MACQUARIE UNIVERSITY

HIGHER DEGREE THESIS
AUTHOR'S CONSENT
DOCTORATE DEGREE

This is to certify that I, Peiyuan Qin being a candidate for the degree of Doctor of Philosophy am aware of the policy of the University relating to the retention and use of higher degree theses as contained in the University's Higher Degree Research Thesis Preparation, Submission and Examination Policy.

In the light of this policy, I agree to allow a copy of my thesis to be deposited in the University Library for consultation, loan and photocopying forthwith.

[redacted]
Signature of Candidate
Date: 31/01/2012

Full Name & Signature of Witness
Date: 31/01/2012

MACQUARIE UNIVERSITY

The Academic Senate on 07 August 2012 resolved that Mr Qin Peiyuan had satisfied the requirements for admission to the degree of Doctor of Philosophy.

This thesis represents a major part of the prescribed program of study.

STUDY OF RECONFIGURABLE ANTENNAS AND THEIR APPLICATIONS IN MIMO SYSTEMS

by

Pei-Yuan Qin

Dissertation submitted in fulfilment of the requirements

for the degree of

DOCTOR OF PHILOSOPHY

Department of Electronic Engineering
Faculty of Science
Macquarie University
Sydney, Australia

January 2012

ABSTRACT

Reconfigurable antennas (RAs) are at the frontier of current antenna research and are excellent antenna candidates for advanced wireless communication applications. The basic structure of a RA is similar to that of a conventional one; however, by using electrical, mechanical or other means to change the fundamental operating mechanism of an individual radiator, the frequency and radiation characteristics of the RA can be varied significantly. This makes a single RA equal to multiple antennas with fixed functionalities. Thanks to the agility and diversity of RAs, they find wide application in Software Defined Radios, multiple-input-multiple-output (MIMO) systems, diversity communication systems, satellite communications, and military communication systems.

One of the greatest design challenges for antenna reconfigurability is changing one characteristic of an antenna, such as the frequency response, without affecting others (polarization or radiation pattern), since the frequency response and the radiation characteristics of an antenna are always highly related. Furthermore, for RAs using electronic components to achieve reconfigurability, the design of an effective dc bias network that has a limited influence on the antenna performance is another important design issue for antenna engineers.

In this dissertation, motivated by the increasing significance of RAs as well as the demand for new design methods for compact RAs with simple dc bias networks, a thorough investigation is presented on RAs in terms of frequency, polarization, pattern, as well as compound frequency and polarization RAs. A few novel RAs with dc bias networks are designed, fabricated and measured. And they have demonstrated many advantages over other corresponding reported

designs.

In addition, a literature review reveals that, although a considerable number of papers on RAs have been published, much fewer are reported on the study of the applications of RAs in wireless communication systems. In order to examine the practical application of RAs, the proposed polarization and pattern RAs are incorporated separately in 2×2 MIMO orthogonal frequency division multiplexing (OFDM) systems. Real-time channel measurements are conducted in both line-of-sight (LOS) and non-LOS (NLOS) scenarios. Compared to the systems with non-reconfigurable antennas, a significant enhancement of the system capacity is accomplished.

STATEMENT OF CANDIDATE

I certify that the work in this thesis has not previously been submitted for a degree nor has it been submitted as part of the requirements for a degree to any other university or institution other than Macquarie University.

I also certify that the thesis is an original piece of research and has been written by me.

In addition, I certify that all information sources and literature used are indicated in the thesis.

Pei-Yuan Qin

ACKNOWLEDGMENTS

First and foremost, I would like to express my sincerest gratitude to my supervisor, Prof Y. Jay Guo (CSIRO ICT Centre, Australia), who has constantly encouraged me to strive for excellence in my career. This work would not have been completed without his remarkable insight, great knowledge, invaluable guidance and generous financial support.

I would also like to acknowledge my supervisors Prof Eryk Dutkiewicz (Macquarie University, Australia) and Prof Chang-Hong Liang (Xidian University, China) for their support, advice and encouragement throughout this work.

Furthermore, I would like to thank the following people from the CSIRO ICT Centre who helped with some of the technical work in this thesis.

I give my thanks to Dr Andrew Weily for his ideas on frequency reconfigurable antenna designs and professional experience in antenna design and measurement.

I would like to extend my gratitude to Dr Trevor Bird and Dr Yong Cai for their advice on reconfigurable antenna designs.

I am grateful for the discussion with Dr Zhuo Chen, Dr Hajime Suzuki and Dr Wei Ni on the subject of MIMO communication.

I also thank Ms Mei Shen and Mr Robert Shaw for the fabrication of reconfigurable antennas.

I owe my sincere thanks to Dr Keith Imrie for proofreading this thesis.

Finally, I am forever indebted to my parents for their infinite support, encouragement and love.

To My Parents

List of Figures

List of Tables

Contents

Chapter 1

Introduction

1.1 Motivation

Antennas are regarded as indispensable and crucial components of wireless communication systems [1-2]. Traditional antennas are normally designed with fixed characteristics and their structures are tailored to fit particular applications. On the other hand, reconfigurable antennas (RAs) are those that have the capability to change their operating frequency, polarization, radiation pattern or combinations of the above by using electrical, mechanical or other means. Compared to RAs, traditional antennas need to be redesigned when the requirements on antenna characteristics are varied, even by a slight margin. As a result, it is quite challenging for traditional antennas to perform their tasks in the following applications or scenarios.

The first scenario is where a number of air-interface communication standards are integrated into a single wireless device. Nowadays, it is common practice for a single radio device to handle several services over a wide frequency range. For example, smart mobile phones or laptops may be required to support different standards, such as wireless local area network (WLAN), Worldwide Interoperability for Microwave Access (WiMAX),

Bluetooth, Global Positioning System (GPS), 3G, 4G, and millimetre-wave WLAN (60 GHz) in the near future. To this end, the antennas need to cover multiple frequency bands.

From the antenna perspective, multiband, wideband and frequency RAs are three potential candidates to be employed in systems requiring multiple operating bands. However, if only a portion of this operating band is required at any given time, such as in a cognitive radio, then a frequency RA would be the most appropriate choice. Compared to multiband and wideband antennas, one of the merits of frequency RAs is that the antenna can provide noise rejection in the bands that are not in use, so that the filter requirements of the front-end circuits can be greatly reduced. In addition, it will be severely challenging for multiband antennas if more and more wireless services are packed into one device, since it is quite difficult to achieve satisfactory bandwidth in each band. Furthermore, compared to multiband or wideband antennas, frequency RAs are more compact so that they will be more suitable for current and future mobile terminal devices. The further advantage of using frequency RAs is that across the entire frequency tuning range the radiation characteristics remain almost stable, which may be a great challenge for multiple and wideband antennas.

The second application is the Software Defined Radio (SDR), which can operate at different frequencies and/or polarizations by using many protocols. For example, a cognitive radio, which serves as a particular form of SDR, is considered as a promising approach to improve the utilization efficiency of radio spectrum resources. A cognitive radio communication system will operate at variable frequencies, thereby requiring frequency agile antennas. For other SDR systems, polarization agility may also be needed. In addition, for military communication systems, in order to enhance the system capability to resist interference and tracking, systems are required to operate at different frequencies in different time slots. To this end, the antennas of such systems should support multiple

frequency bands.

The third scenario is affordable and compact beam-scanning systems. It is known that the cost, the bulk and the complicated structure of currently available phased array systems usually prevent their extensive use in many commercial applications. Therefore, a single antenna, or an antenna array without phase shifter that is capable of steering the beam, will be a promising solution for applications requiring low cost and compact beam-scanning arrays.

The last application is in diversity communication systems, such as multiple-input-multiple-output (MIMO) systems, exploiting antenna diversity to enhance the received radio signal quality and/or increase spectrum efficiency in multipath environments. Antenna pattern and/or polarization agilities are usually employed to provide diversity for those systems.

If traditional antennas are employed for the applications mentioned above, where the characteristics of the antennas should be variable, the number of antennas of a single communication system will be increased. The drawbacks of the increasing number of antennas are the higher cost, larger volume of system, and system performance deterioration due to the mutual coupling of the antennas. Therefore, in order to satisfy the requirements of modern communication systems for flexibility of antenna performance, reconfigurable antennas that are capable of changing their frequency and radiation characteristics are highly sought after [5]-[101].

1.2 Review of the Current Research on RA Designs and Applications

In 1981, antenna engineers started to use shorting posts to change the frequency and polarization of microstrip patch antennas [6], although this reconfigurability cannot be

electrically controlled. In 1982, Bhartia proposed a frequency reconfigurable antenna by mounting varactor diodes on the radiating edges of a microstrip patch [7], and this is the first work on RAs. In 1999, 12 well-known universities, research institutes and companies in the United States participated in a project named "Reconfigurable Aperture Program (RECAP)", launched by the United States Defence Advanced Research Projects Agency (DARPA) [8]. After that, numerous research papers on RAs have been published in antenna-related journals and conference proceedings.

Based on the reconfigurable parameters, the research work can be divided into four main categories:

- Frequency RA
- Polarization RA
- Pattern RA
- Combinations of the above categories

Based on the techniques used to realize reconfigurability, RAs can also be classified into three main groups:

- Using electrical devices, such as PIN diodes, varactor diodes, radio frequency microelectromechanical system (RF-MEMS)
- Using mechanical changes
- Using material changes

In the following sub-sections, the current research on RA designs will be introduced based on the antenna parameters that are made reconfigurable.

1.2.1 Frequency RAs

Frequency RAs can change the antenna operating frequency continuously or discretely while maintaining the polarization and radiation pattern stable across the entire frequency tuning range. Frequency RAs can be classified into four main groups based on the type of antennas employed. They are microstrip patch antennas, microstrip dipole antennas, planar inverted F antennas (PIFA) and microstrip slot antennas. The following introduction to frequency RAs will be presented using the above classification.

Initial work [7], [9-14] proposed to implement frequency RAs by loading the radiating edges of a patch antenna with varactor diodes. By changing the bias voltages of the varactor diodes, the effective electrical size of the patch can be varied, which can produce a 1.1-1.2 frequency tuning ratio [7], [9]. By increasing the number of varactor diodes, the frequency tuning ratio can be increased to 1.6 [10]. It is worth noting that varactor diodes mounted on the non-radiating edges of a patch can also realize frequency-agile antennas [11-12]. The structure shown in Fig. 1.1 (a) is a high-gain partially reflecting surface RA [12]. The operating frequency is electronically tuned by incorporating an array of phase-agile reflection cells on a thin substrate above the ground plane of the resonator antenna, where the reflection phase of each cell is controlled by the bias voltage applied to a pair of varactor diodes. The antenna shown in Fig. 1.1 (b) is a differentially-fed frequency-agile microstrip patch antenna [14]. By loading three pairs of varactor diodes on the microstrip patches, the antenna can achieve a 2.0 frequency tuning ratio. Antennas proposed in [15-21] employ PIN diodes to realize frequency discrete tuning. The tuning mechanism is similar to those using varactor diodes, namely changing the resonant length of a patch antenna. The drawback of microstrip patch frequency RAs is the small impedance bandwidth, as with traditional microstrip patch antennas.

In [22-29], RAs were designed by loading varactor or PIN diodes on dipole or monopole antennas. The advantage of such RAs is that the antenna has a larger impedance band-

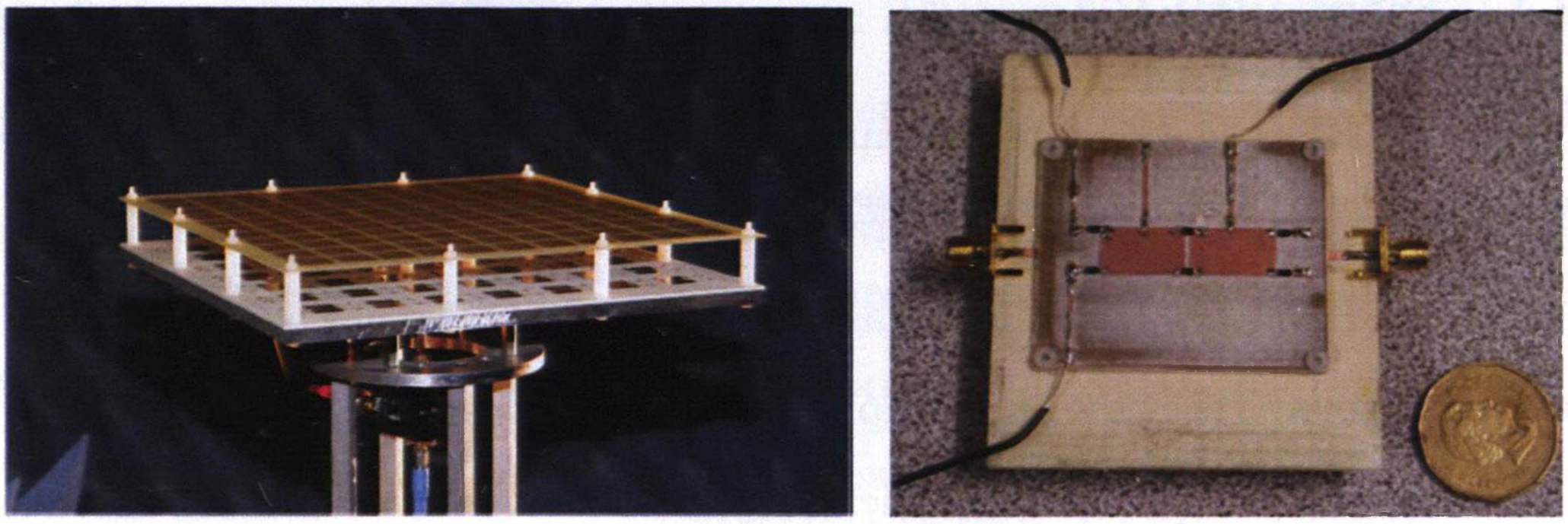

(a) (b)

Figure 1.1: (a) High-gain partially reflecting surface RA [12]; (b) Differentially-fed frequency-agile microstrip patch antenna [14].

width than microstrip RAs and the radiating elements can serve as part of the dc bias lines for the diodes [22], [25], thus simplifying the dc bias network or eliminating the need for extra bias lines around the radiating parts of the antenna, so that the radiation pattern of the antenna can be kept almost unchanged. In Chapter 3, three frequency RAs based on microstrip quasi-Yagi folded dipole antennas are proposed by the author [25-27]. They can achieve discrete or continuous frequency tuning while maintaining the radiation characteristics. In [24], a reconfigurable printed dipole antenna was implemented using two silicon photoconducting switches. By using light from two infrared laser diodes to control the states of the switches, the electrical length of the dipole can be changed, thus the resonant frequency of the antenna is varied. Using fibre-optic cables to activate optical switches has benefits of being electromagnetically transparent and not needing any bias network. However, it is quite challenging to electrically tune the antenna when it is integrated in a wireless communication system since the switches on the antenna should be controlled by extra light sources.

In [30-33], frequency RAs were developed based on the PIFA to realize dual-band frequency tuning by using varactor diodes [30-31] or PIN diodes [32-33]. In [30], a varactor-

tunable slim antenna was proposed that can cover the band of the digital cellular system (DCS; 1710-1880 MHz), personal communication service (PCS; 1850-1990 MHz), universal mobile telecommunications system (UMTS; 1900-2200 MHz), WiBro (2300-2390 MHz), and wireless LAN (WLAN; 5725-5850 MHz) by using varactor diodes. In [31], a simple PIFA-based tunable internal antenna for multifunctional wireless personal communication devices was presented. Multiple resonances are created by cutting slots in the PIFA element. A varactor diode is implemented at an appropriate location in the PIFA structure to obtain the tuning performance over several targeted frequency bands. In [32], an oppositely shorted dual-band stacked patch PIFA was developed. The frequency tuning is achieved by using RF switches integrated to the shorting straps of the stacked patches. In [33], a dual-band frequency reconfigurable PIFA antenna was introduced that can operate in four frequency bands. The frequency reconfigurability of the PIFA antenna is realized by a tuning circuit that is composed of RF switches and discrete passive components.

Microstrip slot antennas are also good candidates for frequency RA designs. By using varactor or PIN diodes to change the length of the slot, the frequency of the antenna can be tuned. Although it is easy to design frequency RAs using slot antennas, and a tuning ratio as great as 3.52 can be achieved [37], slot RAs have the drawback of lower gain and efficiency, particularly in the lower frequency bands. Therefore, frequency-agile slot antennas are attractive for those applications where low-efficiency antennas are required to cover a large frequency range. In addition, dual-polarized RAs can be designed by using slot antennas. In [39], single- and dual-polarized tunable slot-ring antennas were demonstrated. If the antenna is fed by one port, the single-polarized antenna can be tuned from 0.95 to 1.8 GHz by using varactor diodes, as shown in Fig. 1.2 (a). If the antenna is fed by two ports, a dual-polarized antenna can be tuned from 0.93 to 1.6 GHz with independent tuning of both polarizations, as shown in Fig. 1.2 (b).

Furthermore, RF-MEMS is an emerging technology that has been used in patch-based

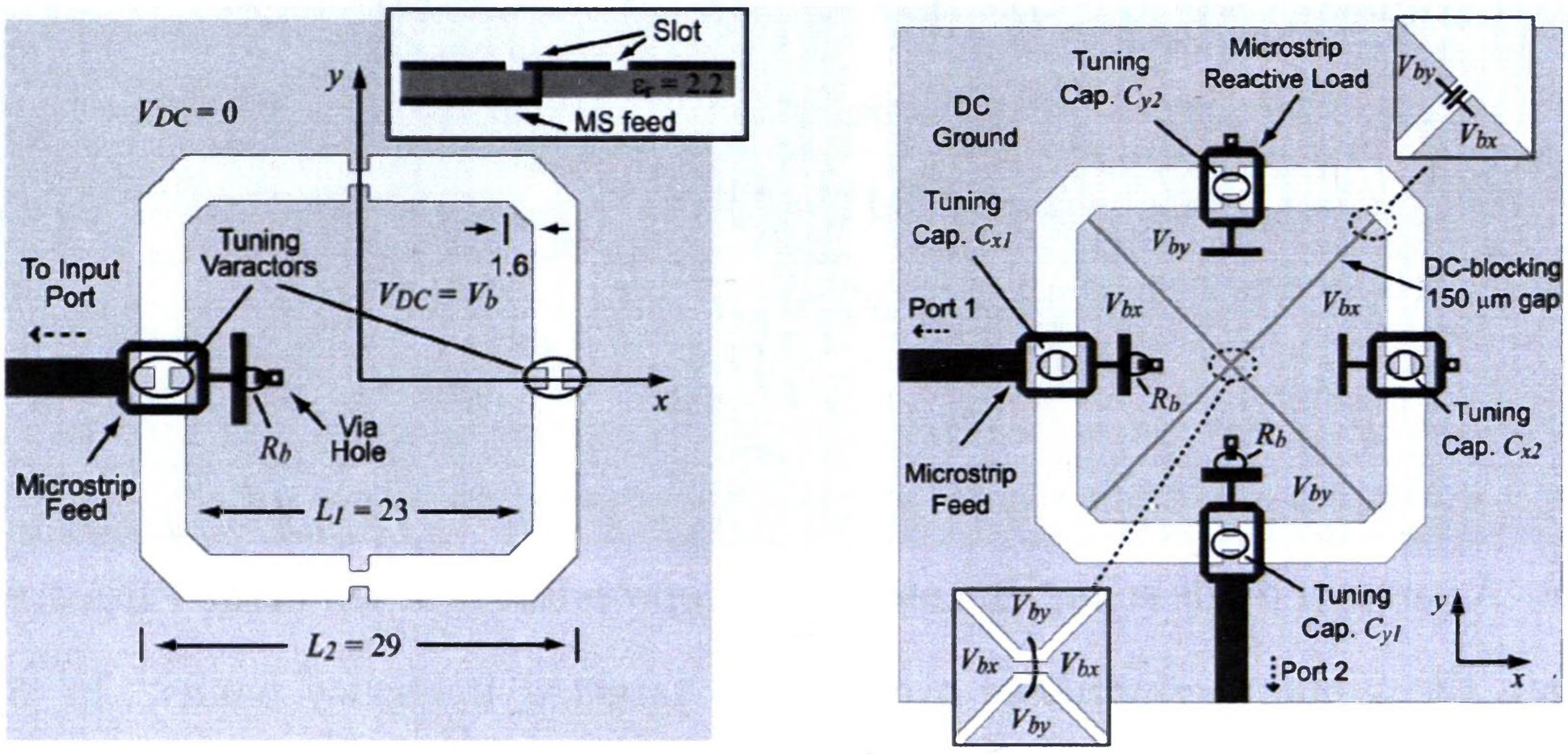

(a) (b)

Figure 1.2: (a) Single-polarized slot-ring antenna [39]; (b) Dual-polarized slot ring antenna [39].

[41] or slot-based [42] RA designs due to the advantages of low loss and high linearity. However, currently available MEMS switches suffer from lower reliability than PIN diodes.

Moreover, mechanical rather than electrical changes in antenna structure [43-44] or changes in the material characteristics of the antenna [45-47] can also deliver frequency tuning. In [43], a mechanically actuated tunable microstrip antenna with a parasitic director was presented. A novel piezoelectric actuation system is used to vary the spacing between the microstrip antenna and the parasitic radiator. The centre frequency, bandwidth, and antenna gain can change as a function of variable spacing between the driven and parasitic elements. In [46], a tunable electromagnetic band-gap (EBG) structure was demonstrated and applied to a switchable microstrip antenna. The EBG structure is loaded with arrays of diode switches. A microstrip patch antenna is located on top of the EBG structure fed by an open-ended microstrip line. The operating frequency of the microstrip patch antenna is tuned by reconfiguring the EBG substrate characteristics.

1.2.2 Polarization RAs

Polarization reconfigurations can take place between different angles of linear polarizations, between left-hand circular polarization (LHCP) and right-hand circular polarization (RHCP), or between linear and circular polarizations. The main difficulty in achieving this kind of reconfigurability is that it must be accomplished without significant changes in antenna input impedance characteristics. Most of the previous work for polarization reconfigurability concentrates on switching between LHCP and RHCP. Relatively few antennas have been presented that can switch between linear and circular polarization because it is difficult to simultaneously realize a good impedance match for circular and linear polarizations. The reason is that circularly polarized radiation is generated by two degenerate orthogonal linear modes, and its input impedance is significantly different from that of the one resonant mode used to generate linearly polarized radiation.

In [48-49], two linearly polarized RAs were presented. In general, this kind of antenna has two operating modes with the same resonant frequency but orthogonal polarizations. By using switches to select between the two operating modes, the antenna can deliver linearly polarized reconfigurability.

In [50-56], polarization RAs were demonstrated that can switch between LHCP and RHCP. Since microstrip patch antennas facilitate the generation of circular polarization, most of the circularly polarized RAs are based on microstrip antennas. Generally, a single microstrip antenna utilizes perturbation [50-55] or an orthogonal dual-fed network [56] to generate two linearly polarized modes with the same magnitude. By using switches to make the phase difference of the two modes equal to $+90^0$ or -90^0, the polarization of the antenna can be reconfigured between LHCP and RHCP.

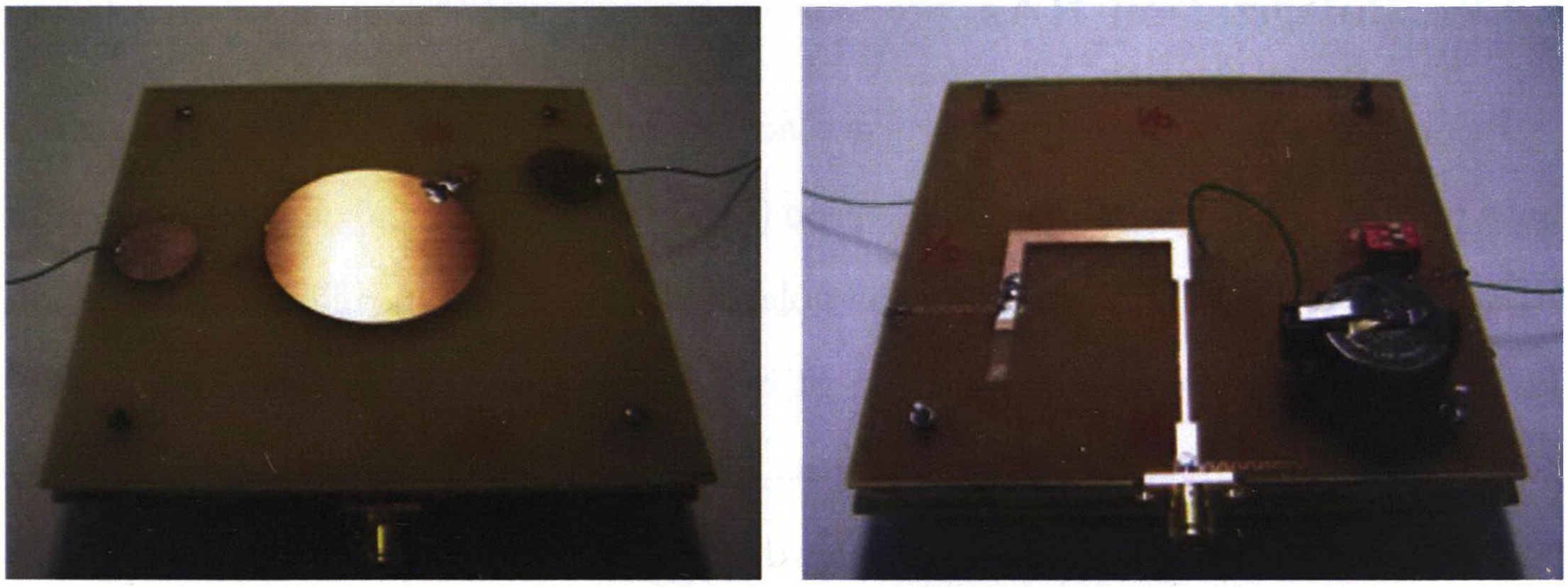

(a) (b)

Figure 1.3: Circular patch polarization reconfigurable antenna [59]: (a) Top layer; (b) Bottom layer.

In [57-61], polarization RAs that can switch between linear and circular polarizations were proposed. In [57], four PIN diodes were used on a corner-truncated square patch. By controlling the states of the PIN diodes, the antenna can produce linear or circular polarization with a small overlapped impedance bandwidth (2.5%). In [58], a perturbed square-ring slot antenna using four PIN diodes was designed that allows radiation with both linear and circular polarization. Unfortunately, the biasing and control circuits were not physically implemented. In [59], a ring-slot-coupled microstrip circular patch antenna was proposed that can switch between linear and circular polarizations, which is shown in Fig. 1.3. It was fabricated on two single FR4 substrates separated by a piece of foam. The overlapped operating frequency bandwidth is 2.2% and it is difficult to integrate such an antenna in a compact wireless device due to its large volume. In [60], an aperture-coupled patch antenna was presented that can provide four polarization states, including two linear polarizations and two circular polarizations. The antenna used two feeding ports and eight PIN diodes, which introduces more losses and increases the complexity of the entire antenna structure. In Chapter 4, a compact U-slot polarization

reconfigurable patch antenna is proposed by the author that can switch between linear and circular polarizations [61] with a wide overlapped impedance bandwidth and axial ratio bandwidth. A simple bias network is used to control the PIN diodes.

1.2.3 Pattern RAs

Pattern RAs have the capability to change the main-beam shape or provide the main-beam scanning. The frequency characteristic should be maintained nearly unchanged for the different states of the antenna. Since the currents on the antenna structure directly determine the antenna radiation pattern, the reconfigurability of the radiation pattern is usually realized by manipulating the current distribution. However, as the current distribution also has a strong impact on the antenna frequency response, it is very challenging to deliver pattern reconfigurability without significant changes in operating frequency. Several methods have been employed to overcome this challenge. One of them is using specific antenna structures, such as reflector antennas or parasitically coupled antennas, so that the input feed port is almost independent from the reconfigured part of the structure, allowing the frequency characteristics to remain largely stable. Another measure is to compensate for the changes in antenna input impedance by using some additional structures or matching circuits.

There are three main techniques that can be used to achieve pattern reconfigurability, namely electrical changes, mechanical changes and material changes. Since most of the designs reported to date focus on the first technology, an introduction to pattern RAs based on electrical changes is given in the following paragraphs.

In general, RAs adopting electrical changes can be further divided into four main groups, which are described in detail below.

The first group uses electrically tuned or switched parasitic elements. By exploiting the coupling between the closely spaced driven and parasitic elements, the array behaviour

can be obtained, but with a single feed point. The changes in the coupling between elements can cause current variation on both the driven and parasitic elements, which can lead to pattern reconfigurability. One of the advantages of this method lies in the high isolation of the driven elements from the tuned elements, which will substantially preserve the frequency characteristics. In addition, this method can be applied to several antenna topologies.

In 1978, Harrington proposed a parasitic dipole array [62], which is shown in Fig. 1.4 (a). The array consists of a driven dipole element surrounded by parasitic dipoles loaded with tunable reactance. Variations in the loading reactance of each parasitic element alter the magnitude and phase of the current on each array element, which allows the main beam of the array to be steered to a desired direction. Based on this idea, a large number of reconfigurable parasitic array designs have been reported [63-66].

Employing switched or tuned parasitic elements to achieve pattern reconfigurability can also be applied to microstrip antennas [67-71]. In [67], a five-element switched parasitic microstrip patch array was presented. The array uses one driven element surrounded by a number of parasitic elements operating near resonance. PIN diodes are used to change the currents on the parasitic patches, which makes some patches act as reflectors and some act as directors. Therefore, steered beams can be achieved. Another similar design using parasitic microstrip dipoles was developed by Zhang [68-69], and is shown in Fig. 1.4 (b). The antenna consists of a single microstrip driven dipole with two parasitic elements parallel to the driven element. The lengths of the parasitic elements can be changed with PIN or varactor diodes, resulting in a variation of the magnitude and phase of the currents on the parasitic elements relative to the driven element. Therefore, the direction of the antenna main beam can be tilted to any of three angles.

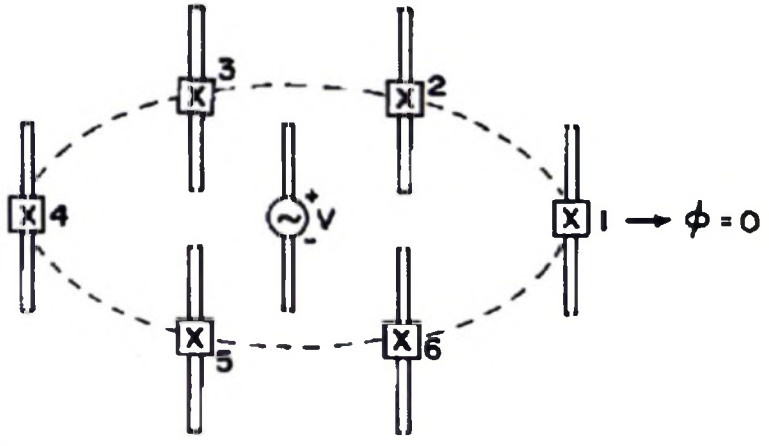

(a)

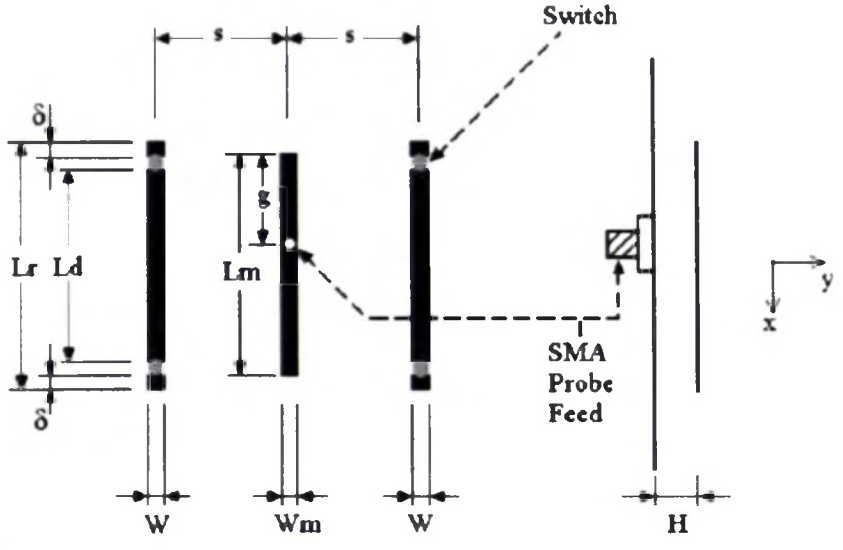

(b)

Figure 1.4: (a) A seven-element circular array of reactively loaded parasitic dipoles [62]; (b) Reconfigurable microstrip parasitic array [68-69].

The second group uses switches to activate one or several elements out of a few radiators, resulting in steered beams [72-73]. As is shown in Fig. 1.5 (a), a planar switched-beam antenna was proposed [72]. It is composed of a four-element antenna array based on an L-shaped slot antenna element. Such an antenna element can deliver a directional radiation pattern in the azimuth plane. Therefore, by using PIN diodes to activate different combinations of the four elements, the maximum-radiation beam can be steered to different directions. In [73], a pattern reconfigurable metallic cubic cavity antenna was presented that can radiate through one or more of six rectangular slots. The configuration of this antenna is shown in Fig. 1.5 (b). PIN diodes are loaded across the slots. When a diode is switched on, the corresponding slot is short circuited and does not radiate. When a diode is switched off, the corresponding slot can radiate. The pattern reconfigurability is achieved by selecting between different combinations of the radiating slots.

The third group integrates reconfigurable phase-shifting elements into an array. Based on this method, beam scanning can be realized by using a phased-tuned reflectarray [74-80]. Specifically, the phase of each element of the reflectarray can be varied by using varactor diodes, MEMS switches or PIN diodes, enabling the array beam to scan across a certain range. A reconfigurable reflectarray requires array elements whose scattered field phase can be adjusted over a broad range (ideally 360^0). In [75], an electronically tunable reflectarray based on elements tuned using varactor diodes was presented. By manipulating the dc voltage across each of the varactor diodes, each individual element can achieve a phase tuning range of 325^0 while maintaining a reasonably flat phase. In [79] and [80], MEMS switches and a combination of PIN and varactor diodes were used to connect or disconnect components for reactive loading to change the phase response of each array element, respectively.

The fourth group alters the operating modes of a single antenna element to change the main-beam shape [81-84]. In [81], a square microstrip spiral antenna was presented.

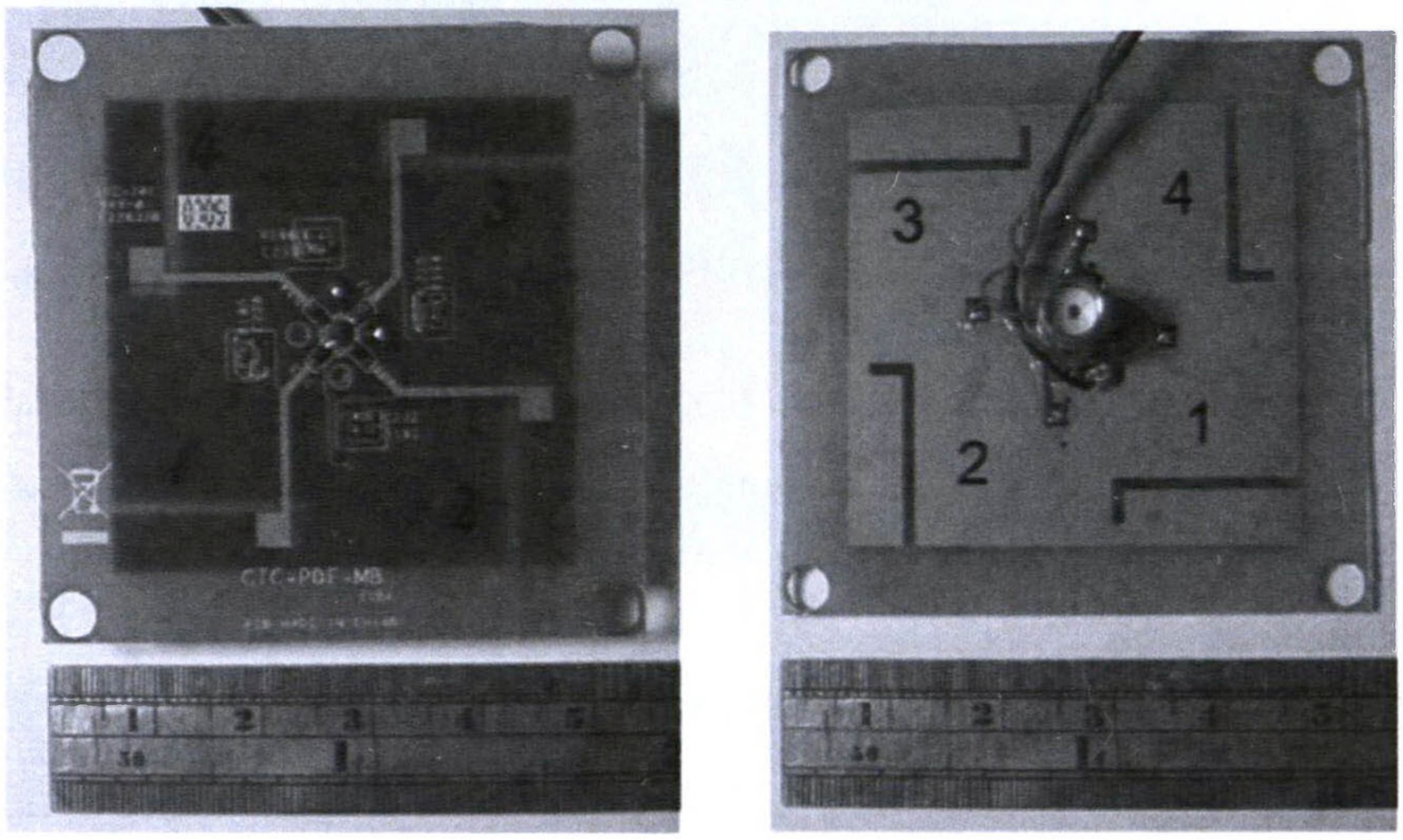

(a)

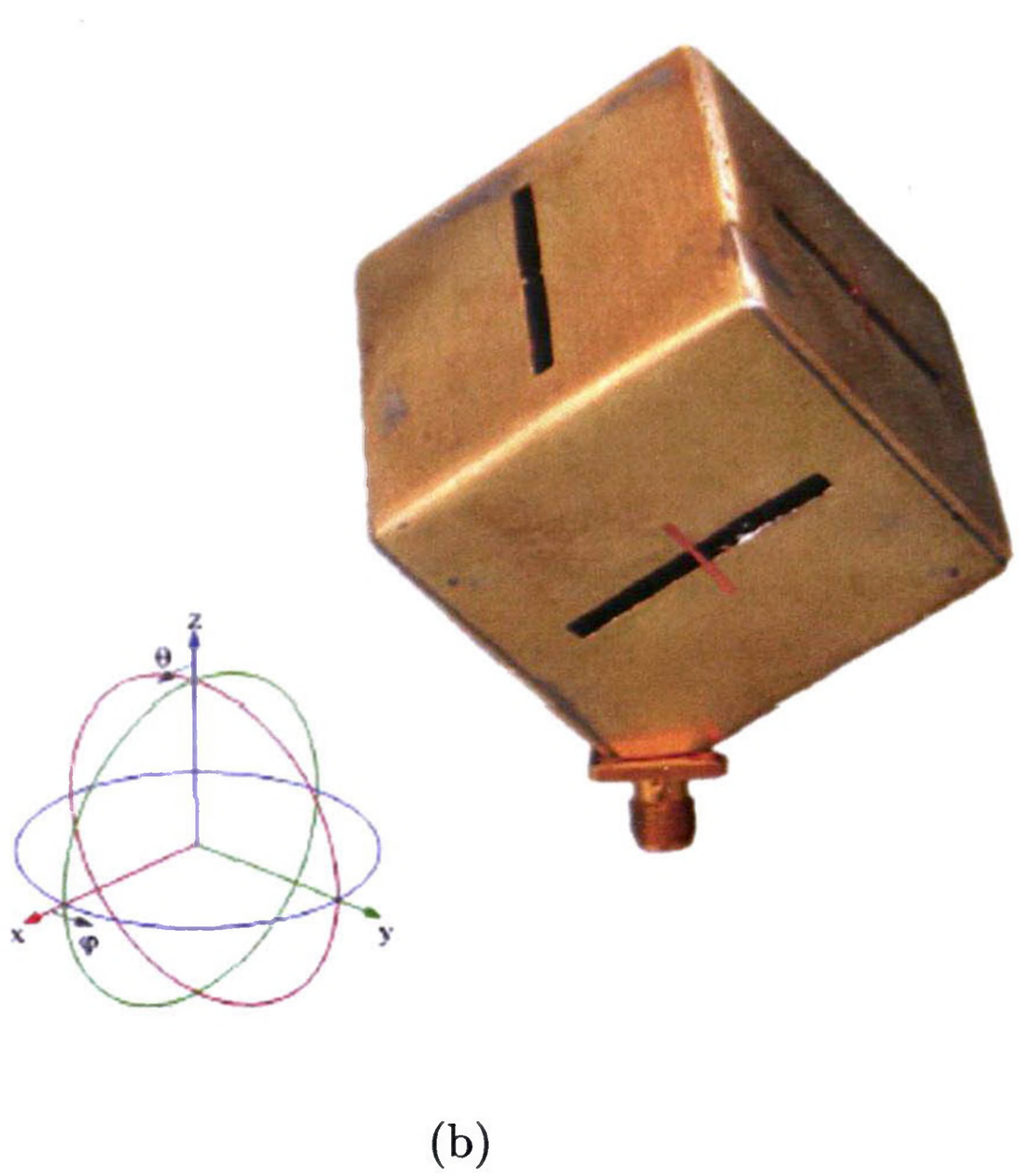

(b)

Figure 1.5: (a)L-shaped slot pattern reconfigurable antenna [72]; (b) Pattern reconfigurable cubic antenna [73].

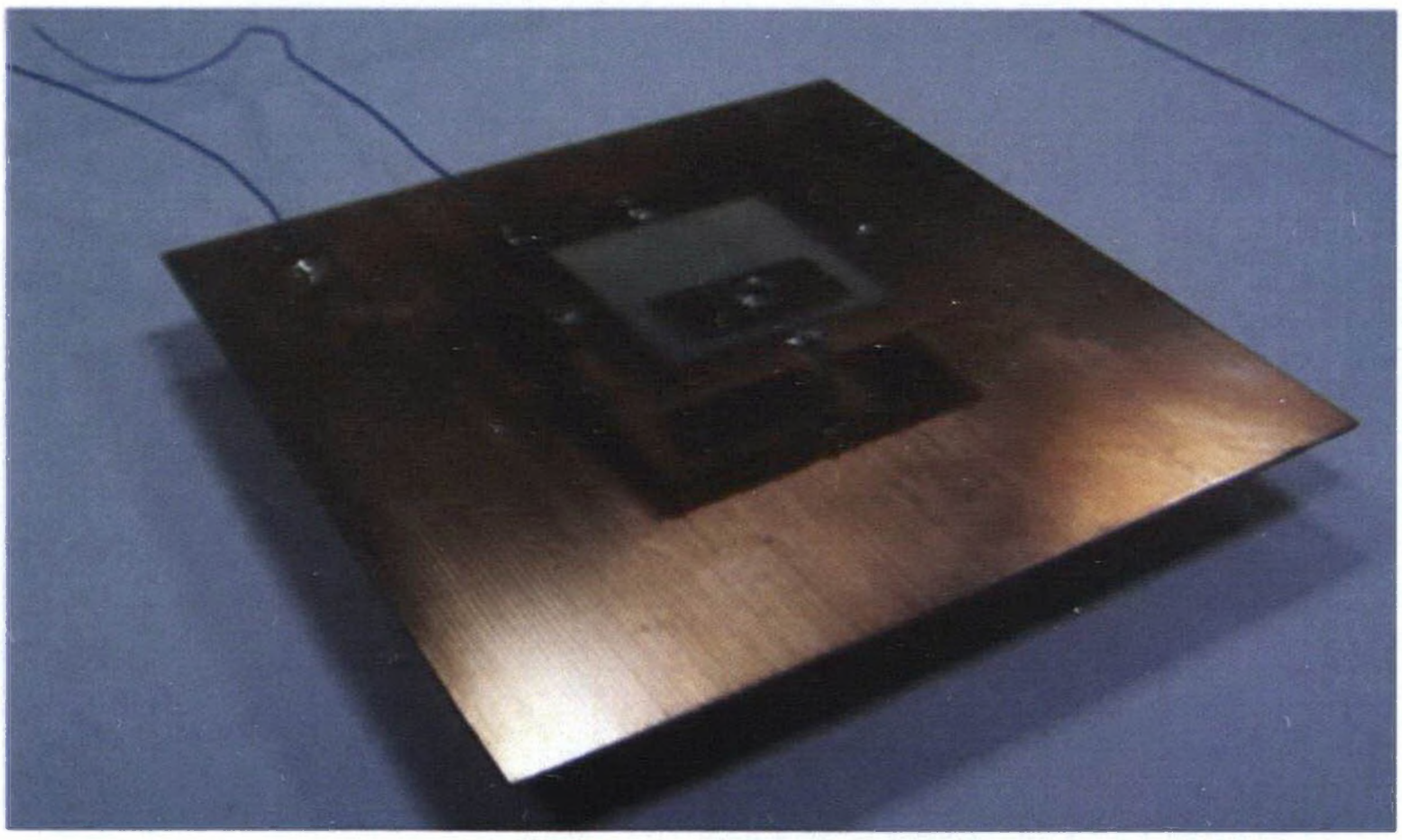

Figure 1.6: Square-ring patch antenna with pattern diversity [84].

RF-MEMS switches are used to change the length of the spiral in order to change the antenna operating modes. The proposed antenna can provide a broadside or 45^0 tilted beam over a common impedance bandwidth. The antennas presented in [82-84] feature the capability to switch between boresight and conical patterns. In [82], a wide-band L-probe circular patch antenna with dual feeds was presented. In order to reconfigure the radiation pattern electrically, an integrated matching network consisting of switches needs to be designed. This will introduce more losses and increase the complexity of the entire antenna structure. In [83] and [84], single feed pattern reconfigurable square-ring patch antennas were designed with air gaps to increase the impedance bandwidth, as shown in Fig. 1.6. Dc bias networks are used to drive the PIN diodes. In Chapter 5, a pattern reconfigurable U-slot patch antenna that can radiate either boresight or conical radiation patterns is proposed by the author [85-86]. The antenna does not need any bias network to control the PIN diodes, which simplifies the antenna structure and makes it easily integrated into wireless communication systems.

1.2.4 Compound RAs

Compound RAs have the ability to independently change the operating frequency, polarization, and radiation pattern of an antenna, which is the ultimate goal of reconfigurable antenna design. Since a compound RA can deliver more flexibility and diversity than a single characteristic reconfigurable antenna, it can bring significant benefits to many wireless communication systems. As discussed in the previous section, it is difficult to separate an antenna's frequency characteristics from its radiation characteristics, which is the major challenge for designing compound RAs. Recently, several groups have achieved combined frequency and radiation pattern reconfigurability [87, 88]. Fig. 1.7 shows an annular slot antenna [87]. By loading PIN diodes across the slot at specific locations (Fig. 1.7 (a)), the direction of the null of the radiation pattern can be changed. In addition, by reconfiguring the matching network shown in Fig. 1.7 (b), the operating frequency of the antenna can also be tuned. In [88], a single-turn microstrip spiral antenna was proposed to reconfigure both the frequency and the radiation pattern.

On the other hand, relatively few reconfigurable antenna designs have been reported that can reconfigure the frequency and the polarization independently. In [89], a frequency tunable aperture-coupled microstrip antenna with vertical and horizontal polarization reconfigurability was reported. However, only the frequency of the vertical polarization can be changed, with a 1.17 frequency tuning ratio. In Chapter 6, a single-feed frequency and polarization reconfigurable microstrip patch antenna is proposed by the author [90]. The antenna can radiate one of three linear polarizations (horizontal, vertical and 45^0 linear polarizations) with a wide independent frequency tuning range for each polarization.

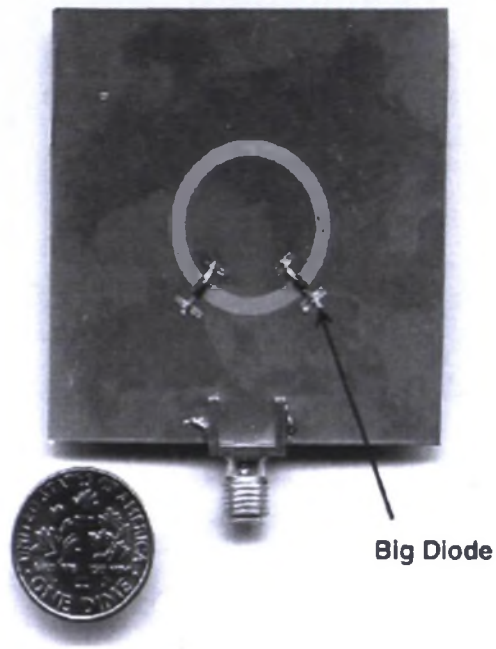

(a)

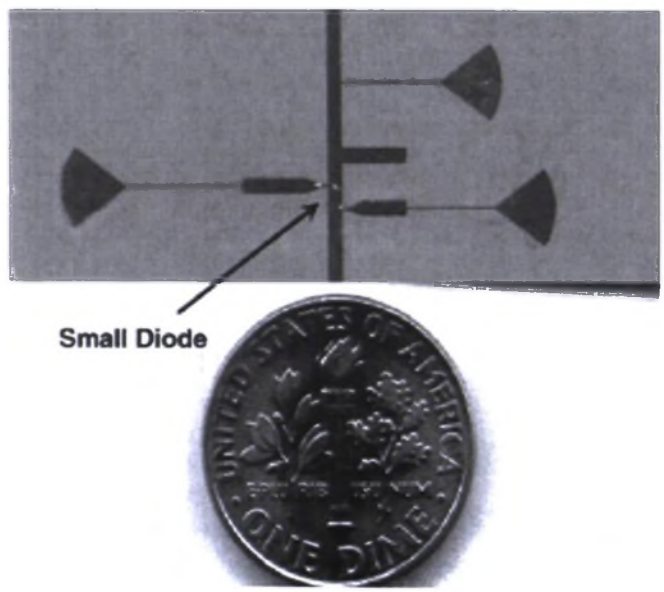

(b)

Figure 1.7: (a) Front side of the annular slot antenna [87]; (b) Back side, the impedance matching network [87].

1.2.5 Applications of RAs in MIMO Systems

MIMO is considered as one of the key potential enabling technologies to enhance the received radio signal quality and/or increase the system spectral efficiency. Recently, reconfigurable antennas have found applications in MIMO systems [91-101], enabling a dynamic change of the radiating characteristics of each antenna element to accommodate the usually fast-changing channel conditions. Specifically, the polarization or pattern diversity provided by reconfigurable antennas can be used to reduce the correlation of the sub-channels of the MIMO systems, thereby increasing the system capacity or improving the signal quality. In [91-96], the applications of polarization reconfigurable antennas in MIMO systems were introduced. In [97-101], applications of pattern reconfigurable antennas in MIMO systems were analysed.

1.3 Contributions and Organisation of the Thesis

1.3.1 Main Contributions of the Thesis

In this dissertation, several novel RAs including frequency, polarization, pattern, and compound frequency and polarization RAs are proposed, prototyped and measured. In addition, the proposed polarization and pattern RAs are incorporated separately in a 2×2 MIMO orthogonal frequency division multiplexing (OFDM) system to demonstrate the improvement in channel capacity. Specifically, the major contributions of this dissertation are summarised as follows:

1. A method of frequency reconfigurability based on a quasi-Yagi folded dipole antenna is proposed in Chapter 3. This method can realize wideband frequency agility while keeping the radiation characteristics stable across the entire tunable frequency range. In addition, the folded dipole allows the dc biasing network to be located far from the

radiating elements of an antenna. Therefore, interference from the bias lines on the antenna performance can be greatly reduced. This biasing method can bring significant benefits for the millimetre-wave frequency reconfigurable antenna design, since in the millimetre-wave band the biasing circuits around the radiating elements will affect the antenna performance considerably. Based on this method, two frequency RAs in the microwave band including one frequency continuous tuning antenna and one frequency discrete tuning antenna are designed [25], [26]. Moreover, a frequency quasi-Yagi folded dipole antenna in the millimetre-wave band is developed [27].

2. A polarization reconfigurable U-slot microstrip patch antenna is proposed in Chapter 4. Most of the previous work on polarization reconfigurability concentrates on switching between right-hand circular polarization (RHCP) and left-hand circular polarization (LHCP). Relatively few antennas have been presented that can switch between linear and circular polarization with a wide overlapped frequency bandwidth and a 3dB axial ratio bandwidth. In order to address this problem, a polarization reconfigurable U-slot antenna is proposed that has the capability to switch between circular and linear polarizations [61]. The antenna is compact and employs a very simple bias network. It has the further advantages of large frequency and polarization bandwidth.

3. A pattern reconfigurable U-slot patch antenna using PIN diodes is proposed for MIMO communication systems in Chapter 5. There are two requirements for pattern reconfigurable antennas that serve for MIMO systems. The first is that the number of radiation patterns that can be reconfigured should be as large as possible. The second is that the correlation coefficient between different patterns should be as low as possible. The proposed pattern reconfigurable antenna can switch between three complementary radiation patterns, and the correlation coefficients between them are very small [85], [86]. Moreover, the overlapped frequency bandwidth is large and the antenna does not need any bias network to control the PIN diodes.

4. A reconfigurable microstrip patch antenna with compound frequency and polarization agility is proposed in Chapter 6. The ultimate goal of reconfigurable antenna design is the ability to independently reconfigure the operating frequency, polarization, and radiation pattern of an antenna. However, relatively few papers have been published on realizing compound frequency and polarization agility. A singly fed compound frequency and polarization reconfigurable microstrip patch antenna with a simple structure is proposed [90]. It can switch between the horizontal, vertical or 45^0 linear polarization, with independent frequency tuning for each polarization state. The tuning ratio is 1.67 for either the horizontal or vertical polarization, and is 1.4 for the 45^0 linear polarization.

5. In order to demonstrate the RA's capability of enhancing MIMO system capacity, the polarization RA proposed in Chapter 4 and the pattern RA proposed in Chapter 5 are incorporated in a 2×2 MIMO-OFDM system separately [86], [96]. This part is described in Chapter 7. Real-time MIMO-OFDM channel measurements are conducted in both line-of-sight (LOS) and non-LOS (NLOS) scenarios. For the MIMO-OFDM system with circularly polarized reconfigurable antennas, the capacity of the system with hybrid polarized antennas is compared to that with the same polarized antennas. For the MIMO-OFDM system with pattern reconfigurable antennas, the capacity of the system with the proposed reconfigurable antennas is compared to that with omnidirectional antennas. The enhancement of the system capacity derived from the pattern diversity is also compared to that reported in other 2×2 MIMO systems with reconfigurable antennas [99]. This work serves as one of the few experimental analyses in the literature of the performance enhancement of an actual MIMO system incorporating RAs.

1.3.2 Organisation of the Thesis

The structure of the thesis is as follows.

Chapter 1 is an introduction, providing a basic insight about RAs and the motivation

for designing RA designs. In addition, it also provides a literature review of the state of the art with respect to previously reported RAs and their applications in MIMO systems.

Chapter 2 briefly introduces the theory of microstrip antennas. Furthermore, it provides the necessary background on MIMO communication systems. This chapter establishes the theoretical foundation for the research work introduced in the following chapters.

Chapter 3 describes three frequency reconfigurable quasi-Yagi folded dipole antennas, including two frequency RAs in the microwave band and one in the millimetre-wave band. The mechanism of the frequency reconfigurability for each antenna is analysed, and the bias network is described. Details of the simulated and measured reflection coefficients, gain and radiation patterns are presented and compared. The effects of the losses of PIN and varactor diodes on antenna gain are discussed.

Chapter 4 presents a polarization reconfigurable U-slot antenna for WLAN applications. Two antenna prototypes with identical dimensions are designed, fabricated and measured. The first antenna prototype enables switching between linear and circular polarization by using a PIN diode and a capacitor located on the U-slot. The second antenna prototype uses two PIN diodes to switch between the two circular polarization senses. The mechanism of the polarization reconfigurability is discussed and the effects of the losses of the PIN diodes on the antenna efficiency are investigated.

Chapter 5 describes a pattern reconfigurable antenna. The operating principle and the equivalent circuits of the antenna with PIN diodes are presented. Three important parameters which affect the input reflection coefficient of the proposed reconfigurable antenna are analysed. An antenna prototype is fabricated and measured. Furthermore, the effects of the losses of PIN diodes on the measured antenna gain and efficiency are discussed.

Chapter 6 presents the design of a compound frequency and polarization reconfigurable antenna. The mechanism of the frequency and polarization reconfigurability is described

and the bias network for the PIN and varactor diodes is discussed in detail. Measured and simulated results on the antenna performance are given.

Chapter 7 describes the applications of the polarization RA proposed in Chapter 4 and the pattern RA proposed in Chapter 5 in a MIMO-OFDM system. The envelope correlation coefficients of the polarization RA and the pattern RA are given. The details of the indoor channel measurement, including the testing environments, antenna array orientation, and measurement process are shown. In a real-time MIMO-OFDM channel measurement, the improvement of the system capacity using RAs is described and analysed, and the factors that can affect the extent of the enhancement are investigated. In addition, the enhancement of the system capacity is compared to that reported in other MIMO systems with reconfigurable antennas.

Chapter 8 summarises the major conclusions of the thesis and future work is discussed.

1.4 List of Publications

Journals

[1] P. Y. Qin, Y. J. Guo, A. R. Weily, and C. H. Liang, A Pattern Reconfigurable U-Slot Antenna and Its Applications in MIMO Systems, IEEE Transactions on Antennas and Propagation, vol. 60, No. 2, pp. 516-528, Feb. 2012.

[2] P. Y. Qin, Y. J. Guo, Y. Cai, E. Dutkiewicz, and C. H. Liang, A Reconfigurable Antenna with Frequency and Polarization Agility, IEEE Antennas and Wireless Propagation Letters, Vol. 10, pp. 1373-1376, 2011.

[3] P. Y. Qin, A. R. Weily, Y. J. Guo, and C. H. Liang, Polarization Reconfigurable U-Slot Patch Antenna, IEEE Transactions on Antennas and Propagation, Vol. 58, No. 10, pp. 3383-3388, Oct. 2010.

[4] P. Y. Qin, A. R. Weily, Y. J. Guo, T. S. Bird, and C. H. Liang, Frequency Re-

configurable Quasi-Yagi Folded Dipole Antenna, IEEE Transactions on Antennas and Propagation, Vol. 58, No. 8, pp. 2742-2747, Aug. 2010.

[5] P. Y. Qin, Y. J. Guo, and C. H. Liang, Effect of Antenna Polarization Diversity on MIMO System Capacity, IEEE Antennas and Wireless Propagation Letters, Vol. 9, pp. 1092-1095, 2010.

[6] P. Y. Qin, C. H. Liang, B. Wu, and T. Su, Novel Dual-Mode Bandpass Filter with Transmission Zeros Using Substrate Integrated Waveguide Cavity, Journal of Electromagnetic Waves and Applications, Vol. 22, pp. 723-730, 2008.

[7] Y. Cai, Y. J. Guo, and P. Y. Qin, Frequency Switchable Printed Yagi-Uda Dipole Sub-Array for Base Station Antennas, accepted for publication in IEEE Transactions on Antennas and Propagation.

[8] B. Wu, C. H. Liang, Q. Li, and P. Y. Qin, Novel Dual-Band Filter Incorporating Defected SIR and Microstrip SIR, IEEE Microwave and Wireless Components Letters, Vol. 18, pp. 392-394, Jun. 2008.

[9] B. Wu, P. Y. Qin, Q. Li, and C. H. Liang, Trisection Cross-coupled Filter with Symmetrical Response Using Split-ring Resonator DGS, Microwave and Optical Technology Letters, Vol. 50, No. 7, pp. 1774-1776, Jul. 2007.

[10] B. Wu, C. H. Liang, P. Y. Qin, and Q. Li, Compact Dual-Band Filter Using Defected Stepped Impedance Resonator, IEEE Microwave and Wireless Components Letters, Vol. 18, pp. 674-676, Oct. 2008.

Conference

[1] P. Y. Qin, Y. J. Guo, and E. Dutkiewicz, Capacity Enhancement of 22 MIMO System Using Pattern Reconfigurable Antennas, Proceedings of 2011 APMC, Melbourne, Australia, Dec. 2011.

[2] P. Y. Qin, A. R. Weily, Y. J. Guo, and C. H. Liang, Pattern Reconfigurable U-Slot Antenna, Proceedings of Twelfth Australian Symposium on Antennas, Sydney, Feb. 2011.

[3] P. Y. Qin, A. R. Weily, Y. J. Guo, and C. H. Liang, Millimeter Wave Frequency Reconfigurable Quasi-Yagi Antenna, Proceedings of 2010 APMC, Yokohama, Japan, Dec. 2010.

[4] P. Y. Qin, A. R. Weily, Y. J. Guo, C. H. Liang, and Y. Cai, A Pattern Reconfigurable U-slot Patch Antenna, Proceedings of 2010 IEEE AP-S/URSI Symposium, Toronto, Canada, Jul. 2010.

[5] P. Y. Qin, A. R. Weily, Y. J. Guo, and C. H. Liang, A Reconfigurable Quasi-Yagi Folded Dipole Antenna, Proceedings of 2009 IEEE AP-S/URSI Symposium, Charleston, USA, Jul. 2009.

[6] P. Y. Qin, A. R. Weily, Y. J. Guo, and C. H. Liang, Frequency Reconfigurable Quasi-Yagi Antenna, Proceedings of Eleventh Australian Symposium on Antennas, Sydney, Feb. 2009.

[7] Y. Cai, Y. J. Guo, and P. Y. Qin, Frequency Switchable Quasi-Yagi Dipole Array for Base Station Antennas, Proceedings of 2011 IEEE AP-S/URSI Symposium, Spokane, USA, Jul. 2011.

[8] Y. Cai, Y. J. Guo, P. Y. Qin, and A. R. Weily, Frequency Reconfigurable Quasi-Yagi Dipole Antenna, Proceedings of 2010 IEEE AP-S/URSI Symposium, Toronto, Canada, Jul. 2010.

Chapter 2

Background

This chapter provides background in two areas. First, a theoretical review of three types of microstrip antennas is given, including a quasi-Yagi dipole antenna, a U-slot patch antenna and a monopolar wire-patch antenna. Since our proposed reconfigurable antennas are based on these microstrip antennas, it is necessary to introduce their operating mechanisms in advance. The second part provides the background of the Multiple-Input-Multiple-Output (MIMO) technology. As applications of the proposed reconfigurable antennas in MIMO systems will be investigated, it is worthwhile to review the basic concepts of MIMO technology.

2.1 Microstrip Patch Antennas

2.1.1 Basic Characteristics

Microstrip antennas are the most common form of printed antennas and have been extensively investigated since the 1970s [103-127]. Presently, they are very attractive for wireless communication systems and mobile radio due to their advantages of low profile, low cost, mechanical robustness, light weight and compatibility with Monolithic

Microwave Integrated Circuit (MMIC) designs.

Often microstrip antennas are referred to as patch antennas [1]. The shape of the radiating patch can be square, rectangular, thin strip (dipole), circular, triangular, or any other configuration. Square, rectangular, dipole and circular are the most common ones due to their ease of analysis and fabrication and low cross-polarization radiation. The structure of a rectangular microstrip patch antenna is shown in Fig. 2.1. It consists of two parallel conductors separated by a thin dielectric substrate that is usually a small fraction of a wavelength ($0.003\lambda_0 < h < 0.05\lambda_0$; λ_0 is the free-space wavelength). The lower conductor acts as a ground plane. By properly choosing the operating mode (field configuration) of excitation beneath the patch, the radiation pattern of the microstrip patch antenna has its pattern maximum normal to the patch (broadside radiation). End-fire radiation can also be realized by judicious mode selection.

There are numerous substrates that can be used for the design of microstrip antennas, and their dielectric constants (relative permittivity) ε_r are usually in the range of 2.2-12. In order to obtain good efficiency and large bandwidth, electrically thick substrates whose dielectric constant is in the lower end of the range are usually selected. These preferred design parameters are in direct contrast to those used in microwave circuits, where thin substrates with higher dielectric constants are desirable.

2.1.2 Analysis Based on the Transmission-line Model

There are many methods of analysis for microstrip patch antennas. The most popular models are the transmission-line [103], [108], cavity [103], [106], [107], and full wave [105], [109]. The transmission-line model is considered to be the simplest analysis method. It can provide good physical insight but with less accuracy. It is also difficult to model coupling. Compared to the transmission-line model, the cavity model is more accurate but more complex. In general, the full wave models are the most accurate and can deal

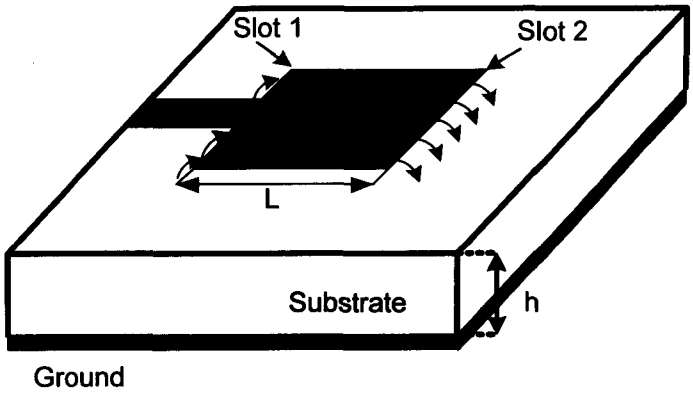

Figure 2.1: Rectangular microstrip patch antenna.

with single elements, stacked elements, arbitrarily shaped elements, arrays, and coupling. However, they are the most complex models and usually give less physical insight. An analysis of the microstrip patch antenna based on the transmission-line model will be shown in the following paragraphs.

In the transmission-line model, a rectangular microstrip antenna is represented as an array of two radiating narrow slots, separated by a low-impedance transmission line of length L. Since the dimensions of the patch are finite along the length and width, the fields at the edges of the patch demonstrate fringing effects, which is illustrated in Fig. 2.1 for the two radiating slots of the microstrip antenna. The amount of fringing is dependent on the dimensions of the patch and the height of the substrate.

For a microstrip line, its electric field lines are shown in Fig. 2.2 (a). It can be noted that the fields exist in two dielectrics: the substrate and air. As can be observed, most of the electric field lines concentrate in the substrate and parts of them reside in air. Since some of the waves travel in the substrate and some in air, an effective dielectric constant ε_{reff} is introduced to account for the fringing effects. The effective dielectric constant is defined as the dielectric constant of the uniform dielectric material so that the line of Fig. 2.2 (b) has identical electrical characteristics [1]. For the microstrip line with air

above the substrate shown in Fig. 2.2 (a), the effective dielectric constant has values in the range of $1 < \varepsilon_{reff} < \varepsilon_r$.

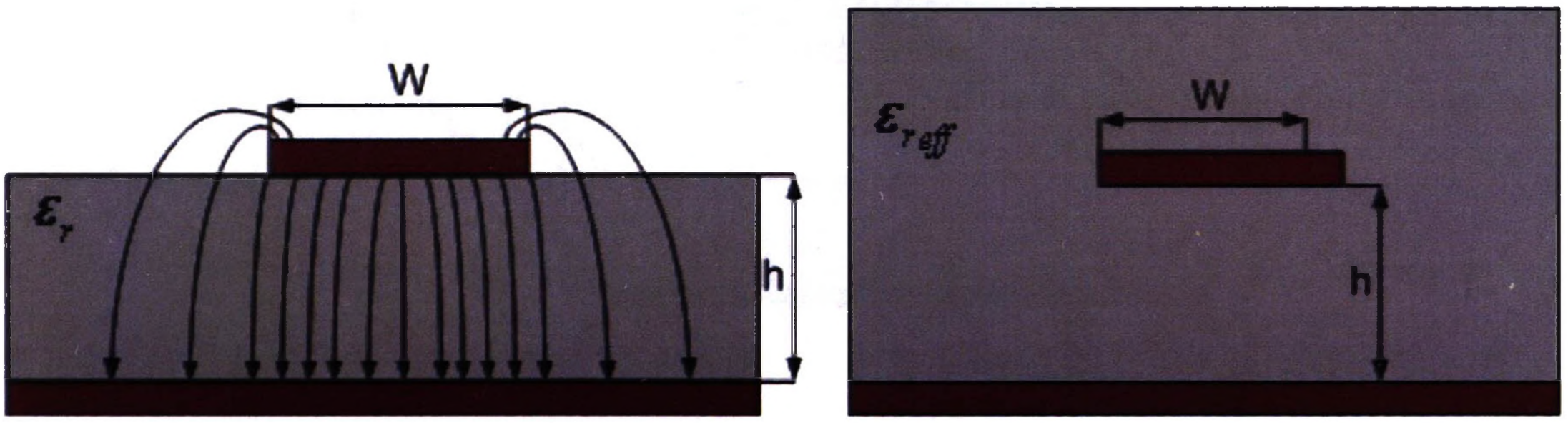

(a) (b)

Figure 2.2: (a) Electric field lines of a microstrip line; (b) Effective dielectric constant.

The effective dielectric constant is a function of frequency. As the frequency increases, the effective dielectric constant approaches the value of the dielectric constant of the substrate since most of the electric field lines concentrate in the substrate. For low frequencies, the effective dielectric constant is given by [110]

$$w/h > 1 \tag{2.1}$$

$$\varepsilon_{reff} = \frac{\varepsilon_r + 1}{2} + \frac{\varepsilon_r - 1}{2}[1 + 12\frac{h}{w}]^{-1/2} \tag{2.2}$$

For microstrip patch antennas, due to the fringing effects, the electrical dimensions of the patch are greater than its physical ones. As is shown in Fig. 2.3, the length of the patch has been extended on each end by a distance ΔL, which is a function of ε_{reff} and the ratio of antenna width to height [1].

$$\frac{\Delta L}{h} = 0.412\frac{(\varepsilon_{reff} + 0.3)(\frac{W}{h} + 0.264)}{(\varepsilon_{reff} - 0.258)(\frac{W}{h} + 0.8)} \tag{2.3}$$

As the length of the patch has been extended by ΔL on each side, the effective length of the patch is now

$$L_{eff} = L + 2\Delta L \tag{2.4}$$

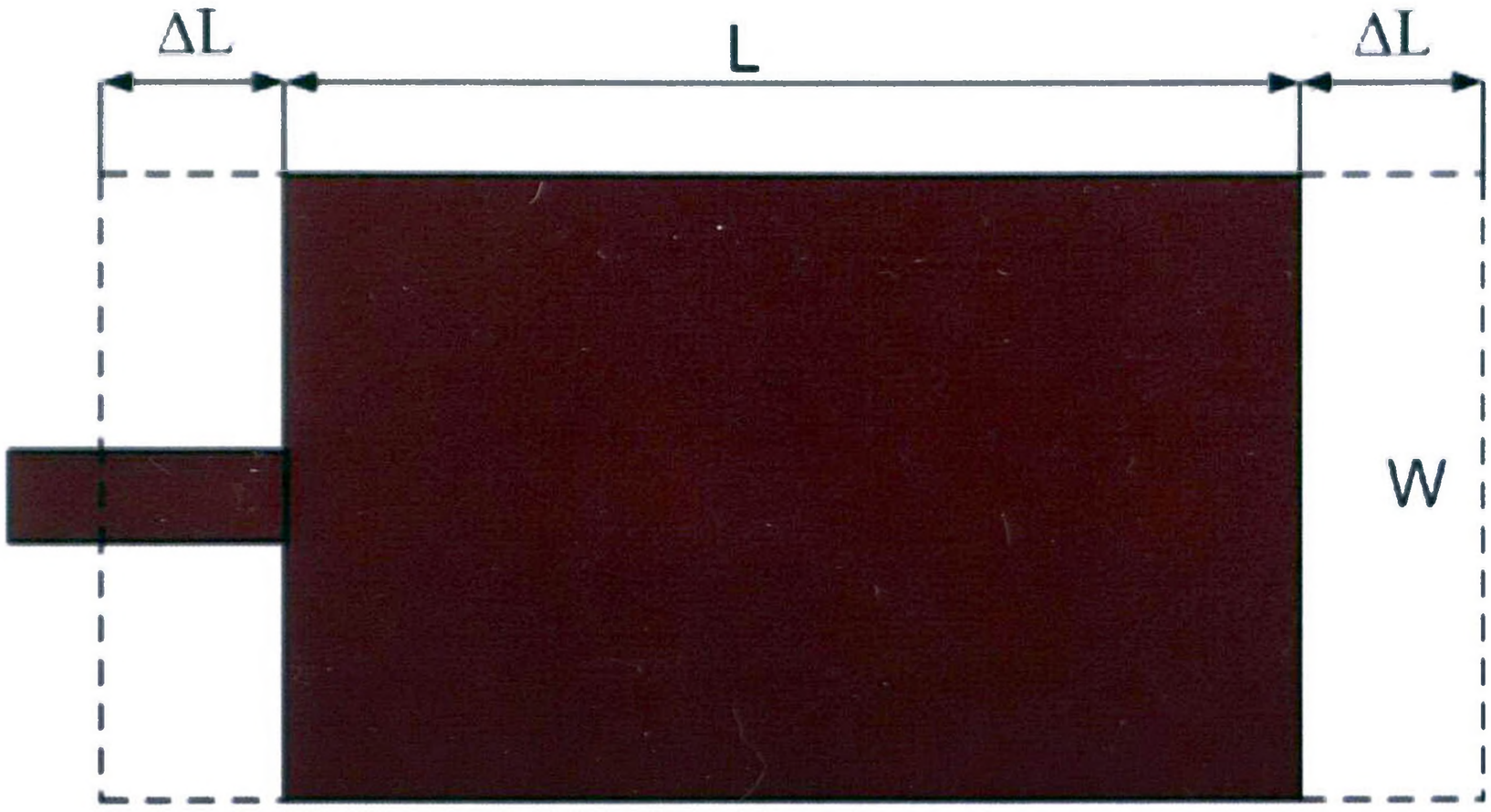

Figure 2.3: Fields fringing effect of a microstrip rectangular patch.

For the dominant TM_{10} mode, the resonant frequency of the microstrip antenna is given by

$$f_r = \frac{1}{2L\sqrt{\varepsilon_r}\sqrt{\mu_0\varepsilon_0}} = \frac{\nu_0}{2L\sqrt{\varepsilon_r}} \tag{2.5}$$

where μ_0 and ε_0 are the permeability of free space and permittivity of free space, respectively, and ν_0 is the speed of light in free space. Since (2.5) does not account for fringing effects, it must be modified to include the edge effects and is given by

$$f_r = \frac{1}{2L_{eff}\sqrt{\varepsilon_{reff}}\sqrt{\mu_0\varepsilon_0}} = \frac{\nu_0}{2(L+2\Delta L)\sqrt{\varepsilon_{reff}}} \tag{2.6}$$

Based on the equations described above, a design procedure is given for the microstrip rectangular patch antenna [1]. The procedure assumes that the resonant frequency, the dielectric constant of the substrate, and the height of the substrate are known.

1. For obtaining good radiation efficiency, the width of the patch is given by [120]

$$W = \frac{1}{2f_r\sqrt{\mu_0\varepsilon_0}}\sqrt{\frac{2}{\varepsilon_r+1}} = \frac{\nu_0}{2f_r}\sqrt{\frac{2}{\varepsilon_r+1}} \tag{2.7}$$

2. Use (2.2) to determine the effective dielectric constant of the substrate.

3. Determine the extension of the length ΔL using (2.3).

4. The actual length of the patch can be determined by

$$L = \frac{1}{2f_r\sqrt{\mu_0\varepsilon_0}\sqrt{\varepsilon_{reff}}} - 2\Delta L \tag{2.8}$$

2.2 Microstrip U-slot Patch Antennas

The major disadvantage of a microstrip antenna is its inherently small impedance bandwidth. Techniques for improving bandwidth have been intensively studied over the past two decades [111-115], including the utilization of parasitic patches [113], coplanar microstrip parasitic subarrays [114], and L-shaped probe feed [115]. In addition, increasing the height of the substrate and using a matching network can improve impedance bandwidths.

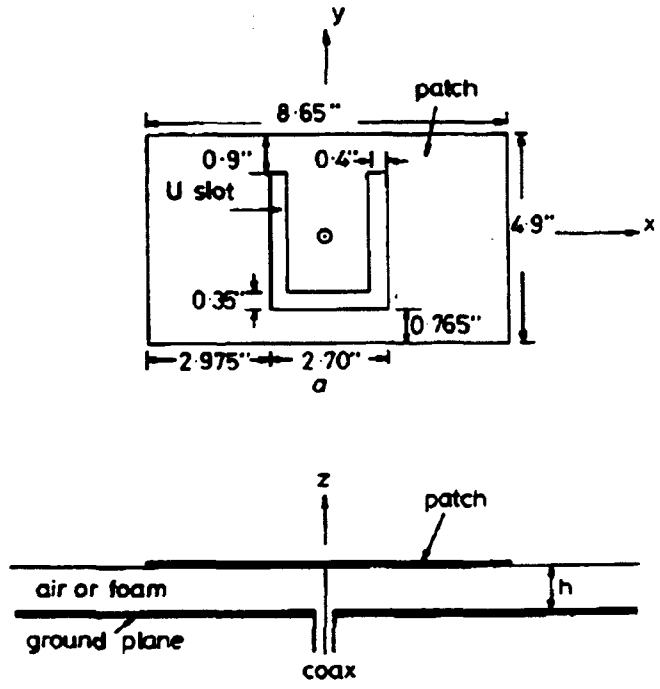

Figure 2.4: U-slot patch antenna [116].

In 1995, Huynh and Lee [116] proposed a novel microstrip U-slot patch antenna with 47% impedance bandwidth, as shown in Fig. 2.4. The dielectric medium between the patch and the ground plane is air. The patch is fed at the centre by a 50Ω coaxial probe. A U-shape slot is inserted into the patch. The measured VSWR is shown in Fig. 2.5. The large impedance bandwidth of the antenna is attributed to the fact that the resonant frequency of the U-slot is close to that of the patch antenna. Therefore, a rectangular patch with a U-slot has a double-looped impedance characteristic on the Smith Chart and can realize a large bandwidth. In [117], the effects of the U-slot dimensions on the antenna resonant frequency are investigated in detail, and a procedure to design a U-slot patch antenna is given.

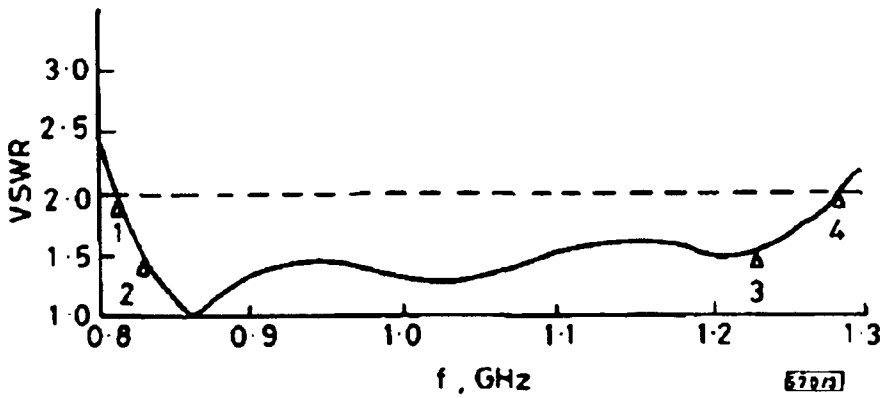

Figure 2.5: Measured VSWR of the U-slot patch antenna [116].

In 2000, Tong proposed a U-slot rectangular patch antenna on a microwave substrate [118] rather than air [116]. The antenna operates at 3.1 GHz and can achieve a 27% input impedance bandwidth.

In 2007, a circularly polarized antenna was designed by Tong based on the U-slot patch antenna, as shown in Fig. 2.6 [119]. An asymmetric U-slot is inserted in the microstrip square patch which sits on the top of a piece of 11-mm-thick foam substrate. The parameters and dimensions of the antenna are shown in Fig. 2.7. By adjusting

the length of the arms of the U-slot (either L_{ul} or L_{ur}) to the optimum position in the y-direction, high-purity circularly polarized radiation can be achieved. In Fig. 2.7, if the left arm of the U-slot (L_{ul}) is longer than the right arm, $L_{ul} > L_{ur}$, the antenna radiates left-hand circular polarization. Right-hand circular polarization can be obtained if L_{ul} is less than L_{ur}. The impedance bandwidth and the 3dB axial ratio bandwidth are 9% and 4%, respectively.

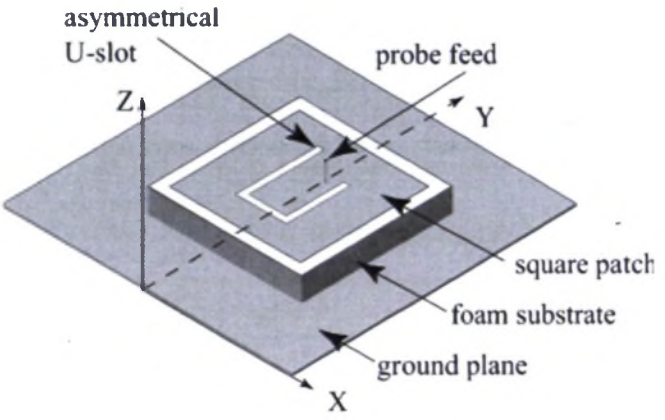

Figure 2.6: Geometry of the circularly polarized U-slot patch antenna [119].

2.3 A Microstrip Monopolar Wire-Patch Antenna

A microstrip patch antenna operating in the dominant TM_{10} mode radiates boresight radiation patterns [120]. By loading two shorting posts between the radiating patch and the ground plane, conical radiation patterns can be achieved [121]. A conical radiation pattern is generally one for which the maximum directivity is off boresight (where boresight corresponds to the direction normal to the plane containing the antenna) and the pattern shape resembles a cone. Such a patch antenna with two shorting posts that works like a monopole is referred to as a monopolar wire-patch antenna [121]. Fig. 2.8 shows its structure and the parameters and dimensions are given in Table 2.1.

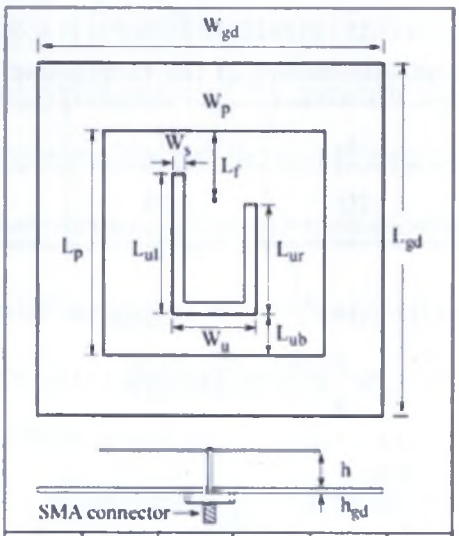

L_p	W_p	h	L_{ul}	L_{ur}	L_{ub}
44.7	44.7	11.0	27.8	21.8	8.3
W_u	W_s	L_f	L_{gd}	W_{gd}	h_{gd}
16.9	2.3	13.9	102	102	3

Figure 2.7: Dimensions of the circularly polarized U-slot patch antenna [119].

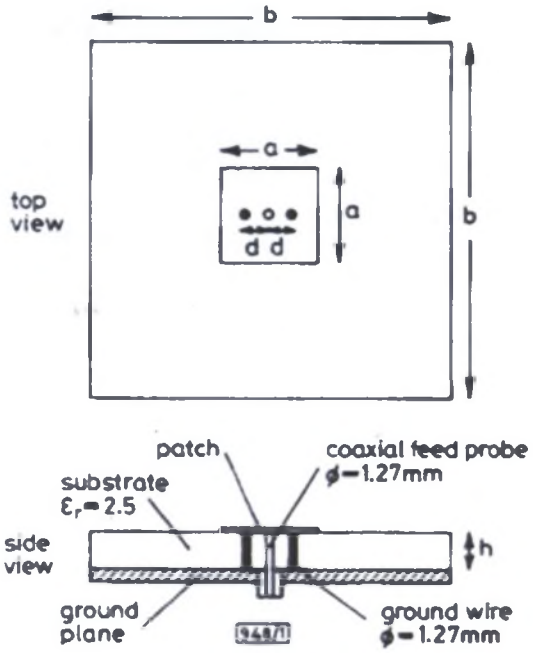

Figure 2.8: Monopolar wire-patch antenna [121].

Table 2.1: Parameters and dimensions of the monopolar wire-patch antenna [121]

Parameter	a	b	h	d
Value (mm)	20	172	10	3.3

The antenna is a classical microstrip patch antenna with a square patch and a ground plane. Two shorting posts are used to connect the patch and the ground plane, which makes currents concentrate on the surface of the shorting posts. In this way, the operating mode of the antenna is changed, thereby producing a conical radiation pattern. The resonant frequency of the antenna described in [121] is 1.74 GHz, which is lower than that of the fundamental mode of a patch antenna.

The height of the antenna is less than 0.05 λ_0, which is a very low profile compared to a quarter-wavelength wire monopole. However, the impedance bandwidth is only 2.8%, which is too narrow for many wireless communication systems. Some research work has been reported that can increase the bandwidth to 15% [122] and 107% [123].

2.4 A Microstrip Quasi-Yagi Dipole Antenna

The Yagi-Uda antenna is a very popular parasitic linear dipole array. The basic structure of a Yagi-Uda antenna consists of a driven dipole, a reflector and a director. It has been used extensively as an end-fire antenna widely at VHF and UHF frequencies. In 1998, Kaneda and Itoh developed a microstrip planar quasi-Yagi antenna that can operate in the microwave/millimetre-wave band [125-127].

The structure of the quasi-Yagi dipole antenna is shown in Fig. 2.9 [127]. The antenna is designed on a 0.635-mm-thick substrate (dielectric constant 10.2) with metallization on both sides. The top side is composed of a microstrip feed, a broad-band microstrip-to-coplanar stripline (CPS) balun, one driven dipole fed by the CPS and one parasitic

director. The bottom plane is a truncated microstrip ground, which serves as the reflector element for the antenna. The combination of the parasitic director and reflector elements directs the radiation of the antenna toward the end-fire direction.

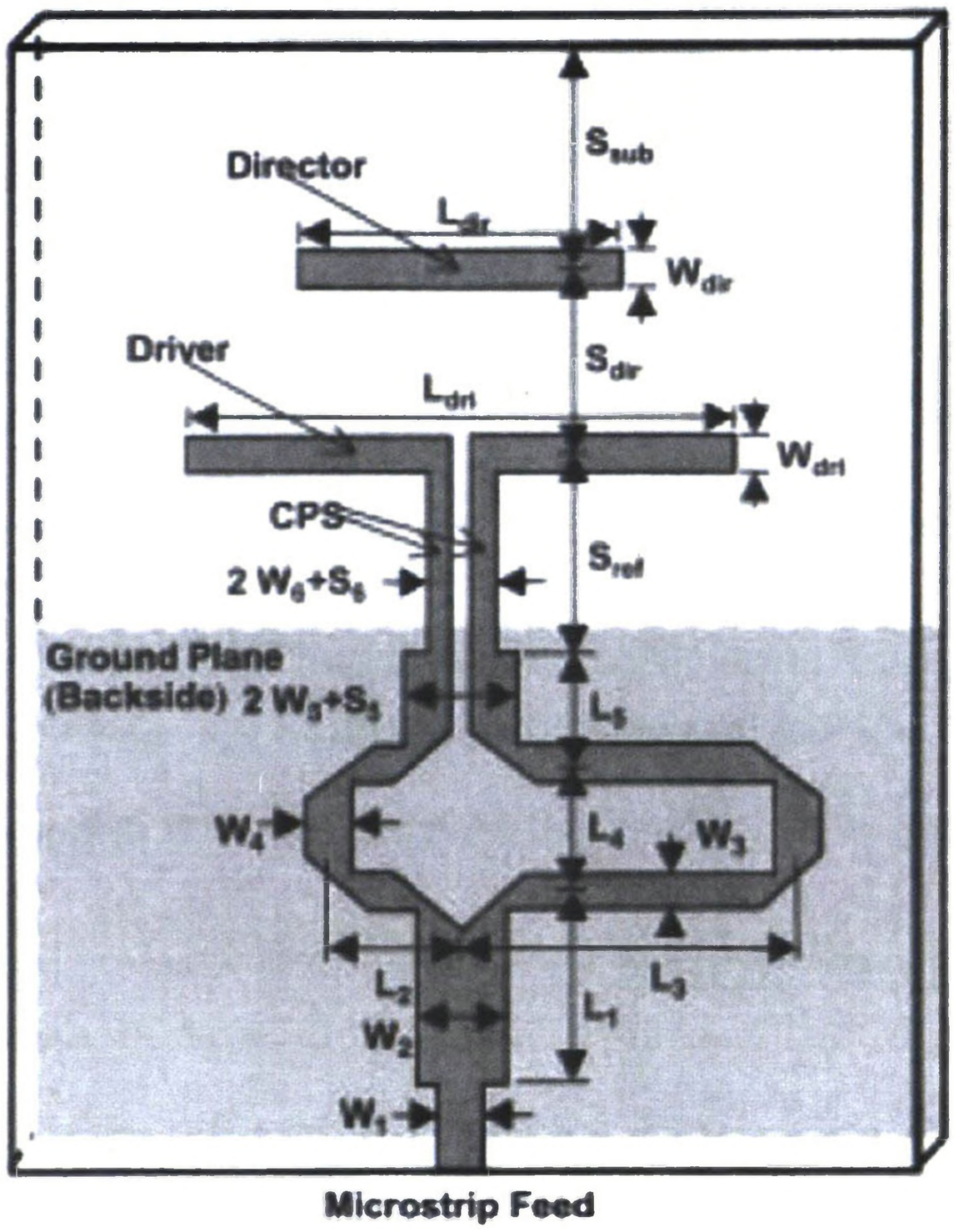

Figure 2.9: Quasi-Yagi dipole antenna [127].

Fig. 2.10 shows the input impedance bandwidth of the antenna. By choosing the antenna parameters properly, the impedance bandwidth can be 40%-50%. The antenna has an end-fire radiation pattern with a front-to-back ratio of about 16 dB and a maximum cross-polarization level of -18 dB.

The quasi-Yagi antenna possesses several advantages over traditional wire antennas. First, the substrate provides mechanical support for the antenna and planar transmission-line compatibility. Second, a truncated microstrip ground plane is employed as the reflecting element, thus eliminating the need for a reflector dipole. This makes the antenna

structure very compact, as well as being compatible with any MMIC devices.

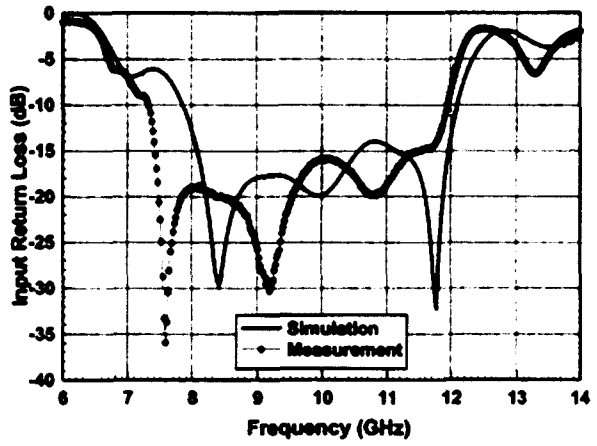

Figure 2.10: Input impedance bandwidth of the quasi-Yagi antenna [127].

2.5 MIMO Technology

2.5.1 Concepts of MIMO Technology

Multiple-Input-Multiple-Output (MIMO) is a technology for wireless communication systems in which multiple antennas are used at the transmitter and/or the receiver to enhance the received radio signal quality and/or increase the spectral efficiency. MIMO technology has attracted considerable research attention since its emergence in the early 1990s, and is still evolving [128-130]. The key characteristic of MIMO technology is that it can provide significant increases in data throughput and link range without additional bandwidth or transmit power.

When a radio-frequency (RF) signal is transmitted towards the receiver, it may encounter objects that reflect, diffract or interfere with the signal, resulting in multiple wavefronts. Therefore, the received signal is a combination of the original signal and the duplicate wavefronts; this is referred to as multipath propagation. The effects of the

multipath propagation include increased signal-amplitude interference, decreased signal-amplitude interference, or a signal null, thereby leading to significant changing of the magnitude of the original signal; this is called multipath distortion or multipath fading. In general, multipath effects will severely affect the quality and reliability of wireless communication.

MIMO technology is an efficient way to overcome multipath fading. Actually, MIMO takes advantage of the multiple signal paths that exist between a transmitter and receiver to significantly improve the quality of the RF signal or data throughput available on a given channel with its defined bandwidth. By using multiple antennas at the transmitter and receiver along with some complex digital signal processing schemes, MIMO technology enables the system to set up multiple data streams on the same channel. If the multipath is rich in the communication environments, the path gains between individual transmit-receive antenna pairs fade independently. In this way, the channel matrix is well conditioned with high probability, and the sub-channels of the MIMO system tend to be independent. By transmitting different information streams in parallel through these independent spatial channels, the receiver can separate the data streams, thereby enhancing the signal quality or increasing the data rate.

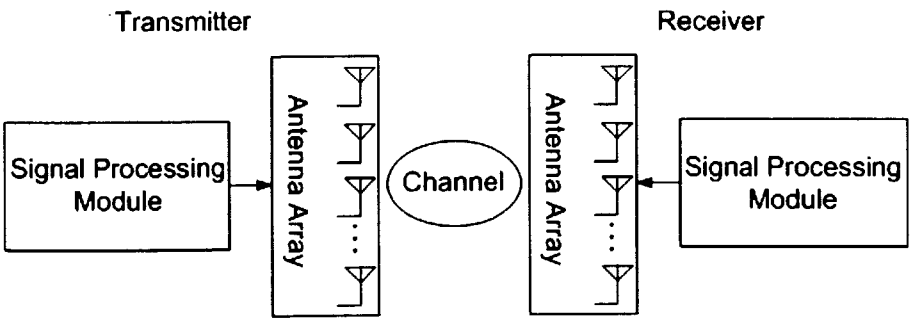

Figure 2.11: MIMO system architecture.

A MIMO system consists of a transmitter and a receiver, as illustrated in Fig. 2.11.

The Transmitter/receiver is composed of a signal-processing module and a physical antenna array. At the transmit end, the data is mapped to transmitting antennas by using different signal-processing methods, such as space-time coding. At the receive end, the data is decoded and recovered.

For a MIMO system consisting of N_r receive antennas and N_t transmit antennas, the transmit streams go through a channel matrix $\mathbf{H}$ which consists of all $N_r \times N_t$ paths between the N_t transmit antennas at the transmitter and N_r receive antennas at the receiver. At a certain time t, the channel matrix $\mathbf{H}$ is given by

$$H(t) = \begin{bmatrix} h_{1,1} & h_{1,2} & \dots & h_{1,N_T} \\ h_{2,1} & h_{2,2} & \dots & h_{2,N_T} \\ \dots & \dots & \dots & \dots \\ h_{N_R,1} & h_{N_R,2} & \dots & h_{N_R,N_T} \end{bmatrix} \tag{2.9}$$

where $h_{i,j}$ is the gain between the ith receive antenna and the jth transmit antenna. When the MIMO channel is completely known to the receiver but is unknown to the transmitter, the Shannon capacity of the MIMO channel is given by [130]:

$$C = log_2[det(I_{N_r} + \frac{SNR}{N_t} HH^+)] \tag{2.10}$$

where C is the system capacity in bits/second/Hz, I_{N_r} is the $N_r \times N_r$ identity matrix, SNR is the average signal-to-noise ratio (SNR), and the superscript $+$ denotes the conjugate transpose.

2.5.2 MIMO Technology Classification

An antenna array used in a MIMO system has many antenna elements placed together. The signals transmitted or received from different antenna elements demonstrate some spatial correlations with each other, which is dependent on both the correlation of the antenna array elements and the communication environments. The correlation coefficient

between two receive signals, ρ, is given by [131]

$$\rho = \frac{E[(r_1 - \bar{r_1})(r_2 - \bar{r_2})]}{\sqrt{E\left|(r_1 - \bar{r_1})\right|^2}\sqrt{E\left|(r_2 - \bar{r_2})\right|^2}} \tag{2.11}$$

where r_1 and r_2 are the envelope values of the two signals, and $\bar{r_1}$ and $\bar{r_2}$ are their average values.

Depending on the degree of the correlations among the sub-channels, MIMO technology can be divided into three categories, namely, spatial multiplexing, diversity, and beamforming.

Spatial multiplexing exploits the scattering properties of the wireless MIMO channels by transmitting different data streams, called sub-streams, in parallel from different antennas to increase link capacity [128]. In spatial multiplexing, a high-rate signal is split into multiple lower-rate sub-streams and each sub-stream is transmitted from a different transmit antenna in the same frequency channel. If these signals arrive at the receive antenna array with sufficiently different spatial signatures, the receiver can separate these sub-streams into (almost) parallel channels. Spatial multiplexing is a very powerful technique for increasing channel capacity at higher SNR. The capacity of the MIMO channel can be measured as the capacity of a single antenna channel times a factor which is called the multiplexing gain. In an ideal MIMO environment, the multiplexing gain is equal to the minimum of the number of the transmit antennas and the number of the receive antennas.

Diversity refers to the use of multiple antennas to improve the link quality between the transmitter and the receiver [128], [130]. It is especially effective at mitigating multipath fading. In diversity methods, multiple copies of the same stream (unlike the multiple different streams in spatial multiplexing) are coded and transmitted by different antennas. With an increasing number of independent copies, the probability that at least one of the copies is not experiencing a deep fade increases, thereby improving the quality and

reliability of reception. A MIMO channel with N_r receive antennas and N_t transmit antennas potentially offers $N_r N_t$ independent fading links, which refers to a spatial diversity order of $N_r N_t$. For digital communication systems, diversity can reduce the bit error rate (BER).

Diversity can be realized in five ways, namely, antenna spatial diversity, antenna pattern diversity, antenna polarization diversity, time diversity and frequency diversity.

Beamforming allows spatial access to the radio channel by means of focusing the energy into some desired directions and nulling others, leading to an increase of the average SNR. The MIMO channel structure and scattering properties are not employed to define independent channels, but to get an equivalent single channel with improved properties. Beamforming can be applied at transmit and/or receive ends of the communication link.

In all, the fundamental benefits available from a MIMO system are diversity and multiplexing. A MIMO system can provide two types of gain: spatial multiplexing gain and diversity gain. However, it is clear that the full benefits of diversity and multiplexing cannot be realized simultaneously. The diversity assumes that the data rate is maintained constant and BER decreases as SNR increases, while multiplexing assumes that BER is held constant and data rate increases with SNR. Usually, some trade-off transmission schemes [132], [133] can be selected to accomplish both multiplexing and diversity gains, but either of them is less than that in a pure multiplexing or diversity scheme.

2.5.3 Antenna Designs for MIMO systems

As mentioned earlier, MIMO systems perform well in rich multipath environments when the correlation between the individual channel gains is low. This correlation is determined by propagation environments as well as antenna array configurations in terms of the correlation between antenna elements. Therefore, in addition to the propagation channel, the design of the antenna array plays a critical role in MIMO system performance.

From an antenna-engineering point of view, the design considerations include not only the conventional parameters of an antenna such as impedance matching, gain, radiation pattern and polarization, but also the envelope correlation coefficient between antenna array elements. The correlation is determined by both the element design and the array configuration such as the spacing of the elements. The envelope correlation coefficient can be calculated by using radiated electric fields assuming that the antennas are lossless and the channels are uniform and random. For a 2-element array, the envelope correlation coefficient ρ_e is given by

$$\rho_e = \frac{\left|\iint_{4\pi} \bar{F}_1(\theta,\phi) \cdot \bar{F}_2^*(\theta,\phi) d\Omega\right|^2}{\iint_{4\pi} \left|\bar{F}_1(\theta,\phi)\right|^2 d\Omega \cdot \iint_{4\pi} \left|\bar{F}_2(\theta,\phi)\right|^2 d\Omega} \tag{2.12}$$

where $\bar{F}_i(\theta,\phi)$ is a complex vector indicating the electric field radiated from the *ith* element. It should be pointed out that this coefficient does not consider the effects of the propagation channel and it is not the correlation coefficient between the two data streams received by the two sub-channels. Therefore, if there is little multipath in the communication environment or if the channel model is a keyhole channel [135], the low correlation coefficient between the two antenna elements cannot guarantee a low sub-channel correlation coefficient. However, for an antenna engineer, the antenna envelope correlation coefficient should be minimized in order to approach the upper bound of the diversity performance of the system.

Chapter 3

Frequency Reconfigurable Antennas

3.1 Introduction

Nowadays, the largest and most desirable portion of the electromagnetic spectrum is allocated to licensed services, resulting in the well-known profound scarcity of this resource for emerging applications. With the rapid proliferation of wireless technologies, spectrum scarcity has become a serious problem since more and more wireless applications are competing for very few spectra. Cognitive radio is viewed as a novel approach for improving the utilization of the spectrum. Cognitive radio, built on a software-defined radio, is defined as a smart wireless communication system. It can intelligently detect which communication spectra are in use and which are not, and instantly move into vacant ones. In this way, spectrum utilization can be improved significantly by making it possible for a secondary user (who is not being serviced) to access a spectrum hole unoccupied by the primary user at the right location and time. As a cognitive radio system will operate in different frequency bands, it is apparent that the antennas of the system are required to be capable of covering multiple bands.

In addition, today, it is common practice for an operator to own several frequency

spectrum bands for one service, such as the GSM system using 900 and 1800 MHz bands as well as WiMAX using 2.5 and 3.5 GHz bands. Moreover, for military applications, in order to enhance the jam resistance, the operating frequency of the system is required to be changed across multiple bands. Consequently, the antennas of the systems mentioned above should support multiple frequency bands.

Multiband, wideband and reconfigurable antennas are three potential candidates to be employed in systems requiring multiple operating bands. However, if only a portion of this operating band is required at any given time, such as in a cognitive radio, then a frequency reconfigurable antenna would be a better choice. Compared to multiband and wideband antennas, one of the merits of frequency reconfigurable antennas is that the antenna can provide noise rejection in the bands that are not in use so that the filter requirements of the front-end circuits can be greatly reduced. Furthermore, compared to a wideband antenna, the frequency reconfigurable antenna is more compact so that it will be more suitable for mobile terminal devices. The further advantage of using frequency reconfigurable antennas is that across the entire frequency tuning range, the radiation characteristics remain almost stable, which is very difficult for wideband antennas.

Most of the frequency reconfigurable antenna designs reported to date are based on the microstrip patch antennas [7-21] or microstrip slot antennas [34-40]. Those two types of antenna can realize a large frequency tuning ratio. However, the impedance bandwidth of those antennas is quite small (around 1-2%), which is not sufficient for many applications. According to our research [25-27], a frequency-agile antenna based on a microstrip dipole or a folded dipole can achieve frequency tuning with a greater impedance bandwidth. In addition, the folded dipole allows the biasing network to be located far from the antenna radiating elements through the metallization of the balun and coplanar-stripline (CPS) feed network, thus eliminating interference from the bias lines. Therefore, this reconfigurable antenna structure with such a biasing scheme can also be employed for

millimetre-wave band reconfigurable antenna design, where the biasing lines around the radiating elements have significant influence on the performance of the antenna.

A literature review shows that few millimetre-wave frequency reconfigurable antenna designs exist. Compared to microwave communication, the millimetre-wave counterpart has advantages of high data rate, large bandwidth, small equipment size, improved security, and interference protection. Furthermore, there is a large quantity of unlicensed spectra available in millimetre wave band. For example, the 60GHz band has been allocated worldwide for short-range wireless communications. This abundant unlicensed spectrum has the potential to enable numerous indoor wireless applications that require large bandwidth and high data rate, such as millimetre-wave Wireless Personal Area Networks (WPAN). Therefore, because of the significant benefits from communicating in the millimetre-wave band, millimetre-wave frequency reconfigurable antenna designs are very necessary and attractive.

In this chapter, a frequency reconfigurable quasi-Yagi folded dipole antenna is proposed for the first time. Two techniques for frequency reconfigurability are presented that allow either continuous tuning by using varactor diodes or discrete frequency tuning by using PIN diodes. Reconfigurability of the operating frequency of the antenna is realized by varying the effective electrical length of the folded dipole driver. Similar end-fire radiation patterns with low cross-polarization levels are realized across the entire tunable frequency range. To validate the concept, two antenna prototypes in the microwave band and one antenna prototype in the millimetre-wave band were designed. For the first antenna, a continuous tuning range of 10% enables this new reconfigurable antenna to cover a total frequency bandwidth of 25% (5.5-7.1 GHz) with about 4.2 to 6.35 dBi gain. For the second antenna, the 5.3-6.6 GHz frequency band or the 6.4-8 GHz frequency band can be covered separately. For the third antenna, the proposed antenna can operate in either the typical millimetre-wave WPAN band (57-66 GHz) or E-band (71-76 GHz).

3.2 Folded Dipole Structures

3.2.1 A Symmetrical Folded Dipole

Before describing the three proposed frequency reconfigurable antennas, it is necessary to introduce the background of the folded dipole [1].

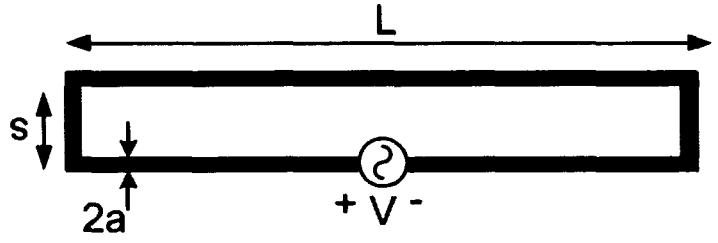

Figure 3.1: Folded dipole.

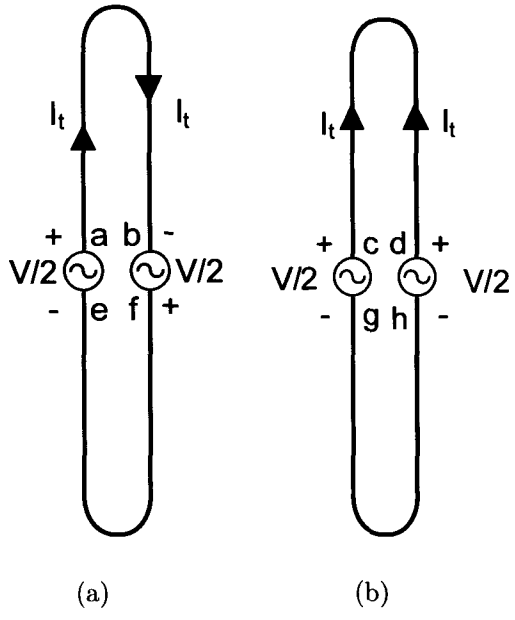

Figure 3.2: Current modes for a voltage V applied to the terminals of a folded dipole.

A folded dipole consists of two parallel dipoles connected at the ends forming a narrow wire loop, as shown in Fig. 3.1. The dimension s is much smaller than L and much smaller

than a wavelength. The folded dipole is essentially an unbalanced transmission line with unequal currents. Its operation is analysed by considering the current to be composed of two modes: the transmission line mode and the antenna mode [136]. The currents for these modes are illustrated in Fig. 3.2.

Suppose that a voltage V is applied across the input terminals of a folded dipole. The total behaviour is determined by the superposition of the equivalent circuits for each mode in Fig. 3.2.

For the transmission line mode of Fig. 3.2 (a), the input impedance at the terminals $a-b$ or $e-f$, looking toward the shorted ends, is given by

$$Z_t = jZ_0 tan\beta\frac{L}{2} \tag{3.1}$$

where Z_0 is the characteristic impedance of the two-wire transmission line.

Since the voltage between the points a and b is $V/2$, and it is applied to a transmission line of length $L/2$, the transmission-line current is given by

$$I_t = \frac{V}{2Z_t} \tag{3.2}$$

For the antenna mode of Fig. 3.2 (b), the current for the antenna mode is given by

$$I_a = \frac{V}{2Z_d} \tag{3.3}$$

where Z_d is the input impedance of a linear dipole of length L and an equivalent radius a_e. The equivalent radius a_e is related to the actual wire radius a by

$$a_e = \sqrt{as} \tag{3.4}$$

The total current on the feed leg (left side) of the folded dipole of Fig. 3.2 is given by

$$I_{in} = I_t + \frac{I_a}{2} = \frac{V(2Z_d + Z_t)}{4Z_dZ_t} \tag{3.5}$$

Therefore, the input impedance at the feed is given by

$$Z_{in} = \frac{V}{I_{in}} = \frac{4Z_d Z_t}{Z_t + 2Z_d} \tag{3.6}$$

When $L = \lambda/2$, it can be shown that (3.6) reduces to

$$Z_{in} = 4Z_d \tag{3.7}$$

From (3.7), it is seen that the impedance of the folded dipole is four times as great as that of an isolated dipole of the same length as one of its sides.

3.2.2 An Asymmetric Coplanar Strip Folded Dipole

The term asymmetric coplanar strip folded dipole means that the widths of the upper and lower strips are different, as shown in Fig. 3.3.

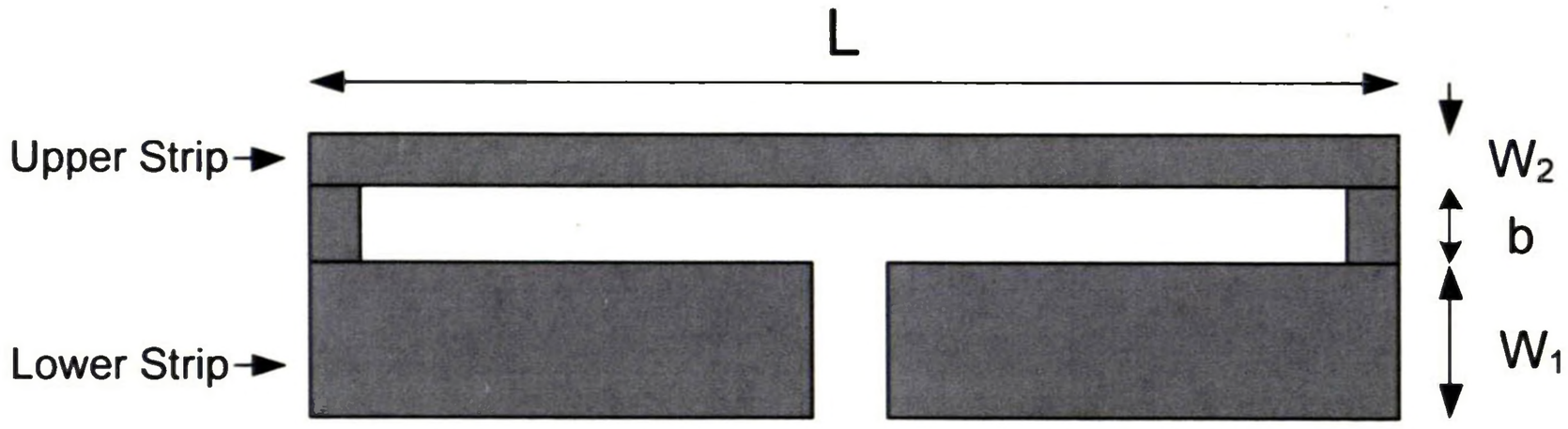

Figure 3.3: Asymmetric coplanar strip folded dipole.

By using a similar analysis method as with the folded dipole, the input impedance of an asymmetric folded dipole of length $L = \lambda/2$ is given by [137]

$$Z_{in} = (1+a)^2 Z_d \tag{3.8}$$

where a is given by [137]

$$a = \frac{ln(4c + 2((2c)^2 - (W_1/2)^2)^{1/2}) - ln(W_1))}{ln(4c + 2((2c)^2 - (W_2/2)^2)^{1/2}) - ln(W_2))} \tag{3.9}$$

$$c = \frac{W_1/2 + b + W_2/2}{2} \tag{3.10}$$

When $W_1 = W_2$, a is equal to 1. The asymmetric folded dipole becomes a symmetric folded dipole. Then Z_{in} is computed using (3.8)

$$Z_{in} = 4Z_d \tag{3.11}$$

Equation (3.11) is identical to (3.7).

3.3 A Frequency Continuous Tuning Quasi-Yagi Folded Dipole Antenna

3.3.1 Antenna Structure and Operating Principle

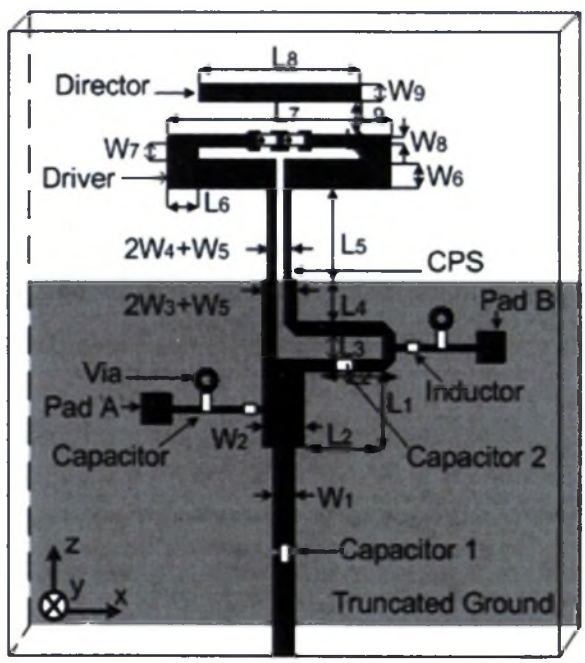

Figure 3.4: Configuration of the antenna.

The configuration of the antenna is shown in Fig. 3.4. The antenna is designed on a two-layer microstrip substrate. The top side of the substrate consists of a microstrip feed,

a quarter-wavelength impedance transformer, a broad-band microstrip-to-CPS balun, a folded dipole driver element fed by the CPS, and a dipole parasitic director element. The bottom side is a truncated microstrip ground, which serves as the reflector element for the antenna. The combination of the parasitic director and reflector elements directs the radiation of the antenna toward the end-fire direction. The parameters and dimensions of the antenna are shown in Table 3.1. It is found that the length of the folded dipole driver L_7, the length of the director L_8 and the ratio of the widths of the upper and lower strips of the folded dipole driver W_8/W_6 are important design parameters which affect the input impedance of the quasi-Yagi folded dipole antenna [137]. In this paper only the electrical length of the folded dipole driver is changed to reconfigure the centre frequency of the antenna in order to simplify the bias network.

Table 3.1: Dimensions of the Antenna

Parameter	W_1	W_2	W_3	W_4	W_5	W_6	W_7	W_8	W_9
Value (mm)	1.8	3.6	1.0	0.6	0.8	2.4	1.2	0.5	1.4
Parameter	L_1	L_2	L_3	L_4	L_5	L_6	L_7	L_8	L_9
Value (mm)	6.5	6.8	2.1	3.6	8.0	2.6	19.4	14.0	3.0

The surface current of the folded dipole was investigated using CST Microwave Studio, as shown in Fig. 3.5. It is found that the current has its maximum value in the middle of the upper strip of the folded dipole driver. Therefore, by mounting varactor diodes in the middle of the upper strip, as shown in Fig. 3.4, the input impedance of the folded dipole will be changed significantly so that the operating frequency of the antenna can be tuned. It is apparent that if the electrical lengths of the upper strip and the lower strip are changed simultaneously, the resonant frequency of the antenna can also be tuned. This case will be studied in detail in the next section.

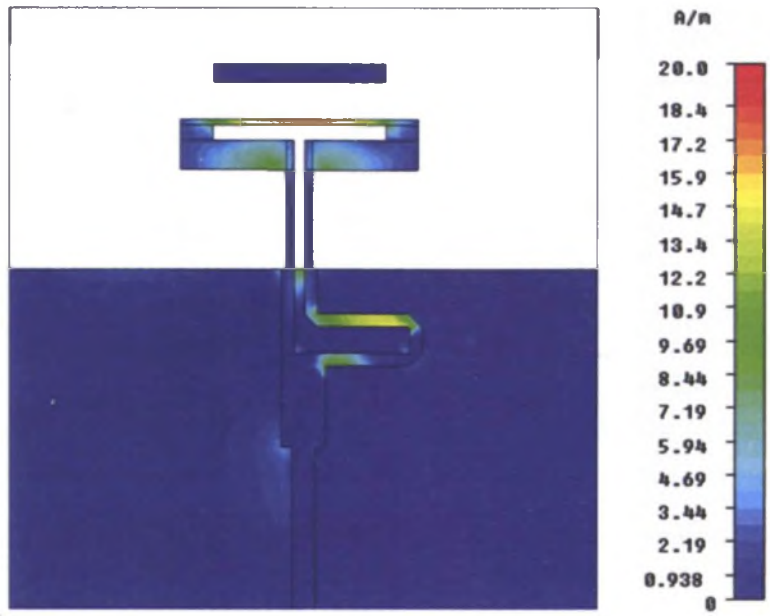

Figure 3.5: Surface current of the antenna.

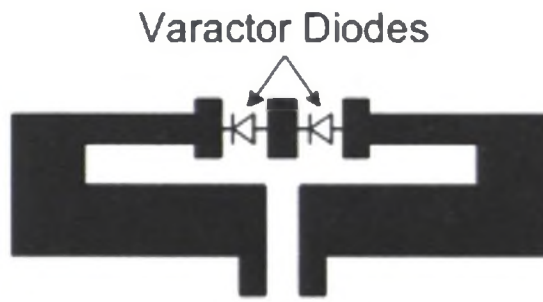

Figure 3.6: Orientation of varactor diodes.

Two low loss varactor diodes (Aeroflex Metelics MGV 125-20-0805-2) with a capacitance range of 0.1-1 pF are placed in series as shown in Fig. 3.4. In Fig. 3.6, the orientation of the varactor diodes inserted on the upper strip of the folded dipole is shown. Fig. 3.7 shows the series RLC equivalent circuit used to model the varactor diodes in the simulation. C_j is the varactor junction capacitance. C_p and L_p are the parasitic capacitance and inductance, respectively. R_p represents the loss of the varactor diode.

Two diodes are used to achieve a larger tuning range, and they are placed at the centre

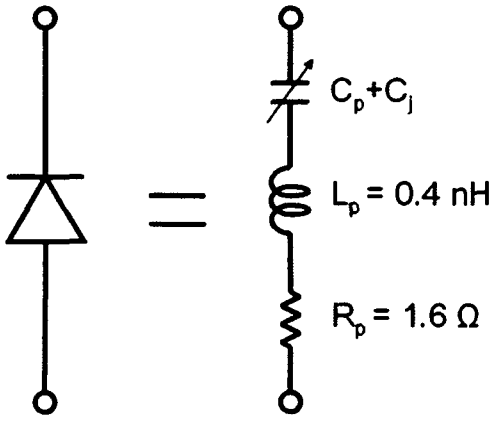

Figure 3.7: Equivalent circuit of the varactor diode (C_p = 0.06 pF, C_j=0.1-1.0 pF).

of the folded dipole where the current is the highest. By varying the junction capacitances of the varactor diodes, the electrical length of the folded dipole driver is varied, thus leading to a change in the input impedance of the antenna. The input impedance of the driven element for different varactor junction capacitances of the antenna with truncated ground plane was analysed using CST Microwave Studio. The results are shown in Fig. 3.8. The model used to calculate the input impedance of the driven element, as shown in Fig. 3.9, is excited by a discrete port but does not include the CPS, the balun and 50Ω microstrip line. The dimensions of the model are given in Table 3.1. As can be seen in Fig. 3.8 (b), the resonant frequency of the antenna is decreased when the junction capacitance increases from 0.1 pF to 1 pF.

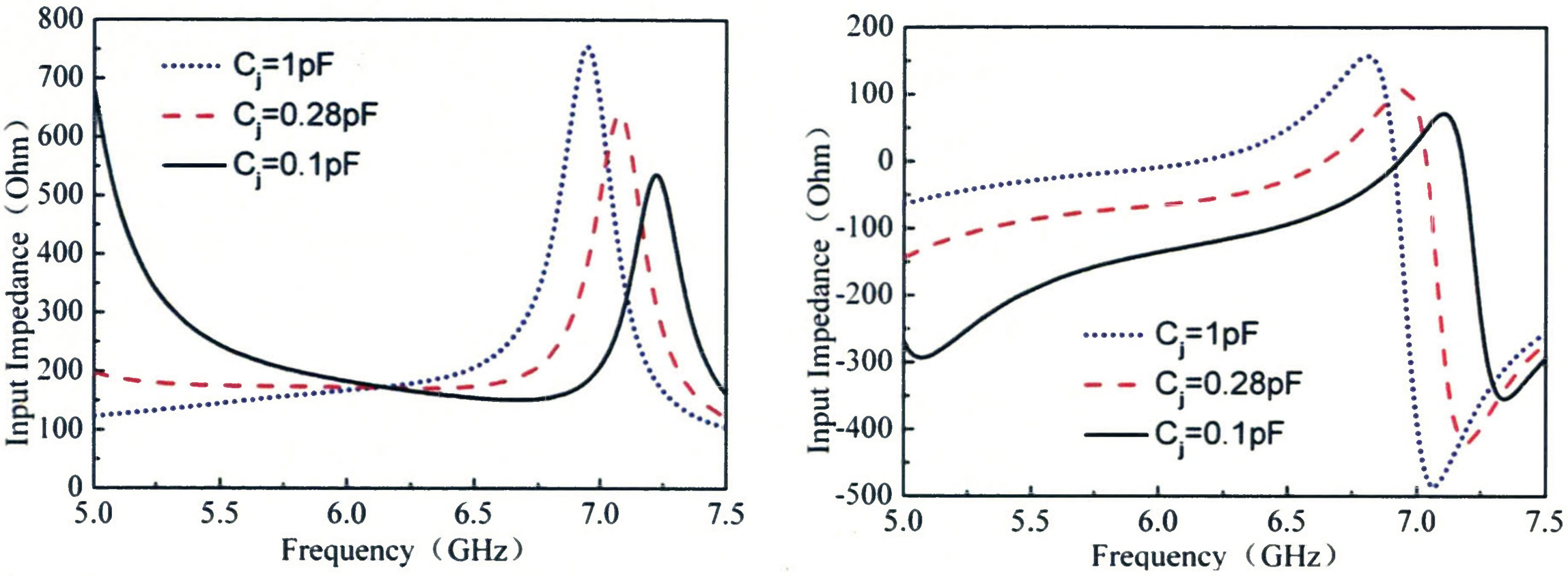

(a) (b)

Figure 3.8: Antenna input impedance for different varactor diode junction capacitances: (a) Real part; (b) Imaginary Part.

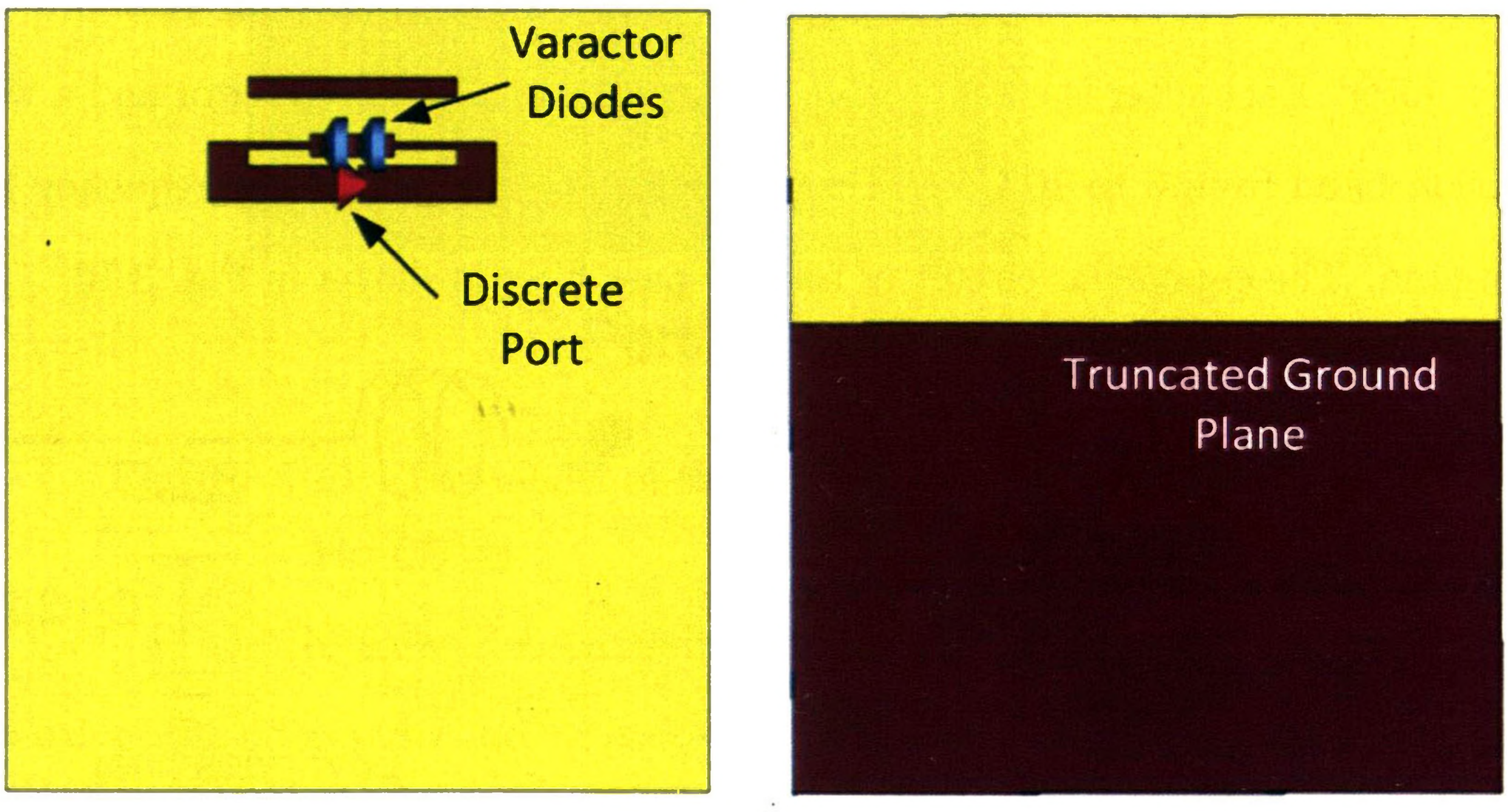

(a) (b)

Figure 3.9: The model used to calculate the input impedance of the driven element. (a) Top layer, including the folded dipole driver, director and a discrete port; (b) Bottom layer, including the truncated ground plane.

3.3.2 Antenna Bias Network

The biasing scheme of the varactor diodes is shown in Fig. 3.4. Since the varactor diodes should be reverse biased, Pad A and Pad B are connected to the positive and negative bias voltages, respectively. The dc bias voltages can be applied to the diodes through the metallization of the balun, CPS and folded dipole. It can be noted that, by using a folded dipole, a closed dc circuit is formed, thereby eliminating the need for extra bias lines to be attached to the folded dipole. If a half-wave dipole is used as the driven element, extra bias lines around the radiating elements would be required, which may cause pattern distortion.

Capacitor 1 is used to prevent the dc bias voltages from flowing into the RF source at the antenna terminal. Capacitor 2 ensures dc isolation between Pad A and Pad B while maintaining the RF continuity of the balun. The dc bias voltage is isolated from the RF signal of the antenna by using two dc bias networks, each consisting of a two-element low-pass filter. Each filter is composed of a chip inductor, a chip capacitor and a via, with a rejection band from 3 to 10 GHz, which covers the entire operating frequency band of the antenna. The equivalent circuit of the low-pass filter is shown in Fig. 3.10.

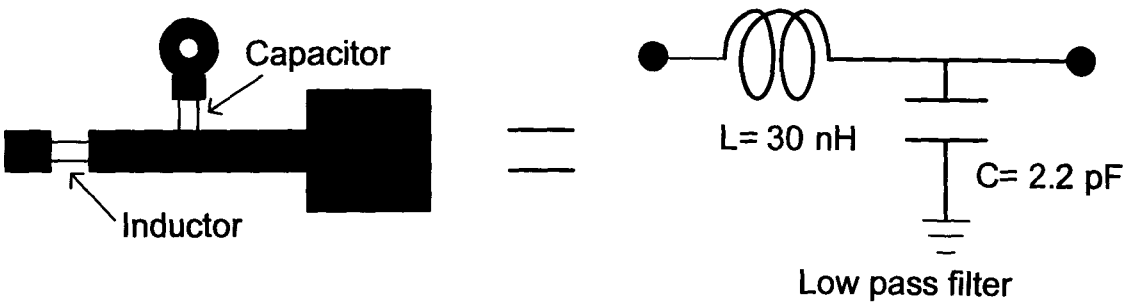

Figure 3.10: Equivalent circuit of the dc bias network used at Pad A and Pad B.

In order to examine the performance of the dc bias network, a microstrip line incorporated with the proposed dc bias network, as shown in Fig. 3.11, was analyzed by CST

Microwave Studio. Regarding the width of the microstrip line, since the bias network connects to both the balun and the quarter-wavelength impedance transformer, two different width that is equal to either W_3 or W_2 are considered. The width of the dc bias line in the model is 0.5 mm, which is the same as that in Fig. 3.4.

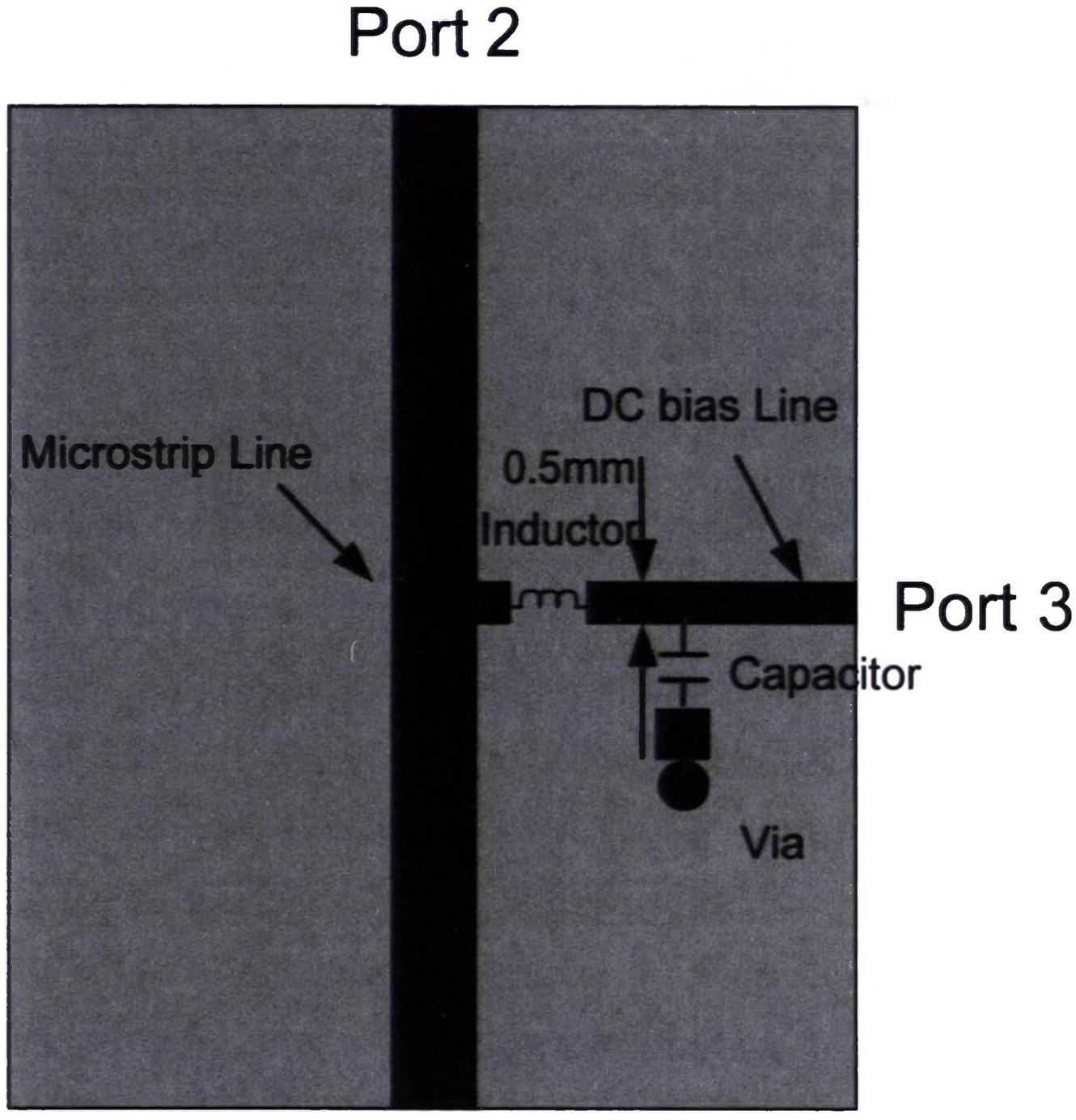

Figure 3.11: The model of the bias network in the simulation.

Fig. 3.12 (a) and (b) show the scattering parameters of the model for the two values of the width of the microstrip line, respectively. It can be seen that in both situations the transmission from port 1 to port 3 $|S_{31}|$ is below -30 dB, which means that the dc bias network can choke the RF signal successfully.

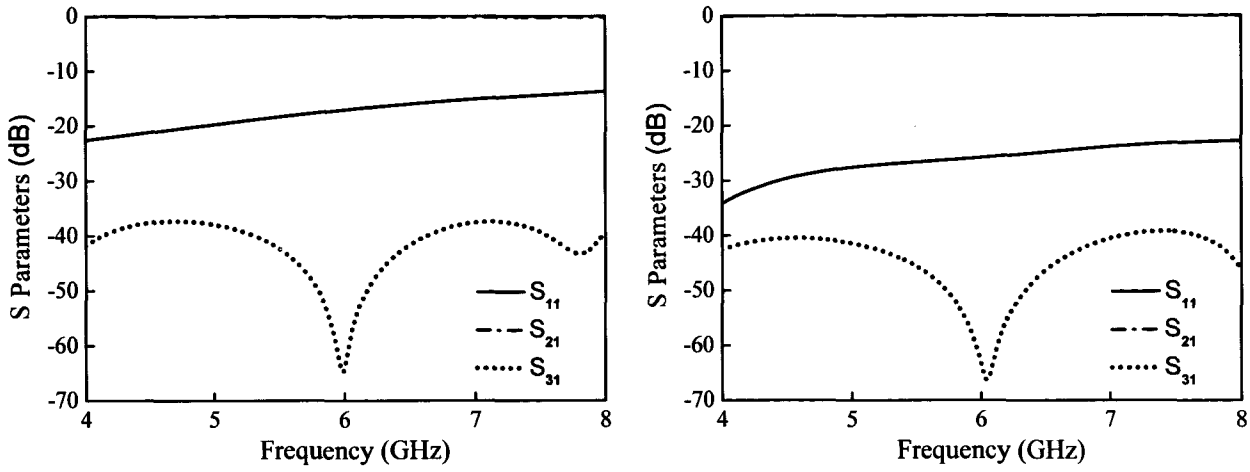

Figure 3.12: Simulation results of the dc bias network with the width of the microstrip line equal to: (a) 1 mm; (b) 3.6 mm.

3.3.3 Simulated and Measured Results

The antenna was fabricated on a single Rogers substrate 4003 (0.813 mm thick and dielectric constant ε_r=3.55). A photograph of the prototype is shown in Fig. 3.13.

The simulated reflection coefficients as a function of frequency for three different varactor diode junction capacitances C_j are given in Fig. 3.14. The corresponding measured results are plotted in Fig. 3.15. From Figs 3.14 and 3.15 it is observed that, by changing the junction capacitance values of the two varactor diodes from 1 pF to 0.1 pF (or by increasing the varactor diode bias voltages), the centre frequency can be continuously tuned from 6 to 6.6 GHz. The reflection coefficient bandwidth ($|S_{11}| \leqslant$ -10 dB) at each frequency is greater than 15%. The frequency tuning range can be further enlarged by employing varactor diodes with a larger capacitance variation. Table 3.2 summarizes the simulated and measured antenna performance across the operating frequency range.

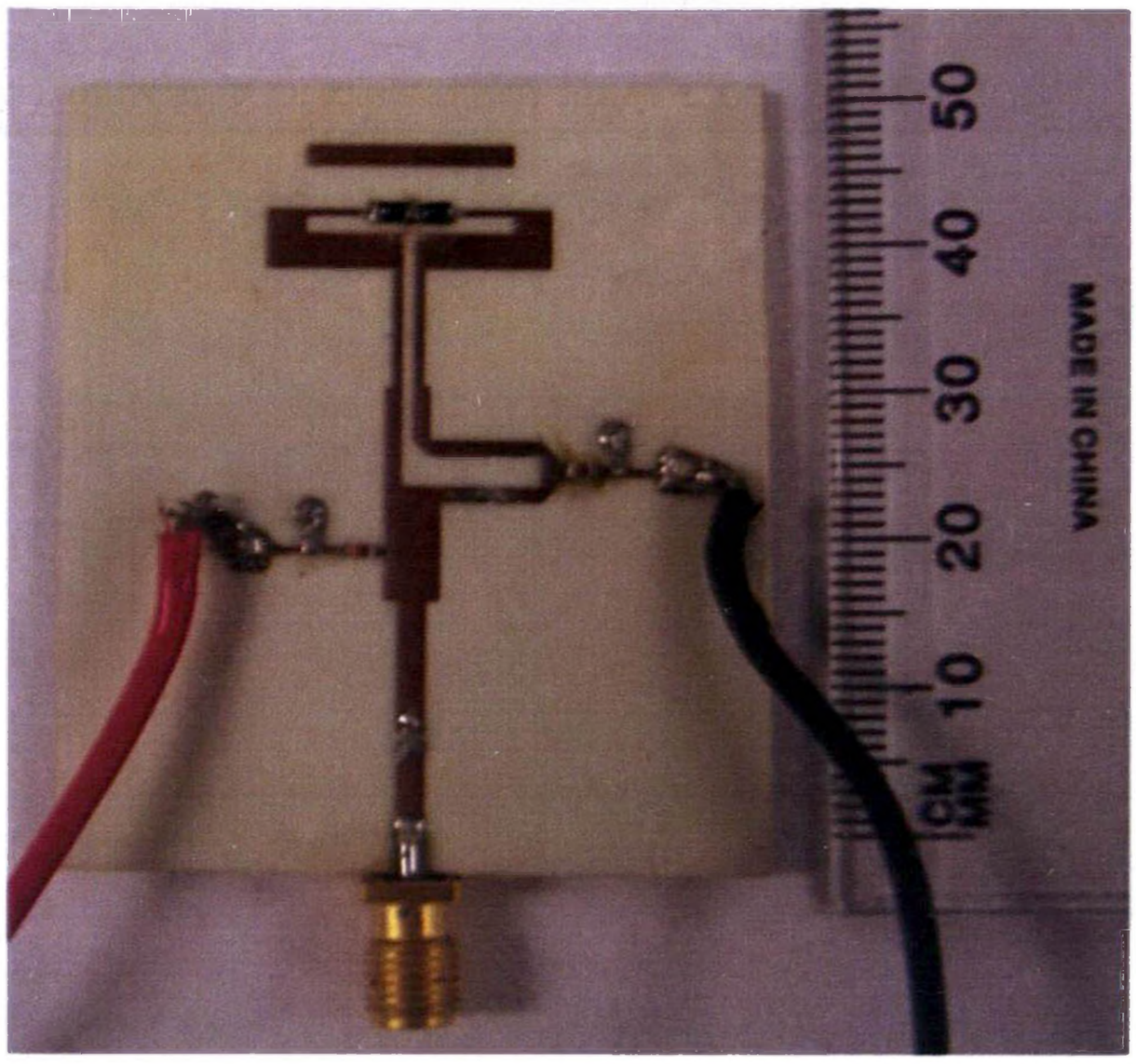

Figure 3.13: Photograph of the antenna.

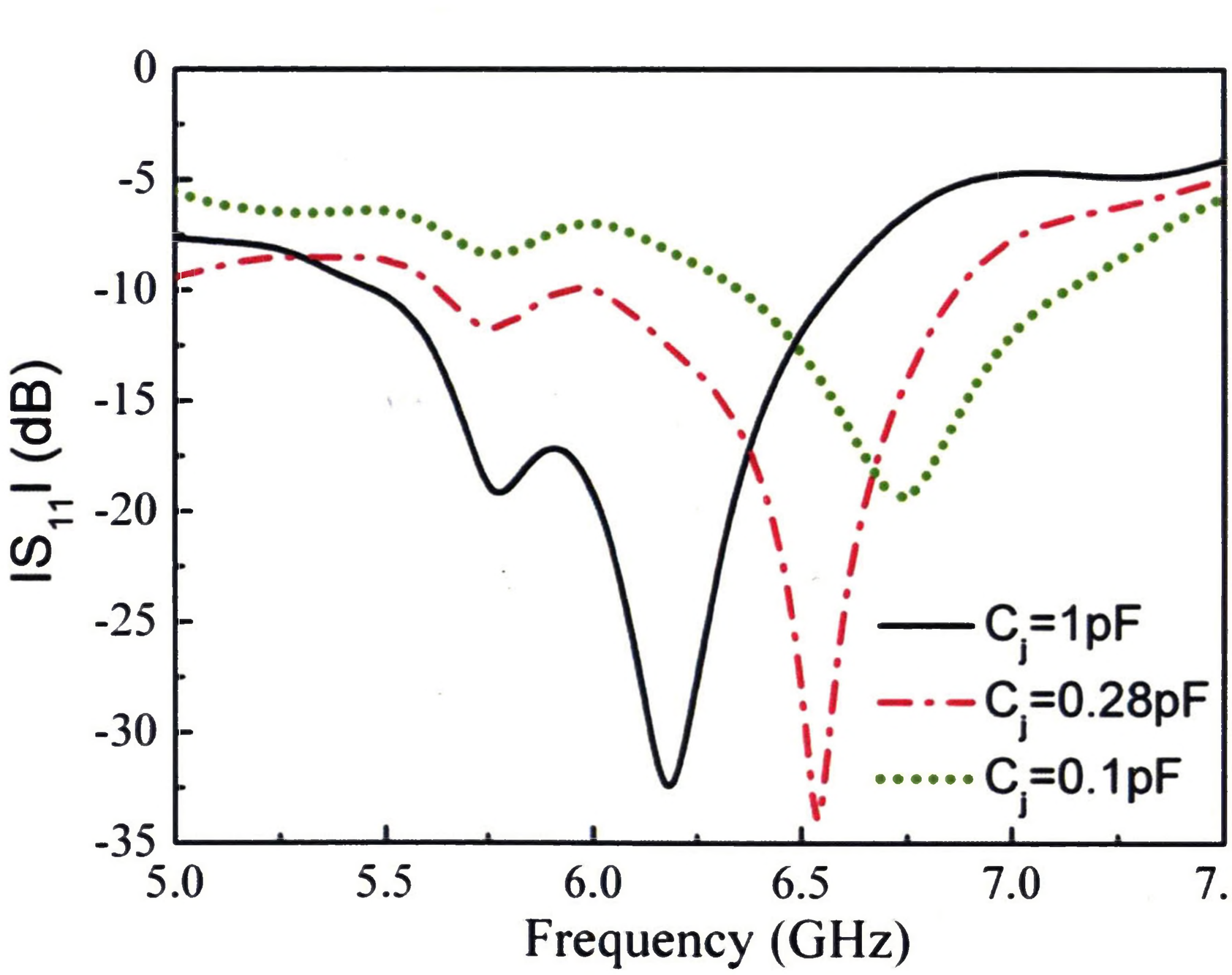

Figure 3.14: Simulated input reflection coefficients for different varactor diode junction capacitances.

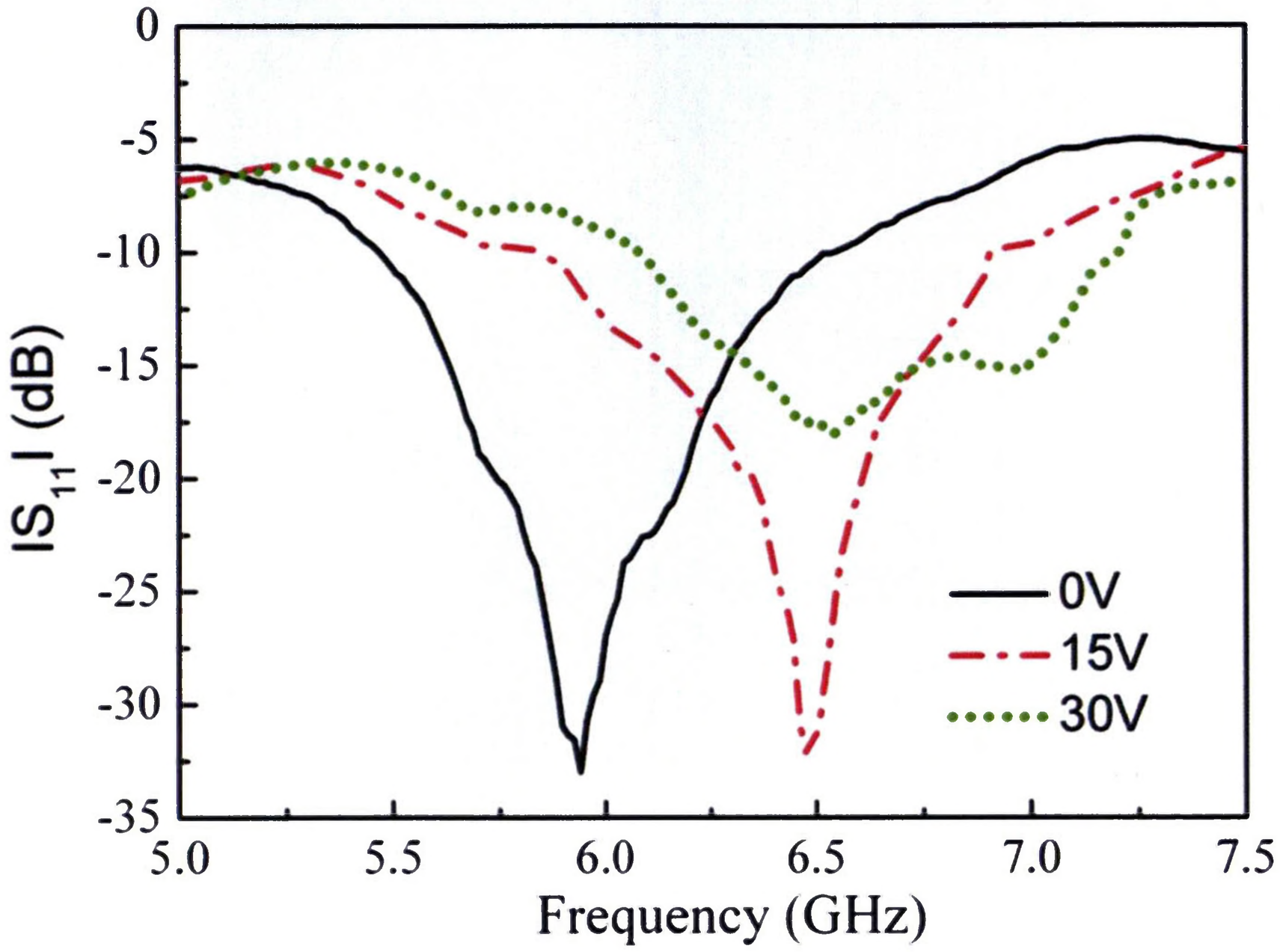

Figure 3.15: Measured input reflection coefficients for different values of varactor diode bias voltage.

Table 3.2: Summary of simulated and measured performance of the antenna

Bias Voltage (V)	C_j(pF)	Centre Frequency (GHz)		Impedance Bandwidth %		Gain (dBi)	
		Meas.	Sim.	Meas.	Sim.	Meas.	Sim.
0	1	6	6	16.7	17.4	4.48	4.8
15	0.28	6.35	6.4	15.7	13.2	5.2	5.4
30	0.1	6.6	6.75	15.0	11.9	5.36	6.45

Radiation patterns were measured using a spherical near-field (SNF) system. Simulated and measured normalized radiation patterns are compared for both the E (z-x) plane and the H(z-y) plane. The orientation of the rectangular coordinate system used in all radiation pattern figures is the same as the one shown in Fig. 3.4. Fig. 3.16 shows the E-plane radiation patterns at 6 GHz, 6.35 GHz and 6.6 GHz for bias voltages of 0 V, 15 V and 30 V, respectively. Fig. 3.17 displays the H-plane radiation patterns at 6 GHz, 6.35 GHz and 6.6 GHz, respectively. Well-defined end-fire radiation patterns can be observed with a maximum cross-polarization level of -15 dB and -10 dB for the E plane and the H plane, respectively. It can be seen that the antenna has similar radiation patterns over the entire tunable frequency range. Further simulations reveal that the radiation patterns do not vary very much with the tuning frequencies and have a front-to-back ratio greater than 15 dB. Unfortunately, due to the blockage caused by the antenna positioner in the SNF chamber, the front-to-back ratio cannot be measured accurately.

The realized gain has also been found by the gain comparison technique [1]. Both the simulated and measured gains of the antenna have been plotted by combining the gain data across the entire tunable frequency range, as shown in Fig. 3.18. From this plot, it is seen that the measured gain varies from 4.2 to 6.35 dBi, while the simulated gain varies from 4.2 to 7.4 dBi, for the entire frequency range. The measured gain is less than the simulated one across the tuning range. This can be mostly attributed to the inaccuracies in the fabrication and measurement process and variations in discrete component parameters from the values given in the manufacturer's datasheet. The loss of the varactor diode is represented by a series resistance of 1.6 Ω. Simulation results show that the gain of the antenna increases by 0.04 dB when the resistance is reduced to zero. Therefore, the effect of the losses of the varactor diodes on the gain of the antenna is very small.

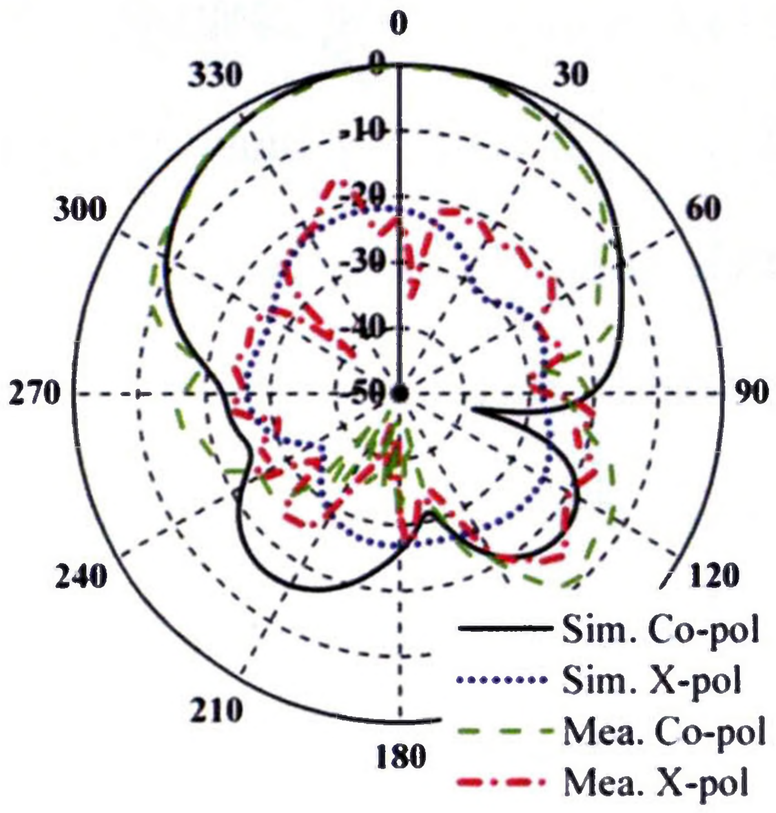

(a)

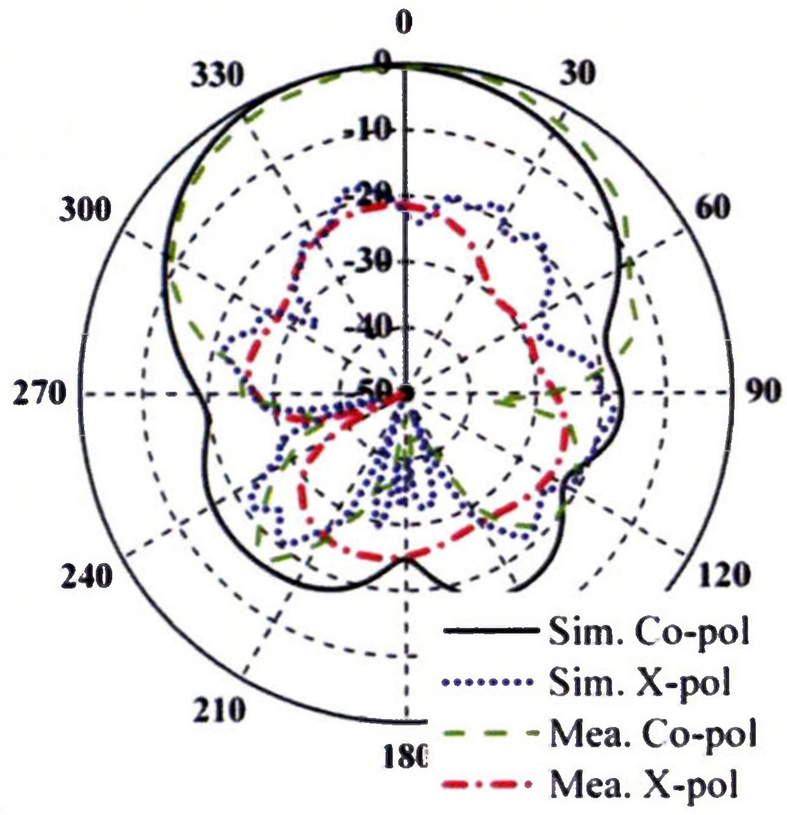

(b)

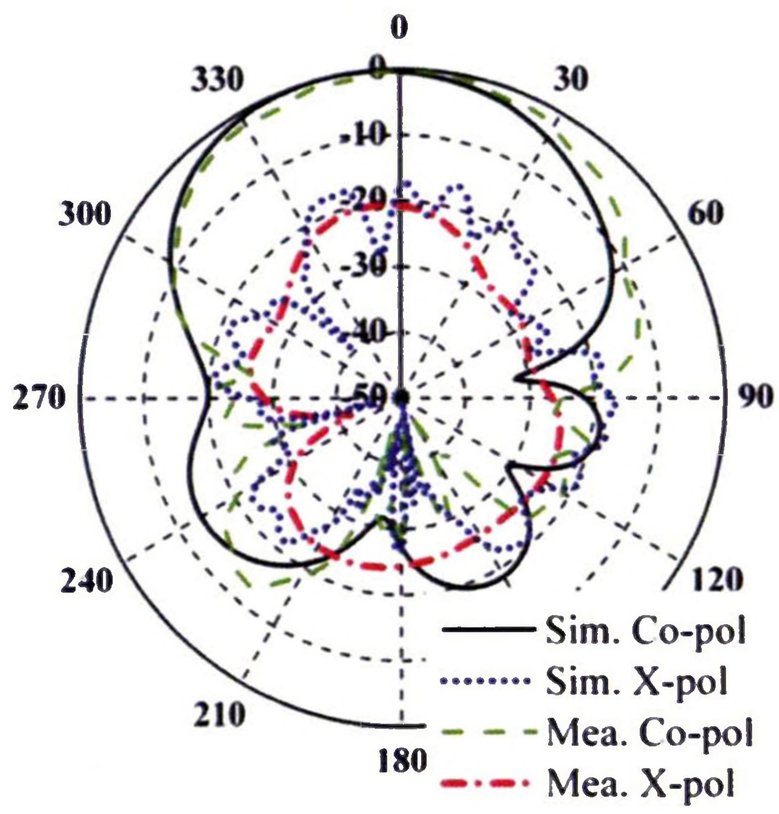

(c)

Figure 3.16: Measured and simulated E-plane (z-x plane) normalized radiation patterns: (a) 6 GHz, bias voltage is 0 V, and theoretical varactor diode junction capacitance is 1 pF; (b) 6.35 GHz, bias voltage is 15 V, and theoretical varactor diode junction capacitance is 0.28 pF; (c) 6.6 GHz, bias voltage is 30 V, and theoretical varactor diode junction capacitance is 0.1 pF.

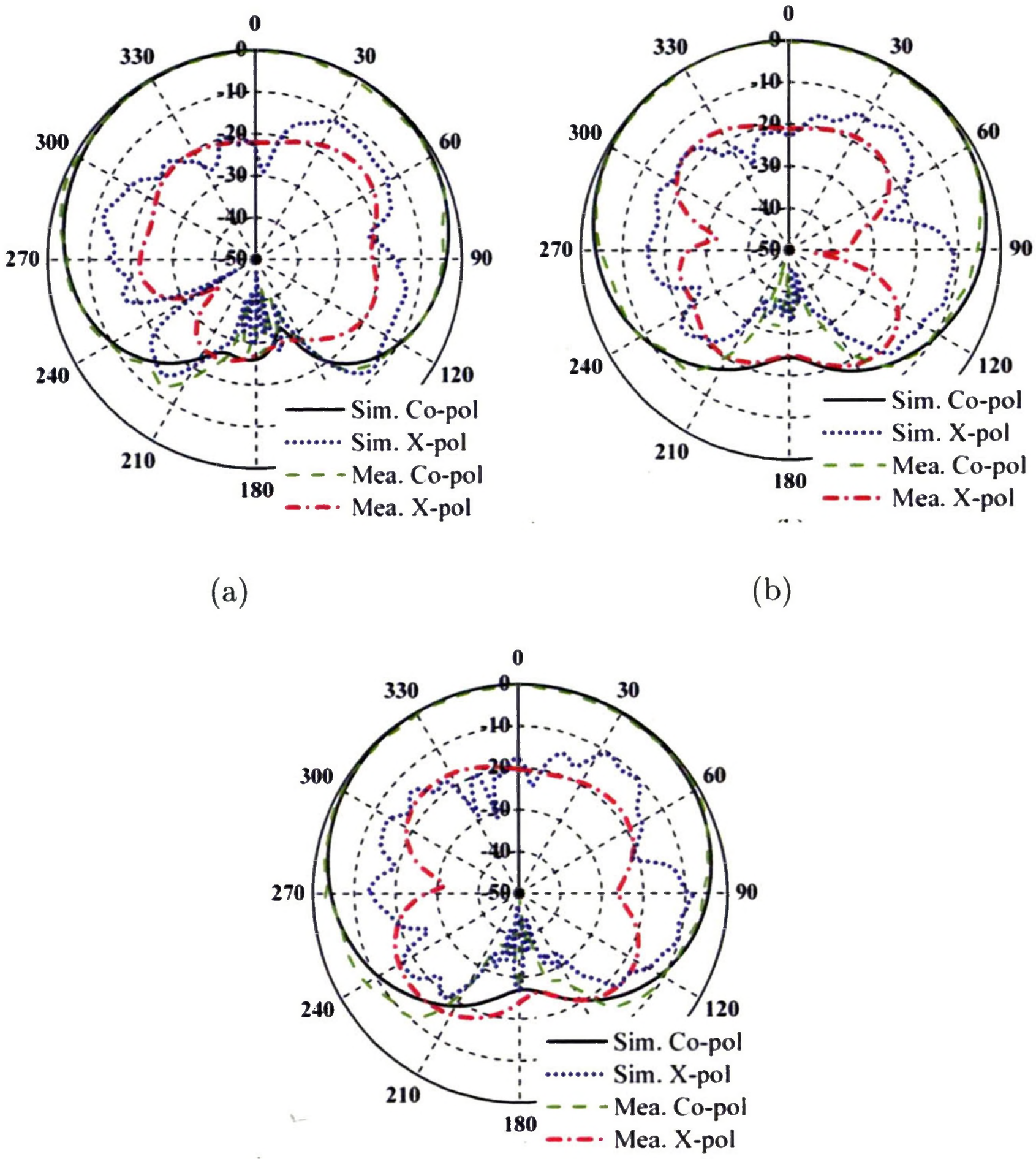

Figure 3.17: Measured and simulated H-plane (z-y plane) normalized radiation patterns: (a) 6 GHz, bias voltage is 0 V, and theoretical varactor diode junction capacitance is 1 pF; (b) 6.35 GHz, bias voltage is 15 V, and theoretical varactor diode junction capacitance is 0.28 pF; (c) 6.6 GHz, bias voltage is 30 V, and theoretical varactor diode junction capacitance is 0.1 pF.

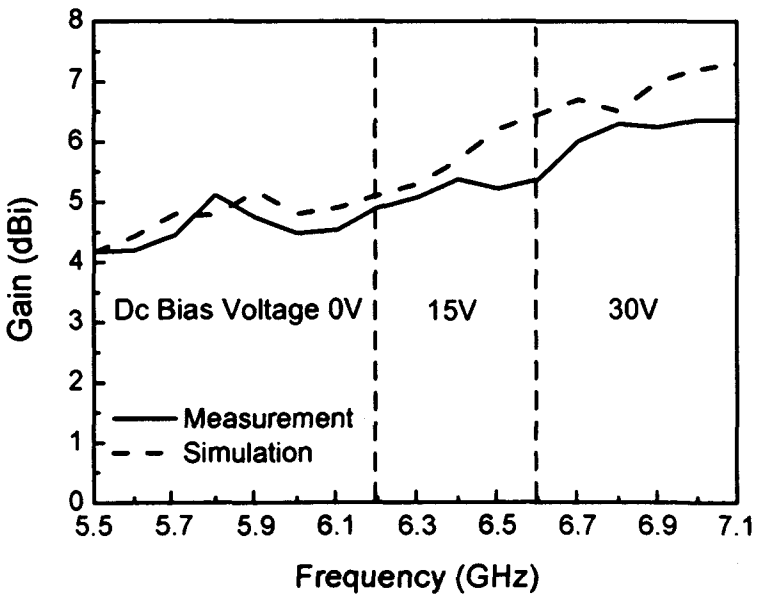

Figure 3.18: Measured and simulated gains of the antenna.

3.4 A Frequency Discrete Tuning Quasi-Yagi Folded Dipole Antenna

3.4.1 Antenna Structure and Operating Principle

The basic structure of the frequency discrete tuning quasi-Yagi folded dipole antenna is similar to the frequency continuous tuning one, and is shown in Fig. 3.19 (a). The main difference is that PIN diodes are used to realize the frequency discrete switching. The folded dipole driver element is printed with six 0.5mm gaps. Six beam-lead PIN diodes (MA4AGBLP912) are mounted across the gaps using electrically conductive silver epoxy. The orientation of the diodes is shown in Fig. 3.19 (b). According to the PIN diode datasheet [138], the diode represents a resistor of 4 Ω (typical value) for the ON state and a parallel circuit with a capacitor of 0.025 pF and a resistor of 10 kΩ for the OFF state. The length of the folded dipole element can be changed by switching between the different states of the diodes. When diodes 1 and 2 are on, and all the other diodes are off, the length of the folded dipole is L_7. In this case, the folded dipole is short and the proposed antenna resonates at a high operating frequency (denoted as State 1). Changing the polarity of the dc voltage turns diodes 1 and 2 off and all the other diodes on. In this case, the length of the folded dipole is increased to $L_7 + 2W_{10} + 2L_{10}$ and the antenna resonates at a lower frequency (denoted as State 2). The bias network for this antenna is exactly the same as the one used in the frequency continuous tuning folded dipole antenna. The parameters and dimensions of the antenna are shown in Table 3.3.

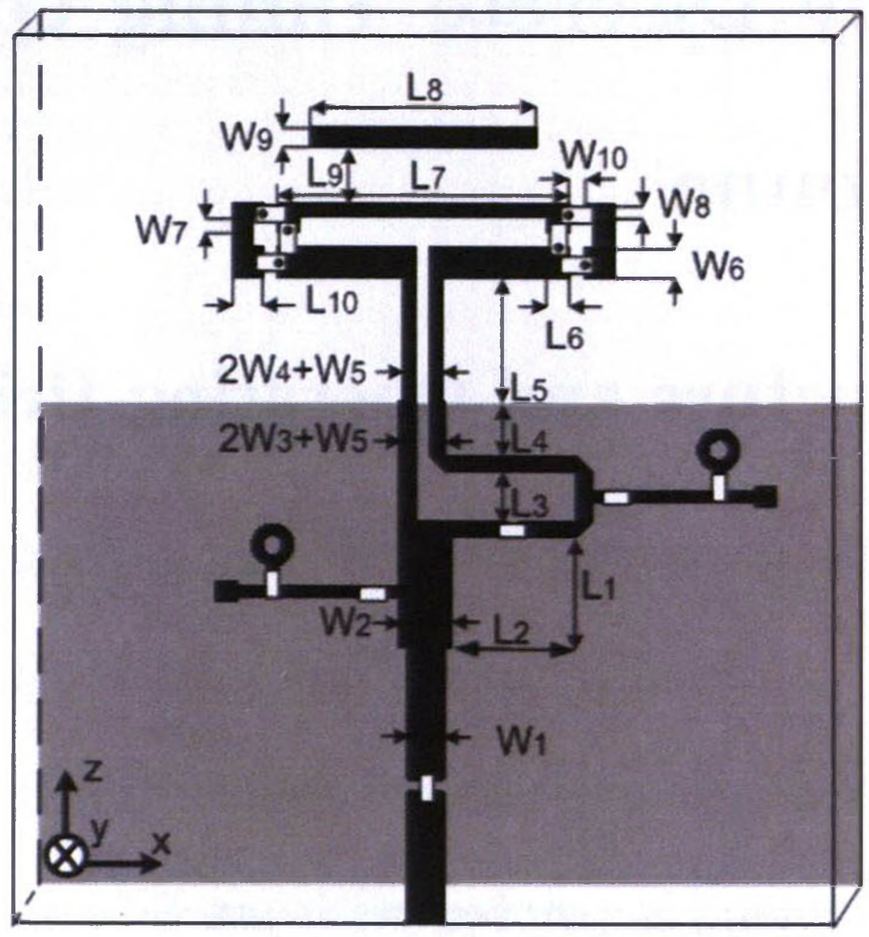

(a)

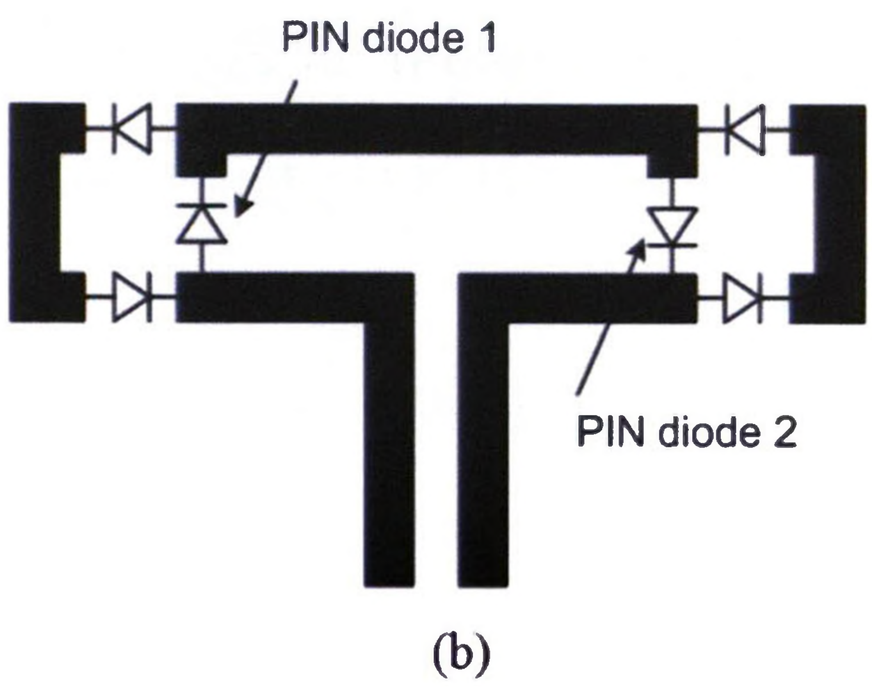

(b)

Figure 3.19: (a) Configuration of the antenna; (b) Orientation of the PIN diodes.

Table 3.3: Dimensions of the antenna

Parameter	W_1	W_2	W_3	W_4	W_5	W_6	W_7	W_8	W_9	W_{10}
Value (mm)	1.8	2.6	0.8	0.6	0.8	1.47	0.7	0.6	1.0	0.5
Parameter	L_1	L_2	L_3	L_4	L_5	L_6	L_7	L_8	L_9	L_{10}
Value (mm)	5.4	6.0	2.4	2.6	6.0	1.05	14.3	11.2	2.7	1.5

3.4.2 Simulated and Measured Results

The antenna was fabricated on a single Rogers substrate 4003 (0.813 mm thick and dielectric constant ε_r= 3.55). The dimensions of the substrate are 40 mm × 50 mm. A photograph of the fabricated prototype is shown in Fig. 3.20.

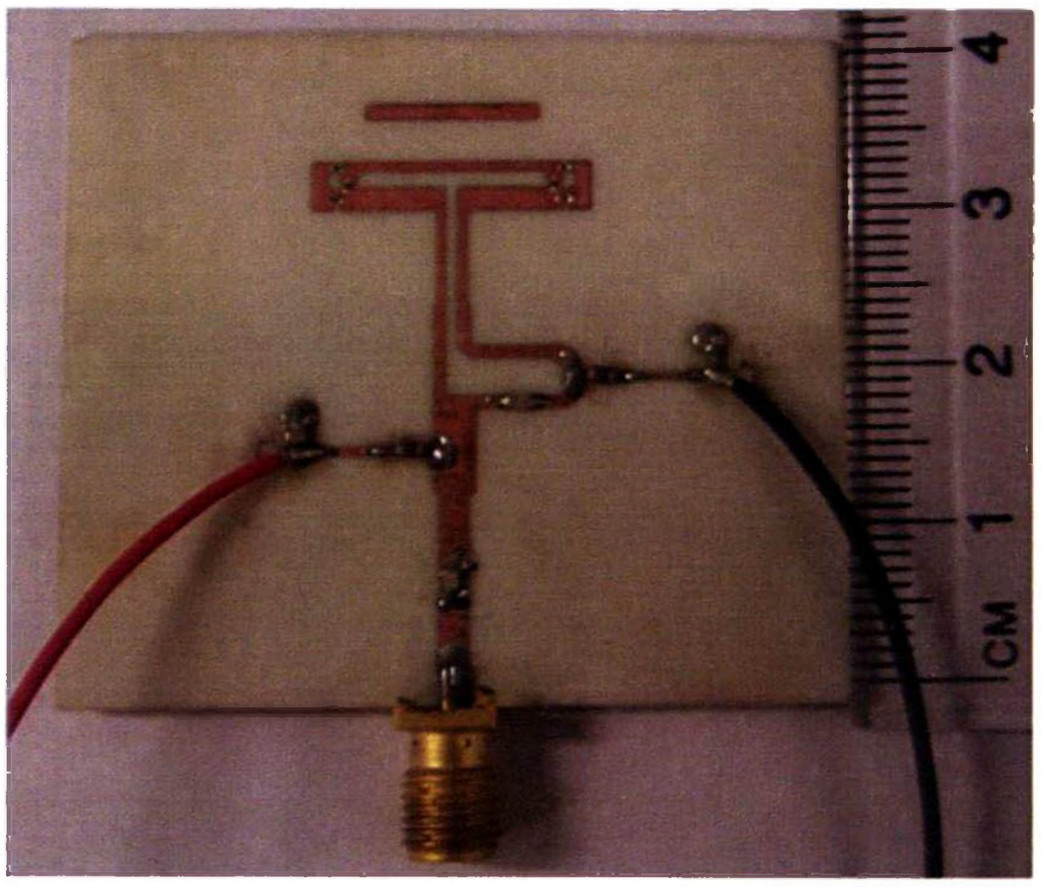

Figure 3.20: Photograph of the antenna.

Fig. 3.21 displays the simulated and measured reflection coefficients as a function of frequency for State 1 and State 2. From State 2 to State 1, the resonant frequency shifts from 5.95 to 7.2 GHz, corresponding to a frequency tuning ratio of 1.21. The impedance bandwidth ($|S_{11}| \leqslant$ -10 dB) is 22.2% and 21.8% for State 1 and State 2, respectively. The frequency tuning range can be further enlarged by increasing the value of L_{10}.

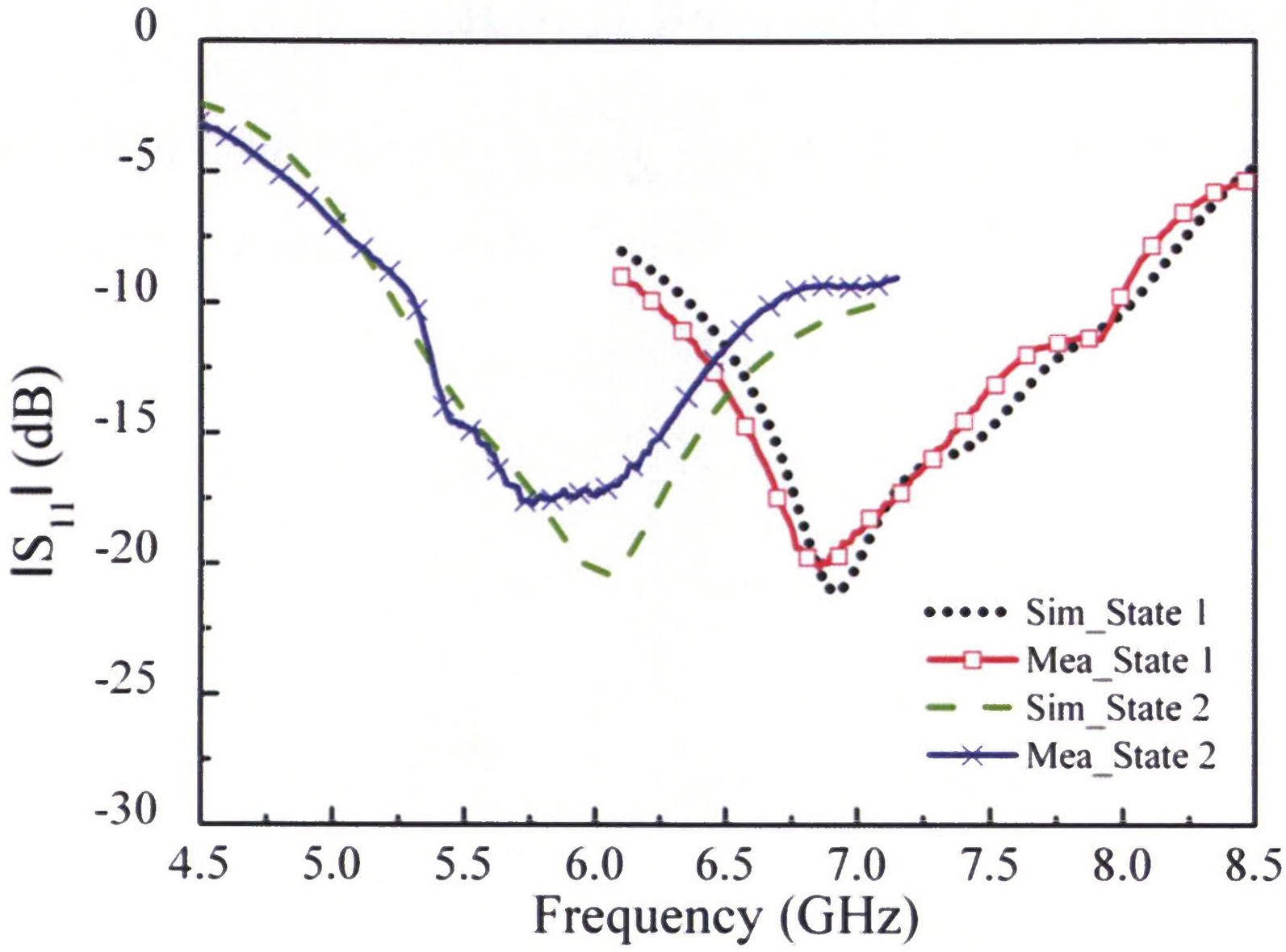

Figure 3.21: Simulated and measured input reflection coefficients for different states of the antenna.

Radiation patterns were measured using a spherical near-field (SNF) system. Simulated and measured normalized radiation patterns are compared for both the E (z-x) plane and the H (z-y) plane planes. The orientation of the rectangular coordinate system used in all radiation pattern figures is the same as the one shown in Fig. 3.19. Fig. 3.22 and Fig. 3.23 show the normalized radiation patterns at 7.2 GHz for State 1 and 5.95 GHz for State 2, respectively. Well-defined end-fire radiation patterns are observed with a maximum cross-polarization level of -15 dB and -10 dB for the E plane and the H plane, respectively. It can be noted that the cross-polarization levels in the beam-maximum direction are typically lower. It also can be seen that the antenna has similar radiation patterns over the entire tunable frequency range. Further simulations reveal that the radiation patterns do not vary very much with the tuning frequencies and have a front-to-back ratio greater than 15 dB. Unfortunately, due to the blockage caused by the antenna positioner in the SNF chamber, the front-to-back ratio cannot be measured accurately.

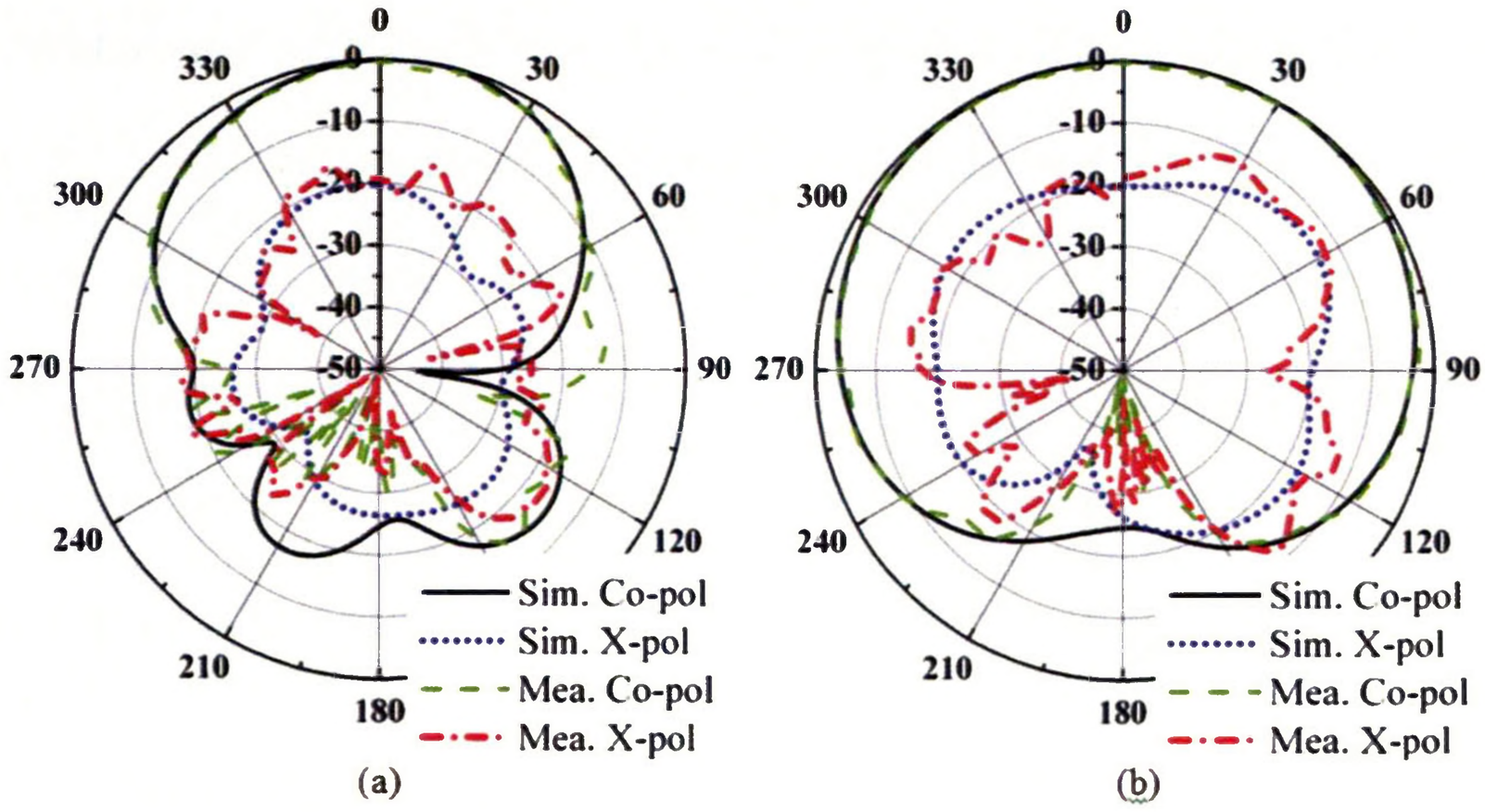

Figure 3.22: Measured and simulated normalized radiation patterns at 7.2 GHz for State 1 of the antenna: (a) E-plane (z-x plane); (b) H-plane (z-y plane).

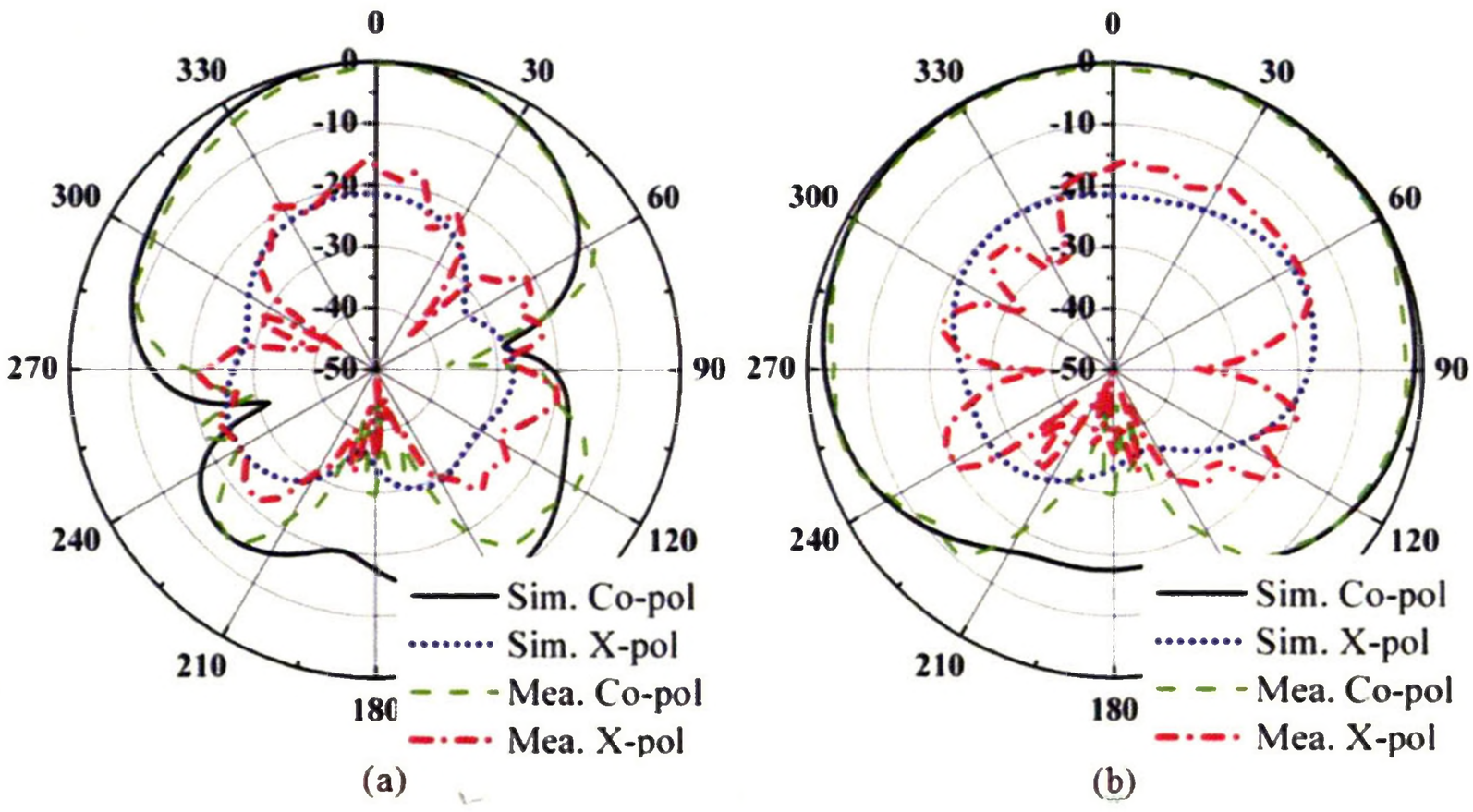

Figure 3.23: Measured and simulated normalized radiation patterns at 5.95 GHz for State 2 of the antenna: (a) E-plane (z-x plane); (b) H-plane (z-y plane).

The realized gain has also been found by the gain comparison technique [1]. The gains in two bands are plotted in Fig. 3.24. The losses included in the simulation are from the forward resistances of the PIN diodes. The measured gains vary from 4.4 to 5.3 dBi for State 1 and 3.5 to 4.5 dBi for State 2. The gain of State 1 is higher than that of State 2, which is due to the fact that fewer diodes are used for State 1, therefore there is less series resistance for State 1. In addition, from Fig. 3.24 it is clear that at some frequency

points the measured gains of the antenna are greater than the simulated results. This is because of the uncertainties in the exact forward resistance of the PIN diode (<4.9 Ω specified by the manufacturer). From the PIN diode data sheet [138], it is known that the forward resistance of the PIN diode is about 4 Ω at 10 GHz. Since the proposed antenna is operating around 6 GHz, there may be variations from the values given in the data sheet. In general, reasonable agreement between the simulated and measured results are noted.

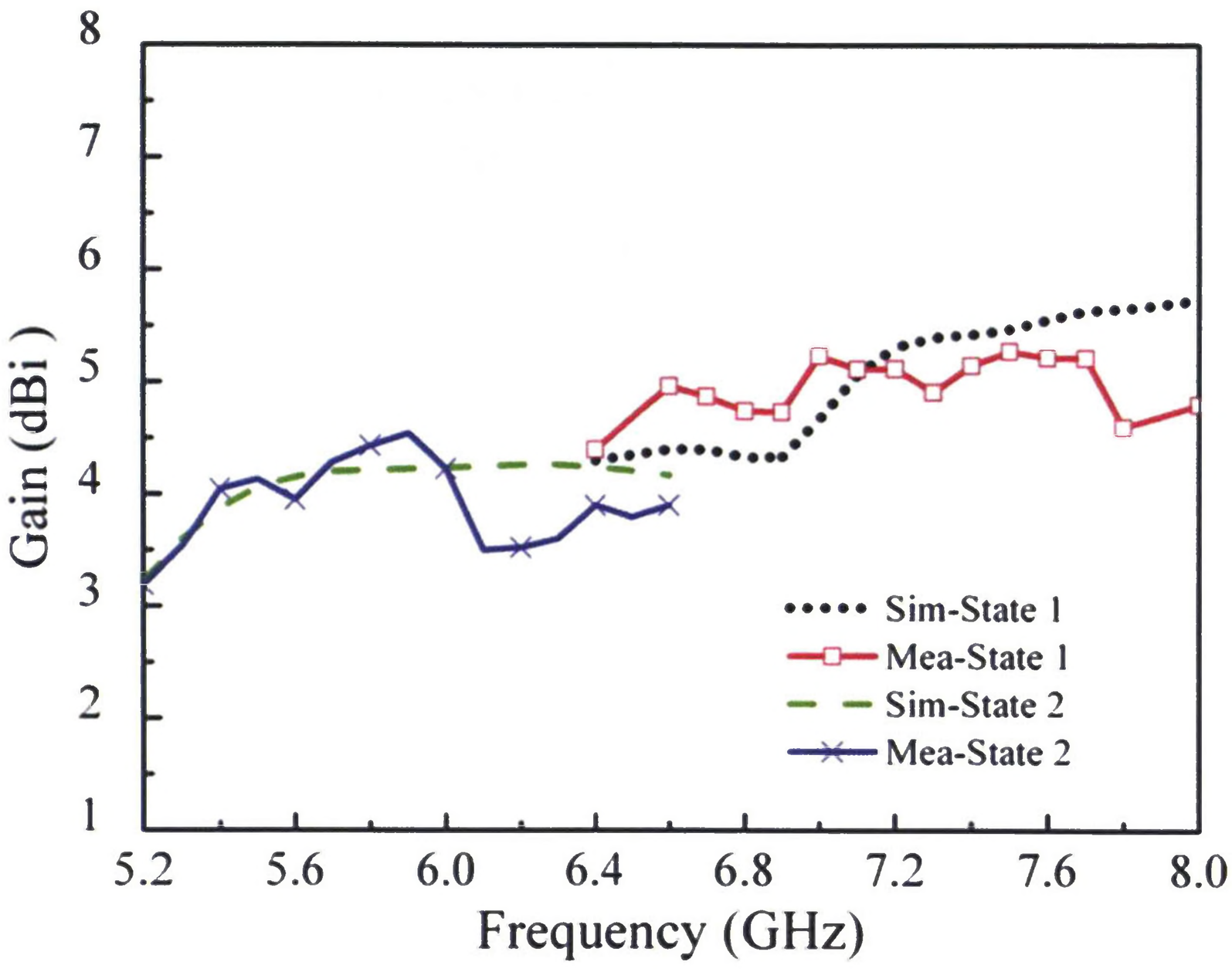

Figure 3.24: Measured and simulated gains of the antenna.

The design and testing of the proposed antenna is useful for another purpose. Due to the fact that the dimensions of the PIN diode (0.6 mm × 0.15 mm) are quite small, the design can be scaled by a factor of ten to provide an antenna design that can tune between a typical millimetre-wave WPAN band (57-66 GHz) and E-band (71-76 GHz).

3.5 A Millimetre-Wave Frequency Discrete Tuning Quasi-Yagi Dipole Antenna

3.5.1 Antenna Structure and Operating Principle

In Section 3.4, a frequency discrete tuning quasi-Yagi folded dipole using 6 PIN diodes is described. The antenna's realized gain is affected by the PIN diodes employed in the antenna. In this section, a new antenna structure that uses only two PIN diodes is proposed for millimetre-wave band applications. By switching between the different states of the PIN diodes, the antenna can operate in either the typical millimetre-wave WPAN band (57-66 GHz) or E-band (71-76 GHz). The basic structure of the antenna is shown in Fig. 3.25, and is similar to those presented in the previous two sections. The top side of the substrate consists of a microstrip feed, a broad-band microstrip-to-CPS balun, a folded dipole driven element with two 0.5mm gaps fed by the CPS, and a dipole parasitic director element. The bottom side is a truncated microstrip ground, which serves as the reflector element for the antenna. The combination of the parasitic director element and the reflector directs the radiation of the antenna toward the end-fire direction. The dimensions of the antenna are shown in Table 3.4.

Table 3.4: Dimensions of the antenna

Parameter	W_1	W_2	W_3	W_4	W_5	W_6	W_7	W_8
Value (mm)	0.23	0.33	0.12	0.09	0.12	0.19	0.08	0.13
Parameter	L_1	L_2	L_3	L_4	L_5	L_6	L_7	L_8
Value (mm)	0.76	0.86	0.47	0.43	0.83	1.92	1.19	0.81

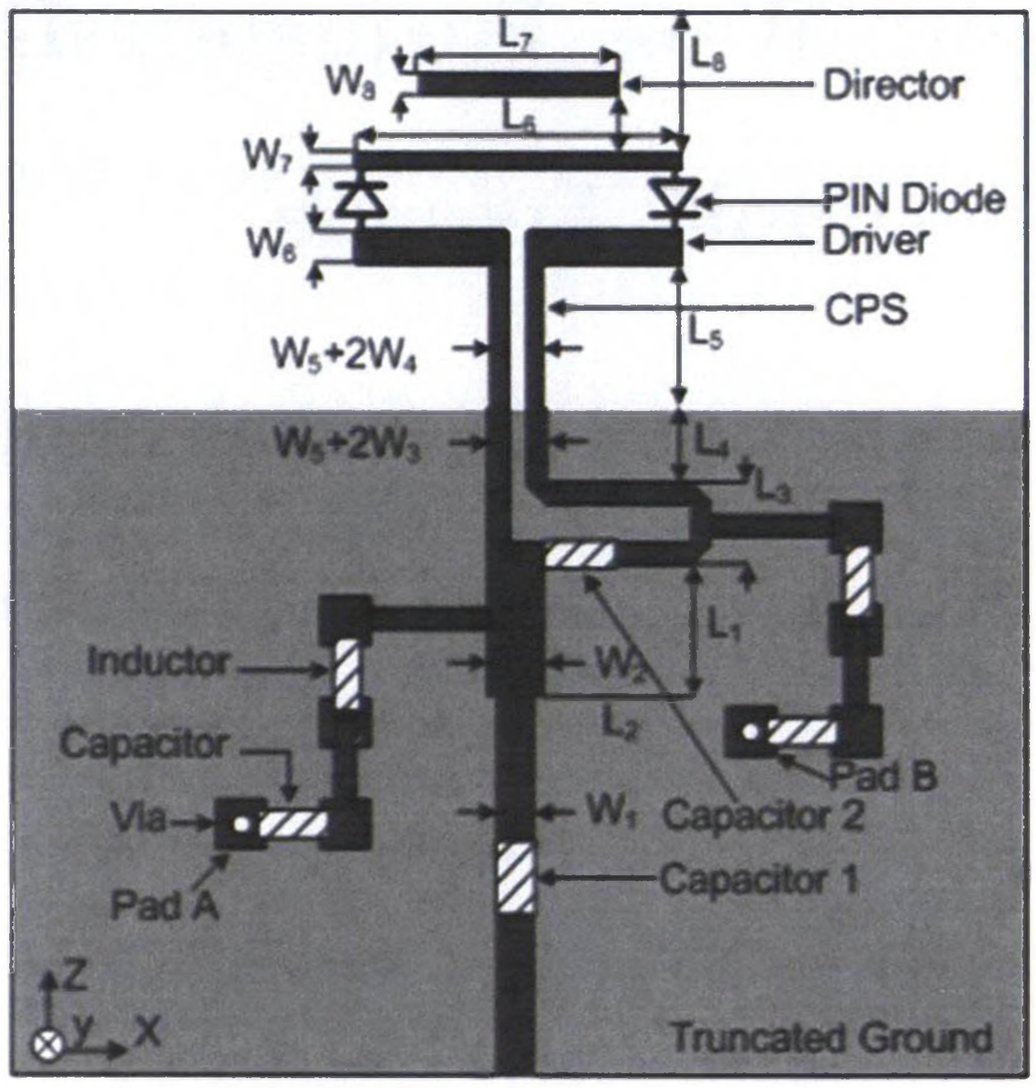

Figure 3.25: Configuration of the antenna.

Two PIN diodes are mounted across the gaps between the upper and lower strips of the folded dipole. The orientation of the diodes is shown in Fig. 3.25. However, since a PIN diode that can work up to 70 GHz was not available at the time of the experiment, in the process of software simulation a thin wire was used for the diode in the forward-bias state and the wire was removed for the diode in the reverse-bias state. It should be noted that, since a bias network is included in the antenna design, practical PIN diodes that can work in the millimetre-wave band can be incorporated in the antenna and be electronically controlled.

The bias network for this antenna is similar to those operating in the microwave band presented in Sections 3.3 and 3.4. Capacitor 1 is used to prevent the dc bias voltage from flowing into the RF source at the antenna terminal. Capacitor 2 ensures dc isolation between Pad A and Pad B while maintaining the RF continuity of the balun. The dc bias voltage is isolated from the RF signal of the antenna by using two dc bias networks, each consisting of a two-element low-pass filter. Each filter is composed of a chip inductor, a

chip capacitor and a via.

When the diodes are forward biased, the driven element is a folded dipole with a parasitic director which makes the antenna operate at 52-68 GHz (State 1). When the diodes are reverse biased, the driven element is a single dipole with two parasitic directors, which allows the antenna to operate at 70-76 GHz (State 2). The operating states of the proposed antenna and the corresponding diode states are summarized in Table 3.5.

Table 3.5: Operating states of the antenna

	PIN Diodes	Operating Frequency
State 1	Forward Biased	57-66 GHz
State 2	Reverse Biased	71-76 GHz

The mechanism of the frequency tuning is attributed to the different impedance characteristics of the driven parts of the antenna in the different states. The input impedance of the driven element with truncated ground plane was analyzed using CST Microwave Studio. Fig. 3.26 (a) and (b) show the input impedance of the driven element for the two states of the proposed antenna. The model used to calculate the input impedance of the driven element is excited by a discrete port but does not include the CPS, the balun and 50Ω microstrip line, as shown in the inset of Fig. 3.26 (b). As is seen from Fig. 3.26 (b), there is a resonance point around 75 GHz. The broad-band microstrip-to-CPS balun and the impedance transformer decrease the high resistance of State 2 around the resonance point to about 50Ω. From Fig. 3.26 (a), it is seen that the imaginary part of the input impedance of State 1 does not cross zero from 50 to 65 GHz. As the same balun and impedance transformer is used for States 1 and 2, the input impedance match for State 1 is worse than that of State 2.

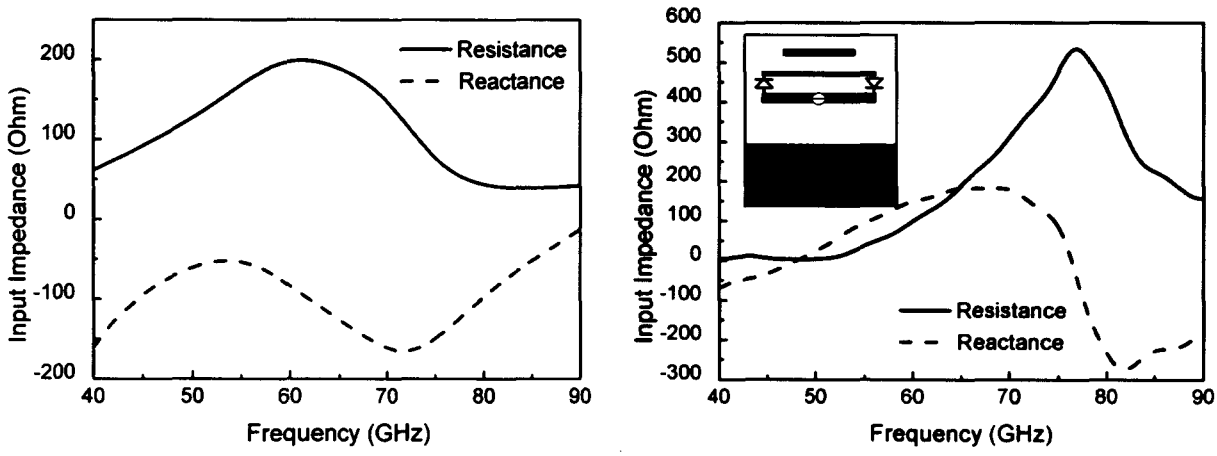

(a) (b)

Figure 3.26: Simulated input impedance of the driven element of the antenna: (a) State 1; (b) State 2.

3.5.2 Simulated and Measured Results

The antenna was fabricated on a liquid-crystal polymer (LCP) substrate (0.1mm thick and dielectric constant ε_r =3.2) with dimensions 7.5 mm × 7.5 mm. LCP has been shown to have a reasonably low loss at millimetre-wave frequencies. A standard waveguide WR-15 (3.76 mm × 1.88 mm) is used to feed the antenna through a waveguide-to-microstrip line transformer. A photograph of the antenna prototype with the waveguide is shown in Fig. 3.27. The waveguide-to-microstrip line transformer is inserted into a metal block that is used to carry the antenna.

For the antenna input reflection coefficient measurements, a thin wire was used for the diode in the forward-bias state and the wire was removed for the diode in the reverse-bias state. Fig. 3.28 displays the simulated reflection coefficients as a function of frequency for State 1 and State 2. For State 1, the impedance bandwidth ($|S_{11}| \leqslant$-10 dB) is 26.6% with a centre frequency of 60 GHz, which can cover the 57-66 GHz band. For State 2, the impedance bandwidth is 8.2% with a centre frequency of 73 GHz, which can cover the 71-

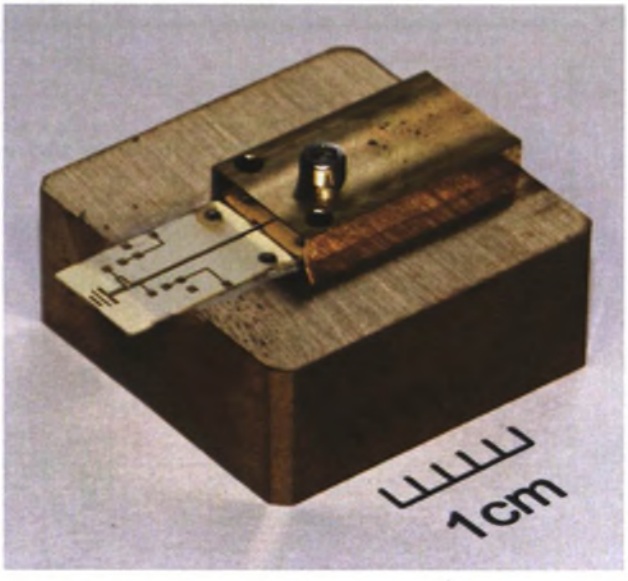

Figure 3.27: Photograph of the antenna.

76 GHz band. The measured results for the two states are shown in Fig. 3.29. For State 1, the impedance bandwidth ($|S_{11}| \leqslant$ -10 dB) is 57-66 GHz. But, at some frequency points, the input reflection coefficients go up to about -9 dB. This can be attributed to the losses of the waveguide-to-microstrip line transformer and the inaccuracies of the assembly process. However, the -9dB reflection coefficient can still be accepted by most applications in the millimetre-wave band. For State 2, the impedance bandwidth is 71-77 GHz. Therefore, the operating frequency of the antenna can be switched between the millimetre-wave WPAN band and the E band.

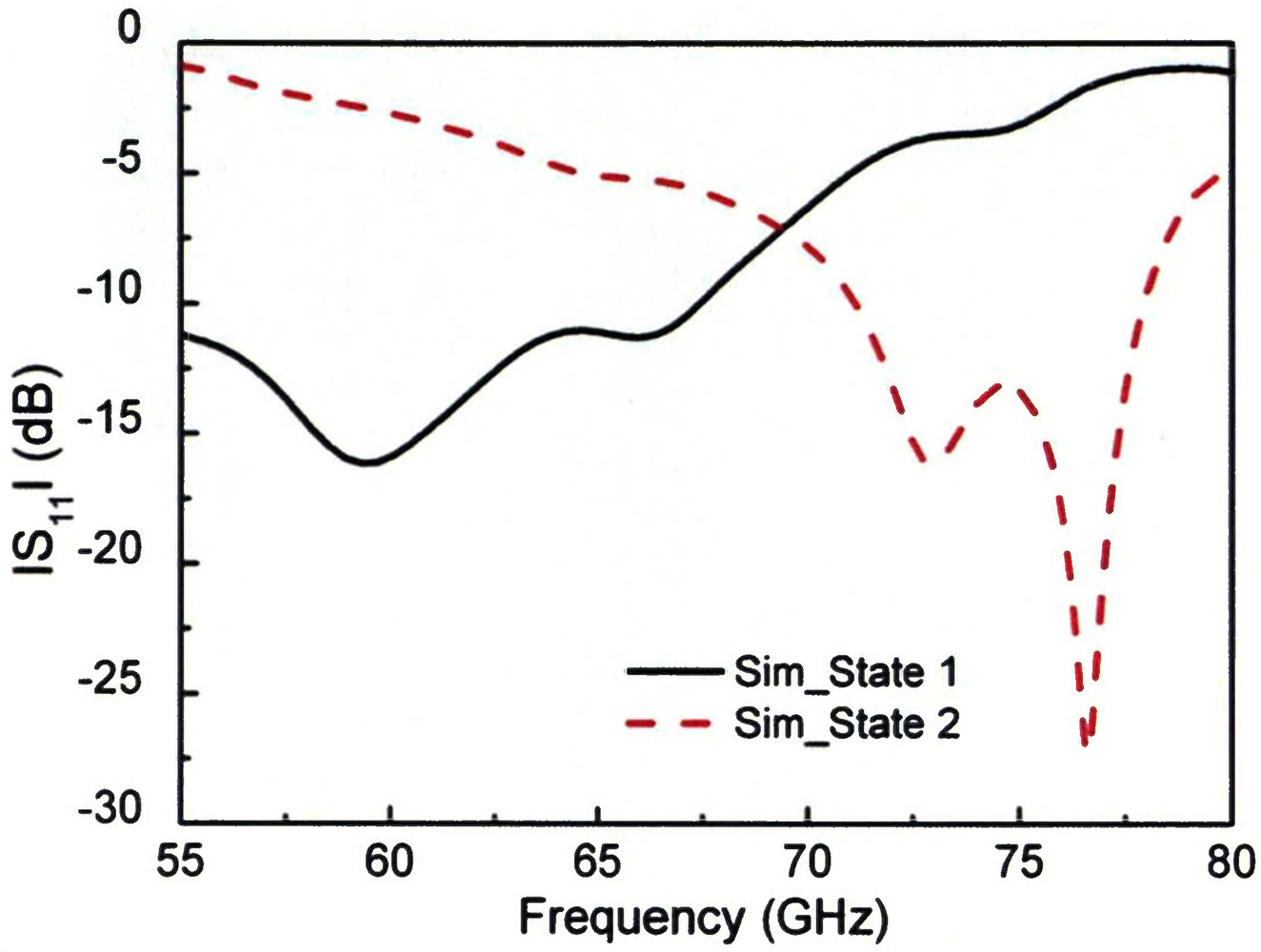

Figure 3.28: Simulated input reflection coefficients for the different states of the antenna.

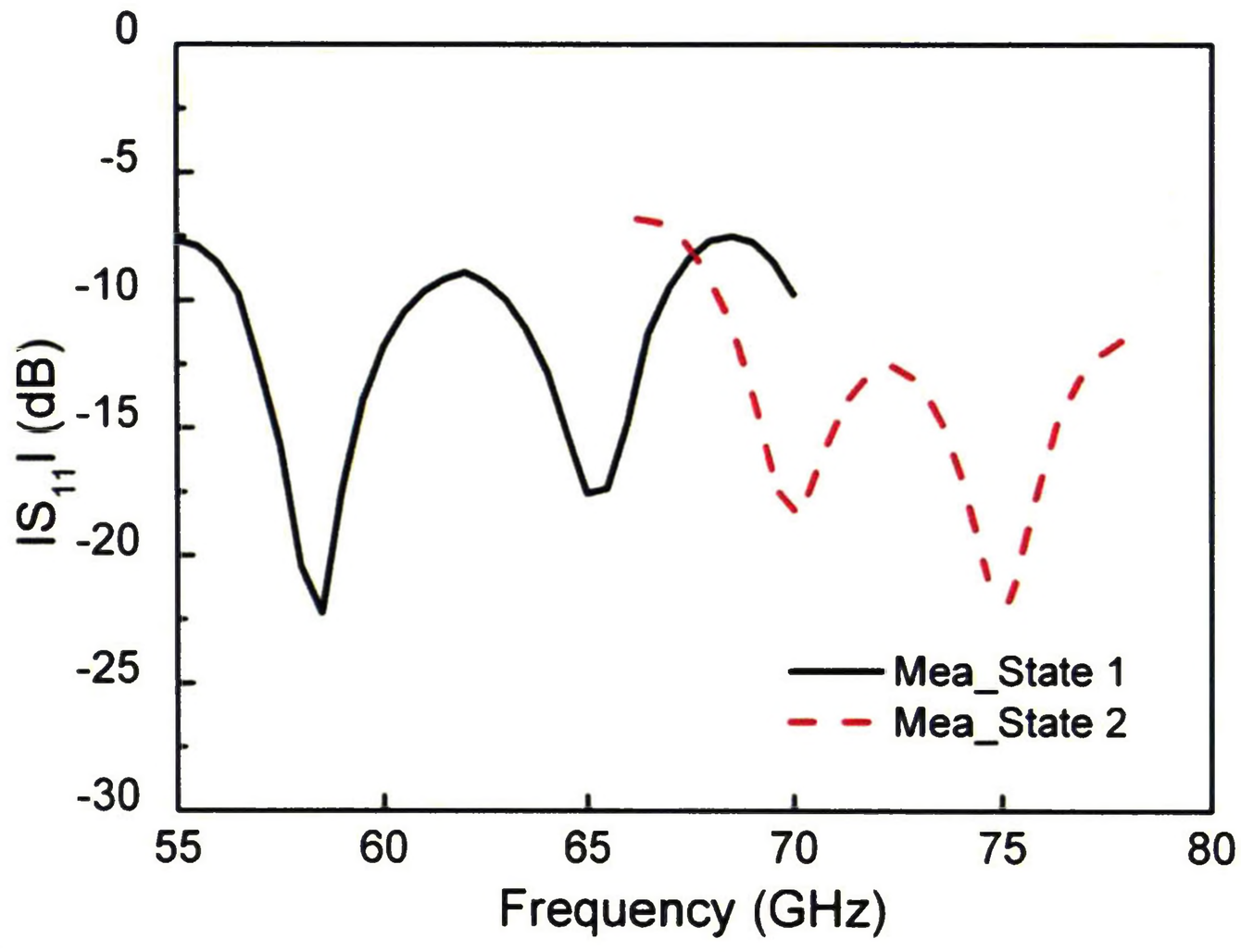

Figure 3.29: Measured input reflection coefficients for the different states of the antenna.

Figs 3.30 and 3.31 show the simulated normalized radiation patterns at 60 GHz for State 1 and 73 GHz for State 2, respectively. The orientation of the rectangular coordinate system used in all the radiation pattern figures is the same as the one shown in Fig. 3.25. For the E-plane (x-z plane) radiation pattern, well-defined end-fire radiation patterns can

be observed and the pattern is symmetrical with respect to the z axis. For the H-plane (y-z plane) radiation pattern, due to the metal block that is used to carry the antenna, the radiation patterns become asymmetrical with respect to the z axis. The simulated gains are 6.4 dBi and 7.4 dBi for 60 GHz and 73 GHz, respectively. The antenna far-field radiation patterns will be measured and reported in our future work.

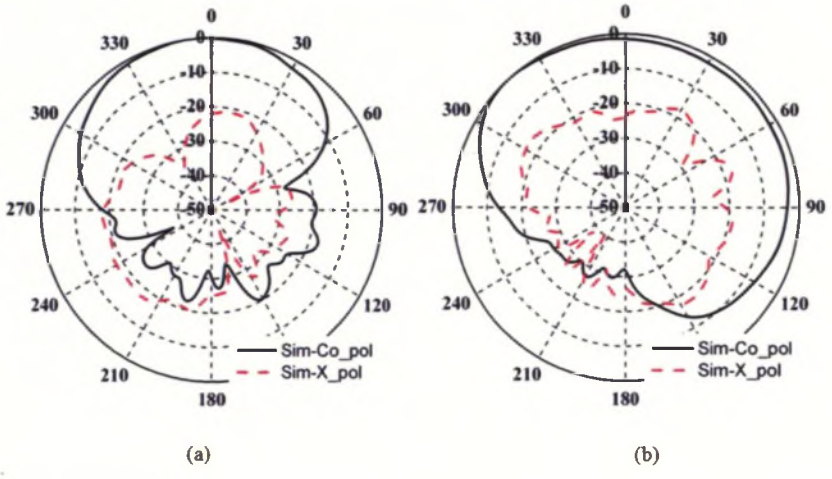

Figure 3.30: Simulated normalized radiation patterns at 60 GHz for State 1 of the antenna: (a) E-plane (z-x plane); (b) H-plane (z-y plane).

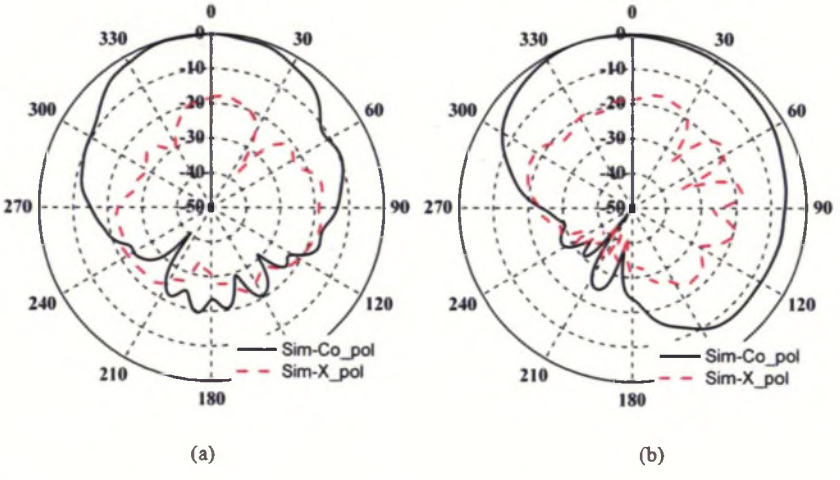

Figure 3.31: Simulated normalized radiation patterns at 73 GHz for State 2 of the antenna: (a) E-plane (z-x plane); (b) H-plane (z-y plane).

Chapter 4

A Polarization Reconfigurable Antenna

4.1 Introduction

Polarization reconfigurable antennas, also known as polarization-agile antennas, have attracted considerable attention due to their ability to improve the performance of wireless communication systems [48-61]. Such reconfigurable antennas can provide polarization diversity to mitigate signal fading in multipath propagation environments and realize double transmission channels for frequency-reuse transceivers. Moreover, polarization diversity can be employed to increase the capacity of a multiple-input-multiple-output (MIMO) system by reducing the correlation of the sub-channels.

Polarization reconfigurable antennas can be classified into three categories: the switch between two orthogonal linear polarizations; the switch between right-hand circular polarization (RHCP) and left-hand circular polarization (LHCP); the switch between circular and linear polarizations. Most of the previous work for polarization reconfigurability concentrates on switching between RHCP and LHCP [48-56]. Relatively few antennas

have been presented that can switch between linear and circular polarizations because it is difficult to simultaneously realize a good impedance match for circular and linear polarizations [51]. The reason is that circularly polarized (CP) radiation is generated by two degenerate orthogonal linear modes, and its input impedance is significantly different from that of the one resonant mode used to generate linearly polarized (LP) radiation. However, it will make the antenna more versatile if switching between linear and circular polarizations can be achieved [57].

Several interesting designs have been proposed to solve this problem [57-60]. In [57], four PIN diodes were used on a corner-truncated square patch to produce LP and CP radiation with a small impedance bandwidth (2.5%). In [58], a perturbed square-ring slot antenna using four PIN diodes was designed that allows operation in both CP and LP modes. Unfortunately, the biasing and control circuits were not physically implemented. In [59], a ring-slot-coupled microstrip circular patch antenna, fabricated on two single FR4 substrates separated by a piece of foam, was proposed that can switch between LP and CP modes. However, the overlapped impedance bandwidth is 2.2% and it is difficult to integrate such an antenna in a compact wireless device due to its large volume. In [60], an aperture-coupled patch antenna was presented that can be operated either in dual-linear polarizations or dual-circular polarizations using two feed ports and eight PIN diodes.

In this chapter, a microstrip U-slot patch antenna is proposed to allow switching either between linear and circular polarizations or between two circular polarization senses. The antenna is compact and can cover the wireless local area network (WLAN) frequency band with good impedance bandwidth and 3dB axial ratio bandwidth. The overlapped impedance bandwidth ($|S_{11}| \leqslant$ -10 dB) for the CP and LP modes is 6.1% with a centre frequency of 5.9 GHz, and the 3dB axial ratio bandwidth is greater than 2.8% with a centre frequency of 5.77 GHz for the CP mode. The proposed antenna is based on the CP U-slot antenna [119] introduced in Chapter 2. Compared to [119], however, the antenna

described in this chapter uses a single-layer microwave substrate for ease of fabrication. In addition, two beam-lead PIN diodes are embedded into the U-slot at specific positions to enable the lengths of the slot arms to be varied. By turning the diodes on or off, the U-slot becomes either symmetrical or asymmetrical, which allows the patch antenna to switch between linear and circular polarization states electronically.

4.2 Antenna Structure and Operating Principle

The configuration of the proposed reconfigurable U-slot patch antenna is shown in Fig. 4.1. The length of the patch, denoted as $L4$, is 0.35 λ_g (14.2 mm), where λ_g is the guided wavelength. This value is obtained from the parametric analysis presented in the next section. λ_g is given by $\lambda_0/\sqrt{\varepsilon_{eff}}$, where λ_0 is the wavelength in free space, $\varepsilon_{eff} \approx (\varepsilon_r + 1)/2$ is the effective dielectric constant of the substrate, and ε_r=2.2 is the dielectric constant of the substrate. A U-slot is inserted into a rectangular patch which is printed on a microwave substrate. As the physical length of the PIN diode is smaller than the width of the slot, conducting pads are placed in the gaps of the U-slot for PIN-diode attachment. The feed probe connected to the U-slot patch through the ground plane and substrate is offset from the top edge of the patch by $L5$. The parameters and dimensions of the antenna are given in Table 4.1.

Table 4.1: Dimensions of the reconfigurable U-slot antenna

Parameter	$W1$	$W2$	$W3$	$W4$	$W5$
Value (mm)	0.5	0.65	5.3	13.8	30
Parameter	$L1$	$L2$	$L3$	$L4$	$L5$
Value (mm)	5.95	9.3	2.9	14.2	5.1

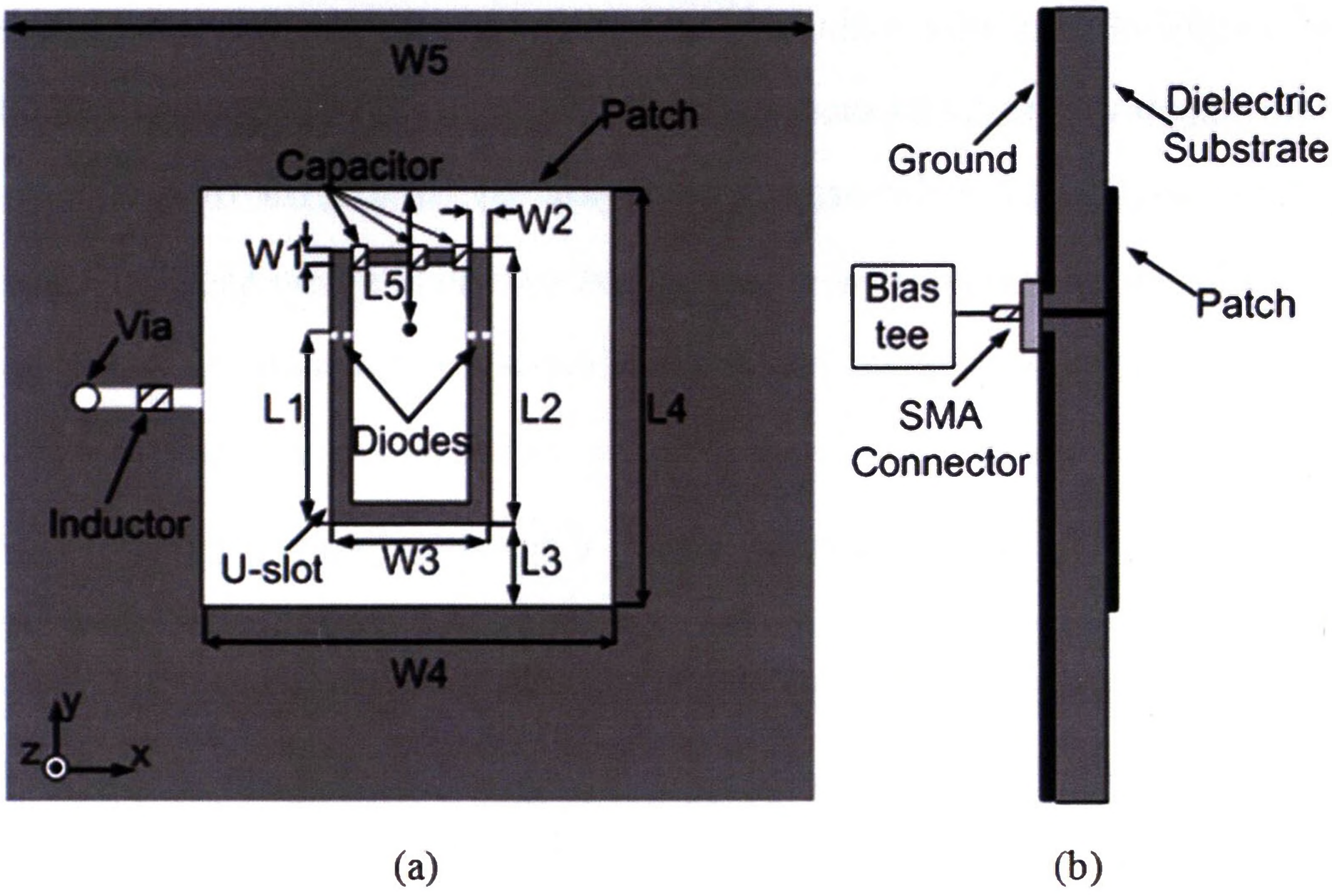

Figure 4.1: Schematics of the reconfigurable U-slot antenna: (a) Top view; (b) Side view.

In order to bias the PIN diodes, another thinner slot is cut on the top of the U-slot in the antenna prototype. It separates the patch into two parts to ensure dc isolation. Three 30pF capacitors are placed across this thinner slot to maintain RF continuity. The outer part of the patch is dc grounded by a shorting pin through an inductor used as an RF choke. Both the dc bias voltage and the RF signal are simultaneously fed through the coaxial probe by using a bias-tee. Fig. 4.2 (a) and (b) show the equivalent circuit and the photograph of the bias-tee, respectively. It is a three-port device that can superimpose the bias voltage on the RF signal.

Beam-lead PIN diodes (MA4AGBLP912) are used as switching elements in the U-slot. According to the PIN-diode datasheet [138], the diode represents a resistance of 4 Ω for the ON state and a parallel circuit with a capacitance of 0.025 pF and a resistance of 10 kΩ for the OFF state.

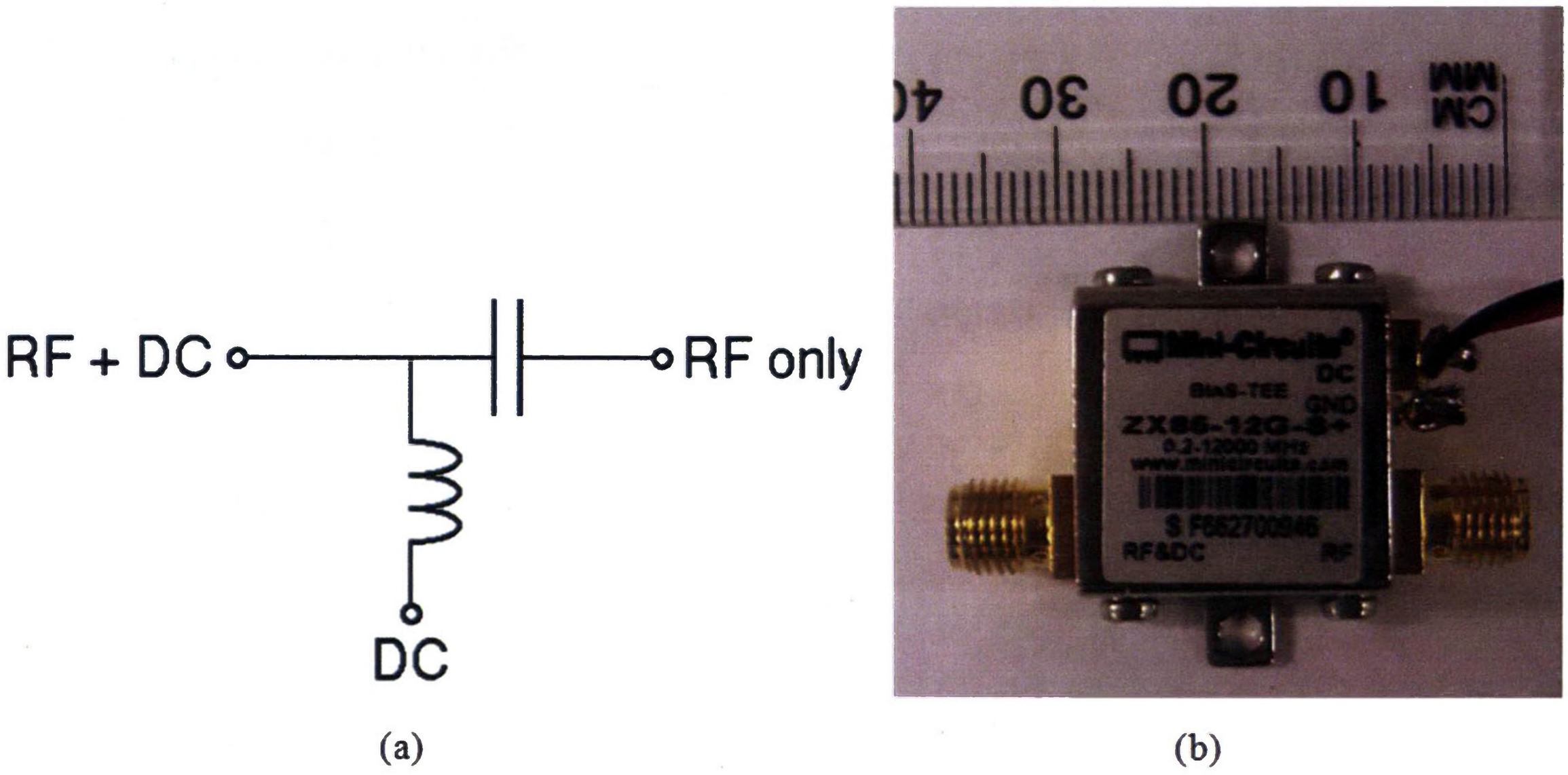

Figure 4.2: Bias-tee: (a) Equivalent circuit; (b) Photograph of the bias-tee.

The electrical length of the U-slot arm can be varied by changing between the different states of the diodes. When the left diode is on and the right diode is off, the RF current can flow across the left arm of the U-slot. In this case, the left arm of the U-slot is shorter than the right arm. In this way, the asymmetrical U-slot can excite two orthogonal modes in the patch. Adjusting the location of the PIN diodes can make the two modes have the same amplitude and a phase difference of 90^0 at a given frequency, thereby enabling the antenna to generate CP radiation. The antenna radiates LHCP when the left arm of the U-slot is longer than the right one. RHCP can be achieved if the right arm is longer than the left one. The U-slot becomes symmetrical when both of the diodes are on or off, which enables the antenna to radiate linear polarization. In this case, the electric-field polarization is parallel to the y-axis in Fig. 4.1. The possible polarization states (RHCP, LHCP and LP) and the corresponding diode states are summarized in Table 4.2.

Table 4.2: Polarization states of the reconfigurable U-slot antenna

	Diode (Left)	Diode (Right)	Polarization
State 1	OFF	OFF	Linear Pol.
State 2	ON	ON	Linear Pol.
State 3	ON	OFF	RHCP
State 4	OFF	ON	LHCP

4.3 Parametric Study of the Patch Length

Two important parameters which affect the input reflection coefficient and axial ratio of the reconfigurable U-slot antenna are the patch length $L4$ and the ratio of the lengths of the asymmetrical U-slot arms. Since a parametric study of the latter has already been reported in [117], we only examine the effects of the former parameter in this section. The other parameters remain constant and their values are given in Table 4.1. To complete the parametric analysis for five different patch lengths, full-wave simulations using CST Microwave Studio have been performed on the antenna shown in Fig. 4.1. As the antenna structure is basically symmetrical along the yz-plane, except for the bias line, the RHCP and LHCP should have similar axial ratio bandwidths and input reflection coefficients. Therefore, for the parametric analysis, only results for LHCP are presented. In addition, the effects on the input reflection coefficients of both LP states are examined.

Fig. 4.3 (a) and (b) show the effects of $L4$ on the resonant frequencies of State 1 and State 2, respectively. From this figure, it is observed that the resonant frequencies of both LP modes decrease as the length of the patch increases. For LP State 1, the input reflection coefficient is too high to be acceptable for most applications. For LP State 2, the impedance match is acceptable for WLAN applications as long as $L4$ is larger than 14.2 mm.

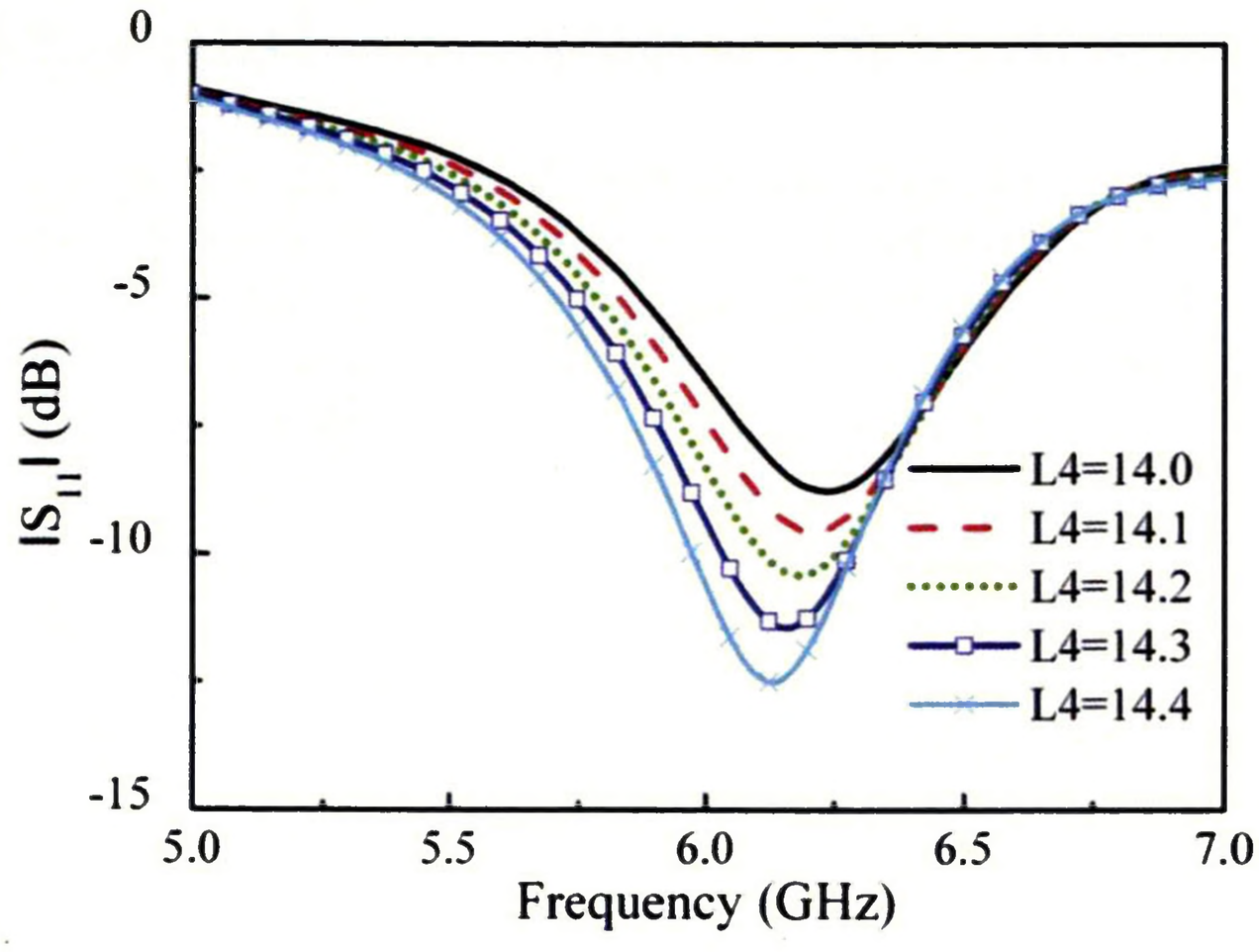

(a)

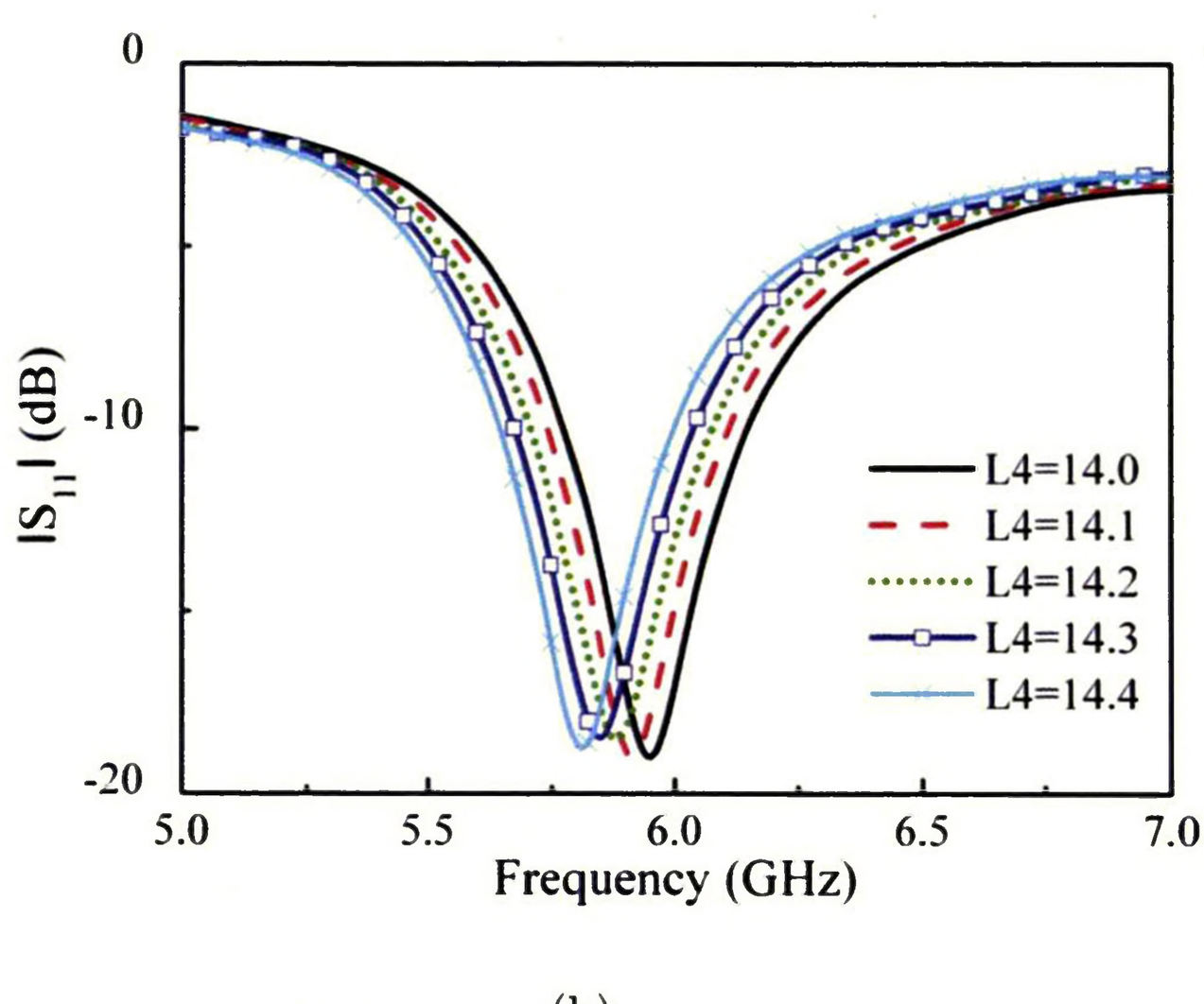

(b)

Figure 4.3: Simulated performance of the antenna as a function of $L4$: (a) Input reflection coefficient for State 1; (b) Input reflection coefficient for State 2.

Fig. 4.4 (a) and (b) show the effects of $L4$ on the axial ratio and input reflection coefficient of the CP mode, respectively. As seen from Fig. 4.4 (a), the 3dB axial ratio bandwidth increases as $L4$ decreases. However, $L4$ cannot be smaller than 14.2 mm if the LP mode is desired. This can be viewed as a compromise in order for the antenna to provide linear polarization; hence the optimum value of $L4$ is chosen to be 14.2 mm.

The 3dB axial ratio bandwidth is 2.8% with respect to the centre frequency of 5.75 GHz when $L4$ is 14.2 mm. From Fig. 4.4 (b), it is seen that the CP operating frequency bands ($|S_{11}| \leqslant$ -10 dB) are all located within the range from 5.6 to 6.3 GHz as $L4$ is varied, which is wide enough to cover the 5.725-5.85 GHz frequency band.

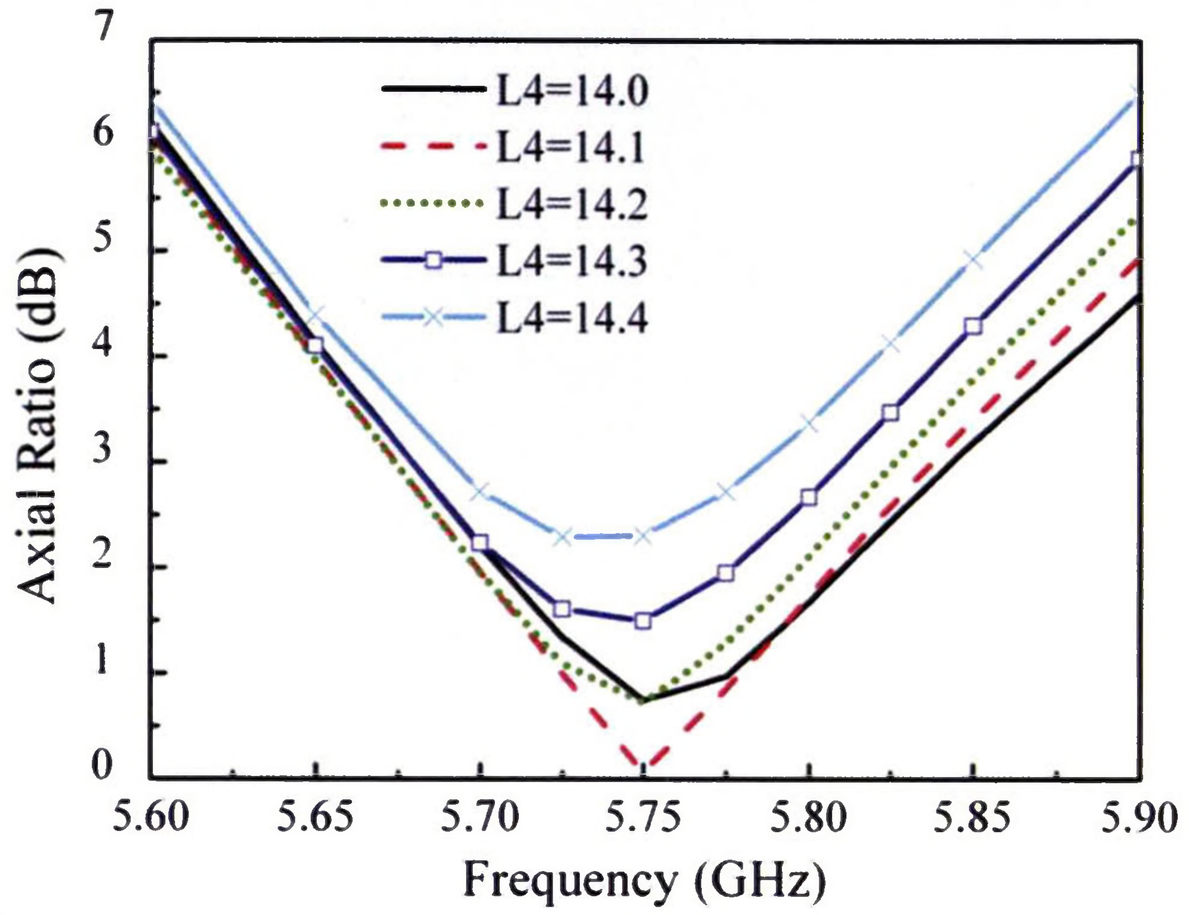

(a)

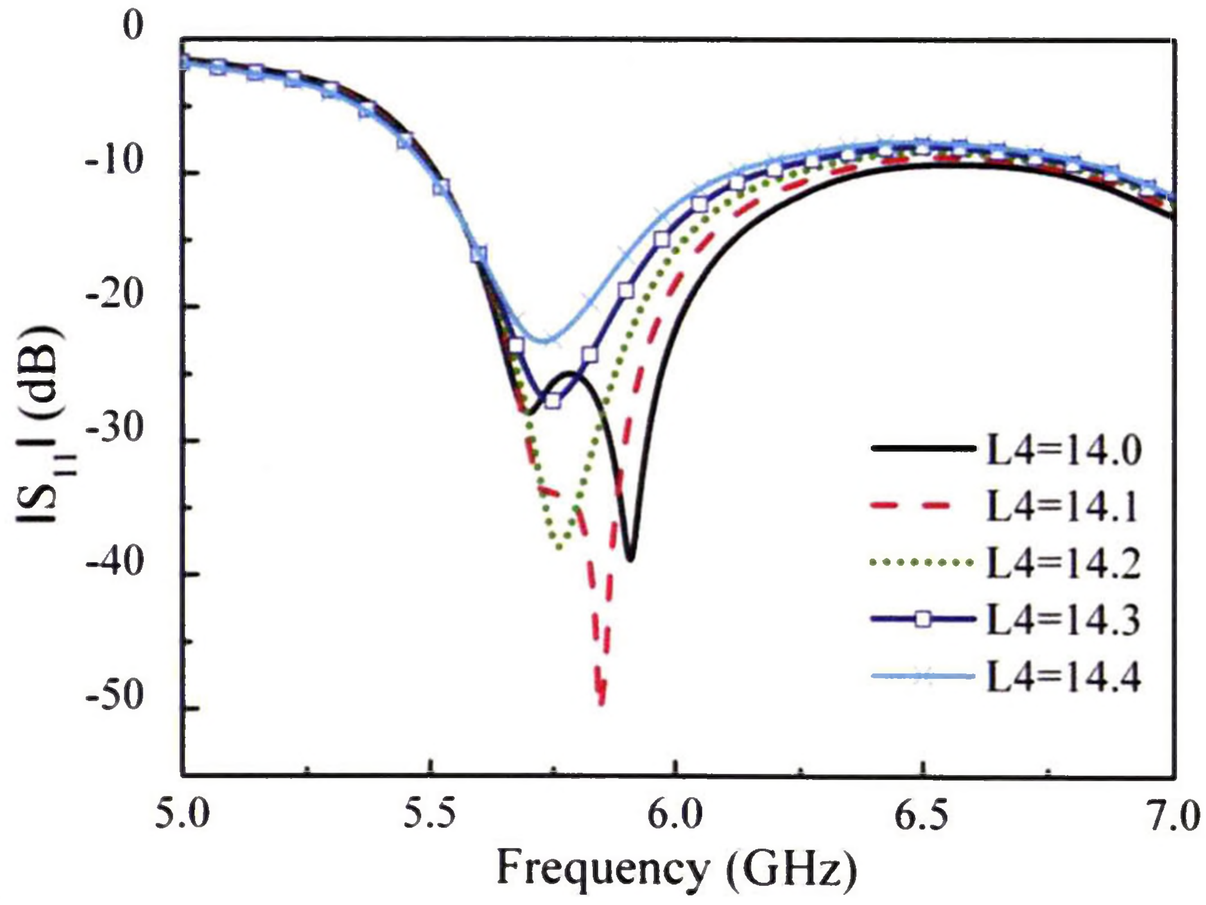

(b)

Figure 4.4: Simulated performance of the antenna as a function of $L4$: (a) Axial ratio; (b) Input reflection coefficient for the CP mode.

4.4 Simulated and Measured Results

According to the above analysis and Table 4.2, a single U-slot antenna that switches between linear polarization, RHCP or LHCP can be designed as long as the diodes are independently biased. Unfortunately, the bias network required will be relatively complicated. Since the aim of the work in this chapter is to validate the design concept, two polarization reconfigurable U-slot antennas with identical structures and dimensions shown in Fig. 4.1 and Table 4.1, respectively, were fabricated. The antennas can switch either between linear and circular polarizations (denoted as Antenna I) or between two circular polarization senses (denoted as Antenna II) by using different electronic elements. Fig. 4.5 (a) and (b) present the configurations of Antennas I and II, respectively.

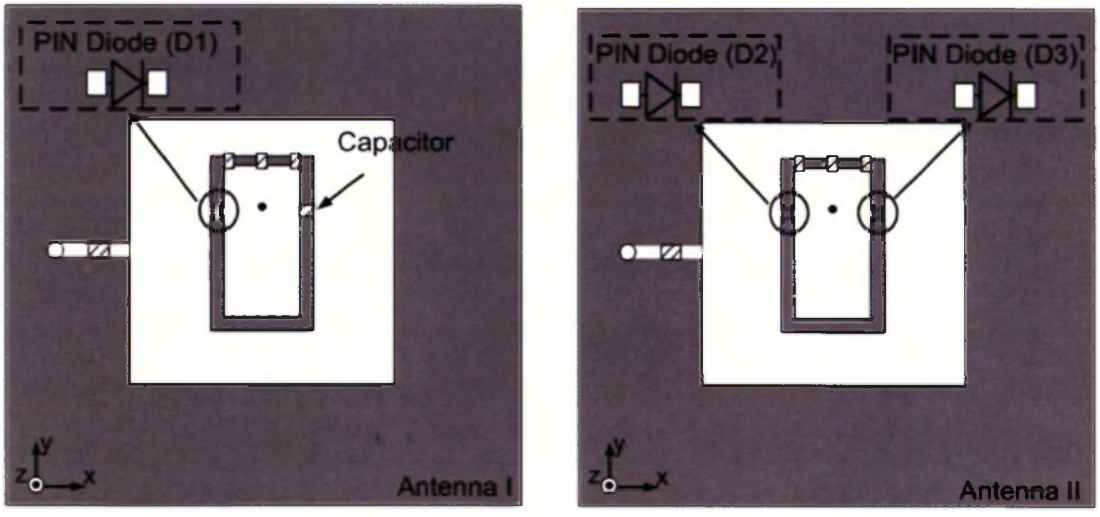

(a) (b)

Figure 4.5: Configurations of the polarization reconfigurable U-slot antennas: (a) Antenna I; (b) Antenna II.

The antennas are printed on a 3.175-mm-thick RT/Duroid 5880 substrate (dielectric constant ε_r=2.2, $tan\delta$=0.0009). Since Antenna I and Antenna II have the same structure but with different electronic elements, a photograph only of Antenna I is given in Fig. 4.6.

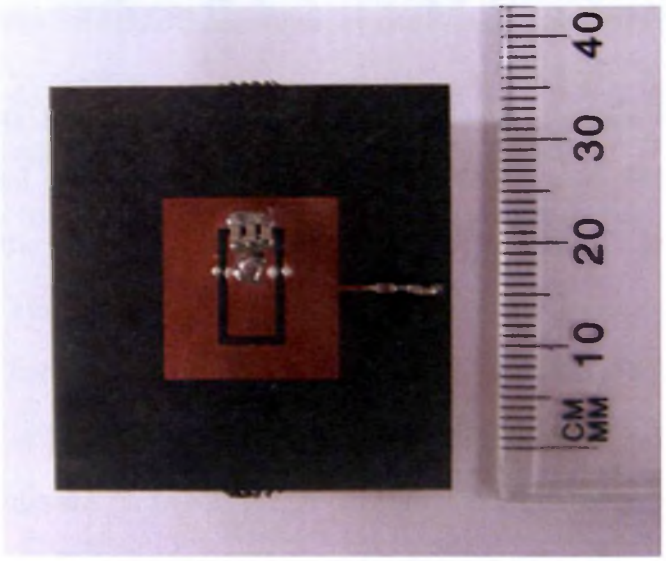

Figure 4.6: Photograph of the antenna.

For Antenna I, a 30pF capacitor is soldered onto the right pad to create a short circuit across the right arm of the U-slot. Meanwhile, a PIN diode $D1$ is mounted across the other arm using electrically conductive silver epoxy. When a forward bias is applied to turn on $D1$, the diode acts as a resistor of 4 Ω and the RF current can flow across the slot. In this case, the two arms of the U-slot are of the same length, which leads to the linear polarization mode. The LHCP mode can be obtained when $D1$ is turned off by changing the polarity of the dc voltage. Antenna I can also provide switching between RHCP and linear polarization if the positions of the capacitor and the pin diode are interchanged.

Simulated and measured input reflection coefficients as a function of frequency for the CP and LP modes are shown in Fig. 4.7. Simulated and measured axial ratios at boresight for the CP mode are given in Fig. 4.8. From the experimental results, it is observed that the impedance bandwidths for the LP and CP modes are 6.1% and 13.5%, respectively, with almost the same centre frequency of 5.9 GHz, which can cover the entire 5.725-5.85 GHz WLAN band. The measured 3dB axial ratio bandwidth at boresight extends from 5.7-5.86 GHz.

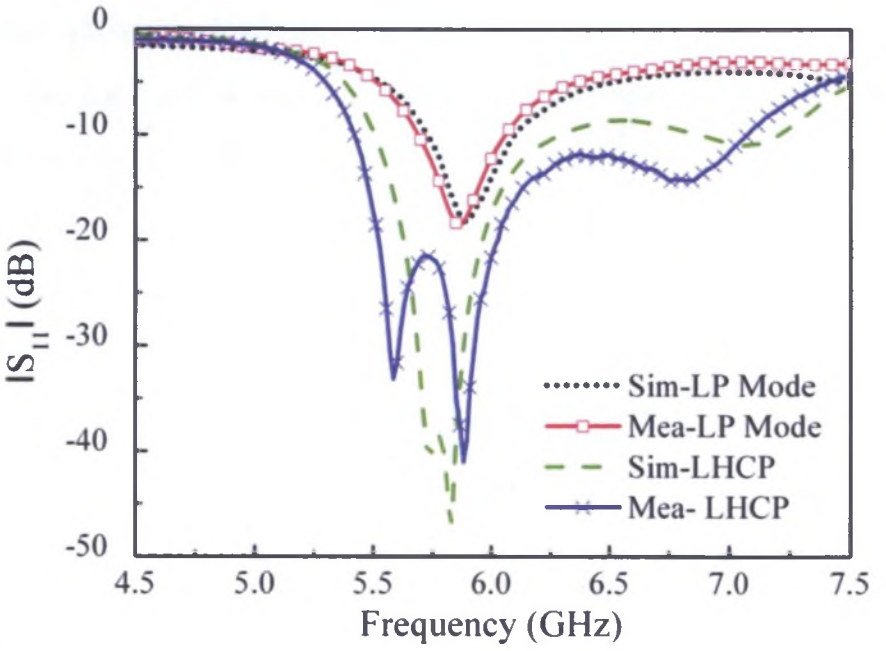

Figure 4.7: Simulated and measured input reflection coefficients for the LP and CP modes of Antenna I.

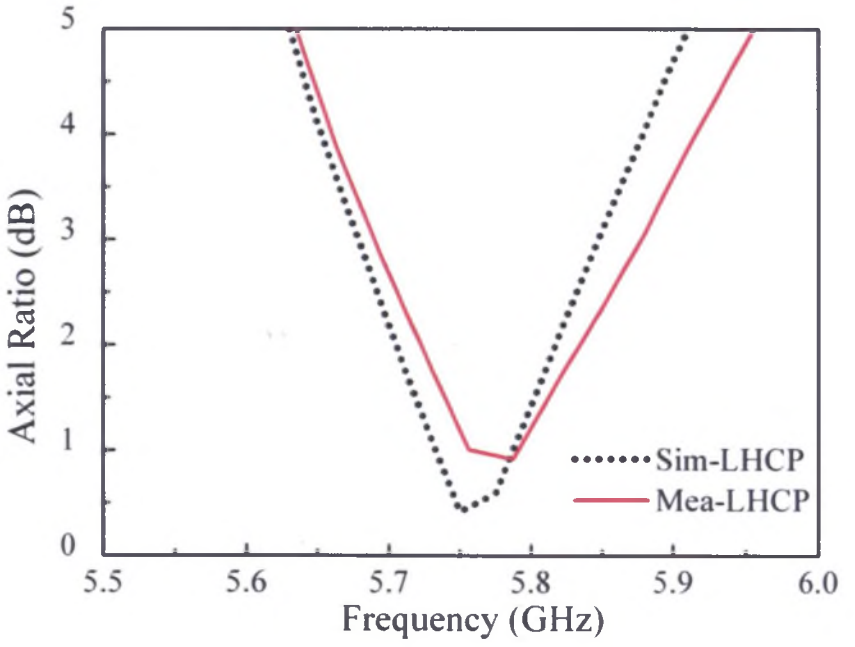

Figure 4.8: Simulated and measured axial ratios for the CP mode of Antenna I.

For Antenna II, two PIN diodes ($D2$, $D3$) are embedded across the two arms of the U-slot. The orientation of the two PIN diodes is shown in Fig. 4.5 (b). As the bias voltage is supplied from the coaxial probe, opposite dc voltage polarities are applied to $D2$ and $D3$. If a positive voltage is supplied, $D2$ is turned off and $D3$ is turned on and the antenna radiates LHCP. When a negative voltage is supplied, $D3$ is turned off and $D2$ is turned on and the antenna radiates RHCP. Fig. 4.9 presents the simulated and measured reflection coefficients as a function of frequency for the LHCP and RHCP modes. It can be observed that the frequency bandwidths of both CP senses are similar to the result of the CP mode of Antenna I in Fig. 4.7. However, it is clear that the impedance match of LHCP is better than that of RHCP, which can be mostly attributed to the existence of the microstrip bias line. Simulations show that if we put the bias line on the other side of the patch, the impedance match of RHCP will be better than that of LHCP.

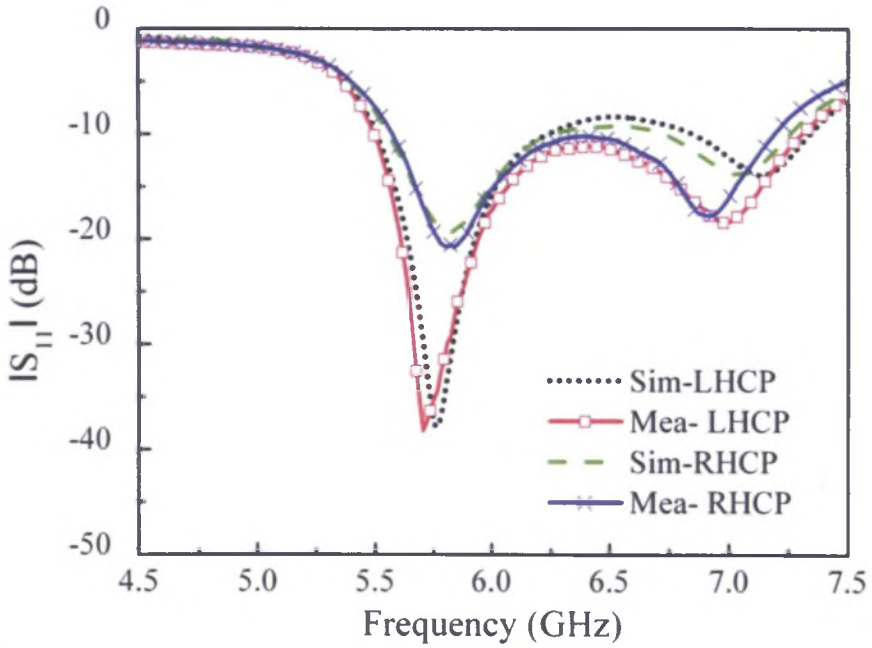

Figure 4.9: Simulated and measured input reflection coefficients for the LHCP and RHCP modes of Antenna II.

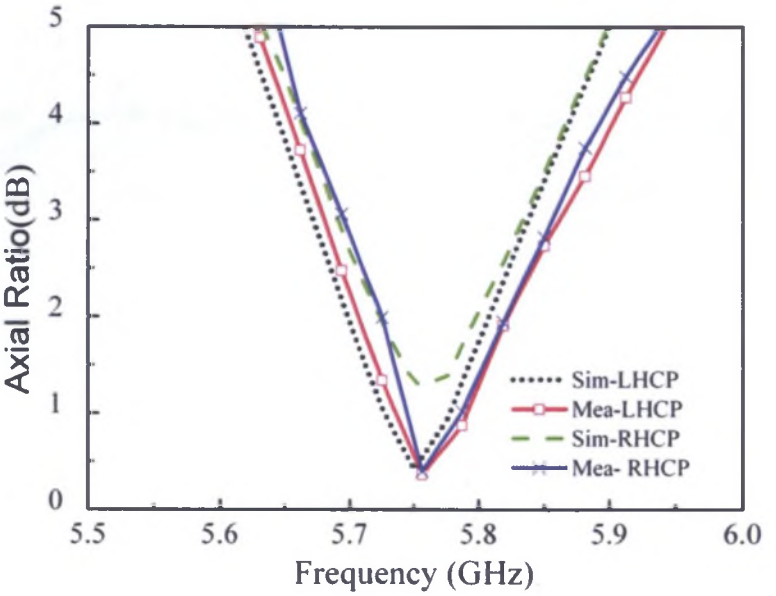

Figure 4.10: Simulated and measured axial ratios for the LHCP and RHCP modes of Antenna II.

Radiation patterns were measured for the LP and CP modes in a spherical near-field (SNF) system. For the CP modes, the axial ratio was measured as well. Fig. 4.10 shows the simulated and measured axial ratios for both CP senses. The 3dB axial ratio bandwidths of LHCP and RHCP are 3.1% and 2.8%, respectively, with the same centre frequency of 5.77 GHz.

In Figs 4.11-4.14, the simulated and measured normalized radiation patterns of both E plane and H plane at 5.78 GHz are compared. The orientation of the rectangular coordinate system used in all radiation pattern figures is the same as the one shown in Fig. 4.1. The radiation plots are as follows: Fig. 4.11 and Fig. 4.12 show radiation patterns for LP and CP modes of Antenna I, respectively; Fig. 4.13 and Fig. 4.14 show radiation patterns for LHCP and RHCP modes of Antenna II, respectively. From Fig. 4.11 to Fig. 4.14, it can be observed that the cross polarization levels for the linear and circular polarizations remain below -12 dB. In addition, it can be noted that the radiation patterns remain almost the same for the different polarization states.

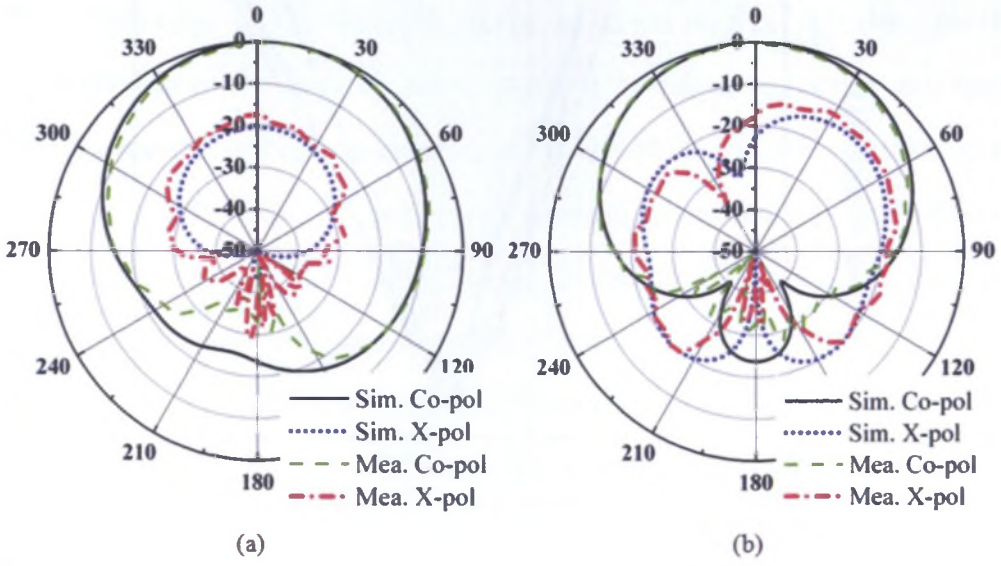

Figure 4.11: Simulated and measured normalized radiation patterns at 5.78 GHz for the LP mode of Antenna I: (a) y-z plane; (b) x-z plane.

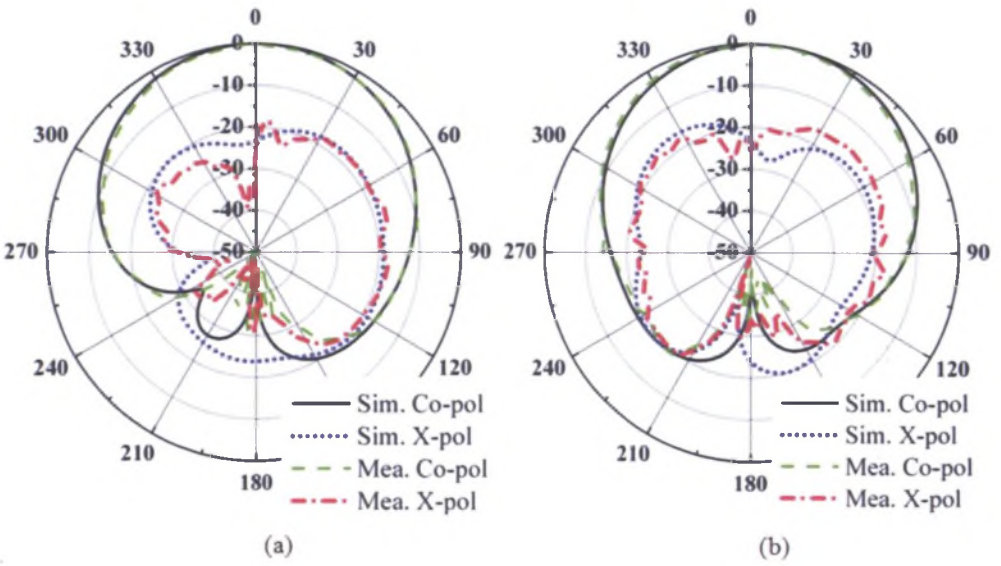

Figure 4.12: Simulated and measured normalized radiation patterns at 5.78 GHz for the CP mode of Antenna I: (a) y-z plane; (b) x-z plane.

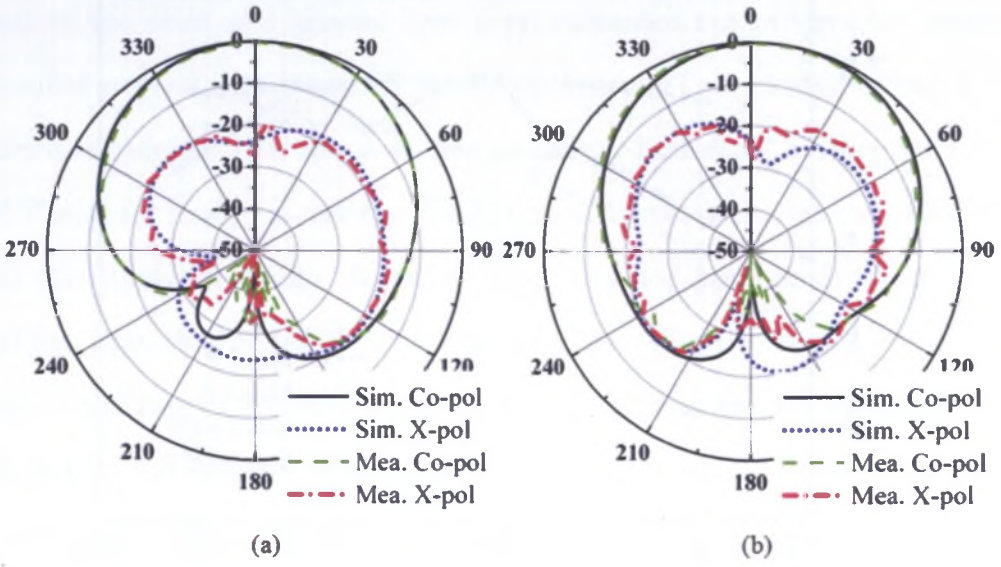

Figure 4.13: Simulated and measured normalized radiation patterns at 5.78 GHz for the LHCP mode of Antenna II: (a) y-z plane; (b) x-z plane.

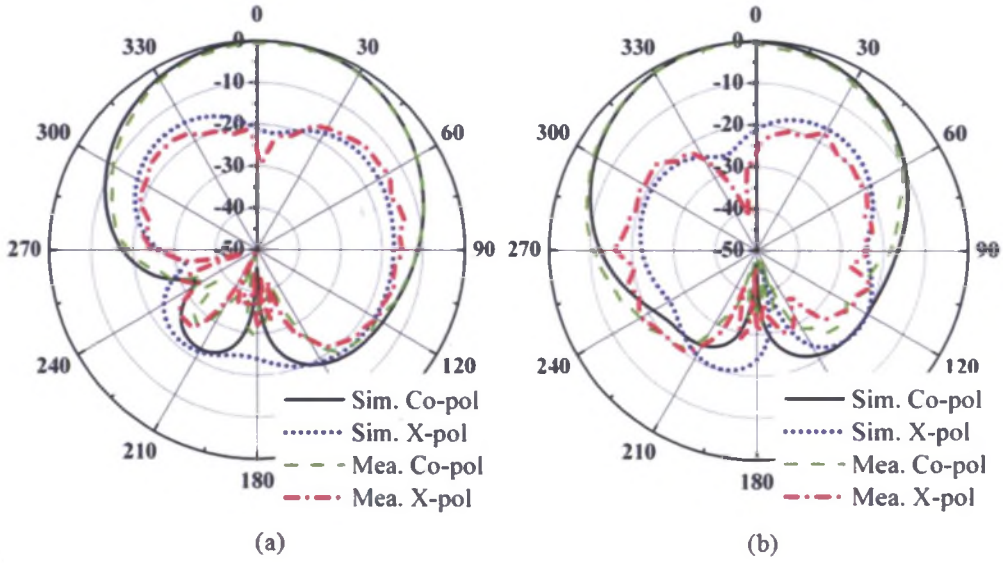

Figure 4.14: Simulated and measured normalized radiation patterns at 5.78 GHz for the RHCP mode of Antenna II: (a) y-z plane; (b) x-z plane.

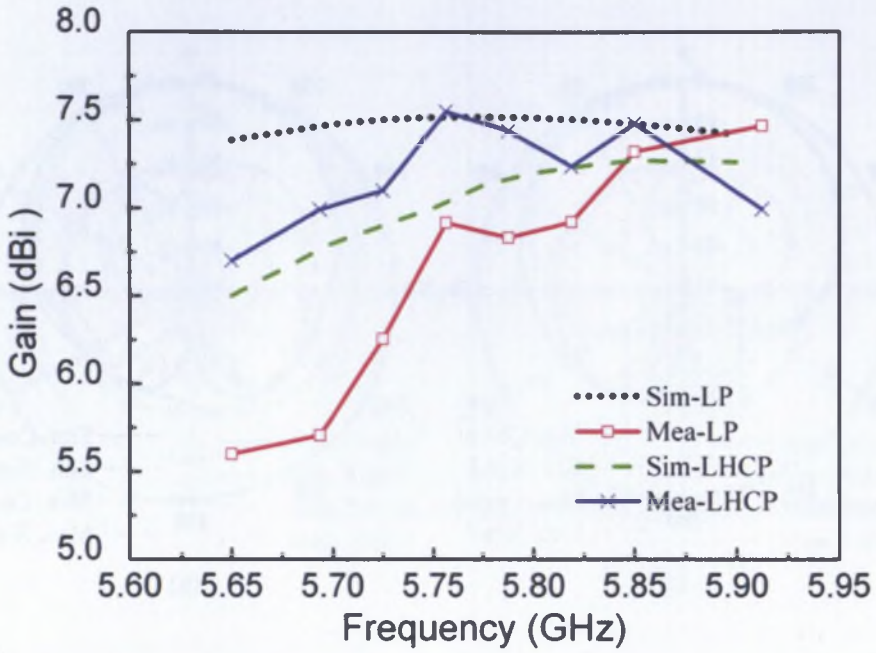

Figure 4.15: Simulated and measured gains for Antenna I.

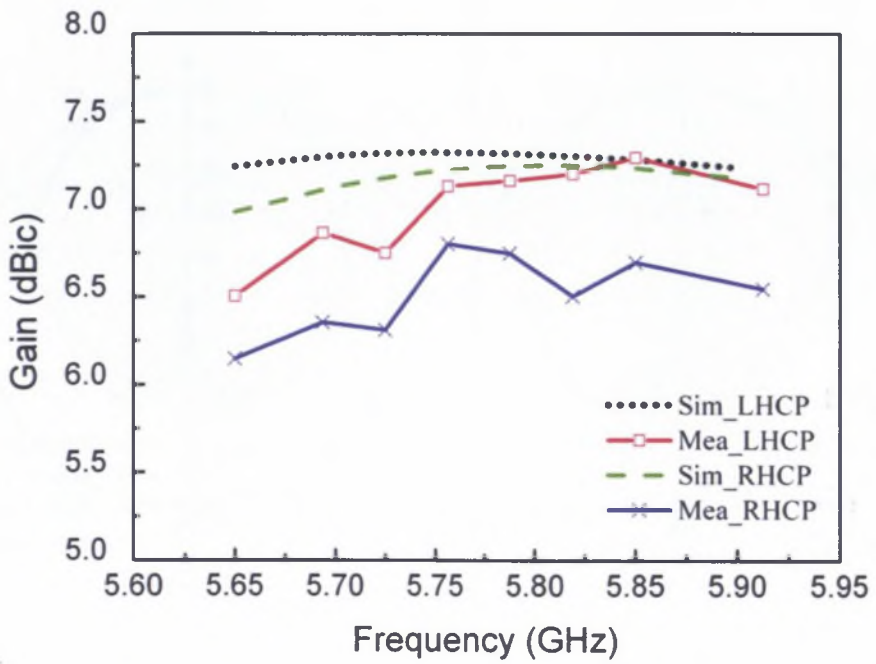

Figure 4.16: Simulated and measured gains for Antenna II.

Additionally, the realized gain was measured using the gain comparison technique. The losses of the cable and bias-tee have been calibrated out of the gain measurement. The measured gains of the LP and CP modes for Antenna I are plotted in Fig. 4.15. From the figure, it is observed that the measured gains vary from 6.3-7.5 dBic and 6.25-7.3 dBi for the CP and LP modes across the WLAN band, respectively, which agree reasonably well with the simulated results. It can be noted that for Antenna II the gain of RHCP is 0.6 dB less than that of LHCP. The reason for the difference is that the values of the resistance of the two PIN diodes for the ON state are not exactly the same; hence the losses caused by the PIN diodes are different. Another possible reason for the difference can be attributed to measurement error.

Moreover, the losses of the PIN diodes also affect the efficiency of the antenna. The measured efficiency is obtained from the difference between the measured gain and directivity. The measured efficiencies of Antenna I for the LP and CP modes at 5.78 GHz are 73% and 82%, respectively. The difference is due to the fact that for the LP mode the PIN diode acts as a 4Ω resistor but for the CP mode the PIN diode is turned off. Therefore, the loss for the CP mode is less than that of the LP mode. In addition, the measured efficiencies of Antenna II for the LCHP and RHCP modes at 5.78 GHz are 86% and 78%, respectively. The efficiencies of Antenna II are different from those of Antenna I since the loss elements for Antenna I and Antenna II are different, and there are also slight variations in the resistance of individual diodes.

Chapter 5

A Pattern Reconfigurable Antenna

5.1 Introduction

Pattern reconfigurable antennas (RAs) have received significant attention due to their ability to improve the performance of wireless communication systems. They can electronically change the far-field radiation pattern characteristics, such as the shape of the pattern or the main-beam location, while maintaining the frequency response. They have the potential to avoid noise sources by changing the null position, to save energy by better directing the signal toward intended users, to mitigate signal fading in multipath environments by using pattern diversity, and to provide better coverage by redirecting the main beam [62-84].

Very recently, pattern reconfigurable antennas have found new applications in multiple-input-multiple-output (MIMO) systems to enhance the system capacity by reducing the correlation of sub-channels. Specifically, this is implemented by switching between different configurations of reconfigurable antenna arrays according to the varying channel conditions. The pattern diversity in some of the configurations can be used to realize low correlation of the sub-channels.

In order for a pattern reconfigurable antenna to be employed in a MIMO system, the correlation coefficient of the different antenna radiation patterns should be as low as possible. Usually it should be lower than 0.5 so that the pattern reconfigurable antenna can provide enough diversity for the MIMO system [134]. Among the reported pattern reconfigurable antenna designs, several [82-84] feature the capability to switch between boresight and conical patterns. A conical radiation pattern is generally one for which the maximum directivity is off boresight (where boresight corresponds to the direction normal to the plane containing the antenna) and the pattern shape resembles a cone. Since the maximum-beam directions of these two patterns are significantly different, the correlation of the two patterns should be quite low. Therefore, this type of pattern reconfigurable antenna can be a good candidate to be incorporated in MIMO systems for improving the system capacity. Unfortunately, regarding the above pattern reconfigurable designs [82-84], the antennas have some disadvantages that will hinder their application to MIMO systems. In [82], a wide-band L-probe circular patch antenna with dual feeds was presented. Nevertheless, an integrated matching network consisting of switches needs to be designed in order to reconfigure the radiation pattern electronically. In [83] and [84], single-feed pattern reconfigurable square-ring patch antennas were designed with air gaps to improve the impedance bandwidth. The air gap increases the antenna volume. In addition, dc bias networks were used to drive the PIN diodes, which increases the complexity for the antenna to be applied into a wireless communication system.

In this chapter, a new pattern reconfigurable microstrip U-slot patch antenna using eight PIN diodes is proposed. Eight shorting posts are implemented around the patch to change the operating mode of the antenna from the monopolar-patch mode to the normal-patch mode. In addition, the two modes are designed to resonate in similar frequency ranges. Therefore, the proposed antenna can electronically reconfigure the radiation pattern between conical and boresight patterns with an overlapped impedance

bandwidth. Furthermore, the plane with the maximum power level of the conical pattern can be varied between two orthogonal planes when the antenna operates in the monopolar-patch mode. Owing to a novel design of the switch geometry, the antenna does not need dc bias lines to control the PIN diodes. The measured overlapped impedance bandwidth ($|S_{11}| \leqslant$ -10 dB) of the two modes is 6.6% with a centre frequency of 5.32 GHz.

Compared with the antennas in [82-84], the proposed antenna has three main advantages. Firstly, only a single bias-tee, which superimposes the bias voltage on the RF signal, is needed to control the PIN diodes in the proposed antenna. Consequently, the complex bias network for PIN diodes or the matching network for dual feeds is not required as part of the printed antenna structure, which greatly simplifies the device. Secondly, the proposed antenna is compact and of low profile since it is designed on a single-layer microwave substrate. Thirdly, compared to the antennas in [82-84] which can switch between two radiation patterns, the proposed antenna has three different patterns in a similar frequency band. A greater number of patterns gives the proposed antenna more flexibility to improve the system capacity of a wireless link.

5.2 Antenna Structure and Operating Principle

5.2.1 Design Guidelines

Microstrip patch antennas excited in the normal-patch mode for boresight radiation and in the monopolar-mode for conical radiation have been reported in [120] and [121], respectively. In [121], the monopolar mode is excited by two shorting posts located to the left and right of the feeding point, as shown in Fig. 5.1 (a). If PIN diodes are used to connect the shorting posts and the microstrip patch, it is possible for this single antenna to operate in the monopolar-patch mode or in the normal-patch mode by switching between the different states of the PIN diodes. However, according to [121], the resonant frequency

of the monopolar mode is much lower than the fundamental normal-patch mode. In order to design an antenna with two modes resonating in similar frequency ranges and having a reasonably large frequency bandwidth, we have taken three measures in the design process.

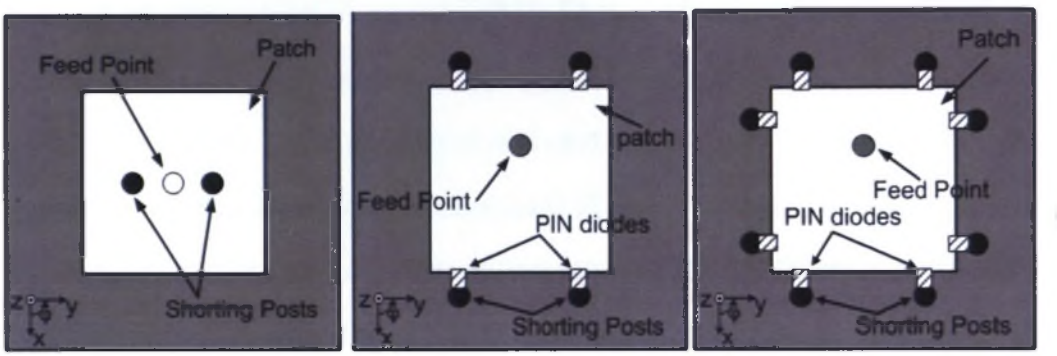

Figure 5.1: Configurations of the patch antenna with PIN diodes: (a) Antenna in Ref. [121] with two shorting posts; (b) Antenna with four shorting posts; (c) Antenna with eight shorting posts.

Firstly, compared with the antenna in [121], we use two shorting posts at either side of the feed point. In order to simplify the bias network, the shorting posts are implemented around the edges of the patch and connected to the patch via PIN diodes, as shown in Fig. 5.1 (b). It is well known that the resonant frequency of a patch antenna loaded with reactive components can be varied depending on the type of reactance used [7], [143]. When the shorting posts are connected to the microstrip patch, the antenna operates in the monopolar-patch mode. In this case, the increase in the number of shorting posts will increase the resonant frequency. On the other hand, when all the shorting posts are disconnected from the patch, the antenna operates in the normal-patch mode. In this case, the increase in the number of shorting posts will reduce the resonant frequency. Therefore, the frequency difference between the two modes becomes smaller as the number of shorting posts increases. The effects of the number of shorting posts on the antenna's

resonant frequency will be detailed in Section 5.3.

Secondly, we examine the normalized far-field radiation patterns for the antennas operating in the monopolar-patch mode in Fig. 5.1 (a) and (b), as given in Fig. 5.2 (a) and (b), respectively. The antennas are analyzed using the time domain solver of CST Microwave Studio. For the antenna in Fig. 5.1 (a), as described in [121], two identical conical patterns are located in two orthogonal planes $\varphi = \pm 45^0$. For the antenna in Fig. 5.1 (b), the maximum power levels of the conical pattern in the plane $\varphi = \pm 90^0$ are 6 dB greater than those in the plane $\varphi = 0^0$. In order to have another similar conical pattern with the maximum power level located at the plane $\varphi = 0^0$ for the antenna in Fig. 5.1 (b), four shorting posts are inserted into the substrate around the other two edges of the microstrip patch, as seen in Fig. 5.1 (c).

Finally, as the probe-fed microstrip patch antenna has a small impedance bandwidth that precludes its use in typical communication systems, a U-slot is etched on the patch to increase its impedance bandwidth [116].

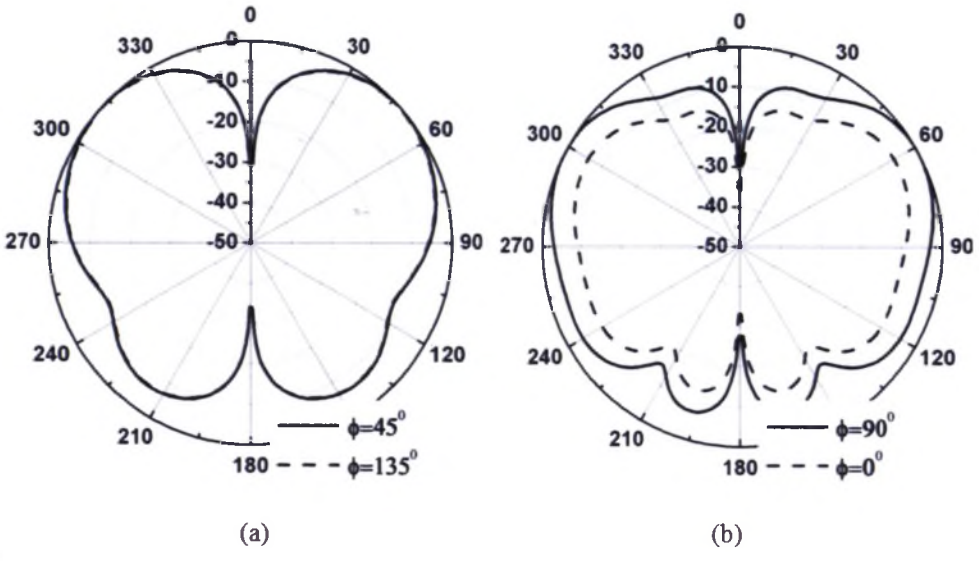

Figure 5.2: Simulated normalized radiation patterns: (a) Antenna in Ref. [121]; (b) Antenna of Fig. 5.1 (b).

5.2.2 Antenna Structure

The layout of the proposed pattern reconfigurable U-slot antenna is shown in Fig. 5.3. A U-slot is inserted into a square patch of dimensions $L1 \times L1$. Each side of the patch is connected to two shorting posts via PIN diodes. The radius of the shorting posts r is 0.7 mm. The feed probe connected to the U-slot patch through the ground plane and substrate is offset from the top edge of the patch by $L5$. Since the length of the PIN diode is less than the width of the gap $L8$, conducting ring pads are placed around the shorting posts to enable attachment of the PIN diodes. The parameters and dimensions of the antenna are given in Table 5.1.

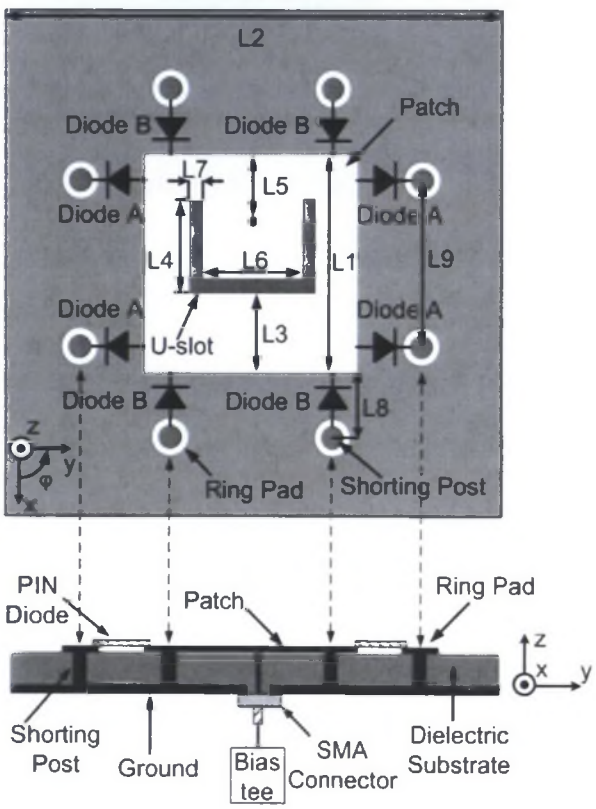

Figure 5.3: Schematics of the pattern reconfigurable U-slot antenna.

Table 5.1: Dimensions of the pattern reconfigurable U-slot antenna

Parameter	$L1$	$L2$	$L3$	$L4$	$L5$
Value (mm)	12.6	50	5.5	5.4	4.2
Parameter	$L6$	$L7$	$L8$	$L9$	r
Value (mm)	4.6	0.7	1.7	9.8	0.7

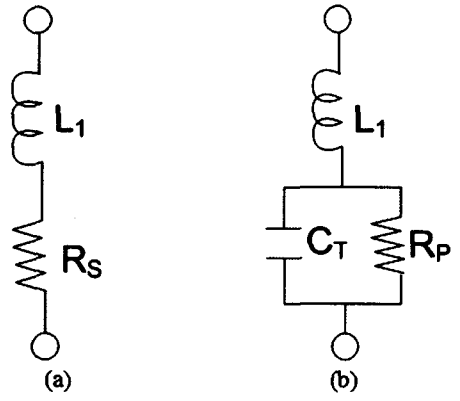

Figure 5.4: Equivalent circuits for PIN diode: (a) Forward biased; (b) Reverse biased.

Beam-lead PIN diodes (MA4AGBLP912) are used as the switching elements. The equivalent circuits used in the simulation software are presented in Fig. 5.4. According to the PIN-diode datasheet [138], the resistor (R_S) is 4 Ω in the forward-bias state and the capacitor (C_T) in the parallel circuit is 0.025 pF in the reverse-biased state. The resistor (R_P) is 10 kΩ representing the net dissipative resistance of the diode in the reverse-bias state. For the zero-bias state, the value of R_P is almost infinity which is equal to an open circuit, and the loss caused by the resistor (R_P) is negligible.

The orientation of the diodes is shown in Fig. 5.3. As all PIN diodes are mounted between the ground and the centre patch, only a bias-tee attached to the SMA connector is needed to control the PIN diodes. When the bias voltage is supplied from the coaxial probe, opposite bias conditions are applied to diodes in groups A and B due to their

reverse orientation. When the dc voltage is zero, all diodes are turned off. In this case, the antenna operates in the normal-patch mode and radiates a boresight pattern (State 1). When the dc voltage is negative, the diodes in group B are on, and the other diodes are off. In this case, the antenna has four shorting posts connected and can be regarded as a monopolar-patch antenna, which radiates a conical pattern with the maximum power level in the z-y plane (State 2). Changing the polarity of the dc voltage from negative to positive, the diodes in group A are on, and all the other diodes are off. In this case, a similar conical pattern can be observed with the maximum power level in the z-x plane (State 3). The possible radiation patterns of the reconfigurable U-slot antenna and the corresponding diode states are summarized in Table 5.2.

Table 5.2: Three states of the pattern reconfigurable U-slot antenna

	Diodes Group A	Diodes Group B	Radiation Patterns
State 1	Zero Biased	Zero Biased	Boresight pattern
State 2	Reverse Biased	Forward Biased	Conical pattern with maximum power level in the z-y plane
State 3	Forward Biased	Reverse Biased	Conical pattern with maximum power level in the z-x plane

5.3 Antenna Equivalent Circuit and Parametric Study

5.3.1 Antenna Equivalent Circuit

Three important parameters which affect the input reflection coefficients of the two modes of the proposed reconfigurable antenna are the radius of the shorting posts, the distance between the shorting post and the patch $L8$, and the number of shorting posts.

Also, it is well known that the U-slot plays an important role in the performance of the patch antenna. Since a parametric study of the U-slot has already been reported [117], we only examine the effects of the former three parameters in this paper. The other parameters remain constant and their values are given in Table 5.1. As the shorting posts have the same effects on the reflection coefficients of States 2 and 3 for the monopolar-patch mode, only the results for State 2 are presented for the parametric analysis.

In order to better analyze the effects of the parameters, the equivalent circuits of the antenna with PIN diodes for States 1 and 2 are given in Fig. 5.5 (a) and (b), respectively. In the equivalent circuits, a parallel resonant RLC circuit is used to model the patch antenna with a U-slot. The purpose of the electrical models in Fig. 5.5 is to give a physical insight into the behaviour of the antenna for the parametric analysis, but not to exactly predict the antenna input impedance. A similar method has been used in [144] for the parametric analysis of a microstrip patch antenna.

Fig. 5.5 (a) shows the equivalent circuit of the antenna operating in the normal-patch mode. The microstrip patch with a U-slot is represented by a RLC circuit (R, L, C). For the normal-patch mode, only the PIN diodes and the shorting posts that are attached to the radiating edges are considered in the equivalent circuit, and the effects of the two PIN diodes and shorting posts at each edge are combined together to simplify the equivalent circuit. As the PIN diodes are all zero biased, according to the PIN diode datasheet, R_P is almost infinity. Therefore, the equivalent circuit of the PIN diode in this state is an inductor L_1 in series with a capacitor C_T. The parasitic capacitance between the shorting posts and the patch is modeled by a capacitor C_2. The shorting post is represented by a shunt inductor L_2. The imaginary part of the input admittance Y_{in} from the reference plane on the right-hand side of Fig. 5.5 (a) was investigated using CST Microwave Studio. Simulation results show that Y_{in} is capacitive with a capacitance C_{in} within the antenna operating frequency range.

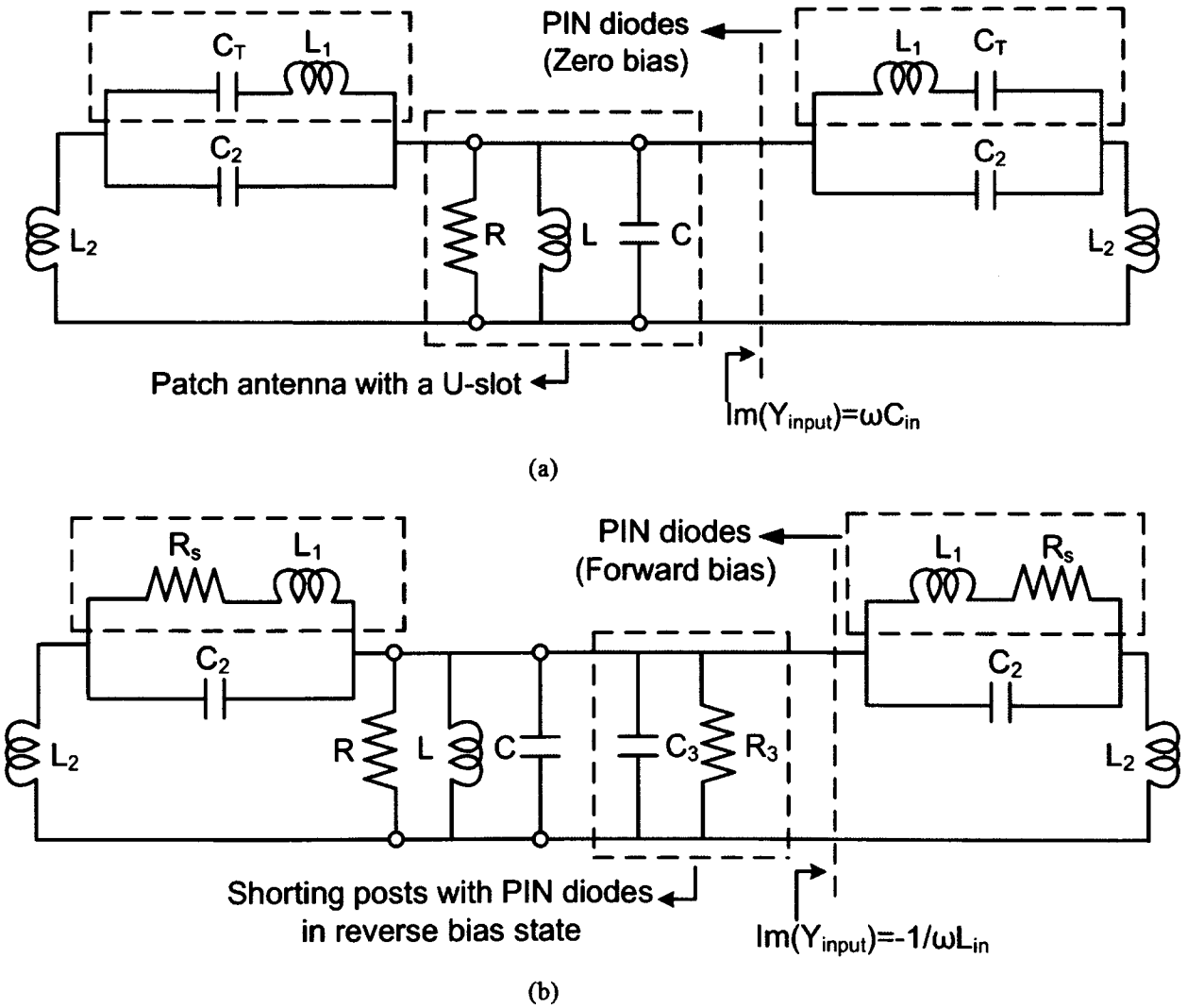

Figure 5.5: The equivalent circuits of the proposed antenna: (a) State 1 (normal-patch mode); (b) State 2 (monopolar-patch mode).

Fig. 5.5 (b) shows the equivalent circuit of the antenna operating in the monopolar-patch mode. As with the circuit of the normal-patch mode, the microstrip patch with a U-slot is also represented by a *RLC* circuit (R, L, C). In the monopolar-patch mode (State 2), four PIN diodes (diodes A) are reverse biased. According to the analysis in the last paragraph, the total effects of the shorting posts with PIN diodes in the zero-bias state is capacitive. The only difference between the zero-bias and reverse-bias states is

the value of the net dissipative resistor R_P of the PIN diodes. Therefore, a capacitor C_3 is used to model the total capacitive effects of the shorting posts connected with diodes A. A resistor R_3 is used to represent the losses in the four PIN diodes. On the other hand, four shorting posts are connected to the patch by PIN diodes B that are in the forward-bias state. Those PIN diodes are modeled by an inductor L_1 in series with a resistor R_s. In addition, the effects of the shorting posts and the parasitic capacitance between the patch and the shorting posts are represented by an inductor L_2 and a capacitor C_2, respectively. The imaginary part of the input admittance Y_{in} from the reference plane on the right-hand side of Fig. 5.5 (b) was investigated. Simulation results show that Y_{in} is inductive with an inductance L_{in} within the antenna operating frequency range.

5.3.2 Parametric Study

Fig. 5.6 (a) and (b) show the effects of the radius of the shorting posts r on the resonant frequencies of the monopolar-patch and normal-patch modes, respectively. It is observed that the resonant frequency of the monopolar patch mode increases with the radius of the shorting posts. This is due to the fact that when the radius increases the inductance from the shorting posts reduces, which makes L_{in} decrease; hence, the resonant frequency of the parallel circuit in Fig. 5.5 (b) increases. For the normal-patch mode, the resonant frequency remains almost unaffected by the radius change of the shorting posts. This is because C_{in} in Fig. 5.5 (a) is almost stable within the changing range of the shorting-post radius, which is evidenced by the simulation results. Therefore, the radius of the shorting posts can change the resonant frequency of the monopolar-patch mode but has little effect on that of the normal-patch mode.

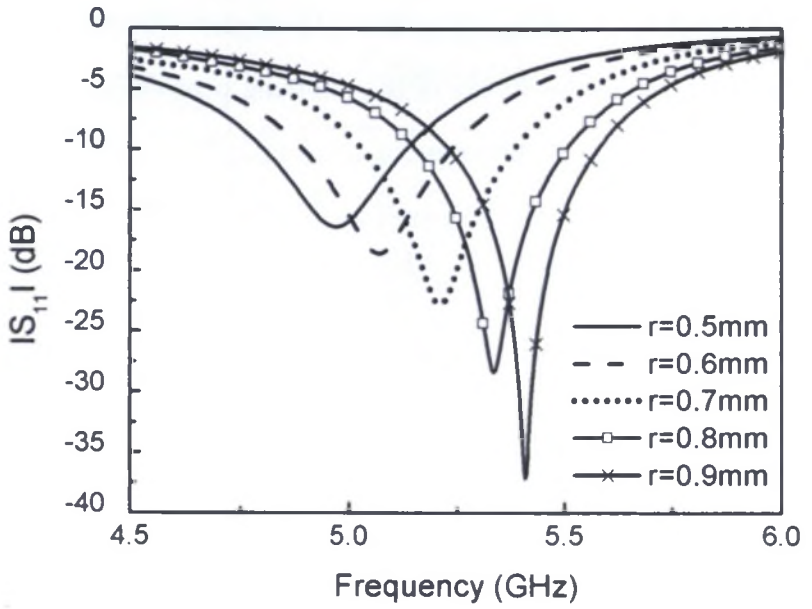

(a)

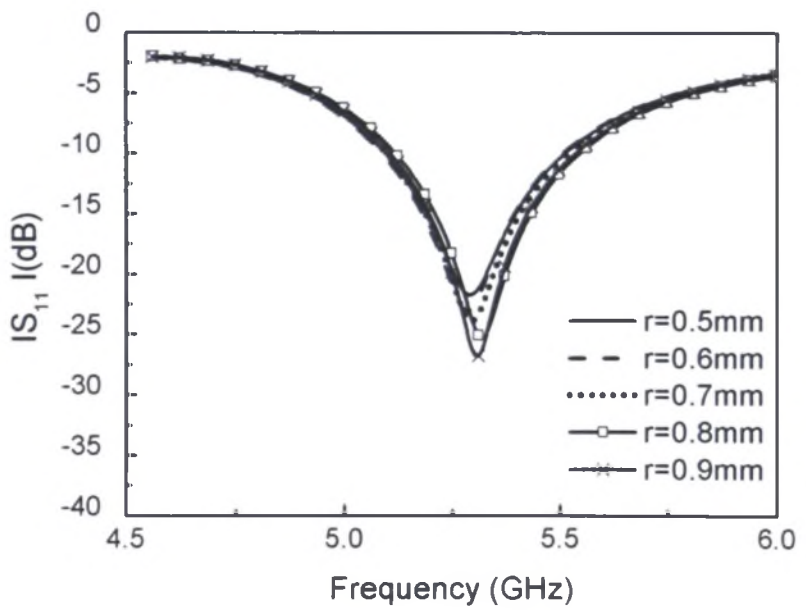

(b)

Figure 5.6: Simulated performance of the proposed antenna as a function of r: (a) Input reflection coefficient of the monopolar-patch mode; (b) Input reflection coefficient of the normal-patch mode.

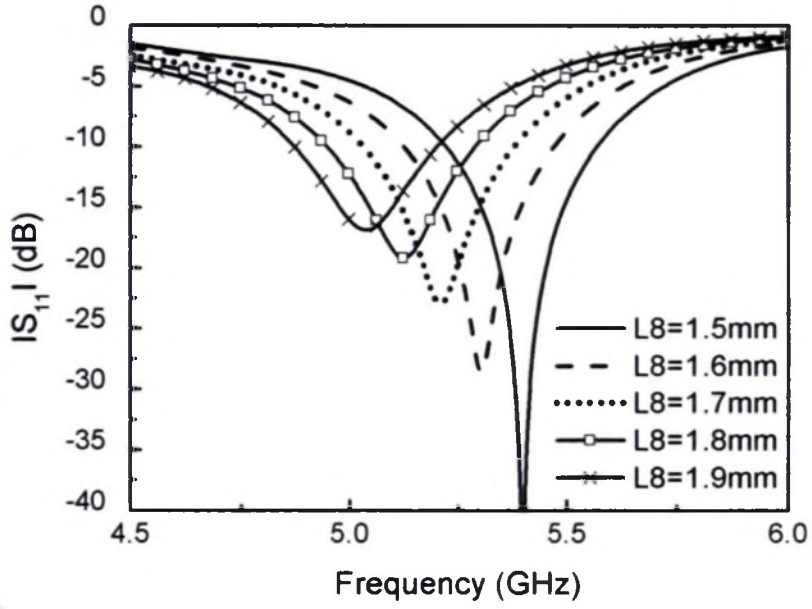

(a)

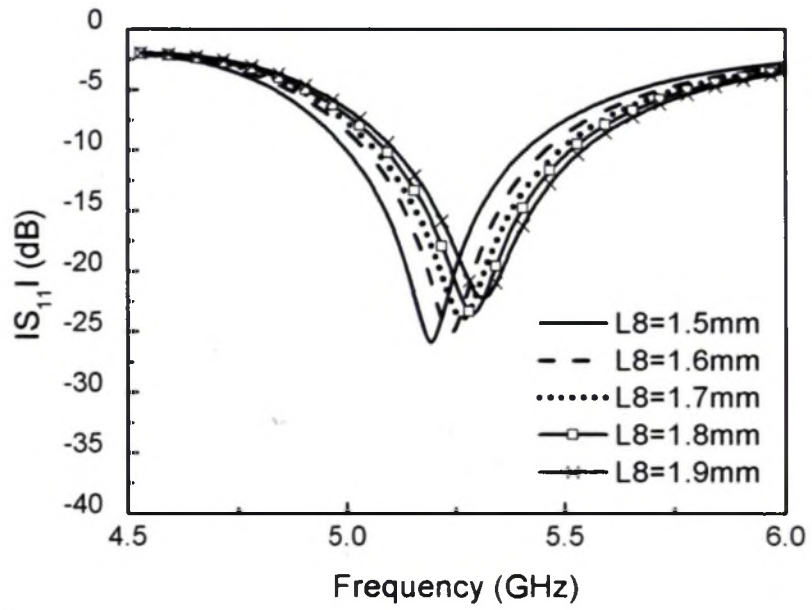

(b)

Figure 5.7: Simulated performance of the proposed antenna as a function of $L8$: (a) Input reflection coefficient of the monopolar-patch mode; (b) Input reflection coefficient of the normal-patch mode.

Fig. 5.7 (a) and (b) show the effects of $L8$ on the resonant frequencies of the monopolar-patch and normal-patch modes, respectively. As seen from Fig. 5.7, the resonant frequency of the monopolar-patch mode increases when $L8$ is reduced. However, the resonant frequency of the normal-patch mode decreases with $L8$. This can be attributed to the fact that, when $L8$ decreases, the parasitic capacitance between the shorting posts and the patch, C_2, increases. The increased capacitance C_2 reduces the inductive effect (L_{in}) from the reference plane in Fig. 5.5 (b), but increases the capacitive effect (C_{in}) from the reference plane in Fig. 5.5 (a) and C_3 in Fig. 5.5 (b). The decreased L_{in} and the increased C_3 have opposite effects on the resonant frequency of the monopolar-patch mode (the resonant frequency of a parallel RLC circuit). However, the simulation results show that the effect of L_{in} outweighs that of C_3, which leads to an increase of the resonant frequency of the monopolar-patch mode. On the other hand, the greater capacitance C_{in} will decrease the resonant frequency of the parallel circuit in Fig. 5.5 (a), which will shift the resonant frequency of the antenna in the normal-patch mode to a lower value.

In the design guidelines (Section 5.2.1), it is stated that an increase in the number of shorting posts will increase the resonant frequency of the monopolar-patch mode, but reduce that of the normal-patch mode. The reason is as follows. For the monopolar-patch mode, the increased number of shorting posts means that, for the diodes in the forward-bias state, more inductors (L_{in}) are paralleled, which makes the effective inductance decrease. On the other hand, for the diodes in the reverse-bias state, more capacitors C_3 are paralleled, which makes the effective capacitance increase. Simulation results show that the decrease of the total inductance outweighs the increase of the total capacitance on the resonant frequency of the RLC circuit in Fig. 5.5 (b). Therefore, the resonant frequency of the monopolar-patch mode is increased when the number of shorting posts increases. On the other hand, for the normal-patch mode, since the PIN diodes connected to the radiating edges are all zero biased, the increased number of shorting posts means

more capacitors are paralleled, which makes C_{in} increase; hence the resonant frequency of the normal-patch mode (the resonant frequency of a parallel RLC circuit in Fig. 5.5 (a)) is decreased.

5.4 Simulated and Measured Results

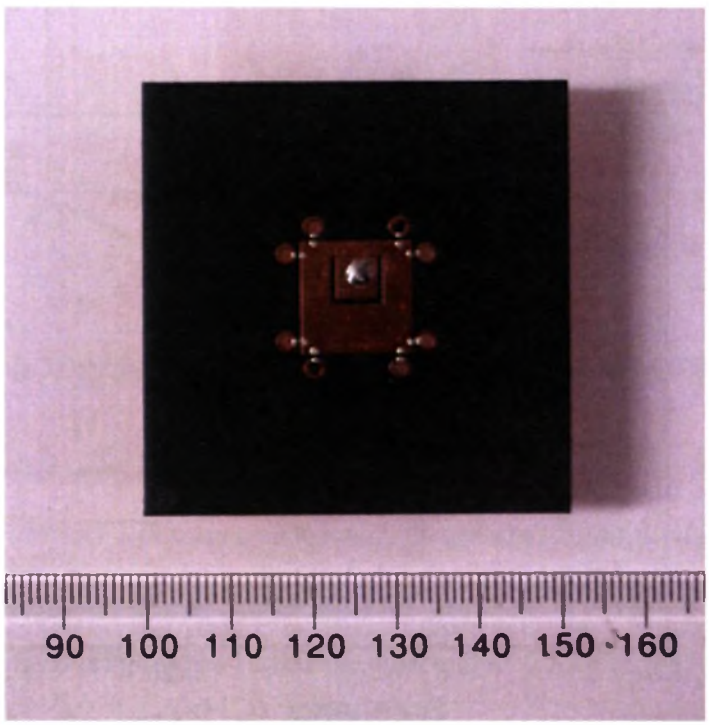

Figure 5.8: Photograph of the pattern reconfigurable U-slot antenna.

Based on the above analysis, a pattern reconfigurable U-slot antenna was designed and fabricated. The proposed antenna is etched on a 3.175-mm-thick RT/Duroid 5880 substrate (dielectric constant ε_r=2.2, $tan\delta$ = 0.0009). A photograph of the fabricated prototype is shown in Fig. 5.8. Figs 5.9 and 5.10 show the simulated and measured reflection coefficients as a function of frequency for three different states of the antenna, respectively. Compared with the simulated results the measured resonant frequencies for

States 2 and 3 are slightly higher. This discrepancy can be mostly attributed to the inaccuracies in the fabrication of the shorting posts. As is shown in Section 5.3.2, the resonant frequency of the monopolar mode is quite sensitive to the radius and position of the shorting posts. However, the simulated overlapped impedance bandwidth ($|S_{11}| \leqslant$ -10 dB) of the three states is 6.5% with a centre frequency of 5.24 GHz. The corresponding measured bandwidth is 6.6% centred at 5.32 GHz, which agrees reasonably well with the simulated results.

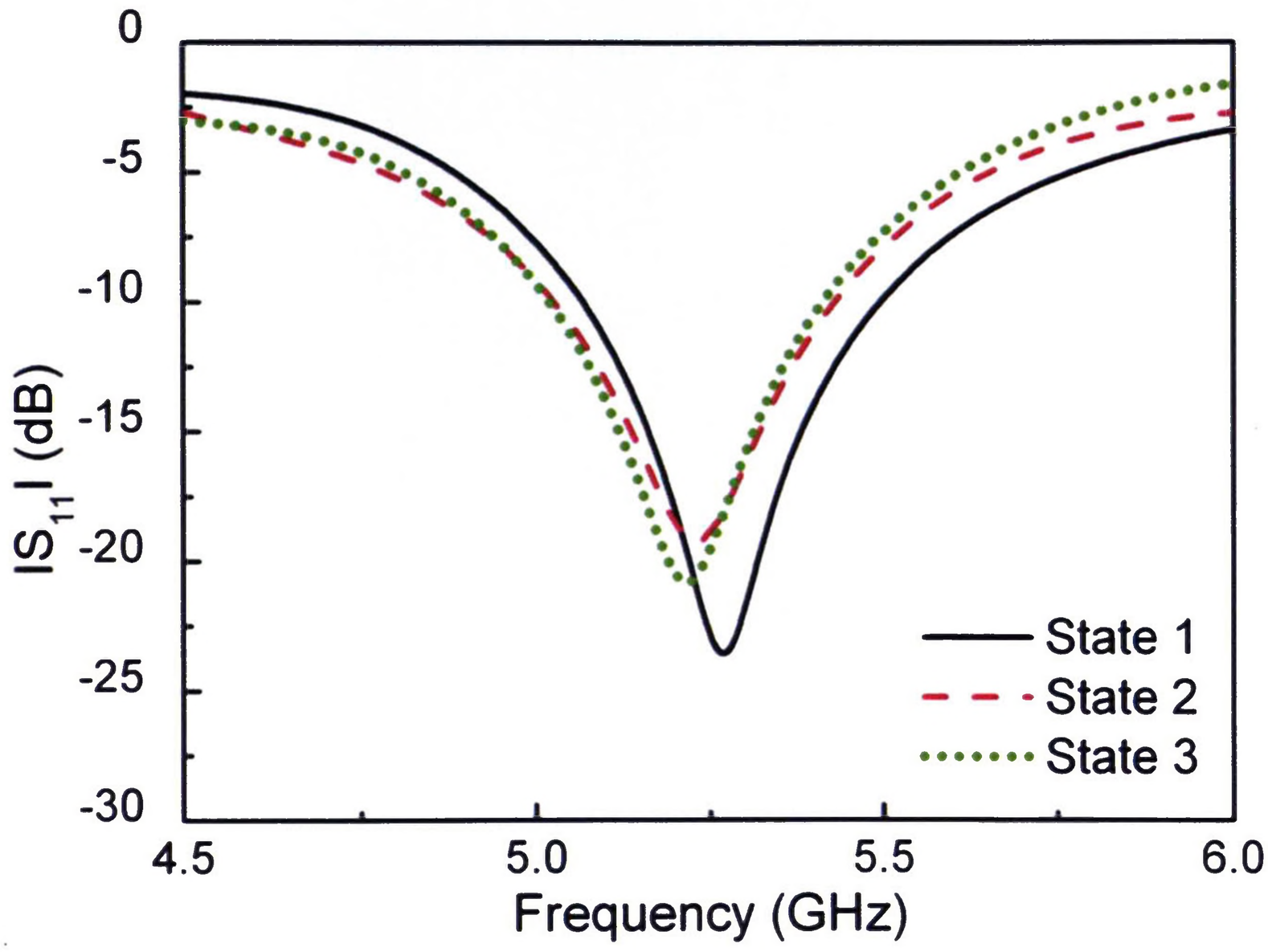

Figure 5.9: Simulated input reflection coefficient of the antenna.

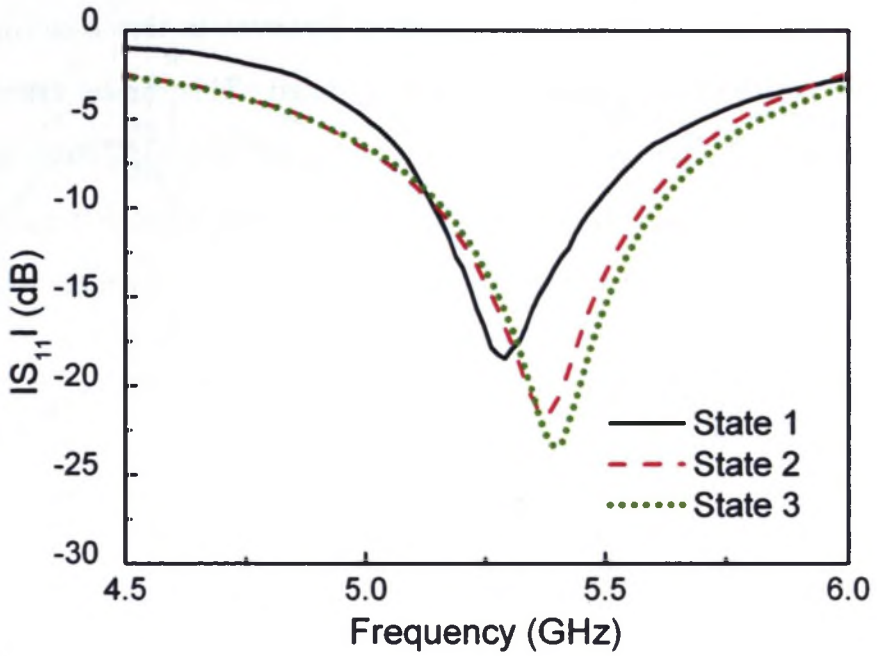

Figure 5.10: Measured input reflection coefficient of the antenna.

Radiation patterns were measured for the three states of the proposed antenna using a spherical near-field (SNF) antenna measurement system. Simulated and measured normalized radiation patterns are compared for both co-polarization and cross-polarization. Figs 5.11, 5.12 and 5.13 display the radiation patterns at 5.3 GHz for State 1, State 2 and State 3, respectively. For State 1, boresight radiation patterns with a maximum cross-polarization level of -20 dB are shown. For State 2, a symmetrical conical pattern with the maximum power level in the z-y plane directed at (elevation angle) 44^0 is plotted in Fig. 5.12 (a) and (b). For State 3, an asymmetrical conical pattern with the maximum power level in the z-x plane directed at (elevation angle) 45^0 is shown in Fig. 5.13 (a) and (b). It can be seen from Fig. 5.13 (a) that the pattern is asymmetrical and there is a 1dB difference between the left and right maximum power levels of the conical pattern. This is due to the position of the probe feed. Simulation results show that, if we put the probe feed at the centre of the patch, the difference between the left and right maximum

power levels in Fig. 5.13 (a) will become smaller. However, in that case the overlapped impedance bandwidth of the two modes will be reduced. This can be viewed as a compromise for the antenna to provide good overlapped impedance bandwidth and radiation patterns. In Figs 5.11, 12 and 13, the simulated cross-polarization patterns for the three states are not given since their values are very small compared to the measured ones.

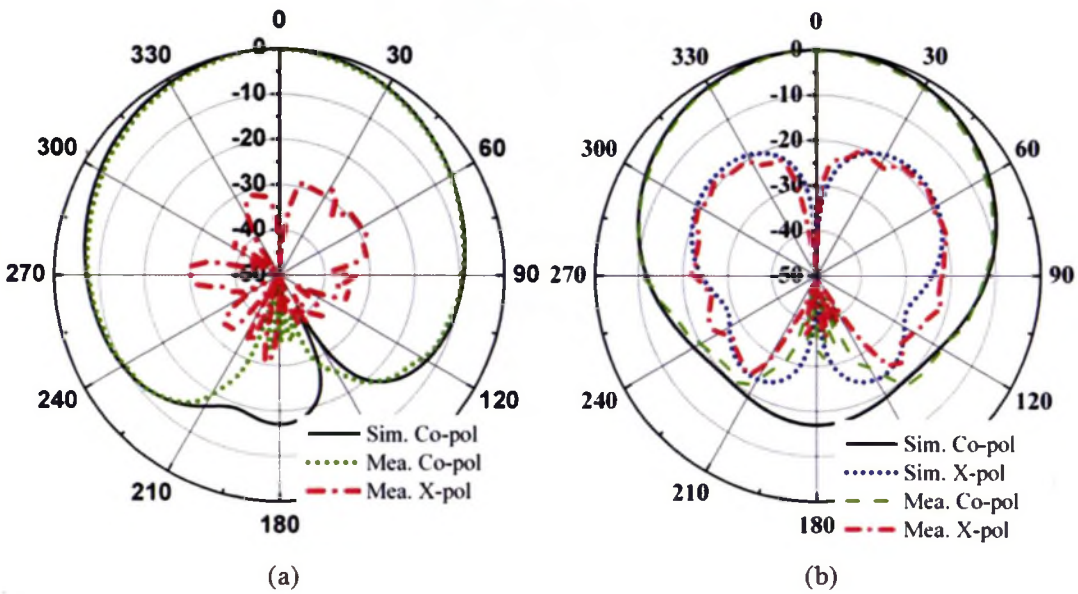

Figure 5.11: Measured and simulated normalized radiation patterns of the antenna at 5.3 GHz for State 1: (a) z-x plane; (b) z-y plane.

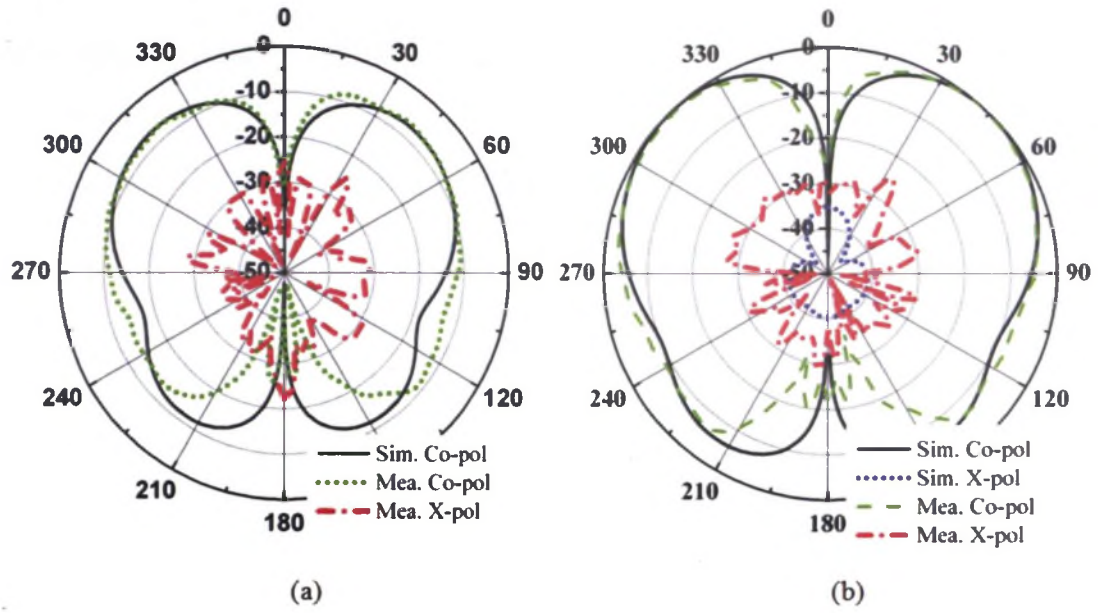

Figure 5.12: Measured and simulated normalized radiation patterns of the antenna at 5.3 GHz for State 2: (a) z-x plane; (b) z-y plane.

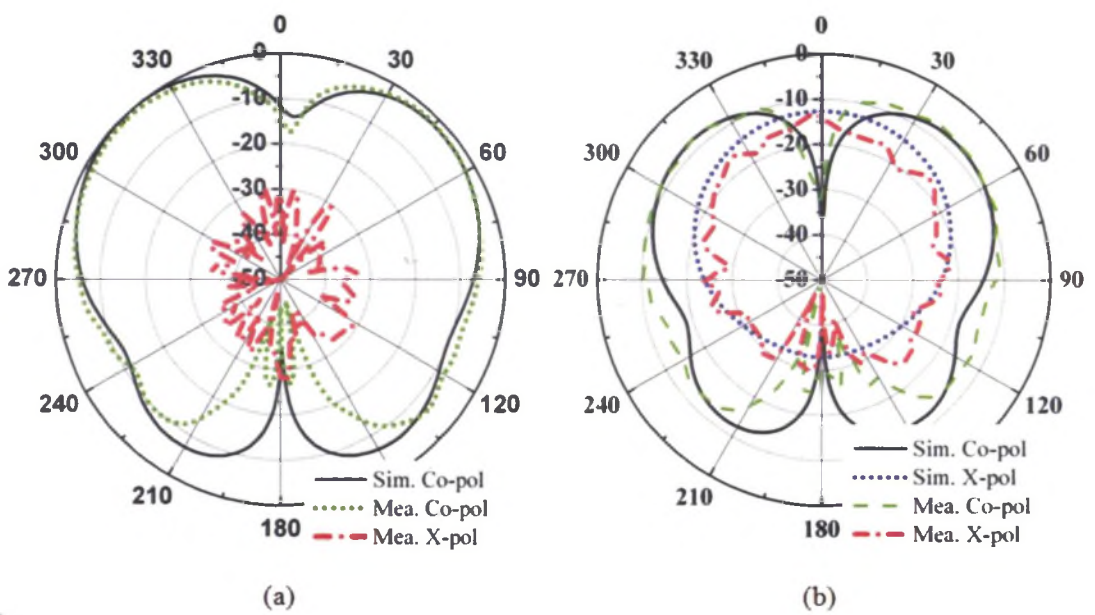

Figure 5.13: Measured and simulated normalized radiation patterns of the antenna at 5.3 GHz for State 3: (a) z-x plane; (b) z-y plane.

Additionally, the realized gain was measured using the gain comparison technique. The losses of the cable and bias-tee have been calibrated out of the gain measurement. The measured gains for the three states are plotted in Fig. 5.14. The measured efficiencies of State 1, State 2 and State 3 at 5.3 GHz are 86.6%, 45.1% and 45.4%, respectively, where the measured efficiency is obtained from the difference between the measured gain and directivity. From Fig. 5.14, it can be seen that the measured gain of State 3 is 0.5 dB greater than that of State 2, which can be mostly attributed to the asymmetry of the conical pattern of State 3 and slight variations in the resistance of individual diodes. Furthermore, at 5.3 GHz the gain of State 1 is approximately 3 dB greater than those of States 2 and 3, which is mainly due to the losses of the PIN diodes. On the one hand, for States 2 and 3, four PIN diodes, each acting as a 4Ω resistor (R_S), are attached to the antenna, but for State 1 all PIN diodes are turned off. To examine the effects of R_S, we have simulated several different values of R_S at 5.3 GHz. Simulation results show that when R_S decreases to zero the realized gain increases by 2 dB and 1.75 dB for States 2 and 3, respectively. On the other hand, for States 2 and 3, diodes with finite value R_P also have more losses than the diodes in the zero-bias state, which is approximately lossless. Simulation results show that at 5.3 GHz when R_P changes from 10 kΩ to infinity the realized gain increases by 0.32 dB and 0.27 dB for States 2 and 3, respectively. Therefore, the losses of States 2 and 3 are much greater than that of State 1 and the corresponding gains are much lower. In order to increase the gains of States 2 and 3, low-loss elements such as radio-frequency microelectromechanical-system (RF MEMS) switches could be used. However, the disadvantages of using currently available RF MEMS are a higher cost and lower reliability than PIN diodes.

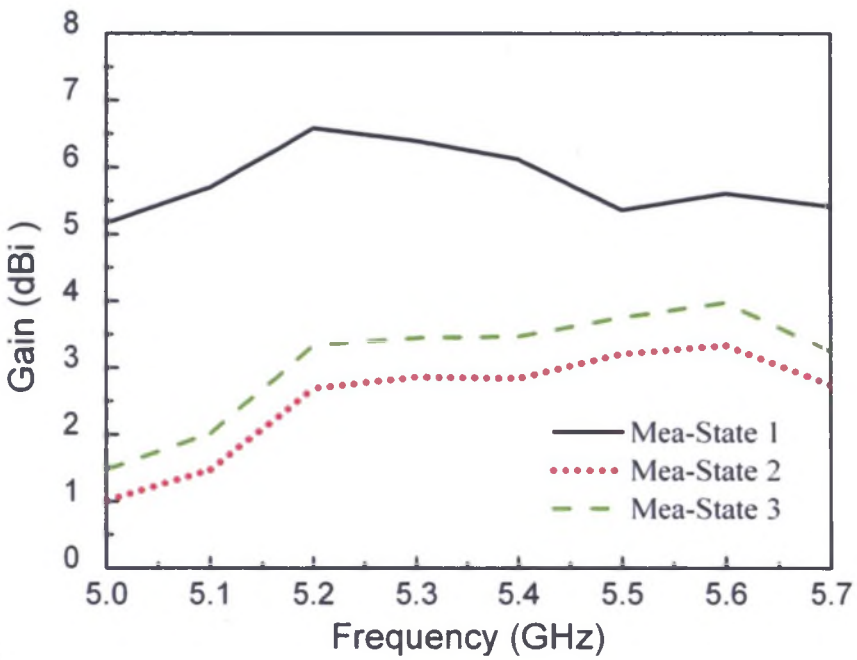

Figure 5.14: Measured gains of the antenna.

Chapter 6

A Reconfigurable Antenna with Frequency and Polarization Agility

6.1 Introduction

The reconfigurable antennas proposed in Chapters 3, 4 and 5 and most of the designs reported to date [6-86] feature reconfigurability of only one characteristic of the antenna rather than multiple reconfigurability. However, the ultimate goal of reconfigurable antenna design is to realize full reconfigurability of the operating frequency, polarization, and radiation pattern of an antenna in order to respond to the usually fast-changing communication environments. A major challenge to achieve this goal is the separation of an antenna's frequency characteristic from its radiation characteristic. Recently, several groups have achieved combined frequency and radiation pattern reconfigurability [87, 88]. An annular slot antenna [87] and a single-turn microstrip spiral antenna [88] were proposed to reconfigure both the frequency and the radiation pattern. Unfortunately, few reconfigurable antenna designs have been reported that can reconfigure the frequency and the polarization independently. In [89], a frequency tunable aperture-coupled microstrip

antenna with vertical and horizontal polarization reconfigurability was reported. However, only the frequency of the vertical polarization can be changed, with a 1.17 frequency tuning ratio. Since a combined frequency and polarization reconfigurable antenna has the capacity to deliver more flexibility and diversity than a single frequency- or polarization-agile antenna, it can bring significant benefits to many wireless communication systems. For example, software defined radios, which can be reconfigured by using many protocols, may operate at different frequencies and/or polarizations.

In this chapter, a single-feed combined frequency and polarization reconfigurable microstrip patch antenna is proposed with a maximum 1.67 frequency tuning ratio. The antenna can radiate one of three linear polarizations with a wide independent frequency tuning range for each polarization. The antenna has a simple structure so that it can be scaled to other frequencies easily. The polarization-agility mechanism is based on the principle presented in [6]. Compared to [6], however, the polarization of the proposed antenna can be electronically controlled by using PIN diodes. Moreover, the frequency of each polarization state can be tuned independently by using varactor diodes. To the best of our knowledge, this is the first single-port reconfigurable antenna design with independent control of the resonant frequency of three polarizations.

6.2 Reconfigurable Antenna Design

6.2.1 Antenna Structure and Operating Principle

The layout of the antenna is shown in Fig. 6.1. The length of the square substrate and the patch is 70 mm and 34 mm, respectively. The feed point is located along the diagonal line and 9 mm from the bottom of the patch edge. The centre of each edge of the patch is connected to a shorting post via a PIN diode (MA4PBL027). The diode represents a forward resistance of 2.8 Ω for the ON state and a parallel circuit with a capacitance of

0.03 pF and a resistance of 10 kΩ for the OFF state. Two varactor diodes (MGV 125-20-0805) with a 0.1 to 1.0 pF junction capacitance tuning range for a corresponding bias voltage from 20 to 2 V are located beside the PIN diode at each edge. The orientation of the diodes is also shown in Fig. 6.1. A Keithley 2400 SourceMeter is used to provide a constant bias current for PIN diodes and variable bias voltages for varactor diodes.

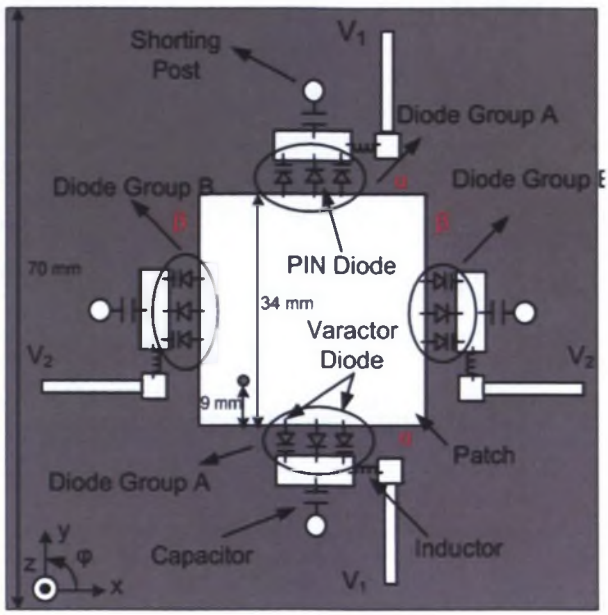

Figure 6.1: Schematics of the reconfigurable antenna.

A square patch antenna fed along the diagonal line without any connection to the ground plane will radiate x- and y- oriented modes, which have the same resonant frequency and equal amplitude and phase. By adding shorting posts in the middle of the patch edges α (Fig. 6.1), the resonant frequency of the y-oriented mode can be increased without affecting the x-oriented mode. This is because edges α are the radiating edges for the y-oriented mode. By attaching shorting posts which can be represented by inductors, the resonant frequency of the y-oriented mode is increased [6]. But the x-oriented mode will not be affected since its radiating edges are β. Similarly, by adding shorting posts in the middle of the patch edges β, the resonant frequency of the x-oriented mode

can be raised without affecting the y-oriented mode. Therefore, a single mode (x- or y-oriented) can be selected by shifting the resonant frequency of the undesired mode to be above that of the desired one. For each mode, two varactor diodes are mounted along the corresponding radiating edges to change the resonant frequency.

6.2.2 DC Bias Network

The diodes are divided into two groups. In order to bias the two groups of diodes separately, two independent dc bias voltages are applied to the terminals labeled V_1 and V_2, respectively, with respect to the square patch. The square patch is dc grounded. A surface-mount inductor (47 nH) is placed in series with each dc feed line at each terminal to choke the RF signal. A surface-mount capacitor (27 pF) is used to maintain the RF continuity (short circuit to the ground) and provide dc isolation between the two diode groups.

When $V_1 < 0$ V, the PIN diodes in group A are turned on and the edges α of the patch are shorted to ground. In this case, the varactor diodes in group A do not work as tunable capacitors since they are forward biased. When $V_1 > 0$ V, the PIN and varactor diodes in group A are reverse biased. The junction capacitance of the varactor diodes decreases when V_1 is increased. It is noted that the PIN diodes used in the antenna can stand a reverse voltage of up to 90 V. Such a high voltage allows the diodes to work with no risk of breakdown since the required reverse-bias voltage for the varactor diodes is only up to 20 V. Diodes in group B can work in the same way as group A since V_1 and V_2 are independent.

When $V_1 < 0$ V and $V_2 > 0$ V (patch is dc grounded), the edges α are connected to the shorting posts. Therefore, the frequency of the y-oriented (undesired) mode is shifted to be above the x-oriented one (desired). We choose the x-oriented one as the antenna operating mode (State I). In this case, the varactor diodes in group B that are attached

to the edges β are used to tune down the frequency of the x-mode continuously according to the junction capacitance (or reverse-bias voltage) of the varactor diodes. The analysis of the frequency tuning of the patch antenna by using varactor diodes is reported in [7], so it is not repeated here.

When $V_1 > 0$ V and $V_2 < 0$ V, we choose the y-oriented mode as the antenna operating mode (State II), and the varactor diodes in group A are used to tune the antenna resonant frequency.

When both V_1 and V_2 are positive, the antenna radiates 45^0 linear polarization (State III). In this case, the varactor diodes in groups A and B should be biased with the same reverse voltage in order to tune the frequency of this polarization. Furthermore, simulation results show that the input reflection coefficient is too high to be acceptable for most applications when both V_1 and V_2 are negative. The possible polarization states of the reconfigurable antenna and the corresponding diode states are summarized in Table 6.1. Fig. 6.2 shows the simulated results of the current distributions on the patch for the three polarization states of the antenna.

Table 6.1: Different polarization states of the reconfigurable antenna

	PIN Diodes in Group A	PIN Diodes in Group B	Polarization	Active Varactor Diodes
State I	Forward Biased	Reverse Biased	x-oriented	Group B
State II	Reverse Biased	Forward Biased	y-oriented	Group A
State III	Reverse Biased	Reverse Biased	45^0-oriented	Group A and B

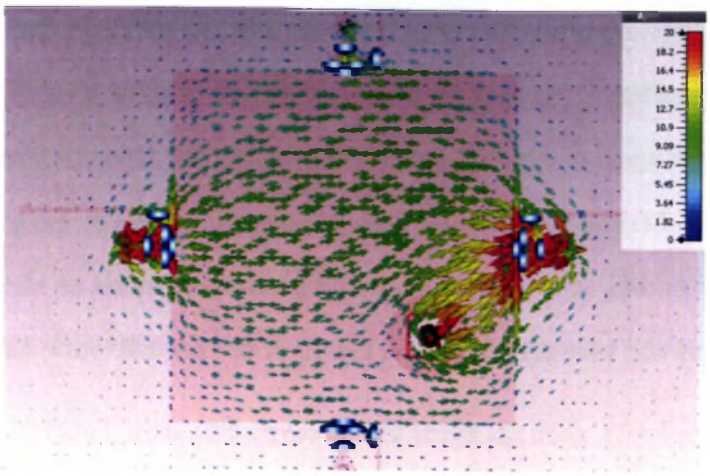

(a)

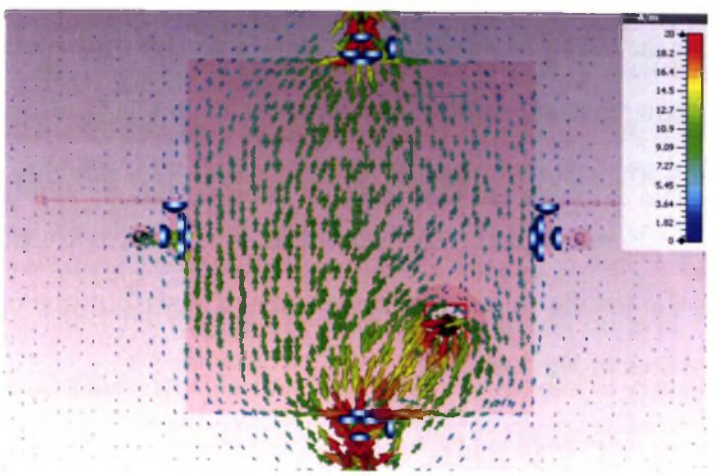

(b)

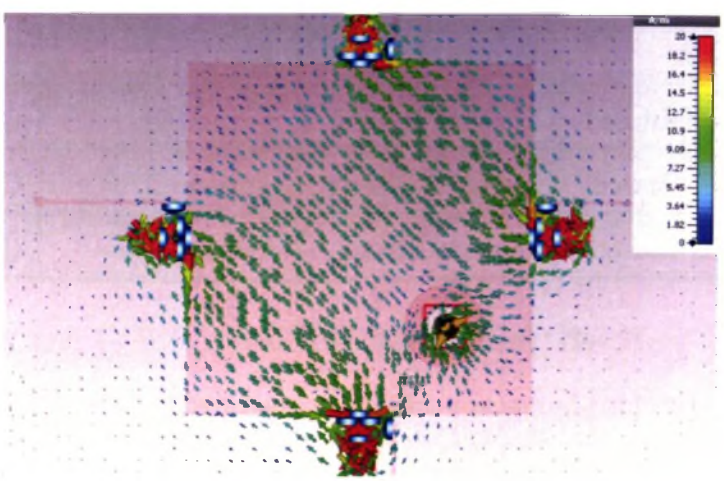

(c)

Figure 6.2: Current distributions on the patch:(a) State I; (b) State II; (c) State III.

6.3 Simulated and Measured Results

6.3.1 Input Reflection Coefficients

Based on the above analysis, an antenna prototype was fabricated on a 3.175-mm-thick RT/Duroid 5880 substrate (dielectric constant ε_r=2.2, $tan\delta$= 0.0009). Fig. 6.3 shows a photograph of the fabricated prototype.

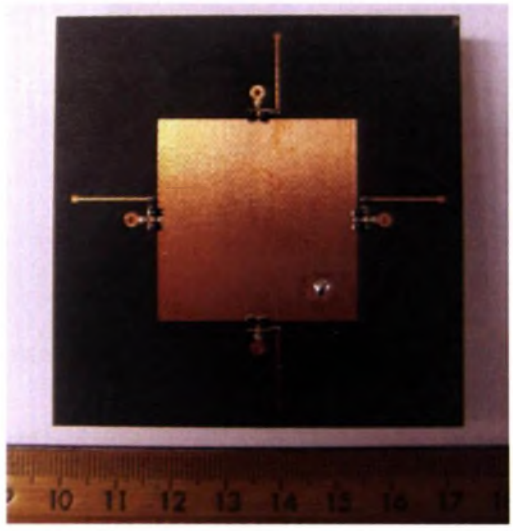

Figure 6.3: Photograph of the antenna prototype.

Figs 6.4 and 6.5 show the measured and simulated input reflection coefficients as a function of frequency under different bias voltages (varactor diode capacitances) for State I and State II, respectively. Due to the symmetrical structure, for different varactor diode capacitances, the simulated results for State I and State II are the same. As is seen from the measured results shown in Figs 6.4 and 6.5, the resonant frequency of the antenna can be tuned from 1.35 GHz to 2.25 GHz by varying the reverse-bias voltage from 2.2 V to 22 V (or 25 V), corresponding to a 1.67 tuning ratio. Minor bias-voltage changes are needed to compensate for the slight performance variations of individual diodes operating in the different polarization states.

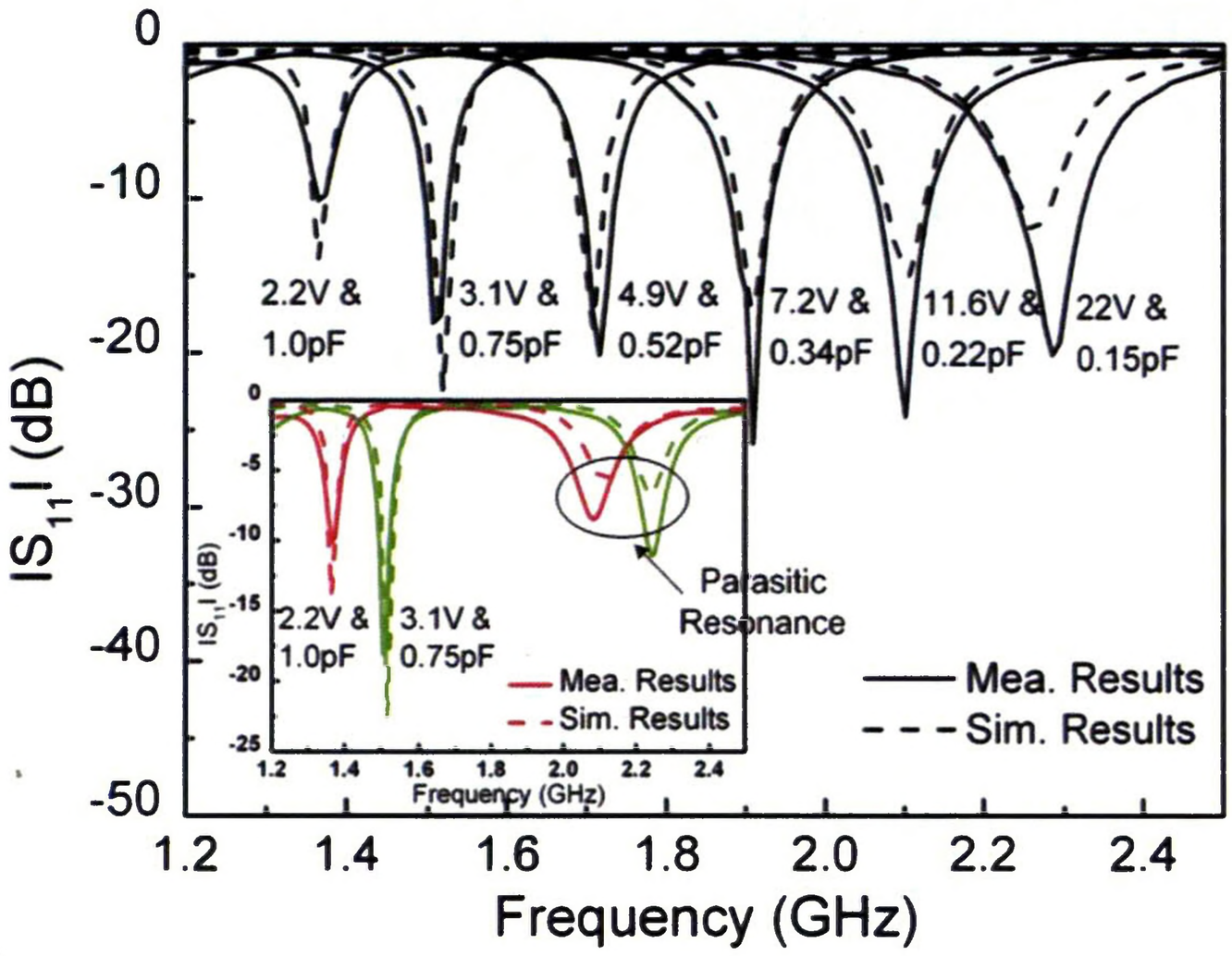

Figure 6.4: Measured and simulated input reflection coefficients for different bias voltages (varactor diode junction capacitances) for State I. The red and the green lines in the inset show the parasitic resonance of the antenna for the bias voltages of 2.2 V (1.0 pF) and 3.1V (0.75 pF), respectively.

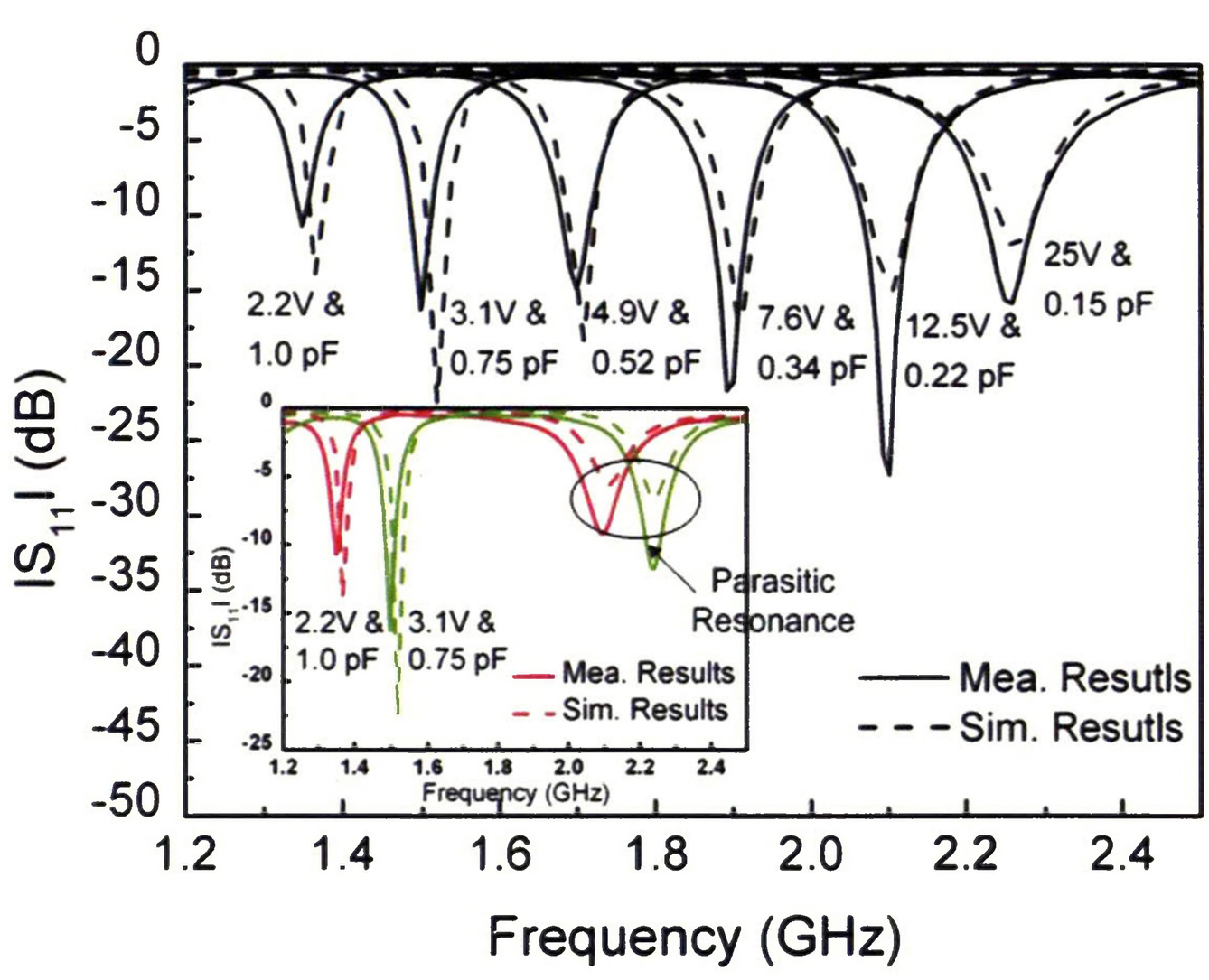

Figure 6.5: Measured and simulated input reflection coefficients for different bias voltages (varactor diode junction capacitances) for State II. The red and the green lines in the inset show the parasitic resonance of the antenna for the bias voltages of 2.2 V (1.0 pF) and 3.1V (0.75 pF), respectively.

In addition, as shown in the insets of Figs 6.4 and 6.5, there are parasitic resonances for the antenna under bias voltages of 2.2 V and 3.1 V (or corresponding capacitances). It should be pointed out that the parasitic resonance will not affect the performance of the operating modes since the radiation patterns at those frequencies, which have a null at boresight, are significantly different from a boresight patch antenna. Moreover, in practice, filters will be implemented in a system to reject other interference signals further. The parasitic resonances of the antenna under other voltages are not shown as they are higher than 2.5 GHz.

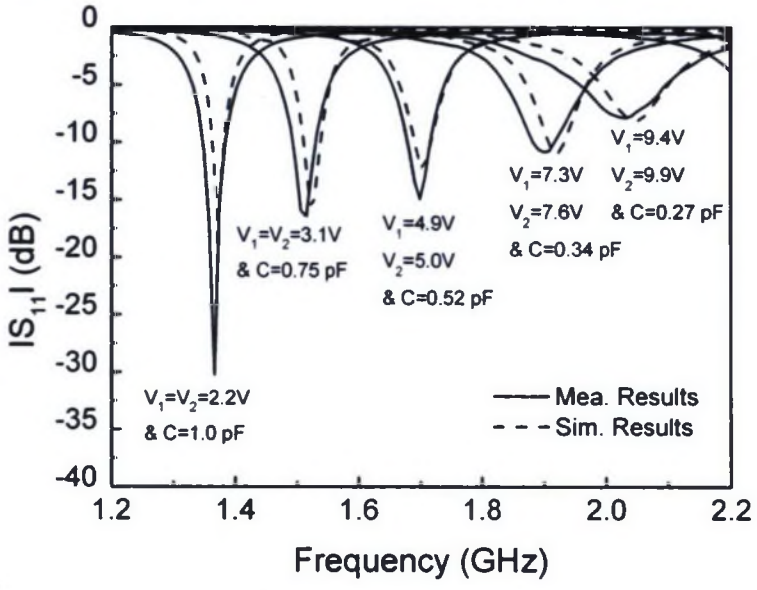

Figure 6.6: Measured and simulated input reflection coefficients for different bias voltages (varactor diode junction capacitances) for State III.

Fig. 6.6 shows the measured and simulated input reflection coefficients of the antenna for State III. From the measured results, it can be seen that the frequency of the antenna can be varied from 1.35 to 1.9 GHz across a bias voltage from 2.2 V to 7.6 V, corresponding to a 1.4 tuning ratio. Compared to State I or II, this tuning range is smaller. This is due to the fact that the feed-point location that determines the antenna impedance match is optimized for States I and II.

The slight discrepancy between the simulated and measured results in Figs 6.4, 6.5, and 6.6 can be mostly attributed to inaccuracies in the fabrication process and variations in the discrete component parameters from the values given in the manufacturer's data sheet. For the three polarization states of the antenna, the impedance bandwidth ($|S_{11}| \leqslant$ -10 dB) is greater than 20 MHz when the resonant frequency of the antenna is above 1.4 GHz.

6.3.2 Far-field Radiation Pattern

Radiation patterns were measured for the three polarization states of the proposed antenna. Simulated and measured normalized radiation patterns are compared in both E and H planes. The E-plane corresponds to the z-x plane ($\varphi = 0^0$) and the z-y plane ($\varphi = 90^0$) for State I and II, respectively. Because of the dc bias lines attached to the antenna, it is difficult to realize a 360^0 azimuth scan. A scan of 180^0 of the principal plane was conducted during the measurement.

Figs 6.7, 6.8, and 6.9 show the radiation patterns at 1.7 GHz for States I, II and III, respectively. In the above figures, boresight radiation patterns can be observed with a maximum cross-polarization level of -15 dB for all the polarization states. The cross-polarization level is less than -10 dB across the entire frequency tuning ranges for all the polarization states. Owing to the limited space, the measured and simulated radiation patterns for other frequencies are not presented.

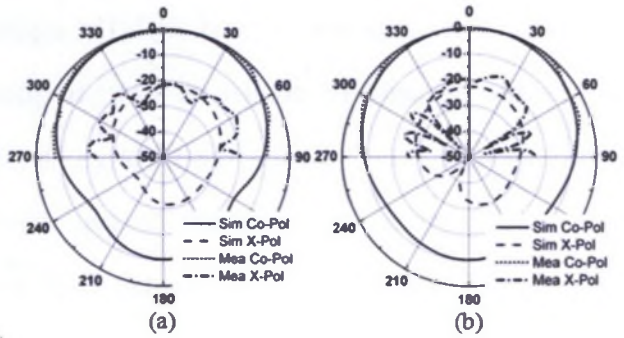

Figure 6.7: Measured and simulated normalized radiation patterns at 1.7 GHz for State I. Figs (a) and (b) are the E-plane and H-plane radiation patterns, respectively.

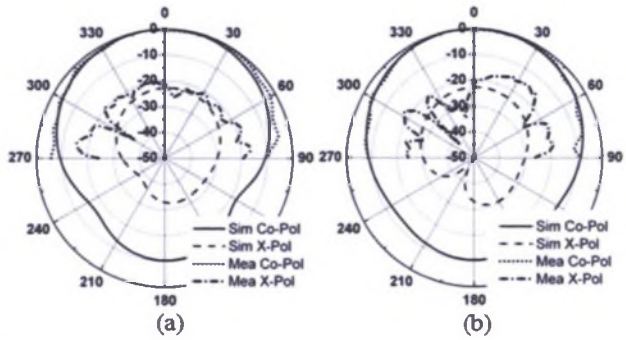

Figure 6.8: Measured and simulated normalized radiation patterns at 1.7 GHz for State II. Figs (a) and (b) are the E-plane and H-plane radiation patterns, respectively.

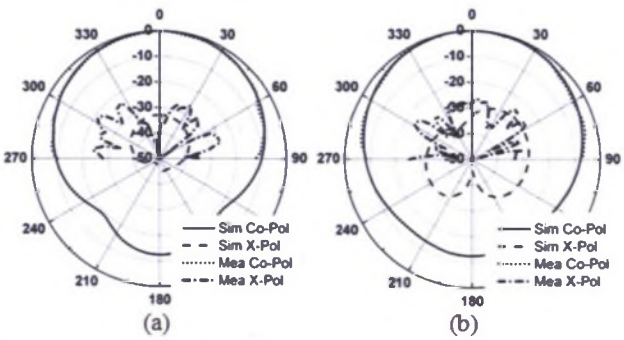

Figure 6.9: Measured and simulated normalized radiation patterns at 1.7 GHz for State III. Figs (a) and (b) are the E-plane and H-plane radiation patterns, respectively.

Additionally, the measured and simulated realized gains were compared for the three polarization states, as shown in Fig. 6.10. The measured realized gain varies from -2.6 to

6.4 dBi from 1.4 to 2.25 GHz. The gains are reduced with the operating frequency. This is because the antenna becomes electrically smaller at lower frequencies. In addition, at high capacitance levels, increased RF current flowing through the diodes makes the I^2R loss increase, which leads to lower gains. In addition, the side effects of PIN diodes and varactor diodes on the antenna gains are examined. For the PIN diode, it acts as a 2.8 Ω resistor when it is switched on. Simulation results show that the antenna realized gain is almost stable when the value of this resistor changes to zero. Therefore, the PIN diodes have little effect on the antenna gain. For varactor diodes, the loss of a varactor diode is represented by a series resistance of 1.6 Ω. Simulation results show that the realized gain of the antenna increases by 1 dB when the resistance is reduced to zero. In order to minimize the effects of varactor diodes on the antenna gain, the diodes with lower series resistance should be used.

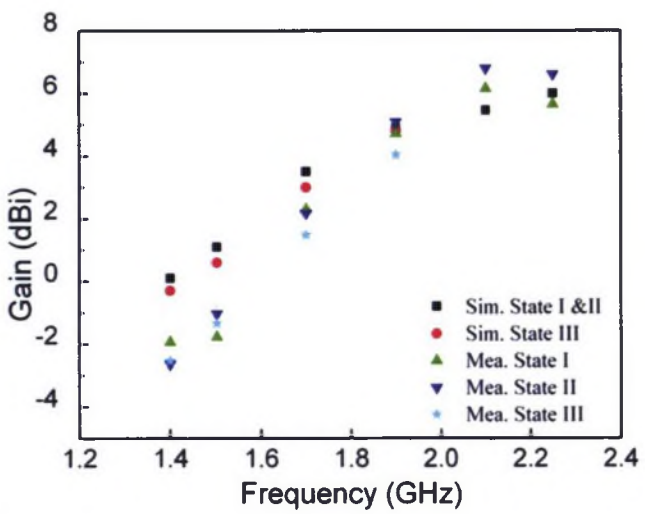

Figure 6.10: Measured and simulated gains of the antenna.

Chapter 7

Applications of Reconfigurable Antennas in MIMO Systems

7.1 Introduction

The multiple-input-multiple-output (MIMO) technique has demonstrated a potential to increase spectral efficiency (more bits per second per hertz) and link reliability (reduced fading). It is characterized by multiple antenna elements at the transmitter and receiver. Compared to single-input-single-output (SISO) systems, MIMO systems exploit the spatial properties of the multipath channel, thereby providing a new dimension which can be used to enhance the communication performance [145-147]. Therefore, MIMO technology is currently being considered as a strong candidate for the physical-layer transmission scheme of next generation wireless communication systems.

Since modern wireless communication environments usually change fast, in order to achieve optimized system performance it is necessary for a MIMO system to be able to change its coding and signal-processing schemes as well as its radiating and receiving characteristics according to the varying channel conditions and system requirements. MIMO

techniques which fulfil this purpose are called reconfigurable MIMO techniques. The MIMO techniques that have the ability to vary the signal-processing algorithms in order to adapt to the changed channel characteristics are called software-reconfigurable MIMO techniques. Those having the capability to change the physical antenna configurations according to some desired antenna array properties, resulting in improved system performance, are called hardware-reconfigurable MIMO techniques. Due to the scope of the research of the author, only hardware-reconfigurable MIMO techniques are investigated. Generally, there are two antenna diversity schemes employed in hardware-reconfigurable MIMO systems, namely polarization diversity and pattern diversity. Since reconfigurable antennas are capable of varying their polarizations and radiation patterns, they can be incorporated in reconfigurable MIMO systems to realize different antenna diversity schemes.

Recently, some research work [91-101] has been devoted to employing reconfigurable antennas to increase MIMO system capacity. Generally, there are two methods to enhance MIMO system capacity by employing reconfigurable antennas. The first is to reduce the sub-channel correlation by using polarization or pattern reconfigurable antennas. Specifically, this is implemented by switching between different configurations of reconfigurable antenna arrays according to the varying channel conditions. The polarization or pattern diversity in some of the configurations can be used to achieve low sub-channel correlation. The second is to increase the received signal power by changing the antenna radiation patterns according to the channel information.

In this chapter, the effects of reconfigurable antennas on MIMO system capacity are investigated. The work is divided into two parts. First, the polarization reconfigurable antennas proposed in Chapter 4 are incorporated in a 2×2 MIMO-orthogonal frequency division multiplexing (MIMO-OFDM) demonstrator and the channel measurements are conducted in both line-of-sight (LOS) and non-LOS (NLOS) indoor environments. Measured results show that transmit/receive antennas radiating different polarizations are

able to improve the system capacity significantly compared to antennas with the same polarization. Second, the pattern reconfigurable antennas proposed in Chapter 5 are incorporated in the same MIMO-OFDM system. Omnidirectional antennas are used as a reference for capacity comparison; similar channel measurements are conducted as for the polarization reconfigurable antennas. It is shown that compared to omnidirectional antennas, pattern reconfigurable antennas can enhance system capacity, with 17% improvement in a LOS scenario and 12% in a NLOS scenario at a signal-to-noise ratio (SNR) of 10 dB.

7.2 Application of Polarization Reconfigurable Antennas in MIMO Systems

Many researchers have investigated the ability of antenna polarization diversity to improve MIMO system capacity [92-94]. In [92-94], the enhancement of MIMO system capacity by using antenna linear-polarization diversity (vertical and horizontal) has been analysed. However, relatively few papers have examined the effects of circular-polarization diversity on MIMO capacity. In [95], the behaviour of a MIMO system with circular-polarization reconfigurable antennas was simulated and the diversity gain was shown, but the capacity gain result was not reported. Therefore, a measurement-based analysis of system capacity is still needed.

In this section, the real-time channel of a 2×2 MIMO-OFDM system with four circular-polarization reconfigurable antennas is measured in both LOS and NLOS indoor environments. System capacities versus SNR are calculated for different antenna configurations.

7.2.1 Polarization Reconfigurable Antennas in the MIMO-OFDM System

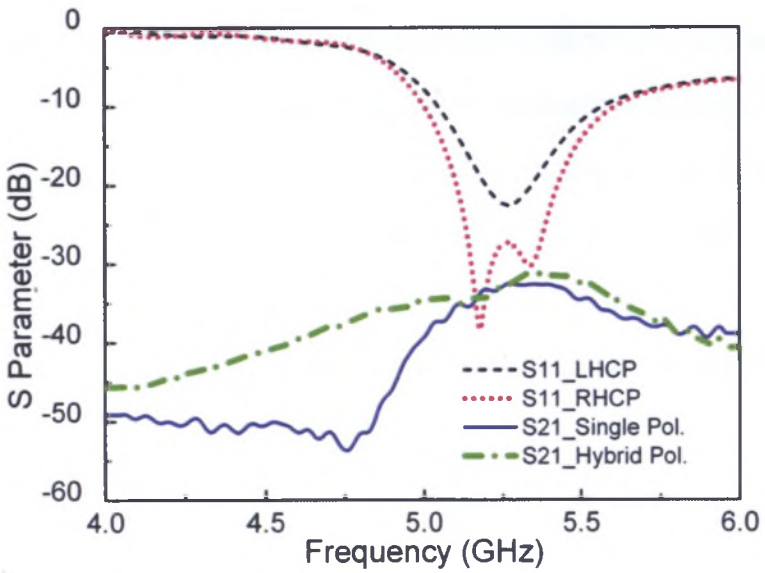

(a)

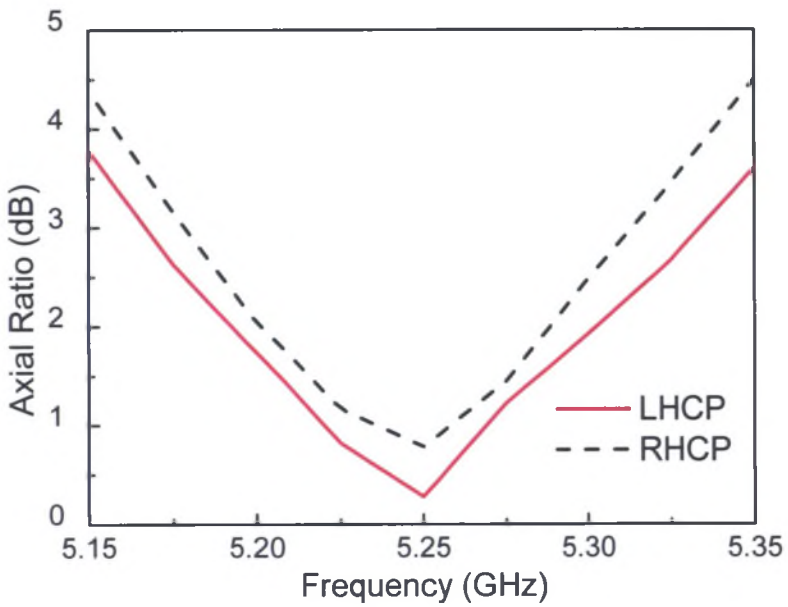

(b)

Figure 7.1: Measured performance of the scaled reconfigurable antennas: (a) S parameters; (b) Axial ratios.

A microstrip U-slot patch antenna that allows switching between RHCP and LHCP has been presented in Chapter 4. The measured overlapped bandwidth ($|S_{11}| \leqslant$ -10 dB and axial ratio less than 3 dB) for LHCP and RHCP is 2.8% centred at 5.77 GHz. Since the MIMO demonstrator designed by the CSIRO ICT Centre (Sydney, Australia) operates at 5.25 GHz, the antenna in Chapter 4 is scaled to work at 5.25 GHz. The measured reflection coefficients and axial ratios of the scaled antenna are shown in Fig. 7.1(a) and (b), respectively. The measured realized gain is about 7.4 dBic for LHCP and RHCP at 5.25 GHz.

Table 7.1: Four configurations of the reconfigurable antennas

Array Configuration	Antenna 1	Antenna 2
1	LHCP	RHCP
2	RHCP	LHCP
3	RHCP	RHCP
4	LHCP	LHCP

At each end of the MIMO-OFDM system, there are two reconfigurable antennas working as a two-element array. However, this does not imply that the array operates as a traditional beamforming array. Rather, each antenna has its own radiation characteristics. As each reconfigurable antenna has two polarization states, there are four configurations of the reconfigurable antennas at each end, as shown in Table 7.1. For each measurement, the configuration of the receive antennas is the same as that of the transmit antennas. In this paper, the system with antenna configuration 1 or 2 is referred to as the hybrid-polarization system, and the system with antenna configuration 3 or 4 is referred to as the single-polarization system.

When two antennas are located close to each other, the mutual coupling can produce pattern distortion and should be eliminated. Therefore, the spacing of the two antennas

at both ends is set to be one wavelength in order to keep the mutual coupling to an acceptable level. Measured results in Fig. 7.1 (a) show that the antenna mutual coupling is less than -25 dB at this spacing for both the single- and hybrid-polarization systems.

When evaluating the MIMO antenna array performance, the envelope correlation coefficient is another critical parameter as it provides a measure of antenna diversity performance. The antenna diversity will be better if the correlation coefficient is lower. The envelope correlation coefficient ρ_e can be calculated using the farfield radiation patterns of the antenna [134]

$$\rho_e = \frac{\left|\iint_{4\pi} \bar{F}_1(\theta,\phi)\cdot\bar{F}_2^*(\theta,\phi)d\Omega\right|^2}{\iint_{4\pi}\left|\bar{F}_1(\theta,\phi)\right|^2 d\Omega\cdot\iint_{4\pi}\left|\bar{F}_2(\theta,\phi)\right|^2 d\Omega} \tag{7.1}$$

where $\bar{F}_i(\theta,\phi)$ is a complex vector indicating the electric field radiated from the ith element. A series of approximations are used to calculate the integrations in (7.1).

$$\int_0^{\pi} f(\theta)sin\theta d\theta = \sum_{i=1}^{N}[f(\theta_i)sin(\theta_i)]\Delta\theta_i \tag{7.2}$$

$$\Delta\theta_i = \frac{\pi}{N} \tag{7.3}$$

$$\theta_i = i\frac{\pi}{N}, i = 1,2,3,...N \tag{7.4}$$

The envelope correlation coefficient between the patterns generated at the two ports of the antenna array for different configurations (Table 7.1) is estimated by using equation (7.1) based on the simulated radiation patterns. Table 7.2 gives the envelope correlation coefficients for different antenna array configurations at 5.25 GHz. It is evident that the envelope correlation coefficients of the configurations (1, 2) having polarization diversity are lower than those (3, 4) with the same antenna polarizations. In addition, it is observed that all the coefficients are below 0.5, which satisfies the criterion for enabling the antenna to provide a good level of diversity [134].

Table 7.2: Envelope correlation coefficients of different array configurations

Array Configuration	ρ_e
1	2.62×10^{-5}
2	2.62×10^{-5}
3	1.12×10^{-2}
4	1.19×10^{-2}

7.2.2 MIMO-OFDM Demonstrator

Actual MIMO-OFDM channel coefficients were measured using the MIMO-OFDM hardware demonstrator [148] designed in the CSIRO ICT Centre. It operates at 5.25 GHz and supports an operational bandwidth of 40 MHz. The receive antennas are connected to an antenna array positioner controlled by a computer. The channel training sequence is designed to estimate the frequency response over 114 OFDM subcarriers in a 40 MHz bandwidth with a subcarrier spacing of 312.5 kHz.

7.2.3 Measurement Location and Process

The 2× 2 MIMO-OFDM channel measurement was conducted in the CSIRO ICT Centre indoor environment, which consists of both concrete and gypsum-board walls, glass windows and wooden doors. The channel is measured in LOS over a 5m distance and NLOS over a 10m distance. The layout of the LOS and NLOS testing scenarios is shown in Fig. 7.2. For the LOS scenario, both the transmitter and receiver are located in the same laboratory (Lab 1) equipped with some metal bookshelves and cabinets. For the NLOS scenario, the transmitter is moved to Lab 2 while the receiver remains in Lab 1.

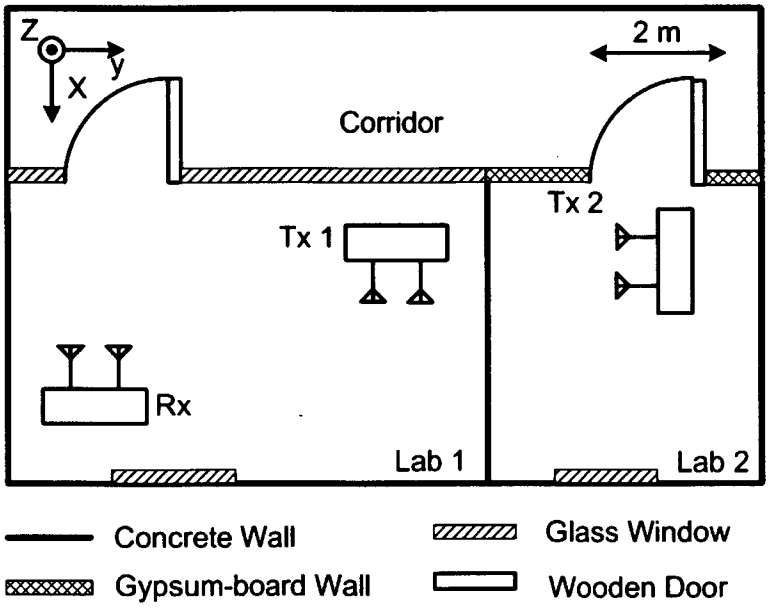

Figure 7.2: Layout of the indoor MIMO-OFDM test environment.

Each reconfigurable antenna is placed vertically as shown in Fig. 7.3. In the LOS scenario, the reconfigurable antennas at transmit (Tx1) and receive ends are configured to face each other. In the NLOS scenario, the reconfigurable antennas at transmit (Tx2) and receive ends are configured to face the negative y and negative x directions, respectively.

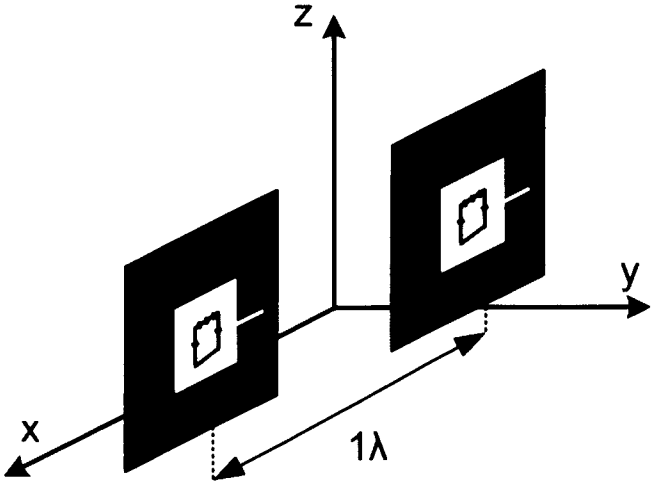

Figure 7.3: Orientation of the reconfigurable antennas.

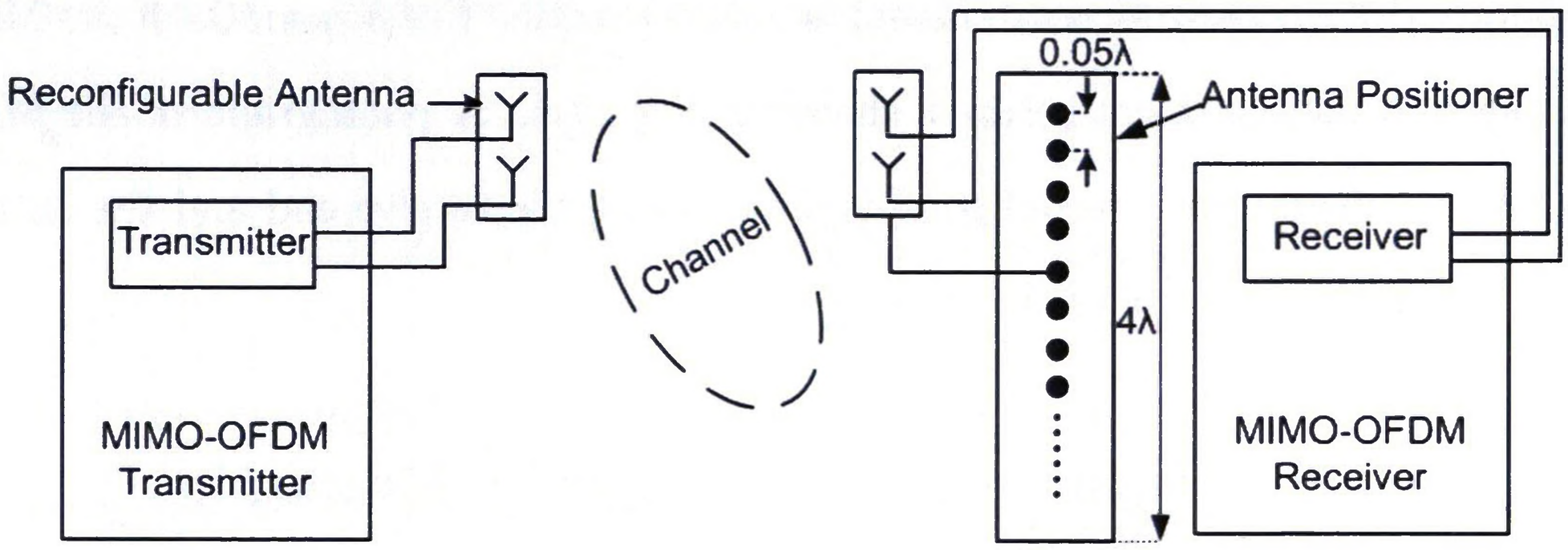

Figure 7.4: The schematic of the MIMO-OFDM system measurement setup. The dc power supply for the reconfigurable antennas is not shown in this schematic.

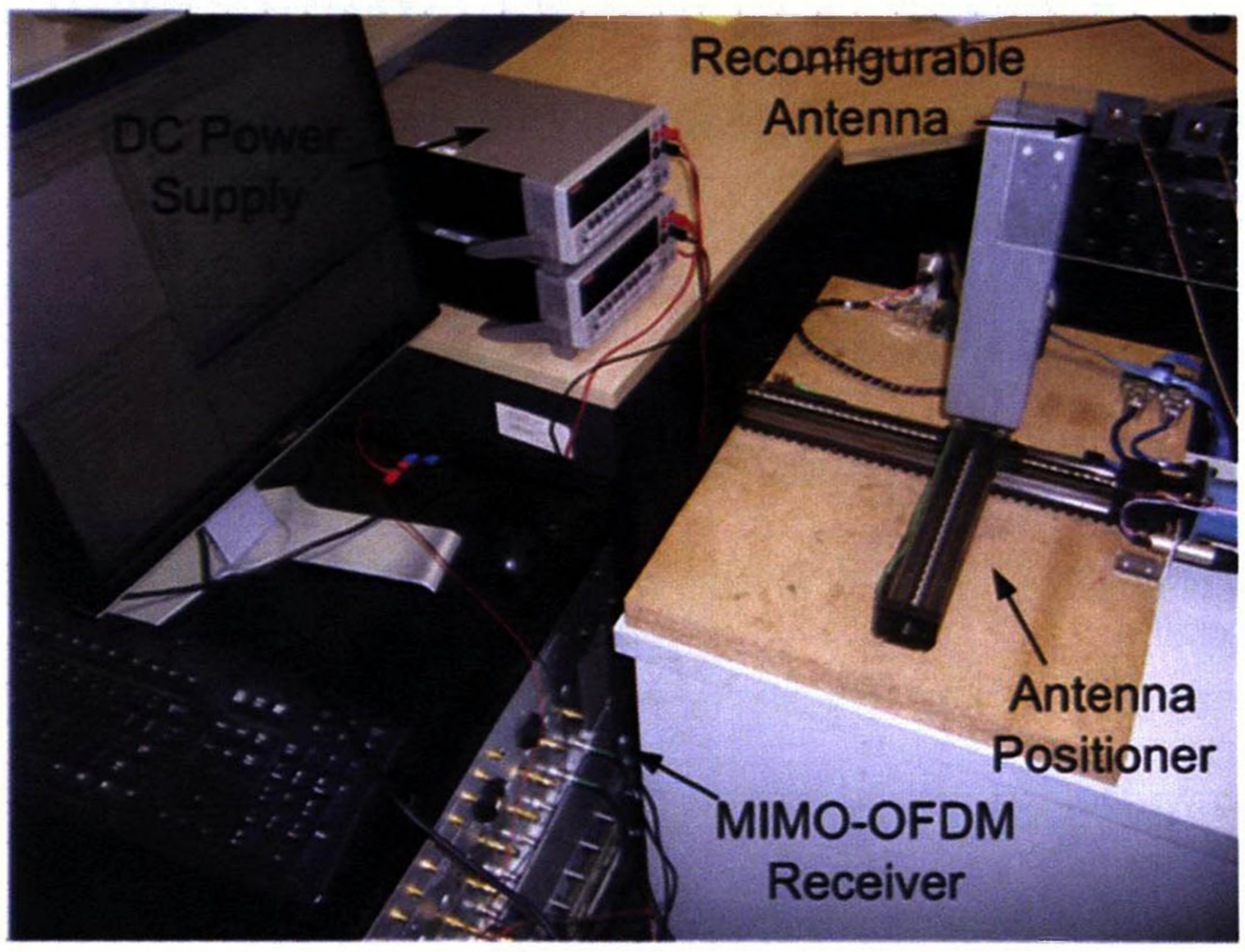

Figure 7.5: MIMO-OFDM receiver with reconfigurable antennas.

For each measurement, the antenna positioner moves the receive antenna array to 80 location samples with 0.05 wavelength increments. The position of the transmit antennas is fixed.

In each scenario only the antenna polarizations are changed. Any other factor that can possibly vary the channel characteristics, such as the number of scatterers and their positions, remains the same. The measurement was performed during the night to avoid

human activities, so the test environment is entirely static. The schematic of the MIMO-OFDM system measurement setup is shown in Fig. 7.4. A photograph of the MIMO-OFDM demonstrator with reconfigurable antennas at the receive end and the dc power supply is shown in Fig. 7.5.

7.2.4 Channel Measurement and Capacity Estimation

The MIMO-OFDM channel is characterized by its coefficient matrix, the elements of which are the complex ratio of the signal output from the *ith* receive antenna over the signal input to the *jth* transmit antenna at the *kth* OFDM subcarrier and the *lth* location sample. The Shannon capacity of a MIMO-OFDM channel is given by [149]

$$C = \frac{1}{m \cdot n} \sum_{l=1}^{m} \sum_{k=1}^{n} log_2 \times [det(I_{N_r} + \frac{SNR}{N_t} \overline{H(i,j,k,l)} \cdot \overline{H(i,j,k,l)}^{+}))] \qquad (7.5)$$

where C is the system capacity in bits/second/Hz, m is the number of sub-carriers, n is the number of location samples, N_r is the number of receive antennas, N_t is the number of transmit antennas, I_{N_r} is the $N_r \times N_r$ identity matrix, $\overline{H(i,j,k,l)}$ is the normalized channel matrix, the superscript + denotes the conjugate transpose, and SNR is the average signal-to-noise ratio over all receive array elements. The capacity of a wideband channel is the value of the capacities averaged over all subcarriers of the MIMO-OFDM system and the 80 location samples.

From (7.5), it is known that there are two ways to improve the capacity of a MIMO system. The first is to increase the amount of power received, which is reflected in the SNR. The second is to reduce the sub-channel correlation coefficient by increasing the diversity of the system, which is reflected in $\overline{H(i,j,k,l)} \cdot \overline{H(i,j,k,l)}^{+}$. The received power and system diversity are related to the performance of the antennas.

It is convenient to use the normalized channel matrix so that the system capacity can be derived as a function of the SNR per receive antenna averaged over all OFDM

subcarriers, receive antenna location samples and MIMO sub-channels. The normalization is performed as follows

$$\overline{H(i,j,k,l)} = \frac{H(i,j,k,l)}{\sqrt{\frac{1}{N_r \cdot N_t \cdot m \cdot n} \|H(i,j,k,l)\|^2}} \tag{7.6}$$

where $\|H\|$ denotes the Frobenius norm of the channel matrix.

When analysing the power transmission of a hybrid-polarization system, it is known that if the transmit antenna is LHCP, the power received by a RHCP antenna will be lower than that received by a LHCP antenna, especially in a LOS scenario. A similar statement can be made for the transmission of a RHCP antenna. Therefore, in a LOS scenario, the hybrid-polarization system always receives less power than the single-polarization system, which will lead to a lower value of $\|H\|$. If the channel matrix of each array configuration is normalized to a common factor, compared to the single-polarization system, the hybrid-polarization system will suffer a capacity loss due to the smaller $\|H\|$. In order to separate the effect of sub-channel correlation on the system capacity from the effect of power gain, two different channel-matrix normalization methods are employed.

The first is that the channel matrix of each antenna array configuration is normalized independently (Method I). In this case, the power gain is not included in the capacity calculation. Therefore, only the effect of the sub-channel correlation is kept in the capacity evaluation. The second is that the channel matrix of each antenna array configuration is normalized with respect to that of a selected configuration (Method II). In this paper, antenna configuration 4 is picked as the reference. In this way, not only the subchannel correlation but also the relative received power difference is preserved in the capacity calculation.

7.2.5 Results and Analysis

Fig. 7.6 (a) and (b) show the system capacity improvement for different antenna array configurations in the LOS scenario calculated by Method I and Method II, respectively. Fig. 7.7 (a) and (b) show the system capacity improvement for different antenna array configurations in the NLOS scenario calculated by Method I and Method II, respectively. For each scenario, the capacity improvement is the difference in capacity between each antenna array configuration and configuration 4. Then the improvement is normalized with respect to the capacity of configuration 4.

From Figs 7.6 and 7.7, it is seen that, in both scenarios and for both calculation methods, the system capacities for array configurations 1 and 2 are very close to each other although there is a small variation. The same happens to configurations 3 and 4. The slight difference can be attributed to two factors. The first is that the channels are not exactly the same when the antennas are switched from configuration 1 to 2 or from configuration 3 to 4 since the polarization of each antenna in the channel is changed. The second is that there is a slight variation in the performance of the four antennas, such as the axial ratio and the realized gain, due to inaccuracies in the fabrication process.

In the LOS scenario it can be noted that, compared with a single-polarization system, its hybrid-polarization counterpart delivers significant improvement to the system capacity for both calculation methods. At an SNR of 15 dB, for instance, the peak improvements are approximately 36% and 16% for Method I and Method II, respectively. This is because by using antenna polarization diversity the subchannel correlation is reduced and the system capacity is improved, especially for the environment with insufficient scatterers. However, it is apparent that the percentage improvement of Method II is lower than that of Method I (20% lower at an SNR of 15 dB). The reason is that the $\|H\|$ of the hybrid-polarization system is smaller than that of the single-polarization system due to the power loss. Using Method II, this effect is taken into account because the chan-

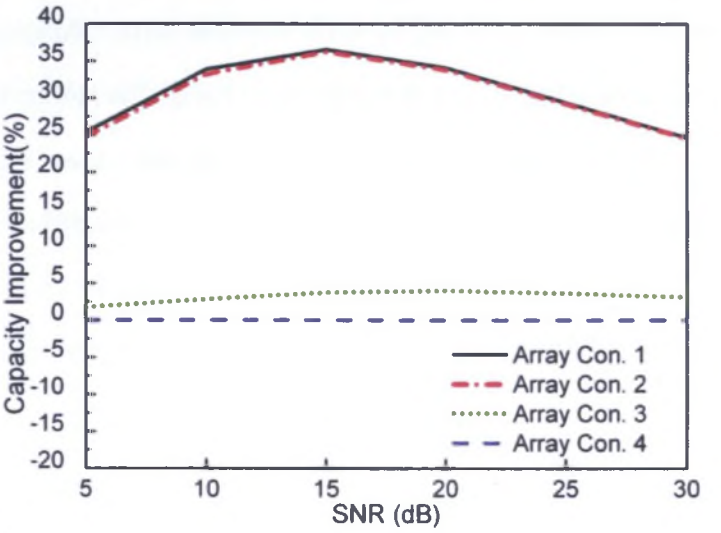

(a)

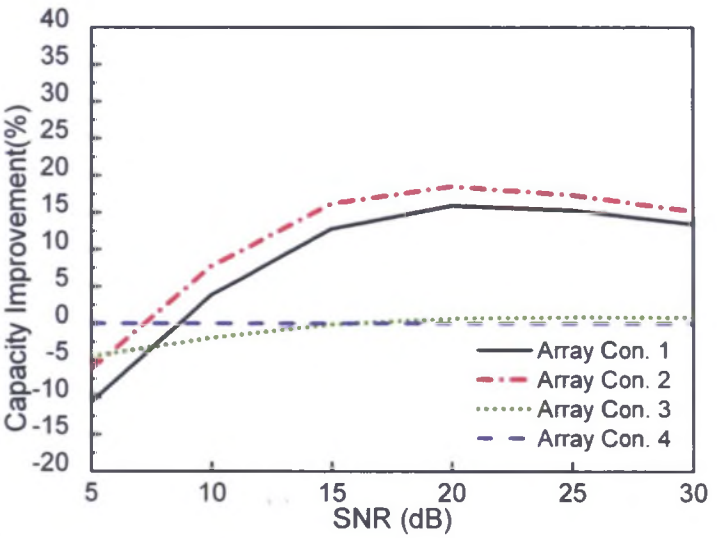

(b)

Figure 7.6: In the LOS scenario, the percentage improvement of the reconfigurable MIMO system capacity versus SNR for: (a) Method I; (b) Method II.

nel matrix of each antenna array configuration is normalized to that of antenna array configuration 4. In this way, the normalized channel matrices of the hybrid-polarization systems are scaled down by a factor due to the normalization; hence the improvement of the capacity is reduced.

In addition, the total power received by each antenna array configuration with respect to that of antenna array configuration 4 is shown in Table 7.3. From the table, it is seen that in the LOS scenario configuration 1 or 2 receives less power than configuration 3 or 4, which agrees well with the analysis in Section 7.2.4. The difference of the received power between configurations 1 and 2 or configurations 3 and 4 can be mostly attributed to the slight variance of the behaviour of the four reconfigurable antennas and the test environments.

Table 7.3: Relative power received for different antenna configurations in LOS and NLOS scenarios

	Con.1	Con.2	Con.3	Con.4
LOS	0.64	0.55	0.90	1.0
NLOS	0.86	0.85	0.92	1.0

In the NLOS scenario, for calculation Method I, it is seen from Fig. 7.7 (a) that the hybrid-polarization system always performs better than the single-polarization system. At an SNR of 15 dB, for instance, the peak improvement is 6.7%. This smaller improvement compared to the LOS case is due to the fact that there is a rich multipath environment in an indoor NLOS scenario so that the subchannel correlation of the single-polarization system has been already quite low. Therefore, the improvement of the system capacity by reducing the subchannel correlation is limited. On the other hand, it can be observed from Table 7.3 that the received power difference between the single- and hybrid-polarization systems in the NLOS scenario becomes smaller. This is mostly attributed to the fact that the scatterers and reflectors that produce rich multipath propagation also scatter much power from the transmit polarization into the orthogonal polarization [150]. Therefore, the hybrid-polarization system will not suffer much power loss in the NLOS scenario. However, the power difference between the hybrid and single polarization systems still

leads to a capacity improvement reduction for Method II. Therefore, at an SNR of 15 dB, the relative increase of capacity is 1.9% with respect to the single-polarization system, as shown in Fig. 7.7 (b).

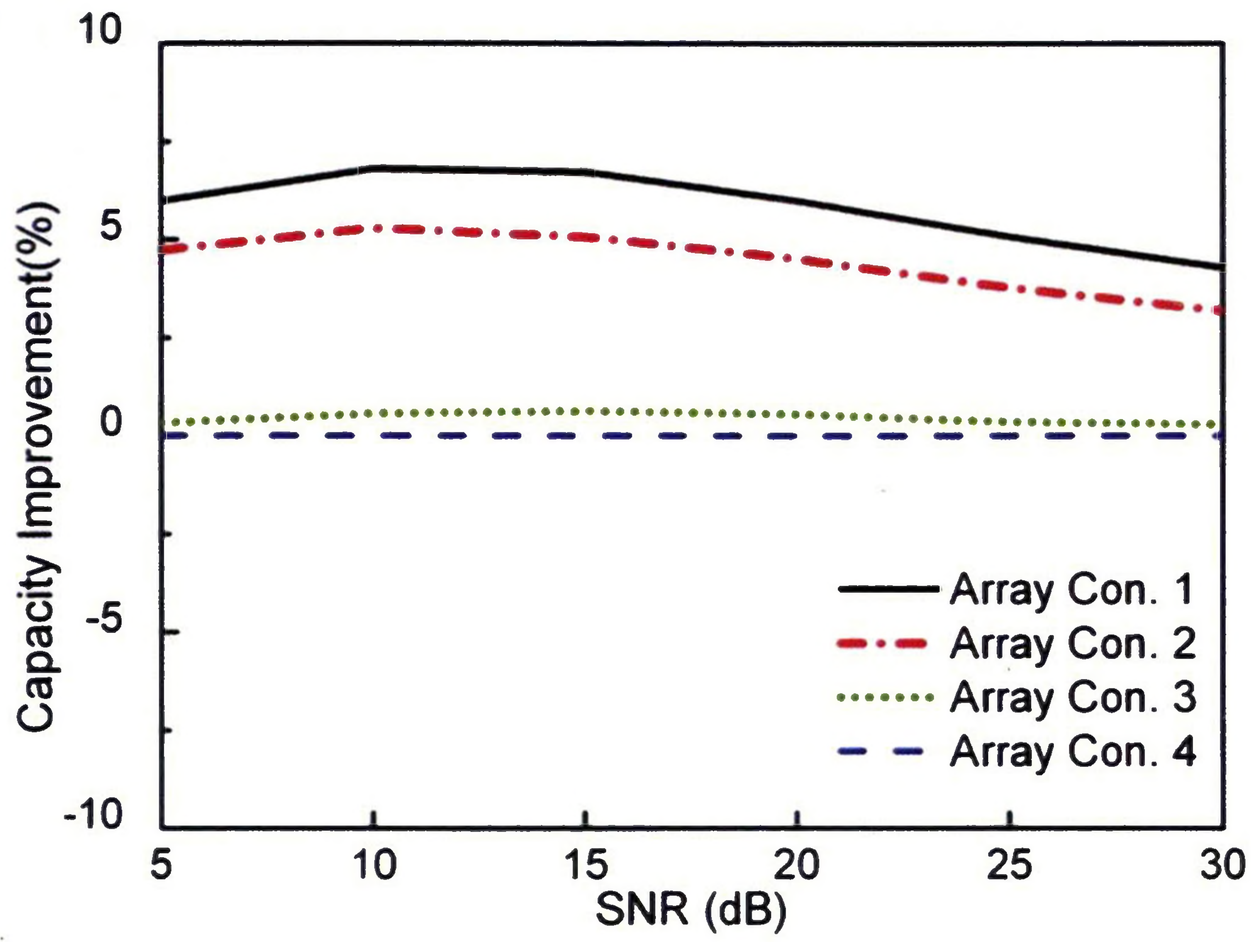

(a)

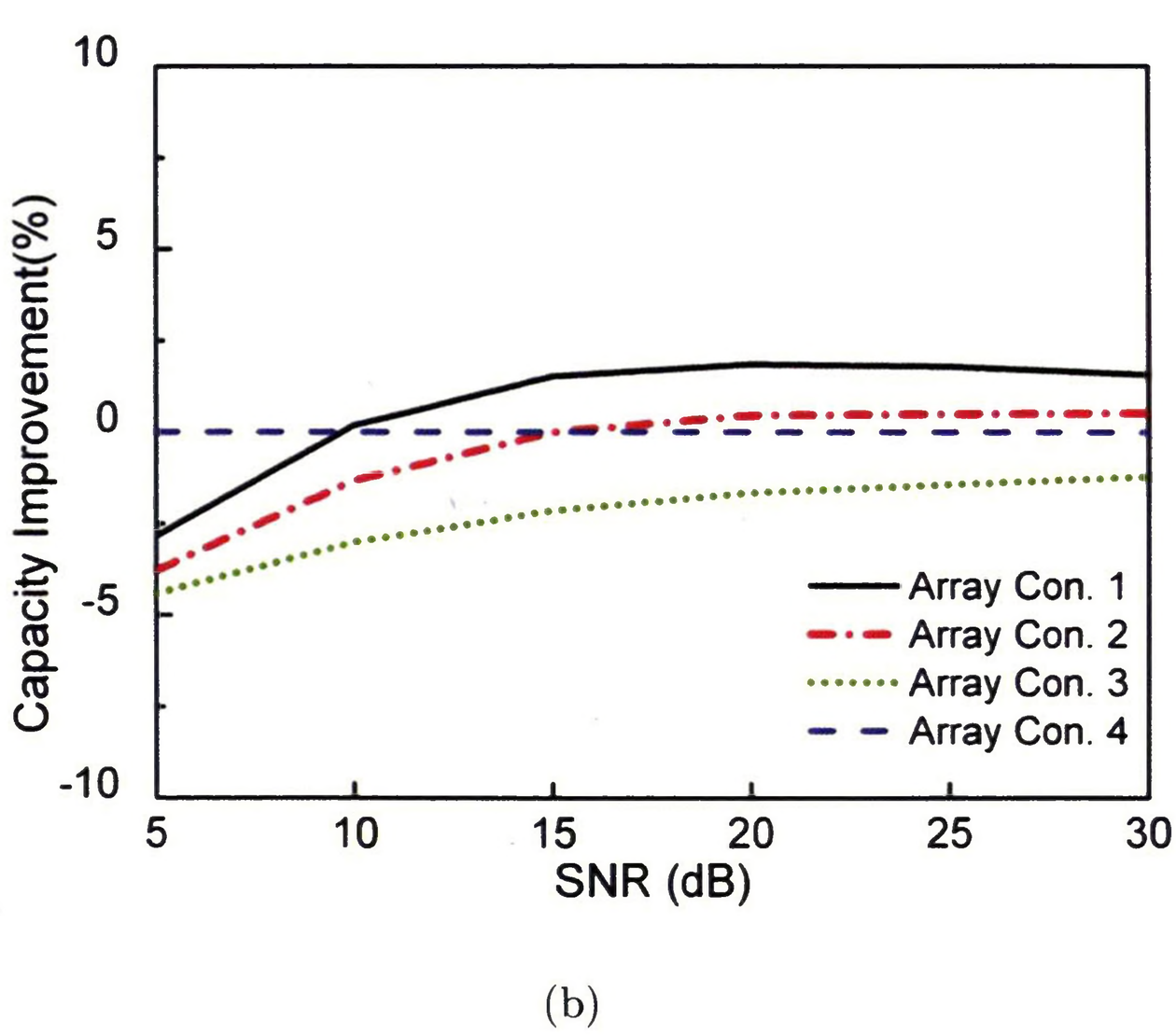

(b)

Figure 7.7: In the NLOS scenario, the percentage improvement of the reconfigurable MIMO system capacity versus SNR for: (a) Method I; (b) Method II.

7.3 Application of Pattern Reconfigurable Antennas in MIMO Systems

Very recently, pattern reconfigurable antennas have found new applications in MIMO systems [97-101]. In [97], a MIMO system with pattern reconfigurable antennas was tested in an anechoic chamber with artificial objects acting as scatterers that make up a multipath environment. The system capacity increase is mostly attributed to the increase of average receiver signal-to-noise ratio (SNR) by changing the main-beam direction. In [98-101], the capacity of a MIMO system was increased by exploiting antenna pattern diversity to introduce sub-channel decorrelation to the MIMO system.

In this section, the pattern reconfigurable U-slot antennas proposed in Chapter 5 are incorporated in a 2×2 MIMO-OFDM system. Channel measurements are conducted in both LOS and NLOS indoor environments. Omnidirectional antennas are used as reference antennas for capacity comparison. It is known that an omnidirectional antenna can receive rich multipath, which can lead to low sub-channel correlation [100]. Therefore, a capacity comparison between systems with reconfigurable and omnidirectional antennas is necessary for highlighting the effect of pattern diversity on the sub-channel correlation.

7.3.1 Pattern Reconfigurable Antennas in the MIMO-OFDM System

The antennas incorporated in the MIMO-OFDM system are the pattern reconfigurable antennas proposed in Chapter 5. At each end of the MIMO-OFDM system, there are two reconfigurable antennas working as a two-element array. However, this does not imply that the array operates as a traditional beamforming array. Rather, each antenna has its own radiation characteristics. As each reconfigurable antenna has three states, there are nine configurations of the antennas at each end. For each measurement, the configuration

of the receive antennas is the same as for the transmit antennas. Table 7.4 gives the nine configurations of the reconfigurable antennas.

Table 7.4: Nine array configurations of the reconfigurable antennas at transmit end

Array Configuration	Antenna 1	Antenna 2
1	State 1	State 1
2	State 1	State 2
3	State 1	State 3
4	State 2	State 1
5	State 2	State 2
6	State 2	State 3
7	State 3	State 1
8	State 3	State 2
9	State 3	State 3

When two antennas are located close to each other, the mutual coupling can produce pattern distortion and should be eliminated. Therefore, the spacing of the two antennas at both ends is set to be one wavelength in order to keep the mutual coupling to an acceptable level. The measured results in Fig. 7.8 show that the mutual coupling is lower than -20 dB for all configurations at this spacing. The mutual coupling results for configurations 4, 7 and 8 are not shown since they have the same results as configurations 2, 3 and 6, respectively.

For the reference antenna, in our study, commercially available omnidirectional antennas (Sky-Cross SMA-5250-UA) are used that have omnidirectional patterns with peak gain at 2.2 dBi. The spacing of the two antennas is also set to be one wavelength to keep the mutual coupling below -20 dB.

The envelope correlation coefficient between the patterns generated at the two ports

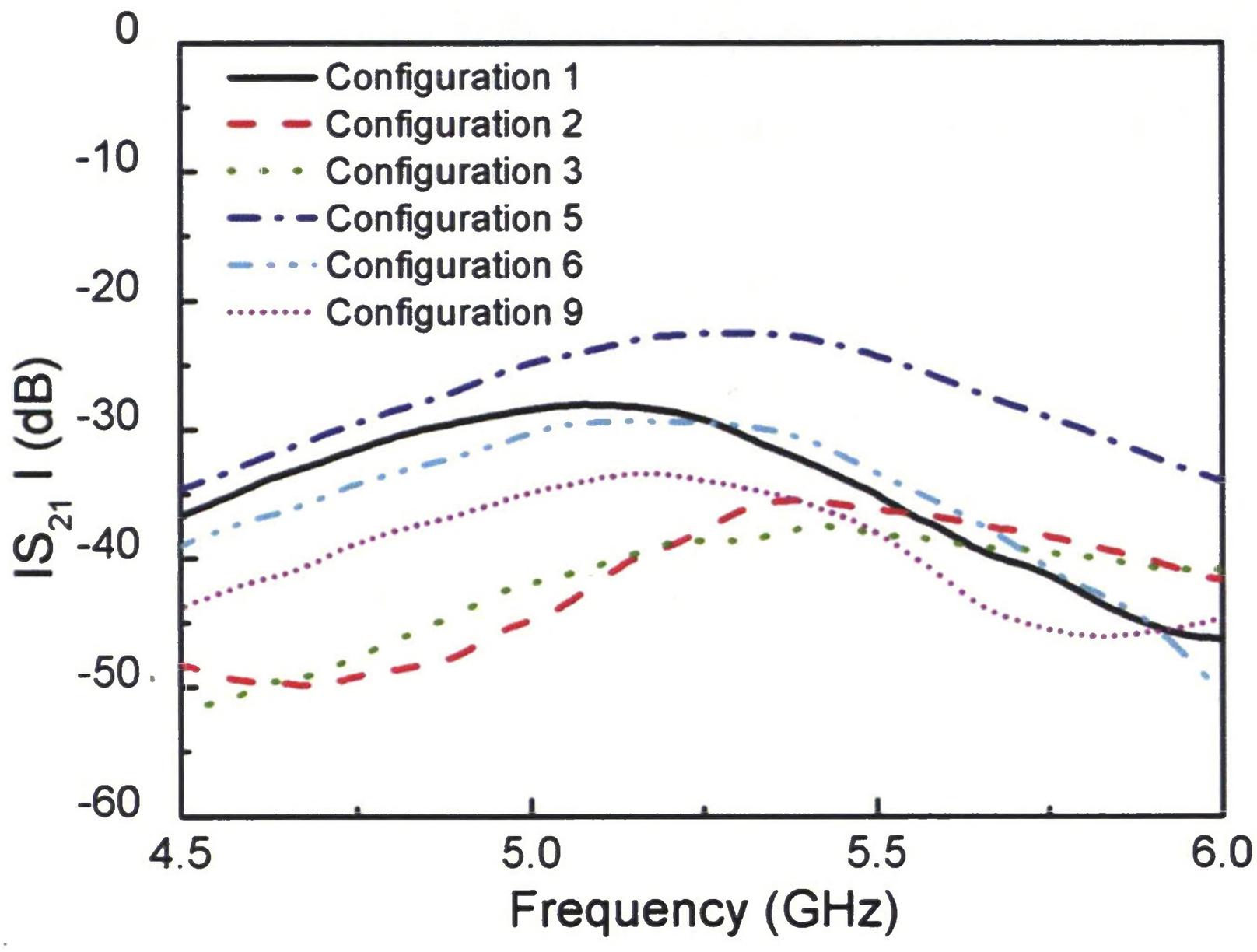

Figure 7.8: Measured mutual coupling coefficients for different antenna configurations.

of the antenna array for different array configurations (Table 7.4) is estimated by using equation (7.1) based on the simulated radiation patterns. Table 7.5 gives the envelope correlation coefficients for different antenna array configurations at 5.25 GHz. It is evident that the envelope correlation coefficients of the configurations (2, 3, 4, 6, 7, 8) having pattern diversity are lower than those (1, 5, 9) with the same antenna patterns, and they are all below 0.5, which satisfies the criterion for enabling the antenna to provide a good level of diversity [134].

7.3.2 MIMO-OFDM demonstrator

The MIMO-OFDM demonstrator is identical to the one reported in Section 7.2.2. Therefore, it is not repeated here.

Table 7.5: Envelope correlation coefficient of the nine configurations of the array

Array Configuration	ρ_e
1	0.85×10^{-2}
2	0.02×10^{-2}
3	0.16×10^{-2}
4	0.02×10^{-2}
5	1.60×10^{-2}
6	0.05×10^{-2}
7	0.16×10^{-2}
8	0.05×10^{-2}
9	4.12×10^{-2}

7.3.3 Measurement Location and Process

The channel test environment and process are the same as those reported in Section 7.2.3. Therefore, they are not repeated here. It should be noted that the reference antennas are located with the omnidirectional pattern aligning with the horizontal plane (x-y plane).

7.3.4 Results and Analysis

The definition of the MIMO-OFDM channel coefficient matrix and the equations to calculate the system capacity and to normalize the channel matrix are the same as those presented in Section 7.2.4, so they are not repeated here.

In the MIMO-OFDM channel measurement, the peak gain of the omnidirectional antenna is 2.2 dBi. But the gains of different states of the reconfigurable antennas vary from 2.8-6.4 dBi at 5.25 GHz. The antenna gain of each configuration is preserved in

$\|H\|$. The lower gain of the omnidirectional antenna can lead to a lower value of $\|H\|$. Therefore, compared to the pattern reconfigurable antenna, if all channel matrices are normalized to a common factor, the reference antenna will suffer a capacity loss due to the smaller $\|H\|$.

In this section, we aim to show that the proposed antenna has the ability to improve the system capacity by using pattern diversity to reduce the sub-channel correlation. If the gain of the antenna is taken into account, the extent of the enhancement of the system capacity derived only from the pattern diversity will not be explicitly shown. Therefore, the gain effect on the capacity should be eliminated in order to realize a fair comparison. In order to separate the effect of pattern diversity on the system capacity from the effect of antenna gain, two different channel matrix normalization methods are employed.

The first is that the channel matrix of each antenna configuration is normalized independently (Method I). In this case, the antenna gain is not included in the capacity calculation. Therefore, only the effect of the sub-channel correlation is kept in the capacity evaluation. The second is that the channel matrix of each antenna configuration is normalized with respect to that of the reference antenna (Method II). In this way, not only the sub-channel correlation, but also the relative received power difference, is preserved in the capacity calculation.

For channel matrix normalization Method I, it can be observed from Fig. 7.9 that, compared with omnidirectional antennas, the proposed pattern reconfigurable antennas improve the system capacity by 17% and 12% for the LOS and NLOS cases, respectively, at an SNR of 10 dB. This is because with antenna pattern diversity the sub-channel correlation is reduced. Therefore, the system capacity is improved, especially for environments with insufficient scatterers. In our experiments the best array configurations, which lead to the largest system capacity improvement, are configuration 6 and configuration 8 for the LOS and NLOS scenarios, respectively. An explanation of this is as follows. Although

the antennas with omnidirectional patterns in the horizontal plane are considered to be a good solution for MIMO systems, as they can receive rich multipath signals in that plane, it turns out that there are still many multipath components outside the azimuth plane which can be received by other states of the reconfigurable antennas. Therefore, system capacity improvement is possible using pattern reconfigurable antennas.

Furthermore, as is seen from Fig. 7.9, the percentage improvement of the system capacity for the LOS scenario is greater than that for the NLOS scenario. This is due to the fact that there is rich multipath in an indoor NLOS scenario so that the subchannel correlation of the system is already quite low. In this way, the improvement of the system capacity by reducing the sub-channel correlation is limited for an NLOS environment. Therefore, the extent of the improvement of the system capacity by reducing the MIMO sub-channel correlation in the LOS scenario is larger than that in the NLOS scenario.

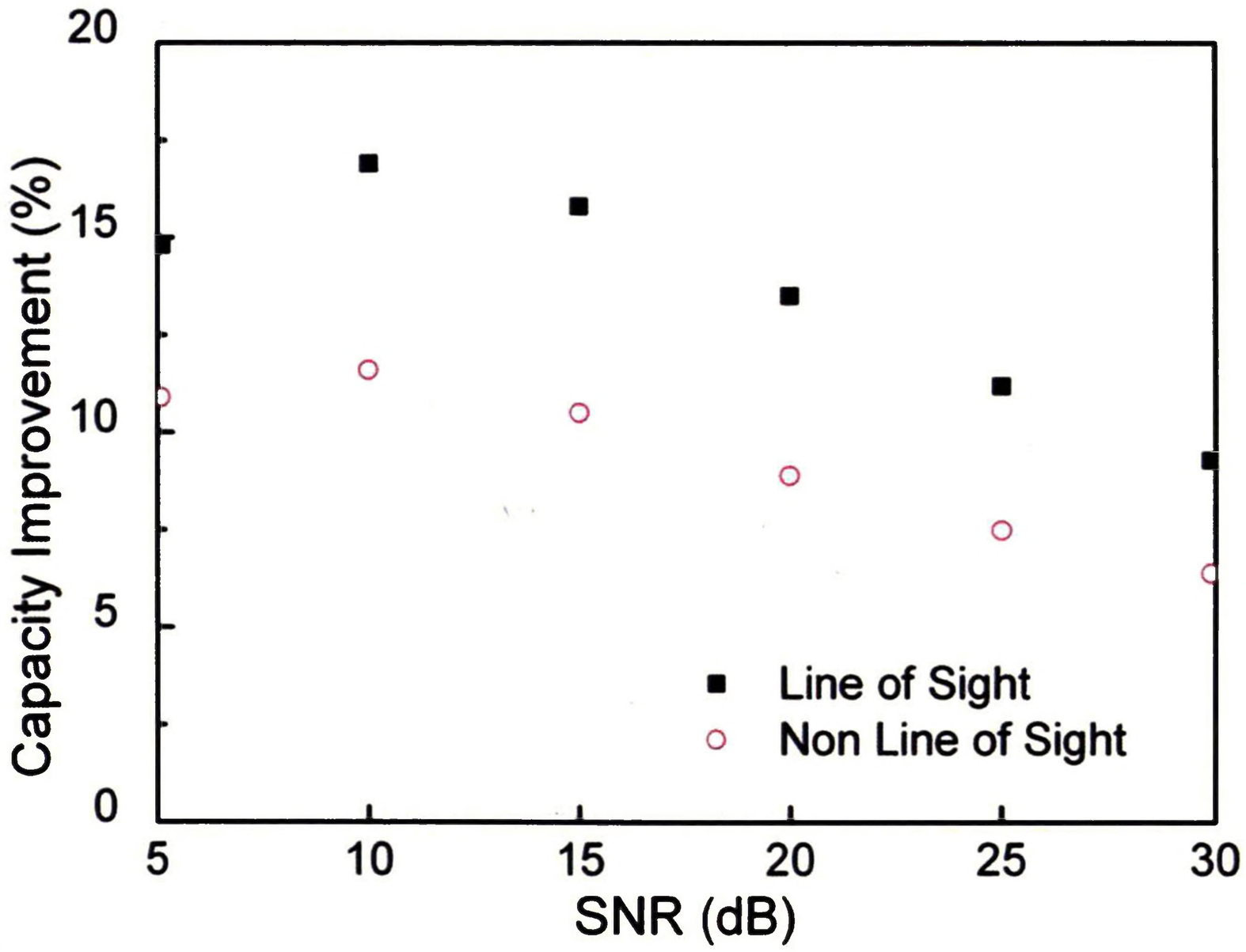

Figure 7.9: Percentage improvement of the reconfigurable antenna MIMO system capacity versus SNR for Method I. The corresponding omnidirectional antenna MIMO system capacity is used as the benchmark.

For channel matrix normalization Method II, the best configuration is antenna array configuration 1 (Table 7.4) in terms of the system capacity for both scenarios. It can be seen from Fig. 7.10 that, at an SNR of 10 dB, the peak improvement is 285% and 264% for the LOS and NLOS scenarios, respectively, which are much higher than those in Fig. 7.9. The reason that antenna configuration 1 outperforms other configurations as well as omnidirectional antennas to such a great extent lies in the higher gain of the antennas in configuration 1. Specifically, the $\|H\|$ of the system with configuration 1 is much greater than that with other configurations. By Method II, this effect is taken into account because the channel matrix of each antenna configuration is normalized to a common value. In this way, the normalized channel matrix of antenna configuration 1 is scaled up by a large factor due to the normalization; hence, the improvement of the capacity is significantly greater.

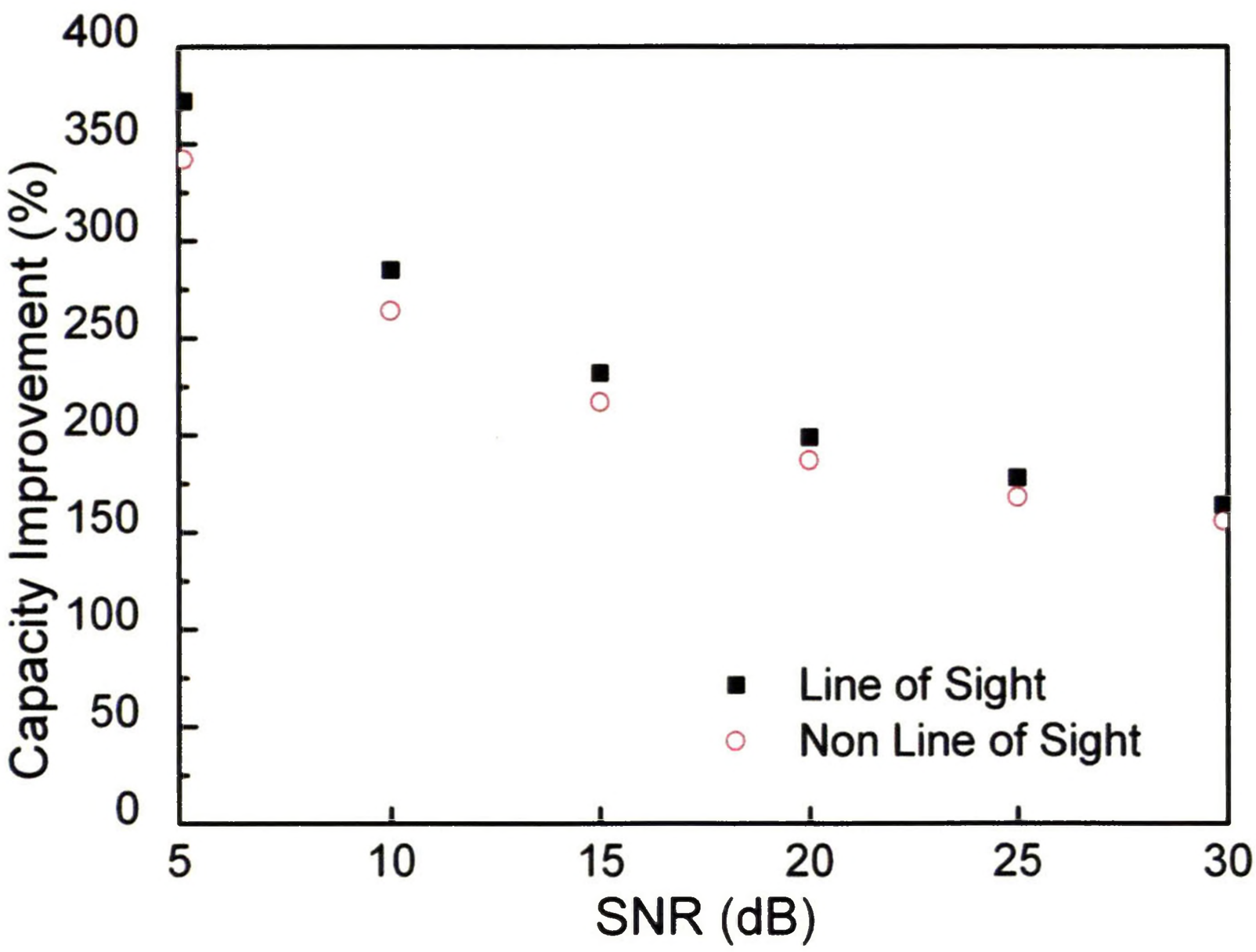

Figure 7.10: Percentage improvement of the reconfigurable antenna MIMO system capacity versus SNR for Method II. The corresponding omnidirectional antenna MIMO system capacity is used as the benchmark.

7.3.5 Discussion

From channel matrix normalization Method I, it is known that the pattern diversity of the pattern reconfigurable antenna can be exploited to improve the system capacity by reducing the sub-channel correlation, which is evidenced by the fact that antenna configurations 6 and 8 outperform the other configurations as well as the omnidirectional one in the LOS and NLOS scenarios, respectively. When the gains of different configurations are considered, however, it is found that the effect of antenna gain outweighs the effect of the channel decorrelation on the system capacity. Therefore antenna configuration 1, which has the largest antenna gain, becomes the best in both scenarios. In this situation, the pattern diversity loses its effect on system capacity due to the large gain difference of the different antenna states.

In order to employ the pattern diversity of the proposed antenna in practice (the gain difference is included in the capacity calculation), we need to improve the realized gains of antenna States 2 and 3. As discussed at the end of the Chapter 5, compared to State 1, the lower gains of State 2 and 3 are mostly attributed to the losses of the PIN diodes. Therefore, low-loss switches, such as RF MEMS, should be used to make the gains of States 2 and 3 close to that of State 1. An updated antenna prototype with RF MEMS could be designed and adopted in our future work.

Reference [99] also demonstrates the capability of a pattern reconfigurable antenna to improve the MIMO system capacity. Compared to [99], our work has three main differences. First, the mechanism of the pattern reconfigurability of the antenna in [99] uses mutual coupling of two closely spaced antennas. The pattern diversity will be reduced if the antenna element distance is increased. Therefore, spatial diversity, which is another effective scheme to improve the system capacity, cannot be efficiently employed together with pattern diversity in a MIMO system. However, as the way to reconfigure the pattern of our antenna is to change the antenna operating modes, there is no space limitation on

our antenna. Second, in our experiments, at an SNR of 10 dB, the capacity percentage improvement is 17% and 12% for the LOS and NLOS scenarios, respectively. These results are better than the average 10% improvement reported in [99]. Admittedly, since the capacity measurement is heavily dependent on the test environment, the improvement could be significantly different for other test scenarios. Third, the reference antenna in [99] is chose to be one particular configuration of the antenna, while in our work omnidirectional antennas are used for reference. Since omnidirectional antennas can receive rich multipath in the horizontal plane, this comparison can highlight the effect of pattern diversity on MIMO system capacity.

Chapter 8

Conclusions and Future Work

8.1 Conclusions

In this thesis, the research work concentrates on the design of new reconfigurable antennas (RAs) and the study of their applications in multiple-input-multiple-output (MIMO) systems. Firstly, a literature review of the previously reported RA designs is given, which demonstrates the available techniques and methods to design RAs. Secondly, motivated by the gaps between the current reported designs and the requirements of diversity systems on RAs, several reconfigurable antennas are proposed including frequency RAs, a polarization RA, a pattern RA, and a compound frequency and polarization RA. The performance of these antennas is summarized as follows:

For the frequency RAs, a planar quasi-Yagi antenna with a folded dipole driver element is employed. The centre frequency of the antenna is tuned by changing the effective electrical length of the folded dipole driver, which is achieved by using either varactor diodes or PIN diodes. Three antenna prototypes are designed, fabricated and measured. The first antenna enables continuous tuning from 6.0 to 6.6 GHz using varactor diodes, and the reflection coefficient bandwidth ($|S_{11}| \leqslant$-10 dB) at each frequency is greater than

15%. The second antenna enables discrete tuning using PIN diodes in either the 5.3-6.6 GHz band or the 6.4-8.0 GHz band. The third antenna operates in the millimetre-wave band and is capable of switching between the millimetre-wave Wireless Personal Area Network (WPAN) band (57-66 GHz) and E band (71-76 GHz). These proposed frequency RAs can provide good out-of-band rejection, thereby reducing the requirements for the filters of the front-end circuits. In addition, the dc biasing network of these frequency RAs is located far from the radiating elements, thus having little influence on the antenna performance. Moreover, the radiation characteristics remain almost unaffected across the entire tunable frequency ranges, and low levels of cross-polarized radiation are realized. The reconfigurable quasi-Yagi antennas have the further advantage of being compact, which makes them suitable for use in fixed- and steered-beam reconfigurable arrays.

For the polarization RA, a U-slot microstrip patch antenna with polarization reconfigurability is designed for wireless local area network (WLAN) applications. PIN diodes are appropriately positioned to change the lengths of the U-slot arms, which alters the antenna polarization states. To verify the design concept, two antenna prototypes with identical dimensions and structures are designed, fabricated and measured. The first prototype switches between linear and circular polarizations, while the second prototype switches between the two senses of circular polarization. The measured impedance bandwidth extends from 5.6 to 6.3 GHz and 5.72 to 6.08 GHz for the CP and LP modes, respectively, which can cover the entire WLAN band. An axial ratio bandwidth of 2.8% with a centre frequency of 5.77 GHz for CP modes is achieved. A simple dc bias network to control the PIN diodes is employed. The reconfigurable U-slot patch antenna is compact and easy to manufacture, which makes it highly suited to advanced wireless communication systems.

For the pattern RA, a compact pattern reconfigurable U-slot patch antenna is presented. Shorting posts around the patch are used to enable the antenna to operate in either a monopolar-patch or a normal-patch mode, which makes the antenna switch be-

tween three different radiation patterns. It is compact but can realize an overlapped frequency bandwidth of 6.6% ($|S_{11}| \leqslant$ -10 dB) with a centre frequency of 5.32 GHz for the two operating modes. Compared to most conventional pattern reconfigurable antennas, the proposed antenna does not need additional dc bias lines to control the PIN diodes, which greatly simplifies the antenna structure. Due to the simple structure and the pattern reconfigurability, the antenna has the ability to improve the performance of wireless communication systems considerably.

For the compound frequency and polarization RA, a new reconfigurable antenna with both frequency and polarization agility is presented. The antenna consists of a square microstrip patch with a single probe feed located along the diagonal line. The centre of each edge of the patch is connected to a shorting post via a PIN diode for polarization switching and two varactor diodes for frequency tuning. By switching between the different states of the PIN diodes, the proposed antenna can produce radiation patterns with horizontal, vertical or 45^0 linear polarization. By varying the dc bias voltages, the operating frequency of each polarization of the antenna can be independently tuned. The frequency tuning range is from 1.35 to 2.25 GHz ($|S_{11}| \leqslant$ -10 dB) for either the horizontal or the vertical polarization and from 1.35 to 1.90 GHz for the 45^0 linear polarization. Compared to most reported frequency or polarization reconfigurable antennas, the proposed design has extra polarization or frequency agility, which makes it more suitable for applications in modern diversity communication systems.

Finally, applications of polarization RAs and pattern RAs in MIMO systems are investigated by incorporating RAs in a 2×2 MIMO- orthogonal frequency division multiplexing (MIMO-OFDM) system. Two different channel matrix normalization methods are employed to separate the effect of sub-channel correlation on the system capacity from the effect of antenna gain. Therefore, the enhancement of the system capacity derived only from the polarization or pattern diversity can be explicitly shown. For the MIMO-OFDM

system with circularly polarized reconfigurable antennas, the capacity of the system with antennas having different polarizations is compared to that having the same polarizations. For the MIMO-OFDM system with pattern reconfigurable antennas, the capacity of the system with the proposed reconfigurable antennas is compared to that with omnidirectional antennas. In real-time MIMO-OFDM channel measurements conducted in both line-of-sight (LOS) and non-LOS (NLOS) scenarios, the system capacity is improved by 36% and 6.7% for the LOS and NLOS scenarios, respectively, at an SNR of 15 dB by using polarization RAs. The enhancement is about 17% and 12% for the LOS and NLOS scenarios, respectively, at an SNR of 10 dB by using the pattern RAs. A comparison of the above improvement using pattern RAs and those reported in other 2×2 MIMO systems with pattern RAs is also made.

8.2 Future Work

1. New and effective reconfiguration techniques for a full agility of the three characteristics (frequency, polarization and radiation pattern).

As illustrated in Chapter 6, most of the reconfigurable antenna designs focus on the reconfigurability of only one characteristic of the antenna. Some of the designs can accomplish the compound reconfigurability of two characteristics. However, to the best of the author's knowledge, there is no reconfigurable antenna reported which can realize a full reconfigurability of all three characteristics. This is mostly attributed to the strong linkage between an antenna's frequency response and its radiation characteristics, which makes it extremely challenging to independently control operating frequency, polarization and radiation pattern. Therefore, new and effective techniques are needed to break the linkage in order to achieve full reconfigurability of an antenna.

2. Reconfigurability of the entire transmitter and receiver.

It is well known that antennas are only one part of the entire transmitter and receiver systems. If reconfigurable antennas are incorporated in wireless communication systems, the other parts of the transmitter and receiver should also be capable of reconfiguring their characteristics. Only in this way can the system utilize the diversity derived from antenna agility, especially for the frequency RAs. Up to now, the research on the reconfigurable antenna and filter is well and extensively conducted. The study of other parts of the transmitter and receiver systems, however, is still in its initial stage.

3. Evaluation of the benefit-to-cost ratio at a system level.

Many researchers, including the author, have investigated the performance enhancement of a MIMO system using reconfigurable antennas. For example, the system capacity can be improved by using polarization or pattern reconfigurable antennas. However, compared to traditional antennas, reconfigurable antennas need extra electronic devices, smart materials or mechanical devices to realize reconfiguration, which increase the total costs of the antenna. So far, there is no mature evaluation system to assess the ratio between the improvement of the system performance and the increased antenna cost. Since the profits are unknown to the investors, there are still barriers for the large-scale commercialization of reconfigurable antennas. However, in some particular fields where the cost of the system is less of an issue, such as national security systems or military communication systems, reconfigurable antennas can find extensive application.

Appendix A

Symbols

λ_0	Free-space wavelength
ε_r	Dielectric constant
ε_{reff}	Effective dielectric constant
Ω	Ohm
H	MIMO channel matrix
H^+	Complex conjugate transpose of H
t	A certain time
$h_{i,j}$	Gain between the ith receive antenna and the jth transmit antenna
$\|\|H\|\|$	Frobenius norm of the channel matrix
N_r	Number of receive antennas
N_t	Number of transmit antennas
$\overline{F_1(\theta,\phi)}$	Complex vector indicating the electric field radiated from the ith antenna
C	System capacity in bits/second/Hz
I_{N_r}	$N_r \times N_r$ identity matrix
$\overline{H(i,j,k,l)}$	Normalized channel matrix

Appendix B

Abbreviations

BER	Bit Error Rate
CPS	Coplanar Stripline
DARPA	Defence Advanced Research Projects Agency
dB	Decibels
DCS	Digital Cellular System
EBG	Electromagnetic Band-gap
GPS	Global Positioning System
LCP	Liquid Crystal Polymer
LHCP	Left-hand Circular Polarization
LOS	Line of Sight
LP	linearly polarized
MIMO	Multiple-Input-Multiple-Output
MMIC	Monolithic Microwave Integrated Circuit
NLOS	Non-LOS
OFDM	Orthogonal Frequency Division Multiplexing
PCS	Personal Communication Service

PIFA	Planar Inverted F Antenna
RA	Reconfigurable Antenna
RECAP	Reconfigurable Aperture Program
RF	Radio Frequency
RF-MEMS	Radio Frequency Microelectromechanical System
RHCP	Right-hand Circular Polarization
SDR	Software Defined Radio
SISO	Single-Input-Single-Output
SNF	Spherical Near-field
SNR	Signal-to-Noise Ratio
UMTS	Universal Mobile Telecommunications System
WiMAX	Worldwide Interoperability for Microwave Access
WLAN	Wireless Local Area Network
WPAN	Wireless Personal Area Network

Bibliography

[1] C. A. Balanis, Antenna theory: analysis and design, 3^{rd} ed. Wiley-Interscience, 2005.

[2] R. Garg, P. Bhartia, I. Bahl, and A. Ittipiboon, Microstrip antenna design handbook, Artech House Publishers, 2001.

[3] S. Haykin, Cognitive radio: brain-empowered wireless communications, IEEE Journal Selected Areas in Communications, Vol. 23, No. 2, pp. 201-220, Feb. 2005.

[4] M. A. Jensen and J. W. Wallace, A review of antennas and propagation for MIMO wireless communications, IEEE Transactions Antennas Propagation, Vol. 52, No. 11, pp. 2810-2824, Nov. 2004.

[5] J. T. Bernhard, Reconfigurable antennas, Morgan & Claypool, 2006.

[6] D. H. Schaubert, F. G. Farrar, A. Sindoris, and S. T. Hayes, Microstrip antennas with frequency agility and polarization diversity, IEEE Transactions Antennas Propagation, Vol. 29, No. 1, pp. 118-123, Jan. 1981.

[7] P. Bhartia and I. J. Bahl, Frequency agile microstrip antennas, Microwave Journal, pp. 67-70, Oct. 1982.

[8] John K. Smith, Reconfigurable program (RECAP), DARPA, 1999.

[9] R. Waterhouse and N. Shuley, Full characterisation of varactor-loaded, probe-fed, rectangular, microstrip patch antennas, IEE Microwave Antennas Propagation, Vol. 141, No. 5, pp. 367-373, Oct. 1994.

[10] E. Bhuiyan, Y.-H. Park, S. El-Ghazaly, V. Nair, and H. Goronkin, Active tuning and miniaturization of microstrip antennas, presented at IEEE Antennas and Propagation Society International Symposium, Jul. 2002.

[11] E. Nishiyama and T. Itoh, Dual polarized widely tunable stacked microstrip antenna using varactor diodes, presented at IEEE International Workshop Antenna Technology, Mar. 2009.

[12] A. R. Weily, T. S. Bird, and Y. J. Guo, A reconfigurable high-gain partially reflecting surface antenna, IEEE Transactions Antennas Propagation, Vol. 56, No. 11, pp. 3382-3390, Nov. 2008.

[13] C. R. White and G. M. Rebeiz, A differential dual-polarized cavity-backed microstrip patch antenna with independent frequency tuning, IEEE Transactions Antennas Propagation, Vol. 58, No. 11, pp. 3490-3498, Nov. 2010.

[14] S. V. Hum and H. Y. Xiong, Analysis and design of a differentially-fed frequency agile microstrip patch antenna, IEEE Transactions Antennas Propagation, Vol. 58, No. 10, pp. 3122-3130, Oct. 2010.

[15] F. Yang and Y. Rahmat-Samii, Patch antennas with switchable slots (PASS) in wireless communications: Concepts, designs, and applications, IEEE Antennas Propagation Magazine, Vol. 47, pp. 13-29, Feb. 2005.

[16] N. Jin, F. Yang, and Y. Rahmat-Samii, A novel patch antenna with switchable slot (PASS): dual-frequency operation with reversed circular polarizations, IEEE Transactions Antennas Propagation, Vol. 54, No. 3, pp. 1031-1034, Mar. 2006.

[17] C. Luxey, L. Dussopt, J.-L. Le Sonn, and J.-M. Laheurte, Dual-frequency operation of CPW-fed antenna controlled by pin diodes, Electronics Letters, Vol. 36, No. 1, pp. 2-3, Jan. 2000.

[18] L. Le Garrec, R. Sauleau, and M. Himdif, A 2:1 band frequency-agile active microstrip patch antenna, presented at European Conference Antennas Propagation, Nov. 2007.

[19] A.-F. Sheta and S. Mahmoud, A widely tunable compact patch antenna, IEEE Antennas Wireless Propagation Letters, Vol. 7, pp. 40-42, 2008.

[20] T. Y. Han and C. T. Huang, Reconfigurable monopolar patch antenna, Electronics Letters, Vol. 46, No. 3, pp. 199-200, Feb. 2010.

[21] J. L. A. Quijano and G. Vecchi, Optimization of an innovative type of compact frequency-reconfigurable antenna, IEEE Transactions Antennas Propagation, Vol. 57, No. 1, pp. 9-18, Jan. 2009.

[22] C. W. Jung, Y. J. Kim, and F. De Flaviis, Macro-micro frequency tuning antenna for reconfigurable wireless communication systems, Electronics Letters, Vol. 43, No. 4, pp. 201-202, Feb. 2007.

[23] C. Zhang, S. Yang, S. El-Ghazaly, A. E. Fathy, and V. K. Nair, A low-profile branched monopole laptop reconfigurable multiband antenna for wireless applications, IEEE Antennas Wireless Propagation Letters, Vol. 8, pp. 216-219. 2009.

[24] C. J. Panagamuwa, A. Chauraya, and J. C. Vardaxoglou, Frequency and beam reconfigurable antenna using photoconducting switches, IEEE Transactions Antennas Propagation, Vol. 54, No. 2, pp. 449-454, Feb. 2006.

[25] P. Y. Qin, A. R. Weily, Y. J. Guo, T. S. Bird, and C. H. Liang, Frequency reconfigurable quasi-yagi folded dipole antenna, IEEE Transactions Antennas Propagation, Vol. 58, No. 8, pp. 2742-2747, Aug. 2010.

[26] P. Y. Qin, A. R. Weily, Y. J. Guo, and C. H. Liang, A reconfigurable quasi-Yagi folded dipole antenna, presented at IEEE Antennas and Propagation Society International Symposium, Jul. 2009.

[27] P. Y. Qin, A. R. Weily, Y. J. Guo, and C. H. Liang, Millimeter wave frequency reconfigurable quasi-Yagi antenna, presented at Asia-Pacific Microwave Conference, Dec. 2010.

[28] Y. Cai, Y. J. Guo, and P. Y. Qin, Frequency switchable quasi-Yagi dipole array for base station antennas, presented at IEEE Antennas and Propagation Society International Symposium, Jul. 2011.

[29] Y. Cai, Y. J. Guo, and A. R. Weily, A Frequency-Reconfigurable Quasi-Yagi dipole antenna, IEEE Antennas Wireless Propagation Letters, Vol. 9, pp. 883-886, 2010.

[30] S.-K. Oh, H.-S. Yoon, and S.-O. Park, A PIFA-type varactor-tunable slim antenna with a PIL patch feed for multiband applications, IEEE Antennas Wireless Propagation Letters, Vol. 6, pp. 103-105, 2007.

[31] V.-A. Nguyen, R.-A. Bhatti, and S.-O. Park, A simple PIFA-based tunable internal antenna for personal communication handsets, IEEE Antennas Wireless Propagation Letters, Vol. 7, pp. 130-133, 2008.

[32] N. Karmakar, Shorting strap tunable stacked patch PIFA, IEEE Transactions Antennas Propagation, Vol. 52, No. 11, pp. 2877-2884, Nov. 2004.

[33] M. Komulainen, M. Berg, H. Jantunen, E. Salonen, and C. Free, A frequency tuning method for a planar inverted-F antenna, IEEE Transactions Antennas Propagation, Vol. 56, No. 4, pp. 944-950, Apr. 2008.

[34] D. Peroulis, K. Sarabandi, and L. P. B. Katehi, Design of reconfigurable slot antennas, IEEE Transactions Antennas Propagation, Vol. 53, No. 2, pp. 645-653, Feb. 2005.

[35] N. Behdad and K. Sarabandi, A varactor-tuned dual-band slot antenna, IEEE Transactions Antennas Propagation, Vol. 54, No. 2, pp. 401-408, Feb. 2006.

[36] P. L. Chi, R. Waterhouse, and T. Itoh, Compact and tunable slot-loop antenna, IEEE Transactions Antennas Propagation, Vol. 59, No. 4, pp. 1394-1397, Apr. 2011.

[37] H. Li, J. Xiong, Y. Yu, and S. He, A simple compact reconfigurable slot antenna with a very wide tuning range, IEEE Transactions Antennas Propagation, Vol. 58, No. 11, pp. 3725-3728, Nov. 2010.

[38] C. R. White and G. M. Rebeiz, A shallow varactor-tuned cavity-backed slot antenna with a 1.9:1 tuning range, IEEE Transactions Antennas Propagation, Vol. 58, No. 3, pp. 633-639, Mar. 2010.

[39] C. R. White and G. M. Rebeiz, Single- and dual-polarized tunable slot-ring antennas, IEEE Transactions Antennas Propagation, Vol. 57, No. 1, pp. 19-26, Jan. 2009.

[40] N. Behdad and K. Sarabandi, Dual-Band reconfigurable antenna with a very wide tunability range, IEEE Transactions Antennas Propagation, Vol. 54, No. 2, pp. 409-416, Feb. 2006.

[41] E. Erdil, K. Topalli, M. Unlu, O. Civi, and T. Akin, Frequency tunable microstrip patch antenna using RF MEMS technology, IEEE Transactions Antennas Propagation, Vol. 55, No. 4, pp. 1193-1196, Apr. 2007.

[42] K. Van Caekenberghe and K. Sarabandi, A 2-bit Ka-band RF MEMS frequency tunable slot antenna, IEEE Antennas Wireless Propagation Letters, Vol. 7, pp. 179-182, 2008.

[43] J. T. Bernhard, E. Kiely, and G. Washington, A smart mechanically-actuated two-layer electromagnetically coupled microstrip antenna with variable frequency, bandwidth, and antenna gain, IEEE Transactions Antennas Propagation, Vol. 49, No. 4, pp. 597-601, Apr. 2001.

[44] J.-C. Langer, J. Zou, C. Liu, and J. T. Bernhard, Reconfigurable out-of-plane microstrip patch antenna using MEMS plastic deformation magnetic actuation, IEEE Microwave Wireless Components Letters, Vol. 13, pp. 120-122, Mar. 2003.

[45] R. K. Mishra, S. S. Pattnaik, and N. Das, Tuning of microstrip antenna on ferrite substrate, IEEE Transactions Antennas Propagation, Vol. 41, No. 2, pp. 230-233, Feb. 1993.

[46] J. Liang and H. Y. David, Microstrip patch antennas on tunable electromagnetic band-gap substrates, IEEE Transactions Antennas and Propagation, Vol. 57, No. 6, pp. 1612-1697, Jun. 2009.

[47] L. Liu and R. Langley, Liquid crystal tunable microstrip patch antenna, Electronics Letters, Vol. 44, No. 20, pp. 1179-1180, Sep. 2008.

[48] A. R. Weily and Y. J. Guo, An aperture coupled patch antenna system with MEMS-based reconfigurable polarization, presented at International Symposium Communications and Information Technologies, Oct. 2007.

[49] B. Poussot, J. M. Laheurte, L. Cirio, and O. Picon, Diversity gain measurements of a reconfigurable antenna with switchable polarization, Microwave Optical Technology Letters, Vol. 49, No. 12, pp. 3154-3158, Dec. 2007.

[50] F. Yang and Y. Rahmat-Samii, A reconfigurable patch antenna using switchable slots for circular polarization diversity, IEEE Microwave Wireless Components Letters, Vol. 12, No. 3, pp. 96-98, Mar. 2002.

[51] M. K. Fries, M. Grani, and R. Vahldieck, A reconfigurable slot antenna with switchable polarization, IEEE Microwave Wireless Components Letters, Vol. 13, No. 11, pp. 490-492, Nov. 2003.

[52] A. Khaleghi and M. Kamyab, Reconfigurable single port antenna with circular polarization diversity, IEEE Transactions Antennas Propagation, Vol. 57, No. 2, pp. 555-559, Feb. 2009.

[53] M. Boti, L. Dussopt, and J. M. Laheurte, Circularly polarized antenna with switchable polarization sense, Electronics Letters, Vol. 36, No. 18, pp. 1518-1519, Aug. 2000.

[54] S. H. Hsu and K. Chang, A novel reconfigurable microstrip antenna with switchable circular polarization, IEEE Antennas Wireless Propagation Letters, Vol. 6, pp. 160-162, 2007.

[55] H. Aissat, L. Cirio, M. Grzeskowiak, J. M. Laheurte, and O. Picon, Reconfigurable circularly polarized antenna for short-range communication systems, IEEE Transactions Microwave Theory Techniques, Vol. 54, No. 6, pp. 2856-2863, Jun. 2006.

[56] K. F. Tong and J. J. Huang, New proximity coupled feeding method for reconfigurable circularly polarized microstrip ring antennas, IEEE Transactions Antennas Propagation, Vol. 56, No. 7, pp. 1860-1866, Jul. 2008.

[57] Y. J. Sung, T. U. Jang, and Y. S. Kim, A reconfigurable microstrip antenna for switchable polarization, IEEE Microwave Wireless Components Letters, Vol. 14, No. 11, pp. 534-536, Nov. 2004.

[58] W. M. Dorsey and A. I. Zaghloul, Perturbed square-ring slot antenna with reconfigurable polarization, IEEE Antennas Wireless Propagation Letters, Vol. 8, pp. 603-606, 2009.

[59] R. H. Chen and J. S. Row, Single-fed microstrip patch antenna with switchable polarization, IEEE Transactions Antennas Propagation, Vol. 56, No. 4, pp. 922-926, Apr. 2008.

[60] Y.-F. Wu, C. H. Wu, D. Y. Lai, and F. C. Chen, A reconfigurable quadri-polarization diversity aperture-coupled patch antenna, IEEE Transactions Antennas Propagation, Vol. 55, No. 3, pp. 1009-1012, Mar. 2007.

[61] P. Y. Qin, A. R. Weily, Y. J. Guo, and C. H. Liang, Polarization reconfigurable u-slot patch antenna, IEEE Transactions Antennas Propagation, Vol. 58, No. 10, pp. 3383-3388, Oct. 2010.

[62] R. F. Harrington, Reactively controlled directive arrays, IEEE Transactions Antennas Propagation, Vol. 26, No. 3, pp. 390-395, May 1978.

[63] R. Schlub, D. V. Thiel, J. W. Lu, and S. G. OKeefe, Dual-band six-element switched parasitic array for smart antenna cellular communications, Electronics Letters, Vol. 36, No. 16, pp. 1342-1343, Aug. 2000.

[64] R. Schlub, J. Lu, and T. Ohira, Seven-element ground skirt monopole ESPAR antenna design from a genetic algorithm and finite element method, IEEE Transactions Antennas Propagation, Vol. 51, No. 11, pp. 3033-3039, Nov. 2003.

[65] D. V. Thiel and S. Smith, Switched parasitic antennas for cellular communications, Artech House, 2002.

[66] D. V. Thiel, Switched parasitic antennas and controlled reactance parasitic antennas: a systems comparison, presented at IEEE Antennas and Propagation Society International Symposium, Jul. 2004.

[67] S. L. Preston, D. V. Thiel, J. W. Lu, S. G. OKeefe, and T. S. Bird, Electronic beam steering using switched parasitic patch elements, Electronics Letters, Vol. 33, No. 1, pp. 7-8, Jan. 1997.

[68] S. Zhang, G. H. Huff, J. Feng, and J. T. Bernhard, A Pattern reconfigurable microstrip parasitic array, IEEE Transactions Antennas Propagation, Vol. 52, No. 10, pp. 2773-2776, Oct. 2004.

[69] S. Zhang, G. H. Huff, G. Cung, and J. T. Bernhard, Three variations of a pattern reconfigurable microstrip parasitic array, Microwave Optical Technology Letters, Vol. 45, No. 5, pp. 369-372, Jun. 2005.

[70] R. J. Dinger, Reactively steered adaptive array using microstrip patch elements at 4 GHz, IEEE Transactions Antennas Propagation, Vol. 32, No. 8, pp. 848-856, Aug. 1984.

[71] R. J. Dinger, A planar version of a 4.0 GHz reactively steered adaptive array, IEEE Transactions Antennas Propagation, Vol. 34, No. 3, pp. 427-431, Mar. 1986.

[72] M. I. Lai, T. Y. Wu, J. C. Hsieh, C. H. Wang, and S. K. Jeng,, Compact switched-beam antenna employing a four-element slot antenna array for digital home applications, IEEE Transactions Antennas Propagation, Vol. 56, No. 9, pp. 2929-2936, Sep. 2008.

[73] J. Sarrazin, Y. Mahe, S. Avrillon, and S. Toutain, Pattern reconfigurable cubic antenna, IEEE Transactions Antennas Propagation, Vol. 57, No. 2, pp. 310-317, Feb. 2009.

[74] S. V. Hum, M. Okoniewski, and R. J. Davies, Realizing an electronically tunable reflectarray using varactor diode-tuned elements, IEEE Microwave Wireless Components Letters, Vol. 15, No. 6, pp. 422-424, Jun. 2005.

[75] S. V. Hum, M. Okoniewski, and R. J. Davies, Modeling and design of electronically tunable reflectarrays, IEEE Transactions Antennas Propagation, Vol. 55, No. 8, pp. 2200-2210, Aug. 2007.

[76] M. Riel and J.-J. Laurin, Design of an electronically beam scanning reflectarray using aperture-coupled elements, IEEE Transactions Antennas Propagation, Vol. 55, No. 5, pp. 1260-1266, May 2007.

[77] A. Petosa, S. Thirakoune, and A. Ittipiboon, Reconfigurable Fresnel-zone-plate-shutter antenna with beam-steering capability, IEEE Antennas Propagation Magazine, Vol. 49, No. 5, pp. 42-51, Oct. 2007.

[78] T. H. Hand and S. A. Cummer, Reconfigurable reflectarray using addressable metamaterials, IEEE Antennas Wireless Propagation Letters, Vol. 9, pp. 70-74, 2010.

[79] H. Rajagopalan, Y. Rahmat-Samii, and W. A. Imbriale, RF MEMS actuated reconfigurable reflectarray patch-slot element, IEEE Transactions Antennas Propagation, Vol. 56, No. 12, pp. 3689-3699, Dec. 2008.

[80] J. Perruisseau-Carrier, Dual-polarized and polarization-flexible reflective cells with dynamic phase control, IEEE Transactions Antennas Propagation, Vol. 58, No. 5, pp. 1494-1502, May 2010.

[81] G. H. Huff and J. T. Bernhard, Integration of packaged RF MEMS switches with radiation pattern reconfigurable square spiral microstrip antennas, IEEE Transactions Antennas Propagation, Vol. 54, No. 2, pp. 464-469, Feb. 2006.

[82] S. L. S. Yang and K. M. Luk, Design of a wide-band L-probe patch antenna for pattern reconfigurable or diversity applications, IEEE Transactions Antennas Propagation, Vol. 54, No. 2, pp. 433-438, Feb. 2006.

[83] W. L. Liu, T. R. Chen, S. H. Chen, and J. S. Row, Reconfigurable microstrip antenna with pattern and polarization diversities, Electronics Letters, Vol. 43, No. 2, pp. 77-78, Jan. 2007.

[84] S. H. Chen, J. S. Row, and K. L. Wong, Reconfigurable square-Ring patch antenna with pattern diversity, IEEE Transactions Antennas Propagation, Vol. 55, No. 2, pp. 472-475, Feb. 2007.

[85] P. Y. Qin, A. R. Weily, Y. J. Guo, C. H. Liang, and Y. Cai, A pattern reconfigurable U-slot patch antenna, presented at IEEE Antennas and Propagation Society International Symposium, Jul. 2010.

[86] P. Y. Qin, A. R. Weily, Y. J. Guo, and C. H. Liang, A pattern reconfigurable u-slot antenna and its applications in MIMO systems, accepted for publication as a special issue on Multiple-Input Multiple-Output (MIMO) Technology (joint with MTT) in IEEE Transactions Antennas and Propagation.

[87] S. Nikolaou, R. Bairavasubramanian, C. Lugo Jr, I. Carrasquillo, D. C. Thompson, and G. E. Ponchak, Pattern and frequency reconfigurable annular slot antenna using PIN diodes, IEEE Transactions Antennas Propagation, Vol. 54, No. 2, pp. 439-448, Feb. 2006.

[88] G. H. Huff, J. Feng, S. Zhang, and J. T. Bernhard, A novel radiation pattern and frequency reconfigurable single turn square spiral microstrip antenna, IEEE Microwave Wireless Components Letters, Vol. 13, No. 2, pp. 57-59, Feb. 2003.

[89] W. C. Wu, J. S. Row, T. Y. Han, and C. Y. D. Sim, An aperture-coupled microstrip antenna with frequency agility and polarization diversity, presented at Asia-Pacific Microwave Conference, Dec. 2009.

[90] P. Y. Qin, Y. J. Guo, Y. Cai, and C. H. Liang, A reconfigurable antenna with frequency and polarization agility, IEEE Antennas Wireless Propagation Letters, Vol. 10, pp. 1373-1376, 2011.

[91] M. A. Jensen and J. W. Wallace, MIMO wireless channel modeling and experimental characterization, in Space-Time Processing for MIMO Communications, John Wiley & Sons, Ltd, 2005.

[92] P. Kyritsi, D. C. Cox, R. A. Valenzuela, and P. W. Wolniansky, Effect of antenna polarization on the capacity of a multiple element system in an indoor environment, IEEE Journal Selected Areas in Communications, Vol. 20, No. 6, pp. 1227-1239, Aug. 2002.

[93] J. W. Wallace, M. A. Jensen, A. L. Swindlehurst, and B. D. Jeffs, Experimental characterization of the MIMO wireless channel: data acquisition and analysis, IEEE Transactions Wireless Communications, Vol. 2, No. 2, pp. 335-343, Mar. 2003.

[94] A. Grau, J. Romeu, M. J. Lee, S. Blanch, L. Jofre, and F. De Flaviis, A dual-linearly-polarized MEMS-reconfigurable antenna for narrowband MIMO communication systems, IEEE Transactions Antennas Propagation, Vol. 58, No. 1, pp. 4-17, Jan. 2010.

[95] B. A. Cetiner, E. Akay, E. Sengul, and E. Ayanoglu, A MIMO system with multifunctional reconfigurable antennas, IEEE Antennas Wireless Propagation Letters, Vol. 5, pp. 463-466, 2006.

[96] P. Y. Qin, Y. J. Guo, and C. H. Liang, Effect of antenna polarization diversity on MIMO system capacity, IEEE Antennas Wireless Propagation Letters, Vol. 9, pp. 1092-1095, 2010.

[97] J. D. Boerman and J. T. Bernhard, Performance study of pattern reconfigurable antennas in MIMO communication systems, IEEE Transactions Antennas Propagation, Vol. 56, No. 1, pp. 231-236, Jan. 2008.

[98] P. Mookiah, D. Piazza, and K. R. Dandekar, Reconfigurable spiral antenna array for pattern diversity in wideband MIMO communication systems, presented at IEEE Antennas and Propagation Society International Symposium, Jul. 2008.

[99] D. Piazza, N. J. Kirsch, A. Forenza, R. W. Heath, and K. R. Dandekar, Design and evaluation of a reconfigurable antenna array for MIMO systems, IEEE Transactions Antennas Propagation, Vol. 56, No. 3, pp. 869-881, Mar. 2008.

[100] D. Piazza, M. DAmico, and K. R. Dandekar, Performance improvement of a wideband MIMO system by using two-port RLWA, IEEE Antennas Wireless Propagation Letters, Vol. 8, pp. 830-834, 2009.

[101] D. Piazza, P. Mookiah, M. DAmico, and K. R. Dandekar, Experimental analysis of pattern and polarization reconfigurable circular patch antennas for MIMO systems, IEEE Transactions on Vehicular Technology, Vol. 59, No. 5, pp. 2352-2362, Jun. 2010.

[102] CST Microwave Studio. Ver. 2009. Darmstadt.

[103] K. R. Carver and J. W. Mink, Microstrip antenna technology, IEEE Transactions Antennas Propagation, Vol. 29, No. 1, pp. 2-24, Jan. 1981.

[104] R. E. Munson, Conformal microstrip antennas and microstrip phased arrays, IEEE Transactions Antennas Propagation, Vol. 22, No. 1, pp. 74-78, Jan. 1974.

[105] M. C. Bailey and M. D. Deshpande, Integral equation formulation of microstrip antennas, IEEE Transactions Antennas Propagation, Vol. 30, No. 4, pp. 651-656, Jul. 1982.

[106] Y. T. Lo, D. Solomon, and W. F. Richards, Theory and experiment on microstrip antennas, IEEE Transactions Antennas Propagation, Vol. 27, No. 2, pp. 137-145, Mar. 1979.

[107] W. F. Richards, Y. T. Lo, and D. D. Harrison, An improved theory of microstrip antennas with applications, IEEE Transactions Antennas Propagation, Vol. 29, No. 1, pp. 38-46, Jan. 1981.

[108] J. R. James and P. S. Hall, Handbook of Microstrip Antennas, Vols 1 and 2, Peter Peregrinus Ltd, 1989.

[109] C. C. Liu, A. Hessel, and J. Shmoys, Performance of probe-fed rectangular microstrip patch element phased arrays, IEEE Transactions Antennas Propagation, Vol. 36, No. 11, pp. 1501-1509, Nov. 1988.

[110] C. A. Balanis, Advanced engineering electromagnetics, Wiley-Interscience, 1989.

[111] D. M. Pozar, A review of bandwidth enhancement techniques for microstrip antennas, in Microstrip Antennas, The analysis and design of microstrip antennas and arrays, Wiley-IEEE Press, pp. 157-166, 1995.

[112] D. Sanchez-Hernandez and I. D. Robertson, A survey of broadband microstrip patch antennas, Microwave Journal, pp. 60-84, Sep. 1996.

[113] R. Q. Lee, K. F. Lee, and J. Bobinchak, Characteristics of a two-layer electromagnetically coupled rectangular patch antenna, Electronics Letters, Vol. 23, No. 20, pp. 1070-1072, Jul. 1987.

[114] W. Chen, K. F. Lee, and R. Q. Lee, Spectral-domain moment-method analysis of coplanar microstrip parasitic subarrays, Microwave Optical Technology Letters, Vol. 6, No. 3, pp. 157-163, Mar. 1993.

[115] C. L. Mak, K. M. Luk, K. F. Lee, and Y. L. Chow, Experimental study of a microstrip patch antenna with an L-shaped probe, IEEE Transactions Antennas Propagation, Vol. 48, No. 5, pp. 354-358, May 2000.

[116] T. Huynh and K. F. Lee, Single-layer single patch wideband microstrip antenna, Electronics Letters, Vol. 31, No. 16, pp. 1310-1312, Aug. 1995.

[117] S. Weigand, G. H. Huff, K. H. Pan, and J. T. Bernhard, Analysis and design of broad-band single-layer rectangular U-slot microstrip patch antennas, IEEE Transactions Antennas Propagation, Vol. 51, No. 3, pp. 457-468, Mar. 2003.

[118] K. F. Tong, K. M. Luk, K. F. Lee, and R. Q. Lee, A broad-band U-slot rectangular patch antenna on a microwave substrate, IEEE Transactions Antennas Propagation, Vol. 48, No. 6, pp. 954-960, Jun. 2000.

[119] K. F. Tong and T. P. Wong, Circularly polarized U-slot antenna, IEEE Transactions Antennas Propagation, Vol. 55, No. 8, pp. 2382-2385, Aug. 2007.

[120] I. J. Bahl and P. Bhartia, Microstrip Antennas, New York: Artech House, 1980.

[121] C. Delaveaud, P. Leveque, and B. Jecko, New kind of microstrip antenna: the monopolar wire-patch antenna, Electronics Letters, Vol. 30, No. 1, pp. 1-2, Jan. 1994.

[122] J. S. Row, S. H. Yeh, and K. L. Wong, A wide band monopolar plate-patch antenna, IEEE Transactions Antennas Propagation, Vol. 50, No. 9, pp. 1328-1330, Sep. 2002.

[123] K.-L. Laù, P. Li, and K.-M. Luk, A monopolar patch antenna with very wide impedance bandwidth, IEEE Transactions Antennas Propagation, Vol. 53, No. 3, pp. 1004-1010, Mar. 2005.

[124] H. Yagi, Beam transmission of ultra-short waves, Proceedings IRE, Vol. 16, pp. 715-741, Jun. 1928.

[125] N. Kaneda, Y. Qian, and T. Itoh, A novel Yagi-Uda dipole array fed by a microstrip-to-CPS transition, presented at Asia-Pacific Microwave Conference, Dec. 1998.

[126] Y. Qian, W. R. Deal, N. Kaneda, and T. Itoh, A uniplanar quasi-Yagi antenna with wide bandwidth and low mutual coupling characteristics, presented at IEEE Antennas and Propagation Society International Symposium, Jul. 1999.

[127] W. R. Deal, N. Kaneda, J. Sor, Y. Qian and T. Itoh, A new quasi-Yagi antenna for planar active antenna arrays, IEEE Transactions Microwave Theory Techniques, Vol. 48, No. 6, pp. 910-918, Jun. 2000.

[128] J. H. Winters, On the capacity of radio communication systems with diversity in a Rayleigh fading environment, IEEE Journal Selected Areas in Communications, Vol. 5, No. 5, pp. 871-878, Jun. 1987.

[129] T. L. Marzetta and B. M. Hochwald, Capacity of a mobile multiple-antenna communication link in Rayleigh flat fading, IEEE Transactions Information Theory, Vol. 45, No. 1, pp. 139-157, Jan. 1999.

[130] G. J. Foschini and M. J. Gans, On limits of wireless communications in a fading environment when using multiple antennas, Wireless Personal Communications, Vol. 6, No. 3, pp. 311-335, Mar. 1998.

[131] P. Kyritsi, D. C. Cox, R. A. Valenzuela, and P. W. Wolniansky, Correlation analysis based on MIMO channel measurements in an indoor environment, IEEE Journal Selected Areas in Communications, Vol. 21, No. 5, pp. 713-720, Jun. 2003.

[132] V. Tarokh, N. Seshadri, and A. R. Calderbank, Space-time codes for high data rate wireless communication: performance analysis and code construction, IEEE Transactions Information Theory, Vol. 44, No. 2, pp. 744-765, Mar. 1998.

[133] J. C. Guey, M. P. Fitz, M. R. Bell, and W. Y. Kuo, Signal design for transmitter diversity wireless communications systems over Rayleigh fading channels, IEEE Transactions Communications, Vol. 47, No. 4, pp. 527-537, Apr. 1999.

[134] R. Vaughan and J. Andersen, Antenna diversity in Mobile Communications, IEEE Transactions on Vehicular Technology, Vol. 36, No. 4, pp. 149-172, Nov. 1987.

[135] P. Almers, F. Tufvesson, and A. F. Molisch, Measurement of keyhole effect in a wireless multiple-input-multiple-output (MIMO) channel, IEEE Communications Letters, Vol. 7, pp. 373-375, Aug. 2003.

[136] W. L. Stutzman and G. A. Thiele, Antenna theory and design, 2^{nd} ed. John Wiley & Sons, Inc., 1998.

[137] R. W. Lampe, Design formulas for an asymmetric coplanar strip folded dipole, IEEE Transactions Antennas Propagation, Vol. 33, No. 9, pp. 1028-1031, Sep. 1985.

[138] M/A-COM data sheet for MA4AGBLP912 beam lead PIN diode, M/A-COM Technology Solutions, Inc., Lowell, MA

[139] B. Razavi, Gadgets gab at 60 GHz, IEEE Spectrum, Vol. 45, No. 2, pp. 45-58, Feb. 2008.

[140] Wireless Personal Area Networks (WPAN), IEEE 802.15.3 Std. [Online], Available: http://www.ieee802.org/15/pub/TG3c.html

[141] [Online], Available: http://www.e-band.com/index.php?id=69

[142] W. H. Tu and K. Chang, Wide-band microstrip-to-coplanar stripline/slotline transitions, IEEE Transactions Microwave Theory Techniques, Vol. 54, No. 3, pp. 1084-1089, Mar. 2006.

[143] D. L. Sengupta, Resonant frequency of a tunable rectangular patch antenna, Electronics Letters, Vol. 20, No. 15, pp. 614-615, Jul. 1984.

[144] R. B. Waterhouse and N. V. Shuley, Scan performance of infinite arrays of microstrip patch elements loaded with varactor diodes, IEEE Transactions Antennas Propagation, Vol. 41, No. 9, pp. 1273-1280, Sep. 1993.

[145] A. J. Paulraj and T. Kailath, Increasing capacity in wireless broadcast systems using distributed transmission/directional reception, U.S. Patent 5345599, Sep. 1994

[146] A. J. Paulraj, D. A. Gore, R. U. Nabar, and H. Blcskei, An overview of MIMO communications - a key to gigabit wireless, Proceedings IEEE, Vol. 92, No. 2, pp. 198-218, Feb. 2004

[147] Y. J. Guo, Advances in Mobile Radio Access Networks, Artech House, 2004.

[148] H. Suzuki, T. V. Tran, I. B. Collings, G. Daniels, and M. Hedley, Transmitter noise effect on the performance of a MIMO-OFDM hardware implementation achieving improved coverage, Journal Selected Areas in Communications, Vol. 26, No. 8, pp. 867-876, Aug. 2008.

[149] H. Suzuki, T. V. Tran, and I. B. Collings, Characteristics of MIMO-OFDM Channels in indoor environments, Journal Wireless Communications Networking, Vol. 2007, No. 19728, Jan. 2007.

[150] D. C. Cox, R. R. Murray, H. W. Arnold, A. W. Norris, and M. F. Wazowicz, Cross-polarization coupling measured for 800 MHz radio transmission in and around houses and large buildings, IEEE Transactions Antennas Propagation, Vol. 34, No. 1, pp. 83-88, Jan. 1986.